



HAL
open science

Thermo-hydro-dynamic consistency and stiffness in general compressible multiphase flows

Eric Heulhard de Montigny

► **To cite this version:**

Eric Heulhard de Montigny. Thermo-hydro-dynamic consistency and stiffness in general compressible multiphase flows. Mathematical Physics [math-ph]. Université Paris-Saclay, 2021. English. NNT : 2021UPASM039 . tel-03821804

HAL Id: tel-03821804

<https://theses.hal.science/tel-03821804v1>

Submitted on 19 Oct 2022

HAL is a multi-disciplinary open access archive for the deposit and dissemination of scientific research documents, whether they are published or not. The documents may come from teaching and research institutions in France or abroad, or from public or private research centers.

L'archive ouverte pluridisciplinaire **HAL**, est destinée au dépôt et à la diffusion de documents scientifiques de niveau recherche, publiés ou non, émanant des établissements d'enseignement et de recherche français ou étrangers, des laboratoires publics ou privés.

Thermo-hydro-dynamic consistency and stiffness in general compressible multiphase flows.

Cohérence thermo-hydro-dynamique et raideur dans les
écoulements multi-fluides compressibles.

Thèse de doctorat de l'Université Paris-Saclay

École doctorale n° 74, mathématiques Hadamard (EDMH)
Spécialité de doctorat: Mathématiques appliquées
Unité de recherche: Université Paris-Saclay, CNRS, ENS Paris-Saclay, Centre
Borelli, 91190, Gif-sur-Yvette, France
Réfèrent: : ENS Paris-Saclay

Thèse présentée et soutenue à Paris, le 20 Décembre 2021, par

Éric HEULHARD DE MONTIGNY

Composition du jury:

Olivier Simonin Professeur, INP Toulouse - IMFT	Président
Philippe Villedieu Directeur de recherche, ONERA - INSA Toulouse	Rapporteur
Hong Luo Professeur, North Carolina State University	Rapporteur
Antoine Llor Directeur de recherche, CEA DAM,DIF	Directeur
Frédéric Pascal Professeur, ENS Paris-Saclay, Centre Borelli	Examineur
Daniel Lhuillier Professeur émérite, en retraite de l'IJLRDA, Université Paris-Sorbonne	Examineur
Robin J. R. Williams Directeur de recherche, Atomic Weapons Establishment	Invité
William J. Rider Directeur de recherche, Sandia National Laboratories	Invité

Titre: Cohérence thermo-hydro-dynamique et raideur dans les écoulements multi-fluides compressibles.

Mots clés: Écoulements multi-fluides, Cohérence thermodynamique, Raideur

Résumé: Prédire l'évolution des écoulements multiphasiques où coexistent des fluides fortement contrastés mobilise les numériciens et les physiciens depuis le développement des codes de sûreté nucléaire. Le défi est d'autant plus grand lorsque les écoulements sont soumis à des chocs forts, possèdent des changements de phases et transportent les espèces sur de longues distances. Les modèles utilisés pour prédire ces écoulements doivent ainsi capturer les variations de volumes de toutes les phases, leurs différentes dynamiques et les couplages entre les flu-

ides qui peuvent être forts et contrastés. Du fait de cette physique complexe, la structure mathématique des modèles s'écarte souvent des lois de conservation hyperbolique comme les équations d'Euler. De nouvelles méthodes numériques doivent donc être conçues afin d'approcher les solutions des modèles avec des ressources numériques finies tout en restant robustes. Ceci contraint les schémas numériques à respecter la cohérence thermodynamique et à être suffisamment stables pour mener à bien les calculs.

Title: Thermo-hydro-dynamic consistency and stiffness in general compressible multiphase flows.

Keywords: Multiphase flows, Thermodynamic consistency, Stiffness

Abstract: Predicting the behaviour of multiphase flows where many contrasted phases coexist is a challenge that has mobilized numericists and physicists since the development of nuclear safety codes. The challenge is especially tough when flows feature strong shocks, phase changes and transport over long distances. Simulation must then incorporate the compressibility of all phases, their different dynamics and the strong and various couplings

occurring between them. Because of this complex physics, the mathematical structure of the models often departs from the Euler classical hyperbolic equations. New numerical methods must be then designed in order to solve these models with finite computational resources and strong robustness which constrained numerical schemes in terms of stability and thermodynamic consistency.



Acknowledgments

Je profite de ces quelques lignes avant d'entrer dans le vif du sujet pour remercier tout ceux qui m'ont aidé à réaliser cette thèse.

Mes premiers remerciements vont tout naturellement à Antoine Llor qui fut mon directeur pendant ces trois ans. Comme beaucoup d'autres thèses, celle ci n'a pas été « un long fleuve tranquille » mais malgré les écueils, j'ai pu trouver chez Antoine un soutien dans les moments difficiles et compter sur sa grande implication quand les différents jalons approchaient. Si la thèse s'est révélée être une expérience pleine de richesses scientifiques, c'est en premier lieu grâce à nos conversations partant du principe de moindre action jusqu'aux idées d'Aristarque de Samos !

Je tiens également à remercier mon jury de thèse, M. Luo et M. Villedieu pour leurs lectures et corrections attentives, M. Lhuillier pour nos échanges durant la thèse sur la modélisation de la phase dispersée, M. Simonin pour avoir accepté de présider mon jury et ses remarques sur le traitement des collisions et M. Pascal pour ses remarques sur le plan numérique. Je tiens également à remercier les membres invités, M. Williams pour sa relecture et ses corrections et M. Rider pour son retour sur les différents aspects de la thèse.

Ensuite, je tiens à remercier le laboratoire du CEA qui m'a accueilli et qui a donné un cadre propice à ma recherche. Merci à ses chercheurs avec lesquels j'ai pu échanger de nombreuses idées et avoir d'autres regards sur la thèse. Merci à Sébastien et Rémy (et à Bastien leur doctorant) pour leurs nombreuses explications et discussions sur les schémas numériques qui ont contribué à ce que les idées du chapitre 3 de cette thèse voient le jour. À Thibaud pour ses explications sur le PMA, le schéma GEEC et sa relecture de l'ébauche d'article centré sur le chapitre 4. À William et Jean-Philippe pour nos échanges sur les idées qui constituent le corps du chapitre 6. Et enfin à Thierry qui m'a accueilli au sein de son laboratoire et qui a veillé au bon déroulement de la thèse.

Hors du CEA, je tiens à remercier Agnès Desolneux du centre Borelli qui m'a suivi administrativement. Je tiens aussi à remercier tout les professeurs dont j'ai reçu l'enseignement dans les formations annexes, notamment Boris Kolev pour ses nombreuses explications pendant et après les cours sur la géométrie différentielle.

Enfin, si j'ai grandement apprécié cette expérience scientifique, c'est parce qu'elle était aussi une expérience humaine. Merci donc à tout les doctorants et stagiaires de Teratec (Adrien, Yohann, Steve et Jean-Baptiste) puis ceux avec qui j'ai partagé mon quotidien une fois sur le centre: à mes co-bureaux (quand je n'étais pas encore SBF), Marie (experte en nœuds fantômes), Albertine (sérieuse concurrente pour le titre de Maître du Mal), Mathilde (qui m'a sauvé plus d'une fois d'un retour en transport) et Corentin H. (force et honneur, c'est la dernière ligne droite). À Mathieu (que je n'ai connu que docteur mais dont l'aura régnait encore sur les lieux) et à son petit-fils de bureau Corentin (la muse qui a inspiré le film camping). Merci aux post-sas, Ronan (le métronome de nos pauses café à la flegme légendaire), Charles (si vous ne l'entendez pas, c'est qu'il n'est pas là), Olivier (ne le lancez jamais sur Dour), Adrien (et ses chemises Hawaïennes), Jean-Cédric (actionnaire principal

du CEA, d'Elior et des cars Suzanne) et aux nouveaux arrivants: Joël (et sa chaise magique), Kevin (le premier nouveau à s'être fait café-scienté) et Etienne (judoka à la fondation fragile). Entre le post sas et mon ancien bureau (parti trop vite) se trouve donc ce fameux couloir où j'ai côtoyé: Sébastien (respo en chef café-science), Nicolas (il paraît qu'il est toujours en stage), Cécile (si elle commence à rire vous n'aurez pas la fin de l'histoire), Baptiste (auteur de 556 362 contributions à Wikipedia), Christina (fournisseur officiel de chocolat du couloir), Mathéo (gentil supporter d'une petite équipe de Premier League), Grégoire (qui a fait sa thèse en famille), Louise (qui a eu le courage de décider de sa voie), Jean-Gabriel (digne héritier de Grégoire), Victor (footballeur et chanteur d'origine trinitadienne), Antoine (ancien Maître du Mal, parti étendre son empire à Bordeaux), Paul (vaillant coureur à la cheville souple) et Bastien (acolyte d'Albertine avec qui je l'espère, la cohabitation sur le trône se passera bien).

J'ai également une pensée pour ma famille et mes amis (mention spéciale à tout ceux qui ont eu le courage de venir m'écouter parler d'écoulements polyphasiques). Mes remerciements à leur égard iraient cependant bien au-delà de la réalisation d'une thèse et ne leur rendraient que peu justice. Aussi, place à la science !

Contents

Acknowledgments	3
List of symbols	8
1 Introduction	11
1.1 Introduction en Français	12
1.1.1 Un bref panorama de la thèse	12
1.1.2 Le développement du polyphasique au CEA	13
1.1.3 Quelques repères dans la compréhension et la simulation des écoule- ments polyphasiques	14
1.1.4 Quelques défis rencontrés par la communauté	16
1.2 Introduction in English	19
1.2.1 A short overview of the thesis	19
1.2.2 The development of multiphase flows at CEA	20
1.2.3 Some landmarks in the understanding and simulation of multiphase flows	21
1.2.4 Some challenges faced by the community	23
2 Selected state of art	27
2.1 The modeling of multiphase flows	28
2.1.1 General description and classification of flows	28
2.1.2 Review of the models	29
2.2 Details on Euler–Euler approach	35
2.2.1 On averaging	35
2.2.2 History of the models	37
2.2.3 Closing the fluctuation forms	41

2.3	Current approach to find and discretize the <i>backbone</i> model	43
2.3.1	Variational approaches	43
2.3.2	The derivation of the backbone model	51
2.3.3	The numerical scheme	57
2.4	On the hyperbolicity in two-phase flow models	59
2.4.1	The link between stability and hyperbolicity	59
2.4.2	Ellipticity and characteristic analysis of the two phase flow model . .	61
2.4.3	What are the vision toward the ellipticity of this model ?	63
2.4.4	Cutoff wavelength by Ramshaw (1978)	64
2.4.5	On the Baer & Nunziato (1986) model	65
2.A	Appendix: computation of the new pressure gradient (2.3.3)	69
3	Taming the “stiff stiffness” of pressure work and relaxation in numerical schemes for compressible multi-fluid flows	71
3.1	Aim: pressure in multi-fluid models and schemes	73
3.2	Background: multi-fluid models and schemes	75
3.2.1	Derivation of multi-fluid models; backbone model	75
3.2.2	Present issue: “stiff stiffness” of pressure work and equilibration . . .	76
3.2.3	Present hydrodynamic scheme: GEEC	77
3.2.4	Present approach: explicit estimates of implicit pressures	78
3.2.5	Some previous approaches	79
3.3	Explicit backbone evolution equations; stiffness	80
3.3.1	Backbone model with explicit pressure work	80
3.3.2	Explicit pressure work in energy equations; stiffness	81
3.3.3	Stiffness of contrasted systems; air–water example	82
3.3.4	Isentropic binary mixture of ideal–stiffened gases	83
3.3.5	Deluding speed of sound; fundamental derivative	84
3.4	Single time-step integration of pressure work	85
3.4.1	An important building block: the “implicit shock”	85
3.4.2	Another building block: the “implicit isentrope”	87
3.4.3	Multi-fluid pressure equilibration	88
3.4.4	EEIP: Explicit estimates of implicit pressures	90
3.5	One-dimensional numerical tests	92
3.5.1	EEIP in the GEEC scheme	92
3.5.2	Selection and design of test cases	93
3.5.3	General numerical conditions, shock dissipation	96
3.5.4	Shock tube tests	97
3.5.5	Isentropic two-fluid expansion test	100
3.5.6	Two-fluid extension of Noh’s test	101
3.6	Conclusion	105
3.A	Other pressure issues in compressible multi-fluid models and schemes	106

3.B	The backbone model	108
3.B.1	Statistical multi-fluid evolution equations	108
3.B.2	Backbone evolution equations	111
3.B.3	Derivation of evolution equations in explicit form	111
3.C	The GEEC scheme for the backbone model	112
3.D	Semi-analytical solution of isentropic two-fluid expansion	115
3.E	Noh’s test for ideal–stiffened gas mixtures	117
4	Preserving isentropic behavior in multi-fluid systems through fundamental energy closures and first principle	121
4.1	Introduction	122
4.1.1	Thermodynamic consistency in multiphase flows	122
4.1.2	Isentropy through variational approaches and first principles	124
4.1.3	Explicit formalization in anticipation of future numerical schemes	126
4.2	Fundamental modeling of some energy reservoirs	127
4.2.1	Energy reservoirs at the cornerstone of non relaxed multiphase models	127
4.2.2	Energies of fluctuations lost by averaging process	129
4.3	Dissipation free models with added fluctuations	136
4.3.1	Lagrangian and momentum equation	136
4.3.2	Forcing pressure equality	139
4.3.3	Kinetic energy equations, conservation of the total energy	141
4.3.4	Explicit internal energy equations	143
4.A	Appendix: pressure evolution equation with added mass and without pressure constraint	147
5	Collisions in Eulerian-Eulerian modeling of dispersed multiphase flows	149
5.1	Introduction	151
5.1.1	The coupling challenge	151
5.1.2	Modeling of collisions	151
5.1.3	Collisions’ challenging aspects	152
5.1.4	The present approaches	153
5.2	The interior collisions	154
5.2.1	Turbulent agitation	154
5.2.2	Energy closure	155
5.2.3	Lagrangian and momentum equation	159
5.2.4	Energy equations	160
5.2.5	Pressure equilibrium	161
5.3	Exterior collisions	161
5.3.1	The main principle	161
5.3.2	Collision model	162
5.3.3	Mass, momentum and energy exchange	163

5.3.4	Closing the model	164
5.4	The final model	165
5.5	Numerical tests	166
5.5.1	Interior collisions tests	166
5.5.2	Exterior collisions tests	168
5.5.3	Complete collision	168
5.6	An extension of the model	170
5.A	Appendix	173
6	Exploratory work on a new hybrid method to model dispersed phases in multiphase flows	177
6.1	Introduction	179
6.1.1	Physics and modeling of dispersed multiphase flows	179
6.1.2	First tracking of particles in Eulerian cell	180
6.2	A new thermodynamic consistent approach	181
6.2.1	Hybrid description of particles	181
6.2.2	Variational approaches in discrete and semi-discrete systems	183
6.3	Application of the method on various systems	184
6.3.1	Full particles systems	184
6.3.2	Dispersed multiphase flows	185
6.3.3	Model with fluid and particles both compressible	187
6.4	Consistent numerical schemes	188
6.4.1	System with only compressible particles	188
6.4.2	System with fluid and non compressible particles	189
6.4.3	System with fluid and compressible particles	191
6.5	Precisions on the numerical schemes	193
6.5.1	On the particle spreading	193
6.5.2	On the transport equation	194
6.5.3	Dissipation forms	195
6.6	Numerical results	195
6.6.1	Incompressible particles in compressible fluids	195
6.6.2	Dispersed curtains	196
6.6.3	Compressible particle in shock and expansion	198
6.A	Appendix	200
6.A.1	Continuous	200
6.A.2	Discrete	202
7	Conclusion	205
	Bibliography	209

List of symbols

<ul style="list-style-type: none"> * φ, ϕ some fluids * φ_b <i>collector</i> fluid of the fluid φ * a^φ a field of φ * c^φ mass fraction * b^φ indicative function * ξ^φ Lagrangian marker * α^φ volume fraction * ρ^φ density * $[\alpha\rho]^\varphi$ their product * v^φ specific volume * u_i^φ velocity , coordinate i * e^φ mass internal energy * β^φ relative compressibility coefficient * p^φ internal pressure * ke^φ mass external turbulence energy * pke^φ external turbulence pressure * k^φ mass internal turbulence energy * pk^φ internal turbulence pressure * ei^φ mass surface tension energy * ai^φ interacial area density * pi^φ surface tension pressure * a^p a field of a particle p * f_p mass distribution of particle p 	<ul style="list-style-type: none"> * π^φ reference pressure of φ * Γ Gruneisen coefficient * γ adiabatic compression coefficient * σ surface tension coefficient * c_s sound speed * $a_{i,j}$ derivative of the i component of a along j * $D_t^\varphi(a)$ Eulerian derivative along φ: $\partial_t(a) + (u_i^\varphi a)_{,i}$ * $d_t^\varphi(a)$ Lagrangian derivative along φ: $\partial_t(a) + u_i^\varphi a_{,i}$ * A added mass coefficient * $A_{,a}$ its derivative with respect to a * Δt^n time between $t^{n-1/2}$ and $t^{n+1/2}$ * $\Delta t^{n+1/2}$ time between t^n and t^{n+1} * $D_{\Delta t}^\varphi$ discrete Eulerian operator along φ * $d_{\Delta t}^\varphi$ discrete Lagrangian operator along φ * $a_c^{\varphi n}$ field a of φ in cell c at t^n * $a_{cd}^{\varphi n}$ a field a of φ from cell c to d at t^n * $s_{cd}^{n\pm 1/2}$ normal from c to d at $t^{n\pm 1/2}$ * $\sigma_{cd}^{\varphi n\pm 1/2}$ off centering factor * a_{pc}^n of field of a particle p in the the cell c
---	---

CHAPTER 1

Introduction

Contents

1.1	Introduction en Français	12
1.1.1	Un bref panorama de la thèse	12
1.1.2	Le développement du polyphasique au CEA	13
1.1.3	Quelques repères dans la compréhension et la simulation des écoulements polyphasiques	14
1.1.4	Quelques défis rencontrés par la communauté	16
1.2	Introduction in English	19
1.2.1	A short overview of the thesis	19
1.2.2	The development of multiphase flows at CEA	20
1.2.3	Some landmarks in the understanding and simulation of mul- tiphase flows	21
1.2.4	Some challenges faced by the community	23

1.1 Introduction en Français

1.1.1 Un bref panorama de la thèse

Ce projet de thèse s’est déroulé au Commissariat à l’Énergie Atomique (CEA), Direction des Applications Militaire (DAM). Il s’inscrit dans la continuité de la thèse de [Vazquez-Gonzalez \(2016\)](#) et est contemporain de celle de [Paulin \(2021\)](#). Il s’agit de répondre à deux objectifs dans le développement des modèles et schémas multiphasiques : être cohérent thermodynamiquement et capturer la raideur inhérente à ces écoulements pour assurer la stabilité. Dans des travaux précédents [Vazquez-Gonzalez et al. \(2020\)](#), un schéma numérique (nommé GEEC pour « Geometric, Energy, and Entropy Compatible ») a été conçu en utilisant des approches variationnelles et mimétiques. Avec ces méthodes, un comportement quasi-isentropique et des conservations exactes ont été obtenus. Cependant, cette proximité avec l’isentropie a rendu le schéma numérique potentiellement vulnérable aux résidus numériques. En effet, comme l’un des objectifs était de capturer l’isentropie, la discrétisation de l’énergie interne a été développée avec une approche mimétique sans aborder les problèmes de raideur.

Dans cette thèse, nous proposons une nouvelle discrétisation des équations d’énergie interne, formellement applicable à tout autre schéma multiphasique, qui traite les problèmes de raideur et de cohérence thermodynamique dans le couplage par la pression. Cette nouvelle approche est appliquée au modèle discrétisé par [Vazquez-Gonzalez et al. \(2020\)](#), connu sous le nom de modèle à 6 équations, qui dérive d’une approche de moyenne dépouillée de toutes les corrélations de second ordre. Ainsi, toute la dissipation et tous les potentiels d’ordre supérieur cachés dans les fluctuations sont éliminés. Par conséquent, le modèle ne représente que des situations idéales et est donc rarement applicable aux écoulements multiphasiques réels sans être complété. Cependant, comme il est à la racine de tous les autres modèles, il est crucial d’en assurer une discrétisation correcte. Dans le prolongement de [Vazquez-Gonzalez et al. \(2020\)](#), une méthode est proposée au chapitre (4) permettant d’introduire des effets isentropiques d’ordre supérieur (tension de surface, turbulence, etc.) tout en maintenant une formalisation du modèle qui rend compte de la raideur et de la cohérence thermodynamique. Pour montrer l’intérêt de la méthode, des couplages au sein de la phase dispersée sont considérés dans des écoulements chargés de particules. Les collisions sont introduites par des approches variationnelles et les équations qui en découlent sont discrétisées en imitant le schéma GEEC. Les couplages dissipatifs avec la phase porteuse sont modélisés par des forces de traînée. Des simulations numériques de croisement de jets valident l’approche.

La dernière partie de la thèse est un travail exploratoire qui se concentre sur les problèmes de cohérence thermodynamique dans la modélisation Lagrange-Euler (LE) d’écoulements de particules dispersées. Une nouvelle description des particules est couplée au principe de moindre action, conduisant à la dynamique couplée des phases dispersées et porteuses. La dynamique discrète est dérivée avec la même procédure. Cette approche est étendue aux particules compressibles. Les simulations numériques conduisent à des résultats contrastés, montrant les possibilités de la méthode mais aussi un besoin d’améliorations.

1.1.2 Le développement du polyphasique au CEA

Le polyphasique au CEA

Dans le cadre de ses missions, le CEA est amené à prédire différents écoulements polyphasiques dans des contextes académiques et industriels. Tout d'abord, le fonctionnement et la sûreté des réacteurs à eau pressurisée (REP) font intervenir plusieurs fluides circulant dans les différents circuits. Ces fluides sont soumis à des cycles au cours desquels se produisent de fortes variations de température et de pression ainsi que des changements de phase. D'autre part, le CEA a étendu en 2010 ses activités au domaine des énergies renouvelables. Les écoulements polyphasiques y sont également rencontrés comme dans le domaine de l'hydrogène par exemple (pile à combustible, électrolyse de vapeur à haute température, etc.). Enfin, l'une des missions de la DAM est de concevoir et de garantir le fonctionnement et la sûreté des armes nucléaires françaises. Depuis la signature du Traité d'interdiction complète des essais nucléaires (TICE) sous la présidence de Jacques Chirac en 1996, la France a cessé ses essais. Dans ce contexte, le programme de simulation a été lancé en 1994 par François Mitterrand. Depuis lors, la DAM s'appuie sur la simulation numérique pour remplir ses missions. L'objectif des scientifiques et ingénieurs de la DAM est alors de développer des modèles analytiques permettant de rendre compte de la physique des armes et des schémas numériques permettant de les résoudre. La complexité du phénomène et la grande précision requise nécessitent d'importantes ressources de calcul. Pour répondre à cette demande, des supercalculateurs sont développés et installés par Atos (anciennement Bull) au CEA DAM Bruyères-le-Châtel. La réalisation et la programmation sur ces supercalculateurs constituent un défi pour les ingénieurs en raison de leurs architectures spécifiques. Pour valider la qualité des simulations numériques, des comparaisons avec des expériences de fusion réalisées avec le Laser Mégajoule (LMJ) et d'autres expériences standards sont effectuées.

La simulations d'écoulements extrêmes

Du fait de ces applications spécifiques, les écoulements polyphasiques que l'on cherche à simuler à la DAM peuvent se révéler très extrêmes. L'utilisation de ce qualificatif fait référence à plusieurs caractéristiques rencontrées par les physiciens et les numériciens.

Tout d'abord, la taille des écoulements concernés est très grande par rapport au maillage typique utilisé dans les simulations. Cette spécificité rend la simulation complète extrêmement coûteuse en termes de ressources de calcul. Même avec les ordinateurs les plus puissants disponibles, certaines méthodes polyphasiques restent alors inaccessibles. De plus, ce point implique le transport de matériaux sur de longues distances ce qui confronte les schémas à la diffusion numérique.

En outre, le nombre de réservoirs d'énergie à l'intérieur des écoulements implique que les modèles doivent respecter les conservations fondamentales (quantité de mouvement, masse et énergie) car une fuite de ces quantités pourrait conduire à un écart critique entre la solution réelle et la solution numérique. Ce problème est naturellement aussi présent dans les

schémas. Il est particulièrement crucial de traiter la propagation correcte des chocs, conditionnée par la vérification des relations de Rankine-Hugoniot. En outre, ce point conduit à l'obligation de respecter la deuxième loi thermodynamique afin d'éviter des résultats non physiques et/ou des calculs instables.

Le dernier point critique est le nombre élevé de matériaux (jusqu'à quelques dizaines) et les contrastes dans leur équation d'état (EOS). Une multiplicité de phases implique un grand nombre de couplages, conduisant à des modèles complexes qui rendent encore plus difficile le respect des conservations et de la cohérence thermodynamique. D'autant plus que la grande quantité d'énergie implique que tous les matériaux peuvent être compressés. Les contrastes entre les matériaux n'ont pas d'impact direct sur les modèles mais contraignent les schémas numériques utilisés pour les résoudre. Ceci contraignent à leur tour la manière dont les modèles sont écrits.

La capture de ces écoulements est également difficile en raison des instabilités potentielles entre les phases qui conduisent à un comportement non linéaire chaotique. Par exemple, dans la simulation de la fusion par confinement interne (ICF), un petit défaut de la capsule conduit à une perte de compression sphérique et diminue ainsi l'énergie apportée au matériau fusible.

Le programme de simulation est ainsi confronté à de nombreux défis pour prédire les écoulements polyphasiques extrêmes rencontrés. Les ingénieurs et les scientifiques ont donc développé des modèles et des schémas spécifiques. Cependant, la prédiction des écoulements polyphasiques était déjà une préoccupation dans de nombreux sites industriels à travers le monde avant que le CEA DAM ne lance son programme de simulation.

1.1.3 Quelques repères dans la compréhension et la simulation des écoulements polyphasiques

Le développement des premiers modèles

Le développement des modèles polyphasiques a commencé il y a quelques décennies. A la connaissance de l'auteur, la première occurrence de la modélisation dans la littérature a été publiée par [van Deemter & van der Laan \(1961\)](#). Cependant, les équations n'étaient écrites que de manière formelle et la turbulence était négligée dans le processus de moyenne et introduite de manière plutôt intuitive dans le tenseur des contraintes. Plus tard, [Hinze \(1963\)](#) a dérivé un autre modèle en considérant l'effet des particules sur la phase continue. Ces modèles ont été construits avec la technique de moyenne qui est toujours la manière la plus utilisée pour construire des modèles polyphasiques. Ces deux références semblent être la première forme moderne de modèles continus avec un ensemble d'équations par fluide impliquant la conservation de la masse, de la quantité de mouvement et de l'énergie. De nombreux modèles inspirés de leurs travaux ont été rapidement développés pour des écoulements chargés de particules dans des tuyaux ([Soo, 1969](#)) ou dans des lits fluidisés ([Anderson & Jackson, 1967](#)). La question de la fermeture des corrélations était déjà une

préoccupation majeure, notamment les tenseurs de contraintes des deux phases. De plus, les instabilités des modèles ont été rapidement identifiées dans les premières études, comme par exemple par Murray (1965) qui a dérivé une relation de dispersion à partir de son jeu d'équations.

Ainsi, de nombreuses questions qui sont encore abondamment étudiées aujourd'hui étaient déjà présentes à l'esprit des premiers chercheurs. De plus, même si la procédure pour obtenir des modèles a été clarifiée et rédigée de manière plus rigoureuse au fil des ans, l'idée principale, qui consiste à calculer la moyenne des équations locales du fluide et à rechercher des fermetures de formes inconnues, était déjà développée. A l'époque, les modèles étaient purement académiques. Cependant, les ingénieurs et les scientifiques les ont rapidement combinés avec les nouveaux ordinateurs afin de simuler efficacement les écoulements polyphasiques.

Quelques applications industrielles originelles

Les modèles et codes industriels précurseurs ont été développés simultanément à plusieurs endroits dans le monde. Leur développement était particulièrement motivé pour assurer la sécurité des réacteurs nucléaires. En particulier, l'accident de perte de réfrigérant (LOCA) a été rapidement prédit avec une physique polyphasique. Cet accident survient lorsque le circuit de refroidissement ne fonctionne plus à la suite de la rupture d'une conduite. Le cas typique consiste à prédire les ondes de raréfaction progressant le long des tuyaux après la rupture.

En France, le code CATHARE a été conçu en 1979 par le CEA, EDF et Framatome et visait à simuler, entre autres cas, les LOCA dans les REP. Le modèle utilisé était un modèle polyphasique complet ne supposant aucune relaxation instantanée de la vitesse ou de la température (Rousseau, 1984). L'utilisation de ce type de modèles polyphasiques était déjà connue au CEA de Grenoble (Bouré, 1973) où Ishii écrivit son manuel standard (Ishii, 1975). Aux USA, selon Lyczkowski (2017), l'histoire des écoulements polyphasiques commence en 1970 avec le code projet SLOOP (Seriated LOOP) chez Aerojet Nuclear Company (ANC sous financement AEC). Avant cela, le LOCA était calculé avec les codes RELAP dont le développement est relaté par Mesina (2016). Le modèle utilisé dans les premières versions de RELAP supposait une relaxation totale entre les phases et diverses entrées empiriques étaient nécessaires pour capturer les effets polyphasiques tels que la trajectoires des bulles. En revanche, le projet SLOOP utilisait des formes modernes des équations des flux diphasiques (Solbrig & Hughes, 1971). C'était apparemment la première fois qu'un modèle d'écoulement polyphasique était implémenté dans un code.

Cependant, les écoulements polyphasiques apparaissent dans de nombreuses autres situations. En Norvège, la prédiction du transport des fluides par les pipelines a été d'un intérêt crucial avec l'exploitation pétrolière par le biais d'une plate-forme offshore lancée en 1971. Ceci a conduit à la construction d'un laboratoire polyphasique en 1984 à Trondheim par une collaboration entre Esso, Roagaland Research et Sintef. En parallèle, le développement d'un code multiphysique à l'Institut pour la technologie de l'énergie (IFE) a débuté en 1979

et a conduit au code OLGA.

D'où qu'ils viennent, les modélisateurs et les numériciens ont rapidement été confrontés aux problèmes sérieux soulevés par les premiers chercheurs. Ces questions ont donné lieu à des recherches approfondies et ne sont pas encore totalement résolues.

1.1.4 Quelques défis rencontrés par la communauté

L'ellipticité

L'un des problèmes les plus étudiés dans la modélisation des écoulements polyphasiques est le caractère bien posé des modèles obtenus par procédures de moyenne. Cette question a été relevée très tôt par [Gidaspow *et al.* \(1973\)](#) et a conduit à une énorme quantité de littérature depuis lors. La recherche suivante: « *two phase flow hyperbolic model* », renvoie environ 8000 réponses sur Google Scholar.

Depuis l'article fondateur de J.Hadamard (1902), le caractère bien posé d'un modèle est liée à trois concepts principaux qui sont l'existence, l'unicité et la stabilité. Ces questions ne concernent pas seulement les modèles polyphasiques mais tous les modèles physiques qui s'écrivent avec des équations aux dérivées partielles (EDP) et concernent donc presque toute la mécanique continue. Les trois points ci-dessus peuvent être reformulés comme suit :

- Existe-t-il une solution qui vérifie l'EDP du modèle ?
- Existe-t-il une seule solution de l'EDP ?
- Quel est l'impact d'un changement des conditions initiales sur la solution finale ?

La nature peut être considérée comme un dispositif de calcul qui suit les lois de la physique et donne toujours une solution unique pour des milieux continus et des conditions initiales données. Par conséquent, les modèles visant à reproduire ce calculateur devraient posséder cette propriété. En outre, même si le changement des conditions initiales peut avoir un impact énorme sur la solution finale (par exemple un système chaotique tel que la météorologie), les perturbations devraient être limitées après un temps fini.

Cependant, le modèle polyphasique trouvé par [Gidaspow *et al.* \(1973\)](#) ne vérifiait pas ces propriétés. Cette découverte a été inspirée par [Mecredy & Hamilton \(1972\)](#) qui, par une analyse de stabilité, montre une atténuation de la vitesse de l'onde aux hautes fréquences dans leur modèle. L'analyse des caractéristiques effectuée par [Gidaspow *et al.* \(1973\)](#) donne une formule analytique pour les valeurs propres en limite compressible qui comprend une partie complexe. Ce résultat a été la prémisse d'une longue série de recherches et de discussions sur la pertinence physique du modèle mal posé et les moyens d'y remédier. Cette question reste ouverte, comme le rapportent [Lhuillier *et al.* \(2013\)](#), [Dinh *et al.* \(2004\)](#) et [Vazquez-Gonzalez *et al.* \(2020\)](#).

Mais le caractère bien posé n'est pas le seul défi rencontré par les premiers chercheurs. D'autres questions, qui n'ont pas été autant examinées, doivent encore être abordées afin de

construire des modèles et des schémas qui prédisent une physique exacte avec suffisamment de robustesse.

La cohérence thermodynamique

Dans ses mémoires personnelles [Lyczkowski \(2017\)](#)[partie 7.5], Lyczkowski raconte les simulations d'explosion dans une canalisation par son groupe. L'objectif était de reproduire correctement par simulation numérique le profil de pression au bout du tube tel que fourni par les expériences. Il était donc nécessaire de capturer correctement l'onde de détente et le changement de phase s'ensuivant. Cependant, en comparant les résultats numériques de leur code aux données issues des expériences de [Edwards & O'Brien \(1970\)](#), ils ont constaté une grande différence sur la pression après le passage de l'onde. Le code prédisait que la pression tombait à zéro alors que l'expérience montrait un plateau. De plus, cette erreur disparaissait lorsqu'aucun changement de phase ne se produisait (en raison d'une chute de pression plus faible à la sortie du tube). Après une analyse minutieuse (détaillée par [Lyczkowski \(2017\)](#)), le terme de transfert de masse entre l'eau et la vapeur (dû à la chute de pression) s'est avéré thermodynamiquement incohérent. Une fois corrigés, les résultats expérimentaux ont été correctement récupérés. C'est un exemple de la manière dont la cohérence avec la thermodynamique est cruciale dans la conception de schémas numériques. Cependant, bien qu'il soit courant de contraindre les codes à suivre la première loi de la thermodynamique ([Burton, 1991](#)), le respect du second principe a reçu moins d'attention.

Pourtant, certains auteurs se sont enquis de sa vérification dans les modèles à l'intérieur des codes de production ([Arnold *et al.*, 1990](#)). De plus, comme le critère d'entropie permet de sélectionner la solution faible correcte pour les problèmes de Riemann, les schémas de Godunov ont été largement étudiés afin d'assurer une dissipation appropriée dans les chocs (comme la correction entropique: [Harten \(1983\)](#); [Leveque \(1990\)](#)). Cependant, ces corrections ont l'inconvénient de faire dissiper les schémas partout et capturent mal les écoulements isentropiques ([Shen *et al.*, 2010](#)). A la lumière des remarques précédentes, la notion de cohérence thermodynamique incarne :

- la préservation de l'énergie totale,
- la préservation du second principe où la dissipation se produit,
- suivre au plus près l'évolution isentropique lorsque la physique est non dissipative

Les deux premiers points doivent être strictement appliqués dans les schémas numériques ainsi que dans les modèles. Cependant, le troisième point doit être examiné plus attentivement. Si un modèle continu peut atteindre une isentropie stricte, un schéma numérique conçu pour le résoudre produira des erreurs de l'ordre du schéma. L'évolution isentropique étant unique, le chemin thermodynamique calculé s'en écartera à l'ordre du schéma. Pourtant, il est possible de concevoir des schémas isentropiques par des approches variationnelles.

Mais la symplecticité et les conservations de la quantité de mouvement et de l'énergie ne peuvent être préservées simultanément (Zhong & Marsden, 1988). Ainsi, les déviations de l'isentropie ne peuvent être évitées.

La raideur dans les écoulements polyphasiques

Dans les écoulements polyphasiques extrêmes tels que décrits plus haut, de nombreuses interactions couplent tous les matériaux. Ces couplages peuvent être de nature très différente : pressions diverses, vitesses, processus de relaxation thermique, forces de pression, turbulences, transferts de masse, etc. Tous doivent être conformes à la thermodynamique, comme expliqué ci-dessus. Cette exigence s'applique aux modèles et aux schémas. Mais les schémas numériques sont également mis au défi par la capture correcte de ces couplages en termes de stabilité et de robustesse en raison de leur raideurs potentielle. Ces raideurs peuvent notamment être due à des relaxations rapides entre phases et à de forts contrastes entre matériaux. Un exemple classique dans la première catégorie est la capture des forces de traînée entre deux phases se déplaçant initialement avec une vitesse relative importante.

Dans cette thèse, nous nous concentrons sur le principal couplage entre phases relevant de la deuxième catégorie : le couplage de pression. La raideur de ce couplage apparaît lorsque les matériaux présentent une compressibilité très contrastée. Dans ce cas, lorsque le mélange est comprimé, l'un des matériaux supportera toute la compression alors que l'autre ne subira quasiment aucune variation de volume. Lorsque des matériaux contrastés ne sont pas soumis à de fortes compressions ou dilatations, l'un des matériaux peut être considéré comme incompressible. Mais dans les cas extrêmes présentés ci-dessus, tous les matériaux peuvent être comprimés et, par conséquent, les couplages de pression raides entre eux doivent être calculés.

Les écoulements qui présentent de telles caractéristiques sont familiers à l'industrie nucléaire où la vapeur et l'eau coexistent sous haute pression. Si les schémas numériques peuvent être adaptés pour traiter la rigidité des termes de relaxation par des choix implicites ou explicites, le couplage par la pression est plus difficile à traiter pour deux raisons principales : il n'apparaît souvent pas explicitement dans les équations et il n'a pas un comportement monotone dû aux compressions ou expansions rencontrées par les écoulements. La raideur du couplage par la pression dans les écoulements polyphasiques a été étudiée dans les modèles du type Baer–Nunziato Baer & Nunziato (1986) (B.N.) (Kapila *et al.*, 2001; Saurel *et al.*, 2009).

Mais cette raideur devrait être présente dans tous les modèles polyphasiques compressibles. En effet, le contraste entre les phases qui conduit à des variations de volume inégales est un phénomène physique qui doit être capturé quelle que soit la méthode utilisée. Comme la raideur dans les modèles (B.N.) apparaît dans les processus de relaxation, les modèles en équilibre complet qui en sont dérivés sont à l'abri du problème de raideur (Hantke *et al.*, 2021): « ... les modèles réduits ont été dérivés en supposant des temps de relaxation nuls. ... Ainsi, l'instabilité inhérente au modèle de non-équilibre est évitée. ... » Cependant, de

nombreux modèles entièrement compressibles à une seule pression ne sont pas une limite d'un modèle de type B.N. (Vazquez-Gonzalez *et al.*, 2020; Munkejord *et al.*, 2009). Mais la raideur due au couplage de pression est bien présente et peut être écrite explicitement dans l'EDP. Un des objectifs de cette thèse est de proposer une solution pour capturer cette raideur par le couplage de la pression tout en gardant la cohérence thermodynamique. L'objectif final est d'améliorer la robustesse et la stabilité des schémas numériques polyphasiques.

1.2 Introduction in English

1.2.1 A short overview of the thesis

This thesis project was carried out at the Commissariat à l'Énergie Atomique (CEA), Direction des Applications Militaire (DAM). It is a continuation of the thesis of Vazquez-Gonzalez (2016) and is contemporary with Paulin (2021). The aim is to address two objectives in the development of multiphase models and schemes: being thermodynamically consistent and capturing the inherent multiphase stiffness to ensure stability. In previous works (Vazquez-Gonzalez *et al.*, 2020), a consistent numerical scheme (named GEEC for 'Geometric Energy and Entropy Compatible') was designed using variational and mimetic approaches. As a result, a quasi-isentropic behavior and exact conservations were obtained. However, this proximity to isentropy made the numerical scheme potentially vulnerable to numerical residuals. Moreover, as one of the objective was to capture isentropy, the internal energy discretization was developed with a mimetic approach without addressing stiffness issues. In this thesis, we propose a new discretization of the internal energy equations, formally applicable to any other multiphase scheme, which addresses the stiffness and the thermodynamic consistency issues in the pressure coupling.

The model discretized by Vazquez-Gonzalez *et al.* (2020), known as the 6-equation model, derives from an averaging approach stripped of all second-order correlations. Thus, all dissipation and higher order potentials hidden in the fluctuations are eliminated. Consequently, the model represents only ideal situations and is therefore seldom applicable to real multiphase flows without being complemented by fluctuation terms. Now, as it is the basis for all other models, it was crucial to ensure its correct discretization from the start. As follow up to Vazquez-Gonzalez *et al.* (2020), we now propose a method to introduce higher-order isentropic effects (surface tension, turbulence, etc.) while maintaining a model formalization that captures stiffness and thermodynamic consistency. To show the interest of the method, four way couplings are considered in dispersed particle-laden flows. Collisions are introduced through variational approaches and the ensuing equations are discretized by mimicking the GEEC scheme. Dissipative couplings with the carrier phase are embodied in drag forces. Numerical simulations of crossing jets validate the approach.

The last part of the thesis is an exploratory work that focuses on thermodynamic consistency issues in Lagrange-Euler (LE) modeling of dispersed particles-laden flows. A new description of particles is coupled to the least action principle, leading to the coupled dynam-

ics of dispersed and carrier phases. Discrete dynamics derived from the same procedure. This approach is extended to compressible particles. Numerical simulations lead to contrasted results, showing the possibilities of the method but also the need of many improvements.

1.2.2 The development of multiphase flows at CEA

Multiphase flows at CEA

In the scope of its missions, the CEA needs to predict various multiphase flows in academic and industrial contexts. First, the functioning and safety of the pressurized water reactors (PWR) involve several fluids flowing into the different circuits. The fluids are subject to cycles in which high variations of temperature and pressure occur as well as phase changes. Secondly, the CEA has extended his activities in 2010 to the renewable energy field. Multiphase flows are also encountered there in the hydrogen field for instance (fuel cell, high temperature steam electrolysis, etc. . .). Eventually, one of the tasks of the DAM is to design and guarantee the functioning and safety of French nuclear weapons. Since the signature of the Comprehensive Test Ban Treaty (CTBT) under Jacques Chirac's presidency in 1996, France has stopped nuclear tests. In this context, the simulation program has been launched in 1994 by Francois Mitterrand. Since then, the DAM has relied on numerical simulation to fulfill its missions. The aim of scientists and engineers at DAM is then to develop analytic models to capture physics of weapons and the numerical schemes to solve them. Because of the phenomenon complexity and the high precision required, huge computational resources are needed. To meet this demand, supercomputers are developed and installed by Atos (former Bull) at CEA DAM Bruyères-le-Châtel. Crafting and programming on these supercomputers is challenging for engineers because of their specific architectures. To validate the quality of the numerical simulations, comparisons with experiments of fusion done with the Laser MegaJoule (LMJ) and other standard ones are made.

Simulation of extreme multiphase flows

Because of its specific applications, the multiphase flows aimed to be simulated at DAM can be very extreme. The use of this qualifier refers to several features encountered by physicists and numericists.

- a First the size of the flows concerned is very large compared to the typical mesh size used in simulations. This specificity makes complete simulation extremely expensive in terms of computational resources. Even with the most powerful computers available, some multiphase methods are then still inaccessible. Furthermore, this point implies transport of materials over long distances which challenges the numerical schemes in term of diffusion. The large size of the domain is also critical because the flows present short scales impacting them. However, due to limited computing resources, standard equations are only captured above a given scale dictated by cost computation

constraints which is higher than these short scales. Thus a sub-scale modeling is necessary.

- b In addition, the amount of energy reservoirs inside the flows implies that models should respect fundamental conservations (momentum, mass and energy) because a leak of such quantities could lead to a critical gap between the real solution and the numerical one. This issue is naturally also present in the schemes. This is especially crucial to deal with the correct propagation of shocks, conditioned by the verification of the Rankine-Hugoniot relations. Also, this point leads to the obligation of respecting the second thermodynamics law in order to avoid nonphysical results and/or unstable computations.
- c The last critical point is the high number of materials (up to few dozens) and the contrasts in their equation of state (EOS). A multiplicity of phases involves a huge number of couplings, leading to complex models which makes it even harder to respect the conservations and thermodynamic consistency, especially because the large amount of energy implies that all the materials can be compressed. Contrasts between materials do not impact the models directly but constrain the numerical schemes used to solve them which in turn constrain the way models are written.
- d Capture of such flows is also highly difficult due to potential instabilities occurring between phases which lead to chaotic¹ nonlinear behavior. An example of such flows is the simulation of the Internal Confinement Fusion (ICF) where a small defect of the capsule leads to loss of spherical compression and thus diminishes the energy brought to the fusible material.

The simulation program is then confronted to many challenges to predict the extreme multiphase flows engineers and scientist encounter. They have thus developed specific models and schemes. Simulating and predicting multiphase flows were already a concern in many industrial places across the world before the CEA DAM launched its simulation program.

1.2.3 Some landmarks in the understanding and simulation of multiphase flows

Development of the first models

The development of multiphase models started few decades ago. To the author's knowledge, the first occurrence of multiphase modeling in literature was published by [van Deemter & van der Laan \(1961\)](#). However, the equations were written only in a formal way and turbulence was neglected in the averaging process but introduced rather intuitively in the stress tensor. Later, [Hinze \(1963\)](#) derived another model by considering the effect of particles on the continuous fluid phase. These models were built with averaging technique which is still the most common way to build multiphase models. These two references appear to

¹it is understood here that an initial small default has a huge impact after a finite time

be the first modern form of continuous multiphase models with a set of per fluid equations involving conservation of mass, momentum and energy. Many models inspired by their work were soon developed for particle-laden flows in pipes (Soo, 1969) or in fluidized beds (Anderson & Jackson, 1967). The question of closing undetermined correlations was already a major concern, notably the stress tensors of both phases. Very challenging as well, model instabilities were soon identified in early studies, as for instance by Murray (1965) who derived a dispersion relationship from his set of equations. Thus, many issues that are still intensely studied today were in the minds of the first investigators. Also, even if the procedure to obtain models has over the years been clarified and written more rigorously, the main idea which consists on averaging the local fluid equations and looking for closures of unknown forms was already developed. These models were academic by this time. However, engineers and scientists soon combined them with the new born computers in order to effectively simulate multiphase flows.

First multiphase flow industrial applications

Precursor industrial models and codes were developed simultaneously in several places of the world. It was especially driven by the need to ensure the safety of nuclear reactors. In particular, the loss of coolant accident (LOCA) was soon predicted with multiphase science. This accident arises when the cooling circuit no longer functions as a result of a pipe rupture. Typical test case consists in predicting rarefaction waves progressing along pipes after the rupture.

In France, the code CATHARE was devised in 1979 by the CEA, EDF, and Framatome and aimed also at simulating, among other cases, the (LOCA) in PWR. The model used is a complete multiphase model assuming no instantaneous relaxation of velocity or temperature (Rousseau, 1984). Using this kind of multiphase models was already known at CEA Grenoble (Bouré, 1973) where Ishii wrote is seminal textbook (Ishii, 1975).

In USA, according to Lyczkowski (2017), the history of multiphase flows begins in 1970 with the SLOOP project code (Serialized LOOP) at Aerojet Nuclear Company (ANC under AEC financing). Before that, LOCA was calculated with the RELAP codes whose development is told by Mesina (2016). The model used in the first RELAP version assumed total relaxation between phases and various empirical inputs were needed to capture multiphase effects such as raising bubbles. In contrasts, the SLOOP project used modern forms of the two phase flow equations (Solbrig & Hughes, 1971). This was apparently the first time a multiphase flows model was implemented in a code.

However, multiphase flows appear in numerous other situations. In Norway, prediction of fluid transport by pipelines has been of a crucial interest with petroleum exploitation through offshore platform launched in 1971. This has lead to the construction of a multiphase laboratory in 1984 at Trondheim by a collaboration between Esso, Roagaland Research and Sintef. In parallel, the development of multiphase code in Institute for Energy Technology (IFE) started in 1979 leads to the well known code OLGA.

Wherever they came from, modelers and numericists were soon confronted with serious issues raised by the early investigators. These issues have lead to extensive investigations and are yet to be fully settled.

1.2.4 Some challenges faced by the community

Ellipticity

One of the most studied issues in multiphase flow modeling is the well-posedness of models derived from averaging procedures. This issue was brought to attention very early in (Gidaspow *et al.*, 1973) and has lead to a huge amount of literature since then. The query “*two phase flow hyperbolic model*” returns about 8000 answers on Google Scholar. Since the seminal paper of Hadamard (1902), well-posedness is related to three main concepts which are existence, uniqueness and stability. These questions need to be addressed not only in multiphase models but in all models aiming to capture physics and written with partial differential equation (PDE) and thus concern nearly all continuum mechanics. The three points above can be reformulated as:

- Is there a solution that verifies the PDE of the model ?
- Is there only one solution of the PDE ?
- What is the impact of changes in initial conditions on the final solution ?

Reality can be viewed as a calculating device which follows the laws of physics and always gives a unique solution for continuous media and given initial conditions. Therefore, models aiming to approach this calculator should posses this property. Furthermore, even if changing the initial conditions may have a huge impact on the final solution (for instance chaotic system such as meteorology), disturbances are supposed to be bounded after a finite time. However, the multiphase model introduced by Gidaspow *et al.* (1973) was ill-posed. This discovery was inspired by Mecredy & Hamilton (1972) who produced a stability analysis which shows wave speed attenuation at high frequencies in their model. The characteristic analysis done in (Gidaspow *et al.*, 1973) shows analytical formula of the complex eigenvalues in the incompressible limit. This result was the premise to a long stream of competing investigations and endless (sometimes bitter) discussions about the physical relevance of model ill-posedness and the ways to “cure” it. This is still an open question as reported by Lhuillier *et al.* (2013), Dinh *et al.* (2004) or Vazquez-Gonzalez *et al.* (2020).

But well-posedness is not the only challenge encountered by early researchers. Other issues, which have not been so much examined, still need to be tackled in order to build models and schemes that predict accurate physics with enough robustness.

Thermodynamic consistency and stiffness

Thermodynamic consistency inside multiphase flows In his personal memoir (Lyczkowski, 2017) [part 7.5], Lyczkowski tells about the simulations of the pipe blow-down

by his group. The aim was to reproduce correctly by numerical simulation the pressure profile along the tube as provided by experiments. It was therefore necessary to capture correctly the expansion wave and the ensuing phase change. However, when they compared their numerical results to the experimental data by [Edwards & O'Brien \(1970\)](#), they found a huge pressure difference after the passage of the rarefaction wave. The code predicted that pressure fell to zero whereas the experiment showed a plateau. Furthermore, this error disappeared when no phase change occurred (due to a smaller pressure drop at the tube exit). After careful analysis (detailed by [Lyczkowski \(2017\)](#)), the mass transfer term between water and steam (due to the pressure drop) was found to be thermodynamically inconsistent. When corrected, the experimental results were properly recovered. This is an example of how consistency toward thermodynamics is crucial in the the design of numerical schemes. However, though it is a common practice to constraint codes to follow the first law of thermodynamics ([Burton, 1991](#)), following the second law has received somewhat less attention. Still, some authors were concerned about its verification in models inside production codes ([Arnold *et al.*, 1990](#)). Also, because the entropy criteria allows to select the correct weak solution for Riemann problems, Godunov schemes have been extensively studied in order to ensure proper dissipation in shocks (entropy fix, [Harten \(1983\)](#); [Leveque \(1990\)](#)). However, these fixes have the disadvantage that schemes dissipate everywhere and poorly capture isentropic flows ([Shen *et al.*, 2010](#)). In the light of the previous remarks, the notion of thermodynamic consistency embodies:

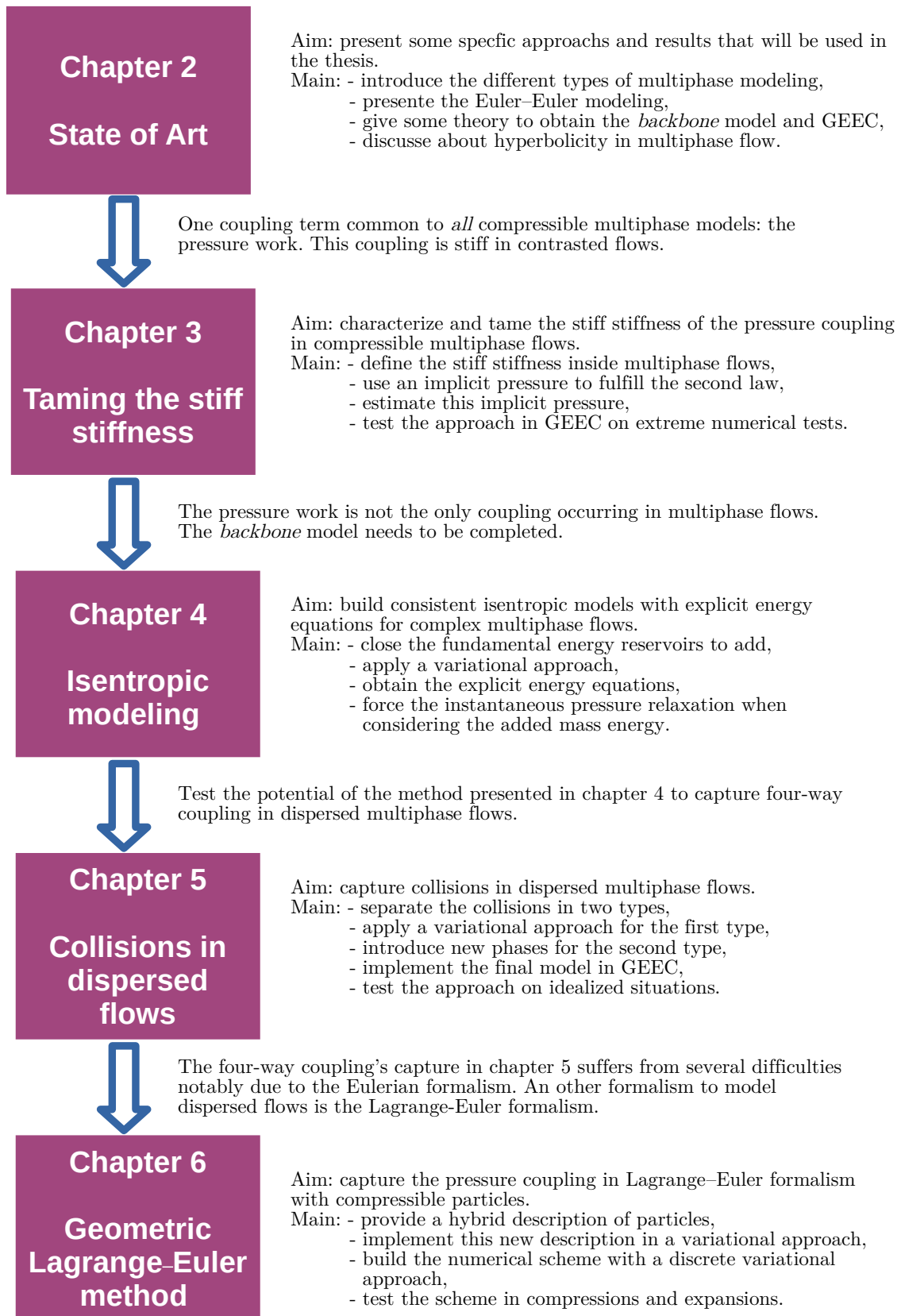
- preservation of the total energy,
- preservation of the second principle where dissipation occurs,
- following as closely as possible the isentropic evolution when the physics is non-dissipative.

The first two points should be strictly applied in numerical schemes as well as in the models. However, the third point needs to be more carefully examined. If a continuous model can achieve strict isentropy, a numerical scheme designed to solve it will produce errors at the order of the scheme. Since the isentropic evolution is unique (for a given set of energies), this will cause the calculated thermodynamic path to deviate from it even though the scheme is expected to deviate as little as possible. Yet it is possible to design isentropic schemes by variational approaches (2.3.1). But symplecticity and the conservation of momentum and energy cannot be preserved at the same time ([Zhong & Marsden, 1988](#)). Thus, deviations from isentropy cannot be avoided.

Stiffness inside multiphase flows In extreme multiphase flows as described above, many interactions couple all the materials. These couplings can be of very different nature: various pressures, velocities, temperature relaxation processes, pressure forces, turbulence, mass transfers, etc... All of them must comply with thermodynamics as explained above. This

requirement applies to models and schemes. But the numerical schemes are also challenged by the correct capture of these couplings in terms of stability and robustness due to their potential stiffness. This stiffness can be notably due to fast relaxations between phases and strong contrasts between materials. A classic example in the first category is the capture of the drag forces between two phases moving initially with a large drift. In this thesis, we focus on the major coupling between phase falling into the second category: the pressure coupling. The stiffness of this coupling occurs when the materials present highly contrasted compressibility. In that case, when the mixture is compressed, one of the materials will bear all the compression whereas the other will experiment nearly no volume variation. Yet, when contrasted materials are not subjected to high compression or expansion, one of the materials can be assumed to be non compressible. But in the extreme cases presented above, all the materials can be compressed and therefore the stiff pressure couplings between them must be computed. Flows which present such feature are familiar to the nuclear industry where steam and water coexists under high pressure. If the numerical schemes can be adapted to tackle the stiffness on the relaxation terms by implicit or explicit choices, the coupling through pressure is harder to cure for two main reasons: it often does not appear explicitly in the equations, and it involves no monotonic behavior due to compression or expansion encountered by the flows.

Pressure stiffness in multiphase has been studied in the very popular [Baer & Nunziato \(1986\)](#) (B.N.) type models ([Kapila *et al.* \(2001\)](#)), ([Saurel *et al.* \(2009\)](#)). But it should be present in all compressible multiphase models. Indeed, the contrast between phases which leads to unequal volume variations is a physical phenomenon that must be captured whatever the method used. Because stiffness in the B.N. models appears in relaxation processes, fully equilibrium model derived from them are safe from stiffness issue ([Hantke *et al.* \(2021\)](#)): *...reduced models have been derived assuming zero relaxation times ... Thus, the stiffness inherent in the non-equilibrium model is avoided...* However, many fully compressible one-pressure models are not a limit of a B.N. type model ([Vazquez-Gonzalez *et al.* \(2020\)](#), [Munkejord *et al.* \(2009\)](#)). But stiffness due to pressure coupling is well present and can be written explicitly in the PDE. One of the goals of this thesis is to propose a solution to capture stiffness due to the pressure coupling while keeping the thermodynamic consistency. The final aim is to improve the robustness and stability of numerical schemes for multiphase flows.



CHAPTER 2

Selected state of art

Contents

2.1	The modeling of multiphase flows	28
2.1.1	General description and classification of flows	28
2.1.2	Review of the models	29
2.2	Details on Euler–Euler approach	35
2.2.1	On averaging	35
2.2.2	History of the models	37
2.2.3	Closing the fluctuation forms	41
2.3	Current approach to find and discretize the <i>backbone</i> model	43
2.3.1	Variational approaches	43
2.3.2	The derivation of the backbone model	51
2.3.3	The numerical scheme	57
2.4	On the hyperbolicity in two-phase flow models	59
2.4.1	The link between stability and hyperbolicity	59
2.4.2	Ellipticity and characteristic analysis of the two phase flow model	61
2.4.3	What are the vision toward the ellipticity of this model ? . .	63
2.4.4	Cutoff wavelength by Ramshaw (1978)	64
2.4.5	On the Baer & Nunziato (1986) model	65
2.A	Appendix: computation of the new pressure gradient (2.3.3)	69

2.1 The modeling of multiphase flows

2.1.1 General description and classification of flows

This thesis is part of the DAM’s approach to build models predicting the behavior of multiphase flows and to develop numerical methods to solve them.. Multiphase flows are flows mixing several phases. A common definition of a phase is a region of space in which the thermodynamic behavior does not vary (same equation of state, same law for heat flux...).

These regions of space are separated by interfaces in which many physical phenomena occur whose capture challenges the model. They can form a countable number of structures (stratified flows in pipe) or multiple disconnected structures (sand grains in water). These two cases define two broad categories of multiphase flows, namely separated flows and dispersed flows. However, these categories are not absolute and depend on the scale at which the flows are observed. A flow with billions of grains of sand in water is considered a dispersed flow (with sand as the dispersed phase and water as the carrier phase), however when zoomed in on a specific grain of sand, the flow can be considered a separated flow with one region corresponding to sand and another to water. Another possible criterion for constructing a classification is then to compare the average size of the interfaces with the typical length of the flow. Of course, within the same flow, the two types of categories can coexist (sand grains through a laminar water flow covering half the pipe).

Also, some classifications consider the state of matter of the phases involved: liquid/solid, solid/gas, etc. . . The multiplicity of possible combinations makes these classifications very complex. Moreover, they consist more in comparing the physical properties of the phases than in questioning their state. Another way of classifying flows in this spirit could be an evaluation of the relationship between the density of the phases, their compressibility, their resistance to deformation, etc. . .

Engineers and scientist use specific models adapted to capture physics inside the multiphase flows depending on their place in classifications. Indeed, several classes of models exist, designed for specific types of flows. In this thesis, two broad classes of models are explored. The first class is able to deal with all type of multiphase flows (but with many pieces of information lost) and the second one is specifically addressed to dispersed multiphase flows.

In industrial applications, pure single-phase flows rarely exist. However, it may not be necessary to consider all phases present if one phase dominates or if they can be merged into one phase with suitable physical properties. However, in many applications, these approximations are not valid and therefore cannot be applied to predict flow behavior with sufficient accuracy. In this case, multiphase flow modeling must be used. Such applications are present in various academic and industrial fields and are crucial to model for the operation of machines or the understanding of nature. Notable examples are the cavity phenomenon in pumps where bursting bubbles can damage engines, the atomization phenomenon of sprayed fuel in combustion chambers which is crucial for engine efficiency, etc. . .

2.1.2 Review of the models

Interface models

Models that reconstruct the interface constitute the direct numerical simulation (DNS) of multiphase flow simulation. They describe the flow down to the interfacial scale. However, if these methods are applicable for flows where the size of the structures is comparable to the characteristic length of the flow, their calculation cost is too high when the size of

the structures is close to the mesoscopic scale. Therefore, they may be used for separated flows but their computational cost is prohibitive for dispersed flows. This is unfortunate because for dispersed flows commonly encountered in industry, such as bubble flows, these methods would have been very accurate. Indeed, surface tension effects are very important (the interfacial area density is higher for small bubbles than for large ones at the same volume fraction). In general, these methods are often used to calculate test cases where only a few structures are initially present in the flow even though they are likely to be strongly deformed: shock bubble interaction (Terashima & Tryggvason, 2009), Rayleigh Taylor instabilities (Glimm *et al.*, 1998, 2001), Richtmyer–Meshkov (Holmes *et al.*, 1995).

Interface tracking Interface tracking has two essential elements, markers to reconstruct the interface and a method to calculate the flow within the structures. The dynamics of the markers are calculated with the propagation front scheme. It conventionally consists of a splitting between the normal direction of the interface and the tangential direction of the interface. There are many variants of this scheme that depend on the approximation of the equations of motion, from simple interpolation of the flow velocity at the marker (Tryggvason, 2012) to more complex algorithms (slope reconstruction, Riemann problem and characteristic methods (Glimm *et al.*, 2001)). Several difficulties exist to follow the front: the management of the interface on itself, the collision and the disappearance of the front (Chern *et al.*, 1986). Far from the interfaces, the domain (called interior) is treated as in the mono-fluid case by taking into account the boundary conditions corresponding to the global edge of the domain or the interfaces.

Interface capturing Interface capture methods reconstruct the interface without assigning it additional ‘numerical’ degrees of freedom (the interface tracking markers). It is therefore necessary to find its position with *fluid* quantities computed by the numerical scheme. Usually, a new variable is introduced to the PDE system whose values will be computed at any point in space (such as pressure or density) and will model the distance to the interface. It is then necessary (as in the case of interface monitoring), to process the discontinuity of the variables and to verify the Rankine Hugoniot relations. Two methods are particularly used, the VOF method and the Level-Set method.

VOF The VOF method was developed by Noh & Woodward (1976) and then introduced by Hirt & Nichols (1981). It consists in transporting a field ‘similar’ to the volume fraction which is 1 when the cell is filled with the fluid and 0 otherwise. An intermediate value of this field in a cell indicates the presence of the interface. The interface must be then reconstructed inside the cell. There are several methods to perform the reconstruction such as the SLIC (simple line interface calculation) method developed by Noh & Woodward (1976) where the interfaces are aligned with the mesh or the PLIC (piecewise linear interface calculation) method developed by Gueyffier *et al.* (1999). In this method, the knowledge of

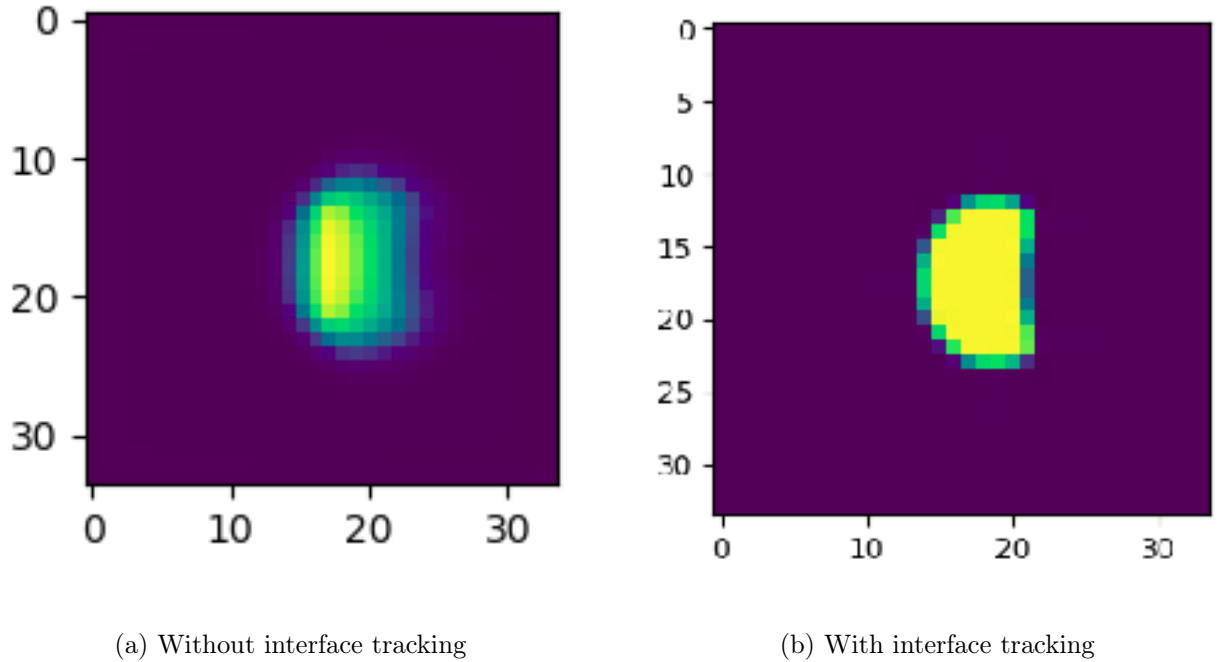


Figure 2.1: Transport of droplet from the free access code of Prof. Tryggvason <https://www3.nd.edu/~gtryggva/MultiphaseDNS/DNS-Solver.pdf>

the VOF at any point of the mesh allows to deduce the normal to the interface by calculating the gradient of the VOF. The interface is then reconstructed in the mesh from the knowledge of the normal and the fact that it must separate the cell into two parts so that their volume respects the value of the VOF. However, this can lead to discontinuous interfaces. It then remains to propagate it and to deduce the new value of the VOF function.

Level set The level set is a method to reconstruct interface that has been introduced by Osher & Sethian (1988) and applied to multiphase flows by Sussman *et al.* (1994). This method is similar to the VOF method in that it uses a new field whose values are calculated in each cell. Its main advantage is that the interface is located more precisely because the value of the level set function is smooth. The interface will be located by looking at the 0 iso value of the level set function. The transport of the level set function is the same as for a scalar field. Thus, it is simpler than the VOF transport, however, it cannot ensure strict mass conservation. This problem is the main drawback of the Level Set method compared to the VOF method and many attempts have been made to correct it van der Pijl *et al.* (2005).

Kinetic approaches

The kinetic approaches represent the dispersed phase stochastically. They consider that the phase is made of an ensemble of particles which possess some parameters. Instead of computing the values of the parameters for each particle, they evaluate the probability of

particles to be in some range of parameters. Its mathematical representation is the probability density function (PDF). Rigorously, for a system of N particles with p parameters, the PDF must be a function of all parameters and variables

$$f_{\text{PDF}} = f(t, x_1^1, \dots, x_p^1, \dots, x_1^N, \dots, x_p^N). \quad (2.1)$$

However, this function may be transformed by integration to the number density function (NDF) which represents the probability that a certain number of particles be within some range of parameters.

$$f = f(t, x_1, \dots, x_p) \quad (2.2)$$

The space of parameters (x_1, \dots, x_p) is made of characteristic variables of a given particle, as an example, the position x , the velocity v , the temperature, etc . . .

The kinetic approaches aim to obtain the (NDF) or at least some relevant information about it such as the moments. The description of its evolution is generally made by a Williams–Boltzmann type equation [Williams \(1958\)](#). With this definition of f , the number of particles at time t in volume $[(x_i, x_f), (v_i, v_f)]$ is

$$N = \int_{v_i}^{v_f} \int_{x_i}^{x_f} f(t, x', v') dx' dv' \quad (2.3)$$

and the density of particles is

$$n(t, x) = \int f(t, x, v) dv. \quad (2.4)$$

In dispersed flows, the space of parameters is generally larger and contains the position x , the velocity v , the temperature θ and a geometric parameter of the particle s . The iso-number part of the Williams–Boltzmann equation is a consequence of the Liouville theorem

$$\partial_t f + \nabla_x \cdot (vf) + \nabla_v \cdot (Ff) + \partial_s(Kf) + \partial_\theta(Rf) = 0, \quad (2.5)$$

F , K , R , standing for the external forces, the mass transfers and the heat exchanges with the carrier phase. The form $\nabla_x \cdot (vf)$ stand for the transport of the particles. This equation can be completed with source terms describing fragmentation or coalescence of the particles, thus changing the total number of particles.

Eulerian approaches The Eulerian approaches associated to kinetic models (not to be confused with the Euler–Euler approaches detailed in (2.2)) aim to compute the moments of the (NDF). The computation presented here is done by considering the simplest possible parametrization of the (NDF) (position, velocity and time) and is there to explain the fundamental mechanisms. The parametrization chosen determines the equation of the (NDF).

$$\partial_t f + (v_i f)_{,x_i} + (F_i f)_{,v_i} = Q \quad (2.6)$$

Q being a collisional operator. The evolution of the moments is computed by integrating (2.6) after multiplication by the associated function.

$$n = \int f dv \quad \Rightarrow \quad \partial_t(n) + (u_i f)_{,x_i} = \int Q dv \quad (2.7a)$$

$$nu_i = \int v_i f dv \quad \Rightarrow \quad \partial_t(nu_i) + \int v_i (v_j f)_{,x_j} dv - F_i = \int v_i Q dv \quad (2.7b)$$

$$ne = \frac{1}{2} \int v_j^2 f dv \quad \Rightarrow \quad \partial_t(ne) + \frac{1}{2} \int v_j^2 (v_i f)_{,x_i} dv - \frac{1}{2} F_i u_i = \int v_j v_j Q dv \quad (2.7c)$$

The last terms in the left hand side (LHS) of the equations have been computed by integration by parts and using the fact that the distribution vanishes for infinite velocity. However, the integration of a form of order p inside the spatial gradient leads to a form of order $p + 1$. Therefore, the evolution equation of an order p moment involves a moment of order $p + 1$. Thus, it is not possible to use this method without closing the higher moment which appears in the last evolution equation (here stopped at order 2 to make the link with hydrodynamic equations). The forms within the spatial gradient illustrate this.

$$\int v_i v_j f dv = \underbrace{\int (v_i - u_i)(v_j - u_j) f dv}_{P_{ij}} + u_i u_j n \quad (2.8a)$$

$$\int v_j^2 v_i f dv = 2u_i ne + \underbrace{\int (v_j - u_j)^2 (v_i - u_i) dv}_q + 2u_j \underbrace{\int (v_j - u_j)(v_i - u_i) dv}_{P_{ij}} \quad (2.8b)$$

The evolution of the moment nu involves the pressure tensor P_{ij} which is of order 2 and the evolution of total energy involves the heat flux q , a moment of order 3. The final equations are then

$$\partial_t(n) + (nu_i)_{,x_i} = \int Q dv \quad (2.9a)$$

$$\partial_t(nu_i) + (nu_j u_i + P_{ij})_{,x_j} = F_i + \int v_i Q dv \quad (2.9b)$$

$$\partial_t(ne) + (nu_i e + q)_{,x_i} + (u_j P_{ij})_{,x_i} = F_i u_i + \int v_j^2 Q dv \quad (2.9c)$$

The system of equation obtained is very similar to Euler's. It must be stressed that pressure form appears as a pure momentum flux and does not involve collisions between particles. As for the heat flux, it is a flux representing the asymmetry of the (NDF). To close this unknown form, several solutions are possible:

- postulate the form of the distribution,
- using analytical function to relate the moment of order $p+1$ to the lower order moment.

There is no discussion here about the collisional operator in which all the dissipative physics occurs (see theorem H). However, basic properties of this operator are conservations of mass, momentum and kinetic energy which occurs effectively during collisions)

- $\int Qdv = 0$ in order to conserve the number of particles,
- For a Maxwellian (NDF), $\int v_i Qdv = \int v_j^2 Qdv = 0$. There is then thermodynamic equilibrium, no dissipation in the equations and the Euler equations are obtained.

In the development made, the (NDF) is only parametrized by the position and the velocity. However, more parameters are needed to represent the dispersed phase, especially the size of particles which is crucial in industrial applications like combustion. However, increasing the phase space also increases the computational effort. In the field of spray for combustion, two variables are generally added which leads to 9 parameters for the (NDF) in 3D. To reduce the computational effort, sectional methods were developed (Tambour, 1980; Greenberg *et al.*, 1993) where moments by integration over velocity and temperature are computed whereas size is discretized in different sections. Clarification about the necessary assumptions of the methods and the full derivation is made in Laurent & Massot (2001). The system obtained after the integration is called the semi-kinetic system and a distribution function of the form $f(t, x, v, \theta, s) = \tilde{n}(t, x, s)f_\theta(t, x, s, \theta)f_v(t, x, s, v)$ is postulated. The functions f_θ and f_v sum to unity by integration on θ resp v . Once the semi-kinetic system is obtained the particle density (conditioned by the size) function is also postulated as $\tilde{n}(t, x, s) = n(t, x)f_s(t, x, s)$ and non dispersion in temperature and velocity by section ($f_\theta(t, x, s, \theta) = \delta(\theta - \bar{f}_\theta(t, x, s))$ and $f_v(t, x, s, v) = \delta(v - \bar{f}_v(t, x, s))$). Then, various assumptions on $f_s(t, x, s)$ lead to different models, the most simple being to assume that there is only one size per section which leads to a bi-fluid model.

Lagrangian approaches In the Lagrangian–Eulerian (LE) approaches, the carrier phase is modeled with the Eulerian description and the Lagrangian phase is described with a point stochastic process, i.e. the particles are within Lagrangian frame whereas the carrier phase is represented in the Eulerian frame. Another denomination is the *trajectory model* Brennen (2005) opposed to the *two-fluid flow model*. These approaches are designed to predict particle-laden flows. In such flows, level of interactions between phases depend on several parameters, notably the volume fraction and the mass loading of the dispersed phase Balachandar (2010). When the carrier phase influences the dispersed phase, the coupling is called one-way coupling, when particles also influences the carrier phase it is called two-way coupling and four way-coupling when particles also interact with each other Elghobashi (1991). This description of the dispersed phase is an approximation of the (NDF) by dirac functions. The various levels of description of the dispersed and carrier phases lead to several categories of models used. A review of the categories is done in Subramaniam (2013). For the discrete phase, there are roughly two levels of descriptions:

- The trajectory of all the particles is computed. The numerical entities represent then physical particles.
- The trajectory of packets of particles are computed. The numerical entities represent then stochastic particles embodying many physical particles.

Equations ruling the particles' evolution are obtained by introducing the (NDF) approximation in the Williams' equation.

$$\frac{dX_i}{dt} = V_i, \quad \frac{dS_i}{dt} = \theta_i, \quad \frac{dV_i}{dt} = A_i(X_i, S_i, t, \{U(x, t)\}) \quad (2.10)$$

with X_i, V_i, A_i the position, velocity and acceleration of the particle i , $\{U(x, t)\}$ values of the carrier phase fields and S_i some other additional particle parameters, as an example a geometric parameter if the particle loss or gain volume (evaporation for a droplet). The acceleration is often modeled by a drag force between particles and carrier phase. However, several other forces may occur, notably unsteady effects such as added mass and Basset force or electrodynamic forces (in hybrid code aiming to simulate plasma for instance). Modeling forces acting on particles is complex because it involves the local perturbations of surrounding flow around them. The scales of the perturbations are generally lower than the grid size and thus they must be captured by subscale modeling.

Diffuse interface model

Diffuse interface models do not consider that phases are separated by interfaces (although they may include interfacial effects) but consider that all phases occupy the whole domain with a certain probability of presence. This approach loses information about the physical discontinuities that exist at the interface between two different phases. However, these methods can be applied to various types of flows and are less computationally expensive than the interface methods. Each phase has its own fields (velocity, density, etc.) which obey to evolutionary equations similar to the Navier–Stokes system. The domain of definition of the fields is the entire domain of the calculation. This is why the phases are said to coexist in the same point of time and space. However, a more precise view is to say that the fields take on the values of a given phase if it would have been present at that point. The principle of these methods is to average the single-fluid equations weighted by the function of the probability of presence of a given phase, and then to close the residuals resulting from this calculation. These closures involve interpretation of the physical meaning of these residuals according to the nature of the flow being modeled and the type of averaging used.

2.2 Details on Euler–Euler approach

2.2.1 On averaging

The computation of the average of equations is an old technique which flourished in fluid mechanics with the study of turbulence. [von Kármán \(1948\)](#) attributes the paternity of

statistical methods to Reynolds (1895). However, time averaging appears earlier in the work of Boussinesq (1877). Nevertheless, Reynolds was first to decompose the movement into an average part and a fluctuating part ¹. A review of the historical development of statistical methods for turbulence is given by Chassaing (2019). The justification for the use of averaged equations is the desire to obtain a deterministic system of equations (thus providing mathematical tools) to model a turbulent phenomenon. The classical averaging operators used in fluid mechanics are the temporal, spatial and ensemble averaging operators.

$$\bar{a}^t(x, t) = \frac{1}{|H|} \int H(t, t') a(t', x) dt' \quad (2.11)$$

$$\bar{a}^x(x, t) = \frac{1}{|G|} \int G(x, x') a(t, x') dx' \quad (2.12)$$

$$\bar{a}^e(t, x) = \frac{1}{N} \sum_i a_i(t, x) \quad (2.13)$$

with $a_i(t, x)$ the value of the quantity a in (x, t) at the i th experiment.

Mass Reynolds averaging is defined with any of these operators as

$$\tilde{a} = \frac{\overline{\rho a}}{\bar{\rho}} \quad a'' = a - \tilde{a} \quad (2.14)$$

with a any fluid quantity of interest. Using this kind of averaging simplifies the averaged equations but lead to a different interpretation of the deviation between averaged quantities and real ones. As an example, the value of \tilde{u} is not anymore the averaged motion of particles in a given domain or period of time but the velocity that correspond to the averaged momentum quantity.

In order to simplify the computation, it may be assumed that operators follow the Richardson & Lynch (1922) rules:

$$\bar{\bar{a}} = \bar{a}, \quad \overline{\bar{a}b'} = 0, \quad \overline{\bar{a} \cdot \bar{b} \cdot \bar{c}} = \bar{a} \cdot \bar{b} \cdot \bar{c}, \quad \overline{\partial_x a} = \partial_x \bar{a}. \quad (2.15)$$

However, these rules are strictly verified only with ensemble averaging but may be acceptable approximations for the other operators. In multiphase flows, averaging methods are used not only to provide deterministic equations of a turbulent system but also to simplify the complexity of the system due to the presence of several phases and their interfaces. The averaging used involves the density and the fluid presence function b^φ noted here b^φ . The averaged fluid presence function gives its probability of presence which is called here (possibly misleadingly) volume fraction and noted α^φ . It should be stressed that the profile of the volume fraction can only give an a priori idea of the shape of the flow. Some misleading comments resulting from an over-interpretation of this field are given here to illustrate this point.

¹even if one of the Reynolds' average, the mass average, is better known under the name of Favre average Favre (1958) in France

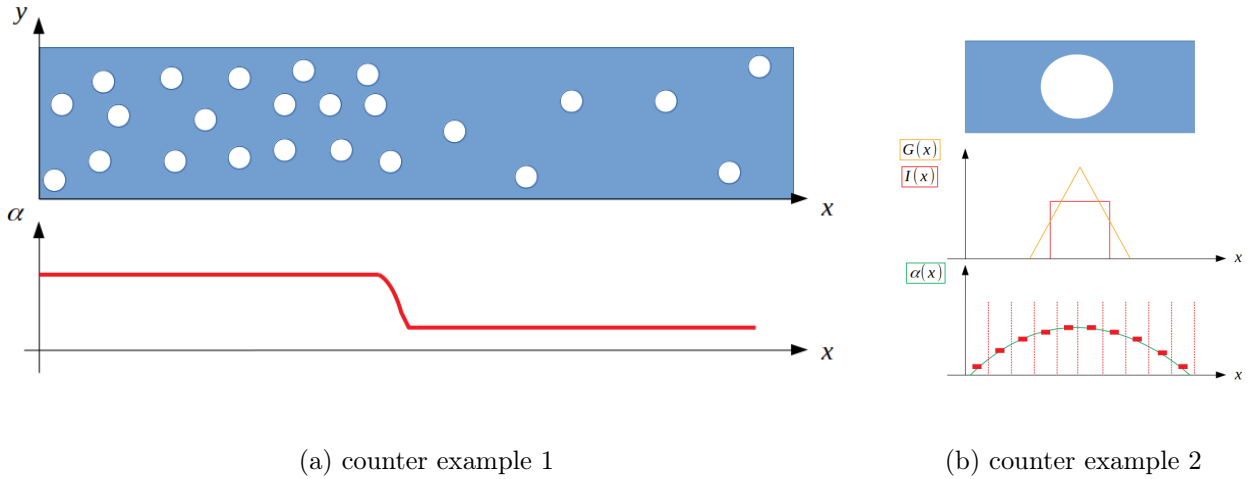


Figure 2.2: Counter examples to some misleading comments

- A sudden change of volume fraction always signals an interface.
- Volume averaging can be used only if the particles are smaller than the size of the averaging width.

The first comment is wrong, a brutal change of volume fraction does not necessarily signals an interface. In the bubbly flow represented in 2.2a, the drawing of the volume fraction profile issued from the space averaging shows that the change of volume fraction corresponds to the disappearance of the bubbles but not to an interface between bubbles and water. Of course, this still represents a variation of interface related quantities like the interface density.

The second comment is wrong as illustrated in 2.2b. The bubble's presence is denoted by I , the kernel by G . The averaging of the presence function is

$$\alpha(x) = \frac{\int I(x')G(x-x')dx'}{\int G(x-x')dx'} \quad (2.16)$$

The volume fraction may be discretized by cells smaller than the bubble's width.

Hence the volume fraction is a very general field which gives only one information: the probability to find a given phase at given point and time. But the volume fraction says nothing about the topology of the flow (dispersed flow, separated flow, etc...). However, if the modeler knows the type of averaging used and the type of flow modeled, more information can be extracted from the volume fraction (the size of the inclusions, the presence of an interface, etc...).

2.2.2 History of the models

The evolution equations of compressible multiphase flows were first found by a conditional averaging of the Euler equations. The conditional averaging or conditional expectation is

made thanks to the introduction of the function of presence (or indicative function) b^φ of the fluid φ . This function takes the values of 1 when the fluid φ is present at (t, x) and 0 else. The conditional averaging can be a time, space or ensemble averaging. Historically, the first developments of this method used space averaging (van Deemter & van der Laan, 1961; Hinze, 1963). They were soon popularized notably by Ishii (1975) and Drew (1983). The first industrial multiphase flow codes, originally designed to insure the safety of nuclear reactor (for instance (Bouré, 1973)), solved models issued from averaging.

Ishii's approach: (Ishii (1975))

In this paragraph, the method used by the precursors of the averaging methods is presented. For the sake of simplicity, the internal energy equation is not averaged here and the stress tensor is reduced to the pressure. The equations that there are going to be averaged are the local continuity equation and the local momentum equation .

$$\partial_t \rho + \underline{\nabla} \cdot (\rho \underline{u}) = 0, \quad (2.17)$$

$$\partial_t (\rho \underline{u}) + \underline{\nabla} \cdot (\rho \underline{u} \otimes \underline{u}) + \underline{\nabla} P = 0. \quad (2.18)$$

These equations are valid at any point of the flow. The presence function of the fluid is transported with the local velocity

$$\partial_t b^\varphi + \underline{u} \cdot \underline{\nabla} b^\varphi = 0. \quad (2.19)$$

The equation (2.19) shows the need to model the spatial derivative of this indicator function. As this function is discontinuous, this derivative will be defined in the sense of the distributions

$$\forall \phi, \int_V \underline{\nabla} (b^\varphi) \phi dv = - \int_{S(V)} \phi \underline{ds}. \quad (2.20)$$

The last element to define is the interface velocity \underline{u}_I . Because the indicator function varies only at the interface, its transport is restated as

$$\partial_t b^\varphi + \underline{u}_I \cdot \underline{\nabla} b^\varphi = 0. \quad (2.21)$$

The next step is the averaging of the two local equations weighted by the indicator function.

$$\int_V b^\varphi \partial_t (\rho) dv + \int_V b^\varphi \underline{\nabla} \cdot (\underline{u} \rho) dv = 0, \quad (2.22)$$

$$\int_V b^\varphi \partial_t (\rho \underline{u}) dv + \int_V b^\varphi \underline{\nabla} \cdot (\underline{u} \otimes \underline{u} \rho) dv + \int_V b^\varphi \underline{\nabla} P dv = 0. \quad (2.23)$$

The averaging operator $\int_V dv$ commutes with the partial derivatives. Therefore, the equations can be developed into

$$\partial_t \overline{b^\varphi \rho} + \underline{\nabla} \cdot \overline{b^\varphi \underline{u} \rho} - \underbrace{\int_V \rho \partial_t (b^\varphi) dv - \int_V \underline{u} \rho \cdot \underline{\nabla} b^\varphi dv}_{\int_{S(V)} \rho (\underline{u} - \underline{u}i) \cdot \underline{ds}} = 0, \quad (2.24)$$

$$\partial_t \overline{b^\varphi \rho \underline{u}} + \underline{\nabla} \cdot \overline{b^\varphi \underline{u} \otimes \underline{u} \rho} - \underbrace{\int_V \rho \underline{u} \partial_t (b^\varphi) dv - \int_V \underline{u} \otimes \underline{u} \rho \cdot \underline{\nabla} b^\varphi dv}_{\int_{S(V)} \rho \underline{u} \otimes (\underline{u} - \underline{u}i) \cdot \underline{ds}} = - \underline{\nabla} \cdot (\overline{b^\varphi P}) - \int_{S(V)} P \underline{ds}. \quad (2.25)$$

After some manipulations, the final forms are obtained.

$$\partial_t([\alpha \rho]^\varphi) + \underline{\nabla} \cdot ([\alpha \rho]^\varphi \underline{u}^\varphi) = m^\varphi, \quad (2.26)$$

$$\partial_t([\alpha \rho]^\varphi \underline{u}^\varphi) + \underline{\nabla} \cdot ([\alpha \rho]^\varphi \underline{u}^\varphi \otimes \underline{u}^\varphi) + \underline{\nabla}(\alpha^\varphi p^\varphi) = \underline{m} \underline{u}^\varphi - \underline{\nabla} \cdot (\overline{b^\varphi \rho \underline{u}' \otimes \underline{u}'}), \quad (2.27)$$

with the following source terms

$$m^\varphi = \int_{S(V)} \rho (\underline{u} - \underline{u}i) \cdot \underline{ds}, \quad \underline{m} \underline{u}^\varphi = \int_{S(V)} \rho \underline{u} \otimes (\underline{u} - \underline{u}i) \cdot \underline{ds} - \int_{S(V)} P \underline{dS}. \quad (2.28)$$

The signification of the source terms is straightforward because they are written in explicit form. They embody mass and momentum transfers through the interface and pressure integration over the interface. However, all of them need to be closed to obtain a system of equation that can be solved.

Current approach in the thesis

In the previous part, the averaging operator was explicitly written and thus specific form of the residuals was obtained. However, the averaging computation can be done without specifying the operator as long as properties such as the Richardson's rules (2.15) are specified. The complete averaging of the non dissipative local equations with the stress tensor reduced to pressure is presented here. The development is roughly the same: averaging of the local equations after multiplying them some function. In the last paragraph, this function was the indicator function. Here, c^φ , the mass fraction of the fluid φ is used instead of the indicator function. This function represents the ratio between the mass of the fluid and the total mass inside a volume whose characteristic size is the hydrodynamic scale. Because, the interface is also spread under the hydrodynamic length, the mass fraction is a good indicator to mark the presence of the interface. In previous developments, the evolution of the indicative function was not trivial because it involved to close the interface's velocity. However, the mass conservation of each fluid coupled to the local mass conservation imposes the evolution of the mass fraction. The procedure is applied to the two local equations (mass, momentum and internal energy)

$$\overline{c^\varphi \partial_t(\rho)} + \overline{c^\varphi (\rho u_i)_{,i}} = 0, \quad (2.29a)$$

$$\overline{c^\varphi \partial_t(\rho u_i)} + \overline{c^\varphi(\rho u_i u_j)_{,j}} + \overline{c^\varphi P_{,i}} = 0, \quad (2.29b)$$

$$\overline{c^\varphi \partial_t(\rho e)} + \overline{c^\varphi(\rho e u_i)_{,i}} + \overline{c^\varphi P u_{i,i}} = 0. \quad (2.29c)$$

After some manipulations, the very general equations are obtained

$$\partial_t(\overline{c^\varphi \rho}) + \overline{(c^\varphi \rho u_i)_{,i}} = \overline{\rho[\partial_t(c^\varphi) + u_i c_{,i}^\varphi]}, \quad (2.30a)$$

$$\partial_t(\overline{c^\varphi u_i \rho}) + \overline{(c^\varphi \rho u_j u_i)_{,j}} + \overline{c^\varphi P_{,i}} = \overline{\rho u_i[\partial_t(c^\varphi) + u_j c_{,j}^\varphi]}, \quad (2.30b)$$

$$\partial_t(\overline{c^\varphi \rho e}) + \overline{(c^\varphi \rho e u_i)_{,i}} + \overline{c^\varphi P u_{i,i}} = \overline{\rho e[\partial_t(c^\varphi) + u_i c_{,i}^\varphi]}. \quad (2.30c)$$

The mass conservation of each fluid without source terms imposes the dynamic of the mass fraction.

$$\partial_t(c^\varphi) + u_j^\varphi c_{,j}^\varphi = 0. \quad (2.31)$$

Some authors (Holmas *et al.*, 2008; Montini, 2011; Vreman, 2011) add diffusion in the continuity equation by the mean of an additional Fick like form

$$D_t^\varphi([\alpha \rho]^\varphi) = (\rho^\varphi \kappa^\varphi \alpha_{,j}^\varphi)_{,j}. \quad (2.32)$$

The momentum equation is then also modified to take into account the diffusion of the momentum quantity. To obtain this diffusion with an averaging method, the transport of the mass fraction (or indicator function) must be modified by adding a diffusion form. This is not developed here. However, this diffusion is introduced without solid physical grounds and is added in the model to stabilize the short wavelengths. This explains its name of artificial diffusion. However, diffusion due to turbulence has physical basis and can be found by an analysis of the turbulent part of the drag force (de Bertonado, 1992; Burns *et al.*, 2004).

With the mass conservation hypothesis (and its consequence 2.31), the momentum equation and the internal energy equation become

$$\partial_t([\alpha \rho]^\varphi u_i^\varphi) + ([\alpha \rho]^\varphi u_i^\varphi u_j^\varphi)_{,j} = -\overline{c^\varphi p_{,i}} - \overline{([\alpha \rho]^\varphi (u^\varphi)'_j (u^\varphi)'_i)_{,j}}, \quad (2.33a)$$

$$\partial_t([\alpha \rho]^\varphi e^\varphi) + ([\alpha \rho]^\varphi e^\varphi u_i^\varphi)_{,i} = -\overline{c^\varphi p u_{i,i}} - \overline{([\alpha \rho]^\varphi (e^\varphi)' (u^\varphi)'_i)_{,j}}. \quad (2.33b)$$

The pressure forms can be expressed after some manipulations. First, the pressure per fluid is defined as $p^\varphi = \frac{\overline{c^\varphi p}}{\alpha^\varphi}$ and $p' = p - \bar{p}$. The LHS may be developed as

$$\partial_t([\alpha \rho]^\varphi u_i^\varphi) + ([\alpha \rho]^\varphi u_i^\varphi u_j^\varphi)_{,j} = -\alpha^\varphi p_{,i}^\varphi - (p^\varphi - \bar{p}) \alpha_{,i}^\varphi + \overline{p' c_{,i}^\varphi} - \overline{([\alpha \rho]^\varphi (u^\varphi)'_j (u^\varphi)'_i)_{,j}}, \quad (2.34a)$$

$$\partial_t([\alpha \rho]^\varphi e^\varphi) + ([\alpha \rho]^\varphi e^\varphi u_i^\varphi)_{,i} = -\alpha^\varphi p^\varphi u_{i,i}^\varphi - \overline{c^\varphi p (u^\varphi)'_{i,i}} - \overline{([\alpha \rho]^\varphi (e^\varphi)' (u^\varphi)'_i)_{,j}}. \quad (2.34b)$$

The residuals inside the momentum equation represent multiphase features. Following the averaging operator used and the type of flow modeled, these residuals have different interpretations. These interpretations will influence their closures, needed to obtain a final solvable system. However, the closure of the momentum equation and the closure of the internal energy equation cannot be set independently in order to respect

- the conservation of total energy
- the consistency between closures of similar residual forms
- the thermodynamic consistency

Another possibility to obtain the internal energy equation is to assume that the mean internal energy of a phase depends only on the mean field of this phase $e^\varphi = e^\varphi(\rho^\varphi, s^\varphi)$. This means that the first principle can be applied as

$$d_t^\varphi(e^\varphi) = p^\varphi \frac{d_t^\varphi \rho^\varphi}{(\rho^\varphi)^2} + T^\varphi d_t^\varphi s^\varphi. \quad (2.35)$$

with the pressure per phase defined as $\frac{p^\varphi}{(\rho^\varphi)^2} = \frac{\partial e^\varphi}{\partial \rho^\varphi}$. However, this equation is implicit in ρ^φ (and s^φ). Thus, using this equation poses problems from the numerical point of view. It will be shown how it may be written explicitly using other relations between pressure and volume fractions and adequate algebraic combinations (2.3.2).

2.2.3 Closing the fluctuation forms

In this part, various momentum equations due to different fluctuations' closures are presented.

Instantaneous relaxation model

The first closure which can be made is to assume that the average pressure \bar{P} and the fluid pressure p^φ are equal. It means that all the fluids share a common pressure. This hypothesis is relevant assuming that the time of pressure relaxation between phases to a common pressure is very small compared to other the typical time scales of the flow (heat relaxation, velocity relaxation, acoustic propagation, etc. . .) which explains the formulation: instantaneous relaxation pressure. This postulate must be assessed by experiments. As an example, shocks in bubbly flow present relaxation time in order of $3\mu s$ (Beylich & Gülhan, 1990) which must be compared to the propagation time of the shock wave toward the domain (about $10^{-2}s$ for a $1m$ size domain). Thus, this hypothesis is perfectly reasonable in these experiments. Closure also needs to be given for the multiphase Reynolds tensor $R_{ij}^\varphi = \overline{([\alpha\rho]^\varphi (u^\varphi)'_j (u^\varphi)'_i)}$ and the pressure fluctuation along the gradient of the function of presence $\overline{p'b_i^\varphi}$. The easiest way is to set these forms equal to zero. The classical one pressure and two velocities momentum equation is then obtained:

$$D_t^\varphi([\alpha\rho]^\varphi u_i^\varphi) = -\alpha^\varphi p_{,i}. \quad (2.36)$$

It can be shown that this momentum equation derives from a least action principle (Vazquez-Gonzalez *et al.*, 2020), thus it is isentropic. The mass conservation and the momentum equation (2.36) are completed by the transport of the entropy, the volume filling constraint and the pressure relation to close the model.

$$D_t^\varphi([\alpha\rho]^\varphi) = 0, \quad (2.37a)$$

$$D_t^\varphi([\alpha\rho]^\varphi u_i^\varphi) = -\alpha^\varphi p_{,i}^\varphi, \quad (2.37b)$$

$$d_t^\varphi(s^\varphi) = 0, \quad (2.37c)$$

$$p^\varphi = p, \quad (2.37d)$$

$$\sum_\phi \alpha^\phi = 1. \quad (2.37e)$$

This model, called the 6-equation model, is often used but is ill-posed due to a lack of hyperbolicity. Also, it can not be written in conservative form due to the pressure gradient weighted by the volume fraction. This prevents to use classical finite volume scheme. Because all residuals are set to zero, this model is at the core of all the other models where additional forms/equations are added. This is why it is called *backbone* model by [Vazquez-Gonzalez et al. \(2020\)](#). In what follows, some examples of the large panel of multiphase models obtained by other closures are presented.

Interfacial pressure

The form $(p^\varphi - \bar{p})\alpha_{,i}^\varphi$ may be interpreted as the difference between the pressure of the phase φ and the pressure at the interface. One of the most famous closure of this form is the Stuhmiller–Bestion closure ([Stuhmiller, 1977](#)) which expresses this difference as a mass times the square of the drift. This closure leads to a conditional hyperbolic model. Many authors write the momentum equation in a conservative way

$$D_t^\varphi([\alpha\rho]^\varphi u_i^\varphi) + (\alpha^\varphi p^\varphi)_{,i} = \bar{p}\alpha_{,i}^\varphi \quad (2.38)$$

and then to close the average pressure \bar{p} with various interpretations.

Pressure relaxation through volume fraction evolution

Another model often used is the 7 equation model. In this model, the relaxation of pressure is not instantaneous but proportional to the variation of the volume fraction. Therefore, the relation between pressure, with here only two fluids denoted + and –, is modified as

$$\{p^\varphi = p\} \Rightarrow \{d_t^+(\alpha^+) = \mu(p^+ - p^-)\} \quad (2.39)$$

Equation 2.39 expresses that pressure equilibrium is reached when the volume fraction of the phases is stable. This illustrates that after a brutal compression (say a shock) in a multiphase flow with contrasted EOS (say bubbly flow), the bubbles continue to oscillate a certain time after the passage of the shock ([Beylich & Gülhan, 1990](#)), which means that the pressure between water and air is not in equilibrium. This time is the relaxation time modeled with the coefficient μ called dynamic compaction viscosity ([Saurel & Abgrall, 1999a](#)). A characteristic analysis of the model shows its unconditional hyperbolic character. A discussion of this model is given in the paragraph (2.4.5).

2.3 Current approach to find and discretize the *backbone* model

2.3.1 Variational approaches

The variational approaches consist on saying that the nature chooses among all the possible trajectories the one that minimizes some functional. Since their successful application in optics by Fermat in 1662, variational methods were used in many domain of physics. Notably, the least action principle (LAP) enunciated by Lagrange in 1756 passed through many revolutions in physics, from the general relativity of Einstein to the quantum electrodynamic of Feynman. In classical mechanics, this principle states that the real trajectory of the system minimizes the integral over time of the difference between kinetic and potential energy. This principle has been reformulated by Hamilton in 1833 giving the Hamiltonian formulation. The LAP (or the Hamiltonian reformulation) is a powerful tool to build trajectory models of complex systems. Indeed, it involves to model the energies of the system rather than the forces. In case of simple systems, where only few components interact, forces are easy to find and so the trajectories. However, if the system contains many non trivial interactions, the LAP is a powerful way to obtain satisfying modeling of the trajectories. If the microscopic systems always posses a variational structure, the macroscopic ones cannot often be modeled with this method due to irreversible process occurring (Berdichevsky, 2009). However, the isentropic evolution of these systems obeys to the variational formalism and therefore, the use of the LAP guaranties to obtain the non dissipative part of the equations. Furthermore, the Noether theorem allows to insure conservations as long as the Lagrangian used present the adequate invariants. Because thermodynamics consistency is a crucial issue in the complex systems of multiphase flows (1.2.4), the LAP is going to be use to build the isentropic part of the models and numerical schemes.

Introduction of the geometric properties of variational methods

To illustrate the reversible character of the trajectories issued from variational principles, some short developments on the Hamiltonian systems inspired by Hairer *et al.* (2006) and Sanz-Serna (1992) are presented. Hamiltonian systems present a great interest because many systems of reference such as pendulum, harmonic oscillator, two-body system, etc... fall into this category. These systems posses $2 \times d$ coordinates $U = [q_1, \dots, q_d, p_1, \dots, p_d]$ whose evolution satisfies

$$\partial_t U = J^{-1} \nabla H(U) \quad (2.40)$$

with $J = \begin{pmatrix} 0_d & I_d \\ -I_d & 0_d \end{pmatrix}$ and H a functional called the Hamiltonian of the system (it is supposed here that H is autonomous, ie it does not depend on time). The simplest example of such

systems is the harmonic oscillator

$$\ddot{x} + w^2 x = 0 \Rightarrow \begin{cases} p = m\dot{x} \\ q = x \end{cases}, \quad H = \underbrace{\frac{1}{2}p^2}_{\text{kinetic energy}} + \underbrace{\frac{1}{2}kq^2}_{\text{potential energy}} \quad (2.41)$$

Hence, the Hamiltonian is equal to the total energy ². One of the properties of the system (2.40) is that its flow ϕ_t conserves this total energy (only for autonomous systems), ie

$$H(\phi_t(p_0, q_0)) = H(p(t), q(t)) = H(p_0, q_0) \quad (2.42)$$

for any admissible initial states (p_0, q_0) (the demonstration is just a composition of derivatives).

The geometric aspect of such systems is inside the matrix J . In 1D, for any parallelogram made of two vectors X and Y , the oriented area of the parallelogram formed by (X, Y) is $a(X, Y) = X^t J Y = x_1 y_2 - x_2 y_1$. The symplectic form, called ω is then defined as

$$\omega(X, Y) = X^t J Y. \quad (2.43)$$

For any couple of vectors in the space p, q as $X = [x_1^p, \dots, x_d^p, x_1^q, \dots, x_d^q]$ and $Y = [y_1^p, \dots, y_d^p, y_1^q, \dots, y_d^q]$, the form ω associates the sum of the oriented areas obtained by projection onto the coordinate planes (p_i, q_i) , ie

$$\omega(X, Y) = \sum_i (x_i^p y_i^q - x_i^q y_i^p). \quad (2.44)$$

The symplectic form measures then a certain volume in the phase space. The central geometric property of the system (2.40) is that the flow of the system preserves this form, ie

$$\nabla^T \phi_t J \nabla \phi_t = J \Leftrightarrow \omega(\nabla \phi_t X, \nabla \phi_t Y) = \omega(X, Y) \quad (2.45)$$

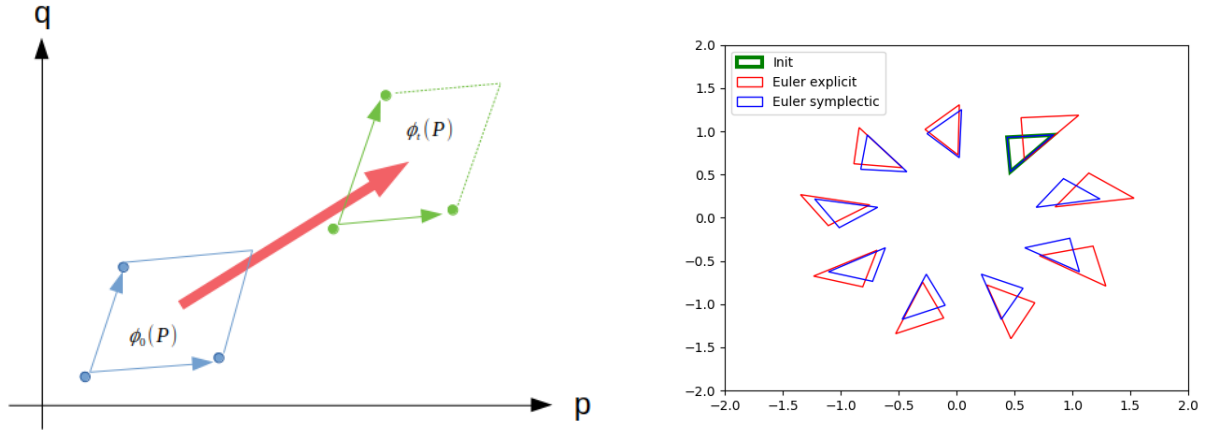
where $\nabla_{(p_0, q_0)} \phi_t(p_0, q_0) = \nabla \phi_t$.

To understand the geometric impact of this formula, let us take a point U_0 in the (p, q) plan and a parallelogram $P = [U_0, U_0 + x, U_0 + y, U_0 + x + y]$ with x and y small vectors. The area of this parallelogram is $\omega(x, y)$. The parallelogram transported by the flow is

$$\begin{aligned} \phi_t(P) &= [\phi_t(U_0), \phi_t(U_0 + x), \phi_t(U_0 + y), \phi_t(U_0 + x + y)] \\ &\approx [\phi_t(U_0), \phi_t(U_0) + \nabla \phi_t(U_0) \cdot x, \phi_t(U_0) + \nabla \phi_t(U_0) \cdot y, \\ &\quad \phi_t(U_0) + \nabla \phi_t(U_0) \cdot x + \nabla \phi_t(U_0) \cdot y] \end{aligned} \quad (2.46)$$

The area of this parallelogram is then at the order one

$$\omega(\nabla \phi_t(U_0) \cdot x, \nabla \phi_t(U_0) \cdot x). \quad (2.47)$$



(a) Transport of a parallelogram with symplectic flow

(b) Euler explicit vs Euler symplectic scheme on the harmonic oscillator

Figure 2.3: Illustration of symplectic properties

If the flow is symplectic, the area of the transported parallelogram is the same as the original one.

Now that these properties have been illustrated in the continuous case, the challenge is to preserve them in the numerical schemes used to solve the differential equations. The conservation of the total energy has been recognized as a crucial feature (in order to obtain correct solution of the Riemann problem as an example) but concerns about preserving the symplectic property in the discrete flow appear in the 60's (de Vogelaere, 1956) and later on (Ruth, 1983; Channell, 1983; Kang, 1984). The discrete flow is the application

$$\phi_{\Delta t}(p^n, q^n) = (p^{n+1}, q^{n+1}) \quad (2.48)$$

and the aim is to preserve the symplectic property (2.45) with this application as illustrated in the figure (2.3). The symplectic Euler scheme is an example of symplectic scheme

$$p^{n+1} = p^n - \Delta t \nabla_q H(p^{n+1}, q^n) \quad q^{n+1} = q^n - \Delta t \nabla_p H(p^{n+1}, q^n) \quad (2.49)$$

For the harmonic oscillator, the discretized flow is

$$\begin{pmatrix} p^{n+1} \\ q^{n+1} \end{pmatrix} = \underbrace{\begin{pmatrix} 1 & -\Delta t \\ \Delta t & 1 - \Delta^2 t \end{pmatrix}}_{\nabla \phi(q^n, p^n)} \begin{pmatrix} p^n \\ q^n \end{pmatrix} \quad (2.50)$$

and straightforward computations lead to $\nabla \phi^T J \nabla \phi = J$.

²In fact, H is the Legendre transformation of the Lagrangian and is equal to the total energy when the Lagrangian possesses a special form.

Variational integrators

The geometric properties of the Hamiltonian systems can be preserved by symplectic integrators. However, many systems do not verify the Hamiltonian structure but fall into the larger class of Lagrangian systems. The Lagrangian systems possess a functional (called Lagrangian) from which their equations of motions can be derived through the LAP. This special property is also a geometric property. However, the symplectic form is not known a priori but can be computed from the integral edge term issued of the variation (Marx, 2008). The flow resulting from the Euler Lagrange equations preserves this symplectic (multisymplectic for the PDE) form ((Marsden & West, 2001) for the EDO and (Marsden *et al.*, 1998) for the PDE).

As for the Hamiltonian systems, the aim is to preserve this geometric property in numerical schemes. The desire to use discrete Lagrangian to build such integrators dates back to the 70's (Cadzow, 1970; Jordan & E.Polak, 1964). To do so, the idea is to discretize the action integral and differentiating it (Logan, 1973). However, a numerical scheme can only possess two of the following properties: symplecticity, energy conservation, momentum conservation (Zhong & Marsden, 1988). A choice must then be made to remove one of these and because conservations are crucial for shock capture, the option in the numerical schemes used in this thesis is to remove the symplecticity. This idea was applied recently by Llor *et al.* (2016) and Vazquez-Gonzalez *et al.* (2020). Because the corrections to conserve the momentum and/or the energy are at the order of the scheme, they are said to be quasi-symplectic.

Application to the Euler equations in continuous

Using the least action principle to find equations of motion in complex systems is a powerful tool. Its use in fluid mechanics started in the years 1900's for incompressible flows with Clebsch (1859)) and with Bateman (1929) to compressible ones. The method of differentiation of the action is not unique because there are two different descriptions of the flow (Eulerian and Lagrangian) and two different ways to incorporate the constraints if the Eulerian coordinates are chosen. The notations used here are the notations that the author have found the most often.

$$\begin{aligned} & \text{Eulerian coordinates: } x, \text{ Lagrangian coordinates: } X \\ & \text{diffeomorphism L to E coordinates: } x = \phi_t(X) \\ & \text{Lagrangian velocity: } \hat{u}(t, X) = \partial_t \phi_t(X) \\ & \text{density: } \hat{\rho}(X, t) \det F(X, t) = \rho_0(X) \\ \text{transformation gradient: } F(X, t) &= \frac{\partial \phi_t(X)}{\partial X} \text{ and its determinant: } J = \det(F) \\ & \text{entropy: } \hat{s}(X, t) = s_0(X) \end{aligned}$$

Lagrangian variations In this approach, there is only one degree of freedom for the system which is the diffeomorphism that links the Eulerian coordinates to the Lagrangian one. All the hydrodynamic fields are related to this diffeomorphism and the derivation of the action is only made with respect to its variation. The presentation done here is inspired by [Morrison \(2006\)](#). The action in the Eulerian frame writes

$$L_{euler} = \int_{V(t)} \frac{1}{2} \tilde{\rho}(x, t) \tilde{u}^2(x, t) - \tilde{\rho}(x, t) e(\tilde{s}(x, t), \tilde{\rho}(x, t)) dx. \quad (2.51)$$

Changing the variable to the Lagrangian frame is straightforward and involves the determinant of the diffeomorphism's Jacobian $J = \det F$ (the entropy is constant along the fluid particle path, ie $\tilde{s}(x, t) = \hat{s}(X, t) = s_0(X)$).

$$L_{lag} = \int_D \left[\frac{1}{2} \dot{\phi}_t^2(X) - e(s_0(X), \frac{\rho_0(X)}{J}) \right] \rho_0(X) dX \quad (2.52)$$

The action can be then written with the following form

$$A = \int_T \int_D L(\phi_i, \dot{\phi}_i, \phi_{i,j}) dX dt \quad (2.53)$$

with ϕ_i the i th coordinate of ϕ_t and $\phi_{i,j}$ its derivative with respect to X_j . The Euler Lagrange equation can be then written as

$$0 = \frac{\partial L}{\partial \phi_i} - \frac{d}{dt} \frac{\partial L}{\partial \dot{\phi}_i} - \frac{d}{dX_j} \frac{\partial L}{\partial \phi_{i,j}} \quad (2.54)$$

The first term in this Euler Lagrange equation is null (there is no dependence on ϕ_i in the kinetic energy nor in the internal energy). The second term gives the acceleration $\rho_0(X) \ddot{\phi}_i$. The last one is the potential derivative

$$\frac{d}{dX_j} \left[- \frac{\partial e}{\partial \hat{\rho}} \underbrace{\frac{\rho_0^2}{J^2}}_{\hat{\rho}^2} \frac{\partial J}{\partial \phi_{i,j}} \right]. \quad (2.55)$$

The Euler momentum equation in the Lagrangian frame is then obtained

$$\rho_0 \ddot{\phi}_i = - \frac{d}{dX_j} \left[\hat{P} \frac{\partial J}{\partial \phi_{i,j}} \right]. \quad (2.56)$$

This equation can be transformed by using the cofactor of the transformation A_j^i (see [Morrison, 1998](#)). This equation is equivalent to the Eulerian counterpart, in 1D, the Eulerian velocity writes

$$\tilde{u}(x, t) = \tilde{u}(\phi_t(X, t), t) = \hat{u}(X, t) = \dot{\phi}_t(X) \quad (2.57)$$

Then by derivation with respect to time

$$\ddot{\phi}_t(X) = \partial_t \tilde{u} + \nabla \tilde{u} \cdot \tilde{u} \quad (2.58)$$

For the second term, in 1 D

$$\frac{d}{dX} \left[\hat{P} \frac{\partial(\partial_X \phi_t)}{\partial(\partial_X \phi_t)} \right] = \frac{d}{dX} \hat{P} = J \partial_x \tilde{P} \quad (2.59)$$

with \tilde{P} the Eulerian pressure, $\hat{P}(X, t) = \tilde{P}(\phi_t(X, t), t) = \tilde{P}(x, t)$.

The Eulerian version of the equation is then found as

$$\underbrace{\frac{\rho_0}{J}}_{\tilde{\rho}} d_t \tilde{u} = -\partial_x \tilde{P}. \quad (2.60)$$

Virtual motions The derivation by the method of the virtual motion is based on considering that there are several degrees of freedom in the flow (velocity, density, etc. . .). However, because all these fields depend only on the diffeomorphism ϕ_t and time, their variations are linked to the variations of ϕ_t . Also, these fields are subject to two constraints, the mass conservation and the entropy conservation. Therefore, the constraints are not present in the Lagrangian but incorporate in the computation of each field's variations. The presentation done here is inspired by the work of [Bretherton \(1970\)](#) and [Gavrilyuk \(2011\)](#).

The fields denoted with a tilde are Eulerian fields, the fields with a hat are Lagrangian fields.

$$\text{Eulerian: } \tilde{f}(t, x, \epsilon) \quad \text{Lagrangian: } \hat{f}(t, X, \epsilon) = \tilde{f}(t, \Phi_t(X, \epsilon), \epsilon) \quad (2.61)$$

Variations of the diffeomorphism ϕ_t are denoted

$$\delta x(t, X) = \frac{d}{d\epsilon} \Phi_t(X, \epsilon)|_{\epsilon=0}. \quad (2.62)$$

The variations of a field in Eulerian and Lagrangian coordinates are then

$$\tilde{\delta} f(t, x) = \partial_\epsilon \tilde{f}(t, x, \epsilon)|_{\epsilon=0} \quad \hat{\delta} f(t, X) = \partial_\epsilon \hat{f}(t, X, \epsilon)|_{\epsilon=0} \quad (2.63)$$

Derivative of the equation (2.61) with respect to ϵ leads to the relation between both variations

$$\hat{\delta} f = \tilde{\delta} f + \delta x \cdot \nabla f \quad (2.64)$$

The interpretation of the difference between both variations is that Lagrangian variations consider changes of the field f and changes of the particles' trajectory. The transformation expresses then $f(X, t) \leftrightarrow f'(X', t)$ with f' and X' the new fields and trajectories. However, the Eulerian variations consider only variations of the field at a given point of space which writes $f(X, t) \leftrightarrow f'(X, t)$. At first order,

$$\begin{aligned} \hat{\delta} f &= f'(X', t) - f(X, t) \\ &= \underbrace{f'(X', t) - f'(X, t)}_{(X'-X) \cdot \nabla_X f} + \underbrace{f'(X, t) - f(X, t)}_{\tilde{\delta} f} \\ &= \delta x \cdot \nabla f + \tilde{\delta} f \end{aligned} \quad (2.65)$$

which is the relation (2.64).

Variations of the fields v , ρ are computed thanks to this relation between Lagrange and Euler point of views combined with the mass constraint and the velocity definition. For density, the equality (2.66) is assumed (its demonstration is recalled by Gavriluk (2011)).

$$\hat{\delta}(\det F) = \det F \operatorname{div}(\delta x) \quad (2.66)$$

Density variations express then

$$\hat{\delta}\rho = -\hat{\rho}\operatorname{div}(\delta x) \quad \tilde{\delta}\rho = -\operatorname{div}(\tilde{\rho}\delta x). \quad (2.67)$$

For the velocity, variations write

$$\hat{\delta}u = \partial_t \delta x \quad \tilde{\delta}u = \mathbf{d}_t \delta x - \delta x \cdot \nabla \tilde{u}. \quad (2.68)$$

As the entropy is only function of Lagrangian coordinates, its variation is simply

$$\hat{\delta}s = 0 \text{ and thus } \tilde{\delta}s = -\nabla \tilde{s} \cdot \delta x. \quad (2.69)$$

The action is written as the integral over the current domain of the Lagrangian. It contains only kinetic energy and internal energy. There is no added constraints in the Lagrangian, however, the mass constraints will be incorporate in the expression of the variations of the virtual motions.

$$A = \int_T \int_{D(t)} \frac{1}{2} \tilde{\rho} \tilde{u}^2 - \tilde{\rho} e(\tilde{\rho}, \tilde{s}) dx dt \quad (2.70)$$

The differentiation of the action along the parameters ϵ is

$$\delta A = \partial_\epsilon A|_{\epsilon=0}. \quad (2.71)$$

Substituting the expression of the variations derived above yields (these are Eulerian fields so the gradients are along Eulerian coordinates)

$$\delta A = \int_T \int_{D(t)} -\left(\frac{1}{2}u^2 - e(\rho, s) - \rho e_{,\rho}\right) \operatorname{div}(\rho \delta x) + \rho u (\mathbf{d}_t \delta x - \nabla u \cdot \delta x) + \rho e_{,s} \nabla s \cdot \delta x dx dt. \quad (2.72)$$

With integration by part and assuming that the variations vanish at the frontiers,

$$\begin{aligned} \delta A &= \int_T \int_{D(t)} \left[\rho \nabla \left(\frac{1}{2} u^2 - e(\rho, s) - \rho e_{,\rho} \right) - \mathbf{D}_t(\rho u) - \frac{1}{2} \rho \nabla u \cdot u + \rho e_{,s} \nabla s \right] \cdot \delta x dx dt \\ \delta A &= \int_T \int_{D(t)} \left[-\rho \left(\nabla \left(e + \frac{P}{\rho} \right) - e_{,s} \nabla s \right) - \mathbf{D}_t(\rho u) \right] \cdot \delta x dx dt \\ \delta A &= \int_T \int_{D(t)} \left[-\nabla P - \mathbf{D}_t(\rho u) \right] \cdot \delta x dx dt \end{aligned} \quad (2.73)$$

The classical Euler momentum equation is then obtained.

Eulerian formalism with constraints in Lagrangian The first attempts to use the least action principle in the Eulerian formalism were unsuccessful because fields were not linked with each other through any constraint. Indeed, the Lagrangian resumes then to

$$L = \frac{1}{2}\rho u^2 - \rho e(\rho) \quad (2.74)$$

and its derivation with respect to the two degree of freedoms u and ρ leads to the Euler–Lagrange equations

$$\rho u = 0 \quad \frac{1}{2}u^2 - e - P/\rho = 0. \quad (2.75)$$

These Euler–Lagrange equations are obviously wrong. The reason of this failure is that both degrees of freedom ρ and u were considered as independent. However, they must be linked through mass conservation (if not, this means that it is possible to create or destroy mass which involves increasing or decreasing the number of particles which is not a degree of freedom of the system). As shown by [Schutz & Sorkin \(1977\)](#), an Eulerian unconstrained variation principle can not produce the correct evolution equations. Therefore, mass conservation must be added in the Lagrangian. In this approach, constraints are introduced through Lagrange multipliers directly in the Lagrangian.

$$L = \frac{1}{2}\rho u^2 - \rho e(\rho) + \Phi D_t(\rho). \quad (2.76)$$

The derivation of the action leads to the Euler Lagrange equations

$$\delta u_i : \quad 0 = \rho u_i - \rho \Phi_{,i}, \quad (2.77)$$

$$\delta \rho : \quad 0 = \frac{1}{2}u^2 - e(\rho) - \rho e_{,\rho}(\rho) - d_t(\Phi). \quad (2.78)$$

The Euler–Lagrange equation obtained by derivation along velocity leads to an unsatisfactory result because it implies that the flow is always potential which means that there are only irrotational flows. The solution to obtain the rotational part of the flow was found by [Lin \(1959\)](#). It consists on adding a constraint over the conservation of a Lagrangian marker denoted ξ which is transported by the flow velocity. The Lagrangian yields then

$$L = \frac{1}{2}\rho u^2 - \rho e(\rho, s(\xi)) + \Phi D_t(\rho) + \Psi d_t \xi \quad (2.79)$$

The entropy is introduced here as a function depending only of the fluid particles label. This is a preservation of the isentropic character of the flow. Discussion about this constraint, its relation to the Clebsch decomposition and its derivation from the Lagrangian framework is made by [Seliger & Whitham \(1968\)](#). Also, its physical interpretation is discussed by [Bretherton \(1970\)](#). The Euler–Lagrange equations of the system are then

$$\delta u_i : \quad 0 = \rho u_i - \rho \Phi_{,i} + \Psi \xi_{,i}, \quad (2.80)$$

$$\delta \rho : \quad 0 = \frac{1}{2}u_j^2 - e(\rho, s(\xi)) - \rho e_{,\rho}(\rho, s(\xi)) - d_t(\Phi), \quad (2.81)$$

$$\delta \xi : \quad 0 = -\rho s_{,\xi} T - D_t(\Psi). \quad (2.82)$$

To obtain the momentum equation, the Eulerian derivative is applied to (2.80).

$$D_t(\rho u_i) = \rho \underbrace{d_t(\Phi_{,i})}_{(d_t\Phi)_{,i}-u_{j,i}\Phi_{,j}} - \xi_{,i} \underbrace{D_t(\Psi)}_{-\rho s_{,\xi}T} - \Psi \underbrace{d_t(\xi_{,i})}_{(d_t\xi)_{,i}-u_{j,i}\xi_{,j}}$$

$$D_t(\rho u_i) = \rho \left[\frac{1}{2} u_j^2 - e(\rho, s(\xi)) - \rho e_{,\rho}(\rho, s(\xi)) \right]_{,i} - \underbrace{\rho u_{j,i} \Phi_{,j} + \Psi u_{j,i} \xi_{,j}}_{\rho u_{j,i} u_j} + \rho T s_{,\xi} \xi_{,i}$$

The derivative of $e(\rho, s(\xi))$ combined with the last term of the formula gives the derivative of the pressure. The classical Euler equation is then obtained

$$D_t(\rho u_i) = -P_{,i}. \quad (2.83)$$

This last approach is the approach that will be used in the following. Some authors prefer the Lagrangian approaches to the Eulerian ones because they seem more natural in the sense that no constraints need to be introduced (Herivel, 1955). Also, some authors prefer the use of the virtual variation methods because they avoid to introduce Lagrangian multipliers in the Lagrangian. ‘The specification (2.80) of the velocity field in terms of potentials is cumbersome, and for some applications is distinctly inconvenient.’ (Bretherton, 1970). However, this approach is simpler than its homologous one because it involves only integration by part. The mass constraint is especially tedious to consider in 3D. For the pure Lagrangian methods, it involves to deal with the cofactor of the transformation gradient (Morrison, 1998). For virtual motions, the theorem (2.66) is not straightforward to prove. Because additional constraints and fields will be introduced in the following, using these two methods may lead to other complex algebras that we avoid by using the pure Eulerian formulation.

2.3.2 The derivation of the backbone model

Using the variational approaches

Using variational approaches to build multiphase flow models dates from the work of Bedford & Drumheller (1978). The authors used the virtual motion techniques (2.3.1) to build models that take into account the micro inertia of the bubbles. The kinetic energy of this micro inertia is the kinetic energy associated to the variation of volume fraction, added to complete the space of parameters originally constituted by the two diffeomorphisms (Sciarra *et al.*, 2003). Introduction of this kinetic energy leads to a Rayleigh-Plesset like equation (Plesset, 1949). Virtual approaches were also used by Sciarra *et al.* (2003) and by Gavriluk & Saurel (2002) where other effects such as the added mass had been added. The approach used in this thesis (2.3.1) was applied first for multiphase flows by Geurst (1980) to build a model for superfluid Helium, then in (Geurst, 1985) to build a model taking into account added mass and is still used as recently (Clausse & López de Bertodano, 2021) to model incompressible flow with inclusion of turbulence. This approach was also used to build the backbone model by (Vazquez-Gonzalez, 2016; Vazquez-Gonzalez *et al.*, 2020). The main steps of the computation are reminded here. The Lagrangian of the system is built with the

kinetic energies and the internal energies of each fluids plus the addition of the constraints by the means of Lagrangian multipliers

$$L = \sum_{\phi} \left(\underbrace{\frac{1}{2}[\alpha\rho]^{\phi}(u_j^{\phi})^2}_{(1)} - \underbrace{[\alpha\rho]^{\phi}e(\rho^{\phi}, \xi^{\phi})}_{(2)} + \underbrace{\Phi^{\phi}D_t^{\phi}([\alpha\rho]^{\phi})}_{(3)} + \underbrace{\Psi^{\phi}d_t^{\phi}(\xi^{\phi})}_{(4)} \right) + \underbrace{\Pi \left(\sum_{\phi} \alpha^{\phi} - 1 \right)}_{(5)} \quad (2.84)$$

with

- (1) the kinetic energy of the fluid ϕ ,
- (2) the internal energy of the fluid ϕ ,
- (3) the mass conservation of the fluid ϕ ,
- (4) the entropy conservation (or equivalently the conservation of the Lagrangian marker) of the fluid ϕ ,
- (5) the volume filling constraint.

The derivative with respect of each degree of freedom leads to the following Euler Lagrange equations

$$\delta[\alpha\rho]^{\phi} : 0 = \frac{1}{2}(u_j^{\phi})^2 - e^{\phi} - \rho^{\phi}e_{,\rho^{\phi}}^{\phi} - d_t^{\phi}(\Phi^{\phi}) \quad (2.85)$$

$$\delta\alpha^{\phi} : 0 = (\rho^{\phi})^2 e_{,\rho^{\phi}}^{\phi} - \Pi \quad (2.86)$$

$$\delta u_i^{\phi} : 0 = [\alpha\rho]^{\phi} u_i^{\phi} - [\alpha\rho]^{\phi} \Phi_{,i} + \Psi^{\phi} \xi_{,i}^{\phi} \quad (2.87)$$

$$\delta \xi^{\phi} : 0 = -[\alpha\rho]^{\phi} e_{,\xi^{\phi}}^{\phi} - D_t^{\phi}(\Psi^{\phi}) \quad (2.88)$$

$$\delta \Phi^{\phi} : 0 = D_t^{\phi}([\alpha\rho]^{\phi}) \quad (2.89)$$

$$\delta \Psi^{\phi} : 0 = d_t^{\phi}(\xi^{\phi}) \quad (2.90)$$

$$\delta \Pi : 0 = \sum_{\phi} \alpha^{\phi} - 1 \quad (2.91)$$

Equations (2.86) shows that all the fluids share the same pressure which is the result found by removing all the fluctuation terms issued from the averaging method. To obtain the momentum equation, the equation (2.87) is derived with the Eulerian derivative and the other Euler Lagrange equations are used to make the pressure gradient appear. The computation is essentially the same as the one done in (2.3.1) and is developed by [Vazquez-Gonzalez \(2016\)](#). The momentum equation is obtained

$$D_t^{\varphi}([\alpha\rho]^{\varphi} u_i^{\varphi}) = -\alpha^{\varphi} p_{,i}. \quad (2.92)$$

Completed by the Gibbs equation, the mass conservation (2.89), the no void constraint (2.91) and the EOS per fluid, the backbone model is formed.

Now that the isentropic part of the model is found, dissipative phenomenon needs to be added. The Gibbs equations will then be written as

$$d_t^\varphi(e^\varphi) = p^\varphi \frac{d_t^\varphi \rho^\varphi}{(\rho^\varphi)^2} + \dot{W}^\varphi \quad (2.93)$$

with \dot{W}^φ the irreversible source term. The implicit character of the equation above makes it difficult to write a numerical scheme due to conservation and robustness issues. Therefore, its explicit version is needed. The necessary development is done by [Vazquez-Gonzalez *et al.* \(2020\)](#) and its main steps are briefly recalled here. First the thermodynamic relation over the pressure (keeping in mind that the fluids share a common pressure) is used.

$$d_t^\varphi p = \gamma^\varphi p \frac{d_t^\varphi \rho^\varphi}{\rho^\varphi} + \Gamma^\varphi \rho^\varphi \dot{W}^\varphi. \quad (2.94)$$

With the mass conservation equation (2.89) this equation becomes

$$\frac{\alpha^\varphi}{\gamma^\varphi} d_t^\varphi p = -p D_t^\varphi \alpha^\varphi + \frac{\alpha^\varphi}{\gamma^\varphi} \Gamma^\varphi \rho^\varphi \dot{W}^\varphi. \quad (2.95)$$

By summation over all the fluid equations and using the volume filling constraint (2.91), the explicit equation over the common pressure is obtained

$$\bar{\gamma}^{-1} \partial_t(p) + \sum_\phi \frac{\alpha^\phi}{\gamma^\phi} u_j^\phi p_{,j} = -p \bar{u}_{i,i} + \sum_\phi \frac{\alpha^\phi}{\gamma^\phi} \Gamma^\phi \rho^\phi \dot{W}^\phi \quad (2.96)$$

with $\bar{\gamma}^{-1} = \sum_\phi \frac{\alpha^\phi}{\gamma^\phi}$ and $\bar{u} = \sum_\phi \alpha^\phi u^\phi$. The pressure equality is assumed here to be maintained even when dissipation is added to the model. Although, the instantaneous relaxation comes from a variational approach which is valid when no dissipation is introduced. Thus, keeping this equality is an hypothesis that allows to stick to the isentropic evolution when the dissipation introduced in the model vanishes. Discussion about the introduction of the dissipation in the pressure relation will be provided in the perspective. However, for the rest of the thesis, we assume that the pressure relation provided by the Euler–Lagrange equation issued from the LAP is valid even when we add dissipation into the model.

Using the explicit pressure evolution leads to the explicit version of the density and the internal energy evolution per fluid.

$$\frac{d_t^\varphi(\rho^\varphi)}{\rho^\varphi} = -\frac{\beta^\varphi}{\alpha^\varphi} \bar{u}_{i,i} + \sum_\phi \frac{\mu^{\varphi\phi}}{\alpha^\varphi p} (u_i^\varphi - u_i^\phi) p_{,i} - \sum_\phi \frac{\mu^{\varphi\phi}}{\alpha^\varphi p} (\Gamma^\varphi \rho^\varphi \dot{W}^\varphi - \Gamma^\phi \rho^\phi \dot{W}^\phi) \quad (2.97)$$

$$D_t^\varphi([\alpha\rho]^\varphi e^\varphi) = \underbrace{-\beta^\varphi p \bar{u}_{i,i}}_{(0)} + \underbrace{\sum_\phi \mu^{\varphi\phi} (u_i^\varphi - u_i^\phi) p_{,i}}_{(1)} - \underbrace{\sum_\phi \mu^{\varphi\phi} (\Gamma^\varphi \rho^\varphi \dot{W}^\varphi - \Gamma^\phi \rho^\phi \dot{W}^\phi)}_{(2)} + \underbrace{[\alpha\rho]^\varphi \dot{W}^\varphi}_{(3)} \quad (2.98)$$

with $\beta^\varphi = \frac{\alpha^\varphi \bar{\gamma}}{\gamma^\varphi}$ and $\mu^{\varphi\phi} = \beta^\varphi \frac{\alpha^\phi}{\gamma^\phi}$. The physical meanings of the different terms are

- (0) total work of pressure weighted by a the relative compressibility of the fluid
- (1) pressure gradient along the drift between fluids
- (2) dissipation exchanges
- (3) dissipation source term

This form of energy equation will be used to construct the numerical scheme for several reasons:

- the conservation at the discrete level
- the possibility to mimic the continuous version to find the discrete operators
- the exhibition of the stiff work of pressure

Because this scheme is quasi-isentropic, there is not enough dissipation to stabilize the shocks (VonNeumann & Richtmyer, 1950). Thus, dissipative mechanisms must be added to spread the shocks in order to capture them. This is done by the introduction of artificial viscosity.

Adding dissipation in shocks

Introduction of the artificial viscosity. Artificial viscosity was published for the first time by VonNeumann & Richtmyer (1950) but was used before its publication as shown by the internal report of Richtmyer (1948). Since its publication, it has been extensively used in Lagrangian numerical schemes (Cournède, 2001; Wilkins, 1963). The name *artificial viscosity* is misleading because it has nothing artificial. In fact, it *replaces the impact of the unresolved microscopic viscosity by a mesoscopically computable force* (Mattsson & Rider, 2015). Also, other mechanisms are able to dissipate in shocks such as thermal diffusion, drag exchanges, etc... However, adding the artificial viscosity is enough to cut the instabilities at short scales (Zel'Dovich & Raizer, 2002). The main idea behind artificial viscosity is to capture shocks by spreading their profile into a prescribed length. This allows to stabilize computations when the mesh is refined by smoothing the ensuing sharp shocks profile.

Artificial viscosity can be closed by mimicking the dissipative Euler equations (Margolin, 2019) and is shown to be deeply linked with thermodynamics through the fundamental derivative (Mattsson & Rider, 2015; Kuropatenko, 1967). This term, often denoted Q , acts as a pressure in the momentum equation and produces dissipation in the energy equation. For a single phase, it is modeled as

$$Q = a_2 \rho \min(0, l \operatorname{div}(u))^2 \quad (2.99)$$

with a_2 a coefficient (that should depends on the fluid EOS) and l the prescribed length on which the shock is spread. In expansion, $\operatorname{div}(u) > 0$ and thus artificial viscosity is

null whereas in compression, $\text{div}(u) < 0$ and thus viscosity is activated. Furthermore, the power squared makes artificial viscosity becomes non negligible only in region of strong compression, ie in shocks. Its discretization is generally made as

$$Q = a_2 \rho \min(0, l \underbrace{\frac{\Delta u}{\Delta x}}_{<0})^2. \quad (2.100)$$

In shocks, approximation of the work of this artificial pressure shows its dissipative character.

$$\delta W = - \int Q dV \approx -a_2 \rho \frac{l^2}{(\Delta x)^2} (\Delta u)^2 S \Delta t \underbrace{\frac{\Delta u}{\Delta x}}_{<0} > 0 \quad (2.101)$$

Thus, the artificial viscosity produces heat inside shocks. When a_2 is at the order of unity, the number of cells on which the shocks will be spread is driven by the length l chosen.

In rarefaction wave, another viscosity may be added to stabilized computations.

$$a_1 l c_s \text{div}(u) \quad (2.102)$$

This new form dissipates everywhere even in shocks but is there negligible compared to the original one.

$$\delta W = - \int Q dV = a_1 \rho c_s \frac{l}{\Delta x} \Delta t (\Delta u)^2 > 0 \quad (2.103)$$

The viscous local Euler equations shed light on the origin of artificial viscosity. The developments here are inspired from (Mattsson & Rider, 2015).

$$D_t(\rho) = 0 \quad (2.104)$$

$$D_t(\rho u) = -\partial_x(P) + \partial_x(\mu \partial_x u) \quad (2.105)$$

$$D_t[\rho(e + \frac{1}{2}u^2)] = -\partial_x(Pu) + \partial_x(u\mu \partial_x u) \quad (2.106)$$

The heat flux in the internal energy equation has not been introduced because the viscosity is enough to stabilize shocks. The source term in the kinetic energy may be developed as

$$u \partial_x(\mu \partial_x u) = \partial_x(u\mu \partial_x u) - \mu (\partial_x(u))^2. \quad (2.107)$$

This means that the internal energy equation is restated to

$$\underbrace{\rho d_t(e)}_{de} = - \underbrace{P \partial_x u}_{PdV} + \underbrace{\mu (\partial_x(u))^2}_{TdS}. \quad (2.108)$$

The dissipation due to the viscous term is formed by the divergence of the volume up to the square which is very similar to the dissipation due to artificial viscosity. This form can be closed with thermodynamic study in shocks.

By integration of the local Euler equations along a stationary shocks of velocity σ , the viscosity form cancels because gradients are null far from the shock. The Rankine-Hugoniot relations are then obtained,

$$\sigma[\rho] - [\rho u] = 0 \quad \Leftrightarrow \quad m[v] - [u] = 0 \quad (2.109)$$

$$\sigma[\rho u] - [\rho u^2 + P] = 0 \quad \Leftrightarrow \quad m[u] + [P] = 0 \quad (2.110)$$

$$\sigma[\rho(e + \frac{1}{2}u^2)] - [\rho u(e + \frac{1}{2}u^2 + \frac{P}{\rho})] = 0 \quad \Leftrightarrow \quad [e] + \bar{P}[v] = 0 \quad (2.111)$$

with $m = \rho(u - \sigma)$, $\bar{P} = \frac{1}{2}(P_f + P_i)$ and v the specific volume $v = 1/\rho$. For the proof of the equation (2.111), use $P_{f,i} = \frac{1}{2}\bar{P} \pm \frac{1}{2}m[u]$ from the equation (2.110). This means that stationary states before and after the shocks are not affected by the viscosity, however, the steepening of the shock depends only on dissipation occurring inside it.

Integration of the equations along the shock from a point upstream to a point inside makes the viscosity gradient appeared.

$$\int_{x_i}^x (2.105) \Leftrightarrow \underbrace{m^2(v(x) - v_i)}_{m[u]} + P(x) - P_i = \mu \underbrace{\partial_x u(x)}_{m\partial_x v(x) = -q(x)} \quad (2.112)$$

$$\int_{x_i}^x (2.106) \Leftrightarrow (e(x) - e_i) + \frac{1}{2}(P(x) + q(x) + P_i)[v] = \underbrace{e_q(x)}_{-\mu u(x)\partial_x(u(x))} \quad (2.113)$$

These equations are restated to

$$P + q - P_i = -m^2(v - v_i) \quad (2.114)$$

$$e + e_q - e_i = -\frac{1}{2}(P + q + P_i)(v - v_i). \quad (2.115)$$

Setting $e_q = 0$ (considering it is absorbed in e), dividing the last equation by $[v]$ and identifying the ensuing term with the Gibbs relation $de = -Pdv + TdS$, the relation between viscosity and dissipation is obtained as

$$q = -T \frac{dS}{dV} \quad (2.116)$$

which means that q rules the entropy production during the compression. This identity combined with results issued from thermodynamics in weak shock (Bethe)

$$T\Delta S = -\frac{1}{6}Gc^2\left(\frac{\Delta V}{V}\right)^3 \quad \frac{\Delta u}{c} = \frac{\Delta V}{V} \quad (2.117)$$

leads to the following viscosity closure

$$q = \frac{1}{6}G\rho_0(\Delta u)^2. \quad (2.118)$$

In strong shock, the initial pressure P_i can be neglected before the final one P_f . Thus, the equation (2.111), (2.110) and (2.109) leads to $\Delta e = \frac{1}{2}\Delta^2 u$. As the work of pressure is negligible before the entropy variation, $T\Delta S = \frac{1}{2}\Delta^2 u = -q\Delta V$. The volume variation in strong shocks can be expressed as $\Delta V = -\frac{2}{\rho_i(\Gamma+2)}$ which leads to

$$q = \frac{1}{4}\rho_i(\Gamma + 2)\Delta^2 u \quad (2.119)$$

in strong shocks.

The artificial viscosity in multiphase flow The isentropic character of the backbone model demands to add dissipation to capture the shocks. It has been shown how this dissipation can be introduced in a single fluid flow by the mean of artificial viscosity closed thanks to thermodynamic relation. In multiphase flows, an infinite number of closures inspired by the single fluid analysis are available. In each closure, two choices must be made: the shape of the artificial viscosity in the momentum equation and the distribution of its work among the fluids. We have retained two main types: the iso dissipation closure (1) and a closure based on the ratio of compressibility (2). The summary of both closures are

$$\begin{aligned}
 (1) \qquad \qquad \qquad (2) \\
 Q = \bar{\rho} \mathbf{Q}(\bar{u}_{i,i}, c_s) \qquad Q = \sum_{\phi} \beta^{\phi} \underbrace{\rho^{\phi} \mathbf{Q}\left(\frac{\beta^{\phi}}{\alpha^{\phi}} \bar{u}_{i,i}, c_s^{\phi}\right)}_{q^{\phi}} \\
 [\alpha \rho]^{\varphi} \dot{W}^{\varphi} = \eta^{\varphi} Q \bar{u}_{i,i} \qquad \qquad \qquad \beta^{\varphi} q^{\varphi} \bar{u}_{i,i}
 \end{aligned}$$

with $\eta^{\varphi} = \frac{\alpha^{\varphi} \Gamma^{\varphi}}{\sum_{\phi} \alpha^{\phi} / \Gamma^{\phi}}$. The closure (2) is especially stiff when the ratio $\beta^{\varphi} / \alpha^{\varphi}$ increases because the resulting dissipation is proportional to the cube of this quantity. It means that special care must be taken to assure its capture in the internal energy equation from a numerical point of view. The closure (1) is canonical in the sense that the form (2) in the internal energy equation (2.98) becomes zero with this choice.

2.3.3 The numerical scheme

To preserve the geometric characteristic of the backbone model into its discretization, the idea is to use the approaches developed in (2.3.1) to build the numerical scheme. Using discrete variational principle to build a scheme for the mono fluid case was done in a semi discrete way by [Fahrenthold & Koo \(1999\)](#) in Eulerian and extend to the ALE formalism by [Koo & Fahrenthold \(2000\)](#). A second derivation is done in the incompressible case by [Pavlov *et al.* \(2011\)](#). The first application to the multi-fluid case was made by [Vazquez-Gonzalez *et al.* \(2020\)](#) and leads to the GEEC scheme presented in this subsection. The acronym G.E.E.C. means Geometric Energy and Entropy Compatible.

- Geometric because the volume variation is coherent with the advection term.
- Energy because the scheme insures the exact preservation of the total energy
- Entropic because the second principle of the thermodynamic is respected and the scheme dissipates as less as possible away from shocks.

The GEEC procedure allows to meet these requirements with three steps: i) the derivation of the discrete momentum equation with a least action principle, ii) the computation of the discrete internal energy equations by mimicry and computation of the discrete kinetic energy equations, iii) the addition of the artificial viscosity presented in the subsection (2.3.2).

The discrete version of the action (2.84) is written

$$A = \sum_c \left[\sum_\phi \left(\frac{1}{2} [\alpha\rho]_c^{\phi n} (\mathbf{u}_c^{\varphi n+1/2})^2 - [\alpha\rho]_c^{\phi n} e(\rho_c^{\phi n}, \xi_c^{\phi n}) + \Phi_c^{\phi n+1} \mathbf{D}_{\Delta t}^\phi([\alpha\rho]_c^{\phi n}) \right. \right. \\ \left. \left. + \Psi_c^{\phi n+1} \mathbf{D}_{\Delta t}^\phi([\alpha\rho]_c^{\varphi n} \xi_c^{\phi n}) \right) - \Pi_c^{n+1} \left(\sum_\phi \alpha_c^{\phi n} - 1 \right) \right]. \quad (2.120)$$

The operators in red are the transport operators which will entirely determine the discretization of the evolution equations. In order to fulfill the stability requirements, they are chosen to be explicit at the first order. Modification of this transport operator in order to reach the second order while preserving isotropic numerical diffusion is developed by Paulin *et al.* (2020, 2021). The derivation of the least action which leads to the Euler–Lagrange equations whose combination leads to the discrete momentum equation is made by Vazquez-Gonzalez *et al.* (2020). The momentum equation per fluid is

$$\mathbf{D}_{\Delta t}^\varphi([\alpha\rho]_c^{\varphi n-1} \mathbf{u}_c^{\varphi n-1/2}) = -\Delta t^n \alpha_c^{\varphi n} \sum_d \sigma_{cd}^{\varphi n-1/2} \mathbf{s}_{cd}^{n-1/2} (p_d^n - p_c^n). \quad (2.121)$$

This equation is not conservative due to the off-centering factor $\sigma_{cd}^{\varphi n-1/2}$ which is equal to 1 when the fluid φ goes from the cell c to the cell d (crossing the oriented surface $\mathbf{s}_{cd}^{n-1/2}$, from c to d , separating both cells) and 0 else. Thus, summation over all the fluids and cell does not cancel under periodic conditions. In order to meet the conservation of the total momentum, this gradient has to be modified. The first attempt to modify it was proposed by Vazquez-Gonzalez (2016)

$$\alpha_c^{\varphi n} \sigma_{cd}^{\varphi n-1/2} \Rightarrow \frac{1}{2} \left(\frac{\alpha_c^{\varphi n} + \alpha_d^{\varphi n}}{2} + \alpha_c^{\varphi n} \sigma_{cd}^{\varphi n-1/2} - \alpha_d^{\varphi n} \sigma_{dc}^{\varphi n-1/2} \right). \quad (2.122)$$

However, this gradient suffers from robustness issue in presence of strong volume fraction gradient due to the presence of the volume fraction in the neighboring cells $\alpha_d^{\varphi n}$. To tackle this robustness issue, the total pressure gradient summed on all the fluid is modified to be conservative and then weighted by the volume fraction for each fluid.

The new pressure gradients is written

$$\mathbf{D}_{\Delta t}^\varphi([\alpha\rho]_c^{\varphi n-1} \mathbf{u}_c^{\varphi n-1/2}) = -\Delta t^n \alpha_c^{\varphi n} \sum_d \bar{\sigma}_{cd}^{\varphi n-1/2} \mathbf{s}_{cd}^{n-1/2} (p_d^n - p_c^n), \quad (2.123)$$

with

$$\bar{\sigma}_{cd}^{\varphi n-1/2} = \frac{1}{2} \sigma_{cd}^{\varphi n-1/2} + \frac{1}{2} \sum_\phi \alpha_d^{\phi n} \sigma_{cd}^{\phi n-1/2}. \quad (2.124)$$

The computation of this pressure gradient is made in (2.A).

To compute the internal energy equation, the continuous equations are mimicked to insure the compatibility between the discrete gradient operator in the momentum equation,

the transport operator and the divergence of the volume. To do so, the kinetic energy equations are computed as

$$\frac{1}{2}(\mathbf{u}_c^{\varphi^{n+1/2}} + \mathbf{u}_c^{\varphi^{n-1/2}}) \cdot (2.123) \quad (2.125)$$

and the pressure is factorized in the right hand side. This leads to the divergence operator

$$[P\text{div}(u)]_c^n = P_c^n \frac{1}{2} \sum_d \mathbf{s}_{cd}^{n-1/2} \cdot \underbrace{[\alpha_c^{\varphi^n} \bar{\sigma}_{cd}^{\varphi^{n-1/2}} (\mathbf{u}_c^{\varphi^{n+1/2}} + \mathbf{u}_c^{\varphi^{n-1/2}}) + \alpha_d^{\varphi^n} \bar{\sigma}_{dc}^{\varphi^{n-1/2}} (\mathbf{u}_d^{\varphi^{n+1/2}} + \mathbf{u}_d^{\varphi^{n-1/2}})]}_{\langle \mathring{V} \rangle_c^n} \quad (2.126)$$

The discrete internal energy equation yields then

$$\begin{aligned} D_{\Delta t}^\varphi([\alpha\rho]_c^{\varphi^n} e_c^{\varphi^n}) &= -\beta_c^{\varphi^n} P_c^n \langle \mathring{V} \rangle_c^n + \sum_\phi \mu_c^{\varphi\phi n} (\langle \vec{u}^\varphi \cdot \vec{\nabla} P \rangle_c^n - \langle \vec{u}^\phi \cdot \vec{\nabla} P \rangle_c^n) \\ &\quad - \sum_\phi \mu_c^{\varphi\phi n} [\Gamma^\varphi \langle \rho^\varphi \delta W^\varphi \rangle_c^n - \Gamma^\phi \langle \rho^\phi \delta W^\phi \rangle_c^n] + \alpha_c^{\varphi^n} \langle \rho^\varphi \delta W^\varphi \rangle_c^n \end{aligned} \quad (2.127)$$

with

$$\langle \vec{u}^\varphi \cdot \vec{\nabla} P \rangle_c^n = \frac{1}{2} \sum_d \bar{\sigma}_{cd}^{\varphi^{n-1/2}} (\mathbf{u}_c^{\varphi^{n+1/2}} + \mathbf{u}_c^{\varphi^{n-1/2}}) \cdot \mathbf{s}_{cd}^{n-1/2} (p_d^n - p_c^n) \quad (2.128)$$

Once the internal energies of all fluids have been computed, a system is solved in each cell to obtain the new values of the densities, volume fraction and pressure.

$$p_c^{n+1} = P^\varphi(\rho_c^{\varphi^{n+1}}, e_c^{\varphi^{n+1}}) \quad \sum_\phi \frac{[\alpha\rho]_c^{\phi^{n+1}}}{\rho_c^{\phi^{n+1}}} = 1 \quad (2.129)$$

2.4 On the hyperbolicity in two-phase flow models

2.4.1 The link between stability and hyperbolicity

Physical laws are often translated into a system of PDE linking time evolution of the variables to their spatial derivatives. To assure the validity and the possibility to use it in practice, some properties on the solutions are needed. These properties define a well posed problem from the definition of [Hadamard \(1902\)](#):

- existence,
- uniqueness,
- stability.

By the mean of stability, it is understood that a solution must depend continuously on the data, ie that a small perturbation of an initial state must be bounded after a finite time.

There are two main reasons to respect this principle, first flows can be unstable within a certain range but the instabilities always *damp*, ie their amplitude never grows infinite. Secondly, a model which is not stable is likely to crash during calculations because small perturbations due to numerical errors appear at each iteration of the numerical solvers used to *solve* the models. Now, is it possible to know if a model will be stable and, even more, is it possible to predict its range of stability ? To answer this question, a theory that classifies the PDE has been developed. Its main result is that the system of PDE must be hyperbolic, ie possess only real non degenerate eigenvalues. The link between this property and the well posed character of a problem has been developed in the mid century (Hersh, 1963; Kreiss, 1970). However, a linear analysis can give a hint to understand the link between characteristic analysis (the hyperbolicity condition) and the stability. Let a system of PDE with an operator D , its Jacobian A , a stationary state U_0 and a perturbation U . The linear perturbation dynamics is

$$\underline{U}_t + \underline{\partial_U D|_{U_0}}(\underline{U}) = \underline{U}_t + \underline{A(U_0)} \cdot \underline{U}_x = 0 \quad (2.130)$$

To proceed to the analysis, the perturbation is projected into waves.

$$\underline{U} = \begin{pmatrix} u_1 \\ \vdots \\ u_n \end{pmatrix} e^{i(\omega t - kx)} = \tilde{U} e^{i(\omega t - kx)} \quad (2.131)$$

with \tilde{U} independent of (x, t) . The ensuing matrix relationship is

$$i\tilde{U}(\omega I - kA(U_0)) = 0. \quad (2.132)$$

This system has a trivial solution which is $\tilde{U} = 0$, to obtain non trivial solution, ω must take on some values which cancel the determinant $|\omega I - kA(U_0)|$. This condition leads to a relation between ω and k called the dispersion relation. The determinant writes

$$|\omega I - kA| = |\omega I - kP\Lambda P^{-1}| = |P\omega I P^{-1} - kP\Lambda P^{-1}| = |\omega I - k\Lambda| = \prod_i (\omega - \lambda_i k) \quad (2.133)$$

with Λ and P the diagonal and transfer real matrix associated to A . If there exists a complex eigenvalue λ_j , there exists another eigenvalue $\bar{\lambda}_j$, conjugate of λ_j and thus there exists one eigenvalue λ_o which posses negative imaginary part. Then the mode associated to this eigenvalue will grow exponentially

$$\tilde{U} e^{-k\text{Im}(\lambda_o)t} e^{ik(\text{Re}(\lambda_o)t - x)}. \quad (2.134)$$

This wave analysis does not constitute a rigorous approach but gives a hint to understand the link between stability and characteristics.

2.4.2 Ellipticity and characteristic analysis of the two phase flow model

The characteristic analysis of the two-velocities, two temperatures and one pressure model shows that it is not hyperbolic and gives a hint to understand the roots of this elliptic character. This feature was pointed early by [Gidaspow *et al.* \(1973\)](#) and here is presented the simple analysis characteristic. The explicit equations are obtained by [Vazquez-Gonzalez *et al.* \(2020\)](#), the demonstration of their computation is made before proceeding to the analysis of characteristics. Starting from (2.37), the equations are combined to obtain explicit evolution of the pressure. The isentropic equation of pressure is

$$d_t^\varphi(p^\varphi) = \gamma^\varphi p^\varphi \frac{d_t^\varphi \rho^\varphi}{\rho^\varphi}. \quad (2.135)$$

With the mass conservation and the pressure equality assumption, this equation is restated as

$$\frac{\alpha^\varphi}{\gamma^\varphi} d_t^\varphi(P) = -P D_t^\varphi(\alpha^\varphi) \quad (2.136)$$

The combination $\sum_\phi (2.136)^\phi$ combined with the void filling condition leads to the following pressure equation

$$\partial_t(P) + \sum_\phi \beta^\phi u_j^\phi P_{,j} + \bar{\gamma} P \sum_\phi (\alpha^\phi u_j^\phi)_{,j} = 0 \quad (2.137)$$

with $\bar{\gamma}^{-1} = \sum_\phi \frac{\alpha^\phi}{\gamma^\phi}$ and $\beta^\varphi = \frac{\alpha^\varphi \bar{\gamma}}{\gamma^\varphi}$. Once the pressure is explicit, the volume fraction equation can be also written explicitly

$$D_t^\varphi(\alpha^\varphi) + \frac{1}{P} \sum_\phi \mu^{\varphi\phi} (u_j^\varphi - u_j^\phi) P_{,j} - \beta^\varphi \sum_\phi (\alpha^\phi u_j^\phi)_{,j} = 0 \quad (2.138)$$

These formulas are valid for any number of fluid and for any dimension. However, we restrict here to two fluid and 1D for the analysis of the characteristic.

The unknowns of this system are $X = (P, \alpha^-, u^-, u^+, s^-, s^+)$

The system yields now as

$$\partial_t X + A \partial_x = 0 \quad (2.139)$$

with

$$A = \begin{pmatrix} \beta^- u^- + \beta^+ u^+ & \bar{\gamma} P \Delta u & \bar{\gamma} P \alpha^- & \bar{\gamma} P \alpha^+ & 0 & 0 \\ \frac{\mu^{+-} \Delta u}{P} & u^- - \beta^- \Delta u & \alpha^- \beta^+ & -\alpha^+ \beta^- & 0 & 0 \\ \frac{1}{\rho^-} & 0 & u^- & 0 & 0 & 0 \\ \frac{1}{\rho^+} & 0 & 0 & u^+ & 0 & 0 \\ 0 & 0 & 0 & 0 & u^- & 0 \\ 0 & 0 & 0 & 0 & 0 & u^+ \end{pmatrix} \quad (2.140)$$

and $\Delta u = (u^- - u^+)$.

The characteristic polynomial is

$$P(\lambda) = (u^- - \lambda)(u^+ - \lambda)[(u^+ - \lambda)^2(u^- - \lambda)^2 - (c^+)^2\beta^+(u^- - \lambda)^2 - (c^-)^2\beta^-(u^+ - \lambda)^2]. \quad (2.141)$$

Then there are two obvious eigenvalues which are u^+ and u^- and correspond to the transport of the entropy. The other eigenvalues are the four roots of the polynomial

$$(u^+ - \lambda)^2(u^- - \lambda)^2 - (c^+)^2\beta^+(u^- - \lambda)^2 - (c^-)^2\beta^-(u^+ - \lambda)^2. \quad (2.142)$$

In the reference frame following the velocity $\frac{u^+ + u^-}{2}$, the polynomial can be restated as

$$(\delta - \lambda)^2(\delta + \lambda)^2 - (c^+)^2\beta^+(\delta + \lambda)^2 - (c^-)^2\beta^-(\delta - \lambda)^2. \quad (2.143)$$

with $\delta = \frac{u^+ - u^-}{2}$. The domain of ellipticity has been found in (Ransom & Hicks (1984)) using a theorem proved in (Wendroff (1979)). It is recalled in (Cournède (2001)) and yields

$$0 < \delta^2 < \frac{1}{4}c_0^2 \frac{[(\alpha^+/\rho^+)^{1/3} + (\alpha^-/\rho^-)^{1/3}]^3}{\alpha^+/\rho^+ + \alpha^-/\rho^-} \quad (2.144)$$

with c_0 the frozen speed of sound

$$\frac{1}{\rho c_0^2} = \frac{\alpha^+}{\rho^+(c^2)^+} + \frac{\alpha^-}{\rho^-(c^2)^-}. \quad (2.145)$$

To understand the development of instabilities, an expansion of this polynomial is made around $\delta = 0$. For $\delta = 0$, there are four characteristics $(0, 0, -c_s, c_s)$ with c_s the zero drag speed of sound $c_s^2 = \beta^+(c^+)^2 + \beta^-(c^-)^2$. With a Taylor expansion around the last two characteristics, the equation

$$P(\delta, \lambda) = \underbrace{P(0, \pm c_s)}_{=0} + (\lambda \mp c_s)\partial_\lambda P|_{0, \pm c_s} + \delta\partial_\delta P|_{0, \pm c_s} = 0 \quad (2.146)$$

leads to the following roots $(-c_s + \delta \frac{\alpha^+/\rho^+ - \alpha^-/\rho^-}{\alpha^+/\rho^+ + \alpha^-/\rho^-}, c_s + \delta \frac{\alpha^+/\rho^+ - \alpha^-/\rho^-}{\alpha^+/\rho^+ + \alpha^-/\rho^-})$

Because the first derivatives around the two first eigenvalues (which are equals to zeros) are null (it is a second order root), a second order expansion is needed

$$P(\delta, \lambda) = \underbrace{P(0, 0) + \lambda\partial_\lambda P|_{0,0} + \delta\partial_\delta P|_{0,0}}_{=0} + \frac{1}{2}\lambda^2\partial_\lambda^2 P|_{0,0} + \frac{1}{2}\delta^2\partial_\delta^2 P|_{0,0} + \delta\lambda\partial_{\lambda,\delta}^2 P|_{0,0} = 0 \quad (2.147)$$

The roots of this equation are:

$$\frac{\delta}{\alpha^+/\rho^+ + \alpha^-/\rho^-} \left(-\alpha^+/\rho^+ + \alpha^-/\rho^- - 2i\sqrt{\alpha^+\alpha^-/\rho^+\rho^-}, -\alpha^+/\rho^+ + \alpha^-/\rho^- + 2i\sqrt{\alpha^+\alpha^-/\rho^+\rho^-} \right) \quad (2.148)$$

Hence the dispersion relation around small values of drift gives the four eigenvalues

$$\lambda^{1,2} = -\frac{\delta(\alpha^+/\rho^+ - \alpha^-/\rho^-)}{\alpha^+/\rho^+ + \alpha^-/\rho^-} \pm 2i\frac{\delta\sqrt{\alpha^+\alpha^-/\rho^+\rho^-}}{\alpha^+/\rho^+ + \alpha^-/\rho^-} \quad (2.149)$$

$$\lambda^{3,4} = \pm c_s + \delta\frac{\alpha^+/\rho^+ - \alpha^-/\rho^-}{\alpha^+/\rho^+ + \alpha^-/\rho^-} \quad (2.150)$$

The expansion around small values of δ shows the growth rate of the Kelvin–Helmoltz instabilities driven by the coefficients $\pm 2i\frac{\delta\sqrt{\alpha^+\alpha^-/\rho^+\rho^-}}{\alpha^+/\rho^+ + \alpha^-/\rho^-}$. These eigenvalues are not associated with sound speed propagation, hence they are present independently of the compressibility of the phases. Indeed, these unstable modes are the Kelvin-Helmoltz (K.H) instabilities which are associated to the volume fraction.

However, all the previous development implies the instability of the linearized model. Nevertheless, non linearities may have impact on the model (Keyfitz (2001)) that stabilizes the flow.

2.4.3 What are the vision toward the ellipticity of this model ?

One vision in the community is that the multi-fluid models must be hyperbolic Romenski & Toro (2004): *At present it is practically conventional fact that the governing equations of compressible two-phase flow model must be hyperbolic.* Many researches on the field have been made to find hyperbolic models of two phases flows. Several points may be raised in response to a non hyperbolic model:

- 1 The physics behind the model is wrong because the model is mathematically incorrect, thus the model should not be used.
- 2 The physics behind the model is correct but incomplete. The model can be used if complemented by additional terms representing effects lost during the averaging process. These additional terms are needed to ensure the hyperbolic character of the model.
- 3 The multiphase flows are unstable as it is seen in nature with many well known instabilities (Kelvin–Helmholtz (KH), Rayleigh–Taylor (RT), etc...). Thus, the model must be unstable on a certain range of frequencies. The added terms (inter-facial effects, relaxation terms, etc...) are here to set a cut-off, ie small wavelength must be damped if they are shorter than the cut-off.

Among the efforts made in the direction of the second remark, notable efforts to add virtual mass effect are made by Geurst (1985); Zhang & VanderHeyden (2002); Drew (1979). It has been shown that for certain a function of the added mass coefficient (depending on the volume fraction), the added mass makes the model hyperbolic. Also, an interface pressure term depending on the square of the drift was introduced by Stuhmiller (1977).

This modification leads to unconditional hyperbolicity and the pressure term is similar as the added mass pressure. [Theofanous & Chang \(2008\)](#) provided a review of notable attempts.

The third remark has been notably studied by [Ramshaw \(1978\)](#) where they add surface tension in the form of a second derivative of the volume fraction. It must be stressed that this expression represents the surface tension because the authors studied a separated flow in a pipe. Thus, a variation of volume fraction represents well a curvature of the interface between both fluids. But this closure would have not the same meaning at all in a dispersed phase flow as an example.

About well posedness, the view which is developed across this thesis can be summarized by the three following remarks.

- The elliptic model presented above (2.3.2) is not wrong but contains only macroscopic non dissipative physics. However, though the microscopic physics is isentropic [Berdichevsky \(2009\)](#), its macroscopic counterpart must contain entropy production. Thus, dissipation terms are missing and the model can not be used as such in industrial applications. Nevertheless, because it is at the root of all other models, it needs to be studied in order to understand the non dissipative physics and to build numerical schemes able to capture isentropy.
- Experiments on multiphase flows show many chaotic behaviors. In order to capture them, models must be unstable over some range of the spectrum. However, these instabilities occur at large scales. Indeed, a microscopic mechanism always exists to prevent high frequency/short wavelengths instabilities: size of the inclusions, surface tension, viscosity. . .
- Therefore, using an unstable model to study a certain part of the physics always present in all multiphase applications is of a crucial importance. Though, this model, which represents only ideal situations, cannot be used to predict real multiphase flows.

To conclude these remarks, the elliptic character of the backbone model (also called 6 equations model) makes it unusable for engineers who want to simulate real multiphase flows. But its study is fundamental for researchers in order to capture correctly isentropic physics present in all of them. Also, its unstable character is not a problem per se. Indeed, it is necessary to be unstable at some range of frequency to capture multiphase instabilities. But the model should be complemented to obtain a cut off scale coherent with physics and the dissipation inherent to macroscopic process.

2.4.4 Cutoff wavelength by [Ramshaw \(1978\)](#)

This paragraph highlights the second item above, ie that the model can be unstable at a certain range of frequencies but must possess a cutoff in the spectrum. In the incompressible model proposed by [Ramshaw \(1978\)](#), the relation between pressure is modified by adding a

surface tension term.

$$p^+ - p^- = -\sigma \partial_x^2(\alpha^+) \quad (2.151)$$

The two phase pressures are closed by a barotropic equation $\rho^i = f(p^i)$. The average pressure is denoted $P = \frac{1}{2}(p^+ + p^-)$. The model they propose is then

$$\partial_t(\alpha^+) + u^+ \partial_x(\alpha^+) + \alpha^+ \partial_x(u^+) = 0 \quad (2.152a)$$

$$\partial_t(u^+) + u^+ \partial_x(u^+) + \frac{1}{\rho^+} (\partial_x(P) - \frac{1}{2} \sigma \partial_x^3(\alpha^+)) = 0 \quad (2.152b)$$

$$- \partial_t(\alpha^+) - u^- \partial_x(\alpha^+) + \alpha^- \partial_x(u^-) = 0 \quad (2.152c)$$

$$\partial_t(u^-) + u^- \partial_x(u^-) + \frac{1}{\rho^+} (\partial_x(P) + \frac{1}{2} \sigma \partial_x^3(\alpha^+)) = 0 \quad (2.152d)$$

Wavelet analysis leads to the following dispersion relation

$$4\alpha^+ \alpha^- k^4 \sigma - \rho^- \alpha^+ (\omega - k u^-)^2 - \rho^+ \alpha^- (\omega - k u^+)^2 = 0 \quad (2.153)$$

which has four square roots

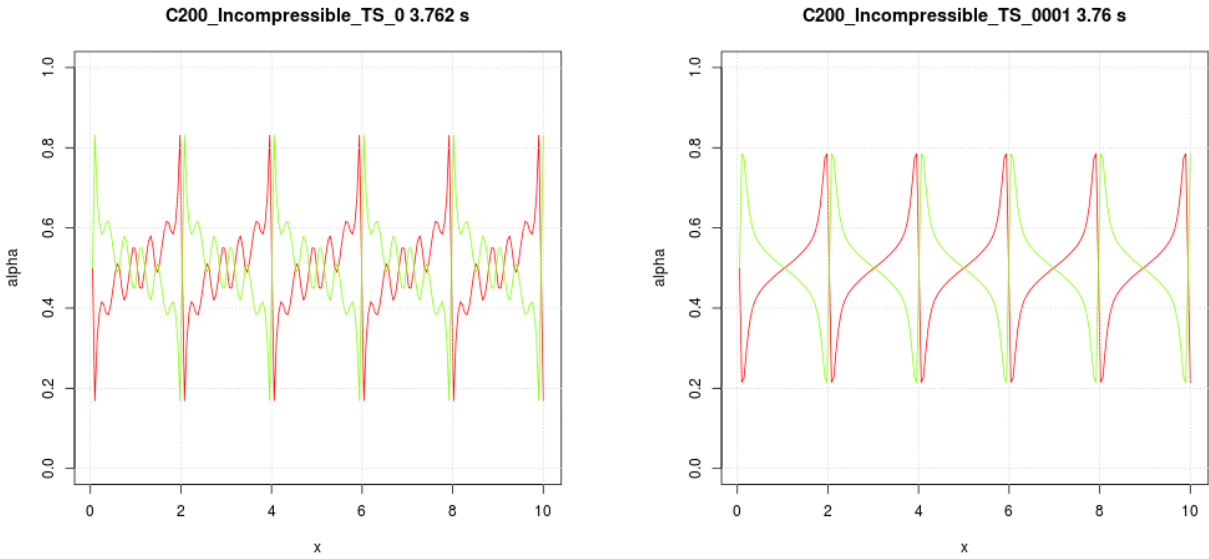
$$\omega = \frac{1}{\alpha^1 \rho^2 + \alpha^2 \rho^1} [(\alpha^1 u^2 k \rho^2 + \alpha^2 u^1 k \rho^1) \mp \left(4\alpha^1 \alpha^2 k^2 \left[\sigma(\alpha^1 \rho^2 + \alpha^2 \rho^1) k^2 - \rho^1 \rho^2 (u^2 - u^1)^2 \right] \right)^{1/2}]. \quad (2.154)$$

If the form under the square root is negative, there is a complex root and thus instable modes (the complex roots goes in conjugate pairs so that at least one will have negative imaginary value). A examination of the roots leads to several remarks. First, the well known influence of the drift on the instability (that notably feeds the KH instabilities) is observed. Secondly, the creation or destruction of instabilities result from a competition between drift and surface tension. But the factor k^2 tells that the surface tension will damp instabilities only at large k (thus short length waves) which are precisely what is needed to capture KH instabilities which are long wave perturbations. However, without surface tension, nothing except the size of the cell can limit short waves instabilities that are then supposed to be evacuated in internal energy through dissipation.

On figure (2.4), the influence of surface tension on the short wavelengths is shown whereas the large wavelengths are unaffected. It must be underlined that in any numerical simulation, a cutoff length always exists which is the typical size of the mesh.

2.4.5 On the Baer & Nunziato (1986) model

The Baer–Nunziato model (Baer & Nunziato (1986)) has been developed to capture the deflagration to detonation transition in granular reactive multiphase flow. It was made popular by Saurel & Abgrall (1999a), notably with the proof of its conservative and unconditionally



(a) Kelvin–Helmoltz instabilities without surface tension (b) Kelvin–Helmoltz instabilities with surface tension

Figure 2.4: Kelvin–Helmoltz instabilities simulation

hyperbolic character. Since then, many authors have used this model to predict other types of flows such as bubbly flow (Saurel & Abgrall, 1999a; Lallemand *et al.*, 2005), as well as granular flow (Gallouet, Thierry *et al.*, 2010; Poroshyna & Utkin, 2019). Models of the type of B.N. models are called seven equations model. This denomination comes from the fact that an evolution equation for the volume fraction is added to the 6 evolution equations. This equation is added to the EOS equations and the volume filling constraint and closes the model. The evolution equation on the volume fraction has been studied by Chang & Ramshaw (2008) to understand the physics behind it. Furthermore, the B.N. model has been reviewed and many remarks are addressed toward its physical tenability to model different types of multiphase flow (Lhuillier *et al.*, 2013; Theofanous & Chang, 2008; Dinh *et al.*, 2004). Notably about the fact that the characteristics exhibit sound speed of the grain which can be true only if they are permanently in contact (as in the granular flows that Baer & Nunziato (1986) originally aimed to model). In (Lhuillier *et al.*, 2013), the authors conclude that: *The use of (3.7) (or its generalization (3.4)) (the evolution equation of the volume fraction) when there are no permanent contacts between the particles is not physically tenable despite its ability to restore hyperbolicity.*

How is the B.N. volume fraction equation found

In this part, the development made by Baer & Nunziato (1986) is presented to understand how they found this seventh equation. All the exchange forms, thermal flux and external sources (which are specific to the type of flow willing to study) are stripped from their

model to keep only the pressure gradient. First, the authors wrote the equations of mass and momentum for each phase following Truesdell (1984)

$$D_t^\varphi([\alpha\rho]^\varphi) = 0, \quad (2.155)$$

$$[\alpha\rho]^\varphi d_t^\varphi u^\varphi = -\partial_x(\pi^\varphi). \quad (2.156)$$

These equations are written under conservative forms which is not the case in many modern models in the literature. Then, they use the first principle to write the internal energy equations: *The remaining conservation law is a statement of the first law of thermodynamics as applied to each phase.* However, they wrote the internal energy equations as

$$[\alpha\rho]^\varphi d_t^\varphi e^\varphi = -\pi^\varphi \partial_x u^\varphi. \quad (2.157)$$

This implies that their potential depends on $[\alpha\rho]^\varphi$ and not α^φ or ρ^φ . Indeed, if π^φ is assumed to be the pressure of the phase, then $p^\varphi = \pi^\varphi$ and the first principle without dissipation would become

$$[\alpha\rho]^\varphi d_t^\varphi e^\varphi = p^\varphi \frac{d_t^\varphi [\alpha\rho]^\varphi}{[\alpha\rho]^\varphi} = -\pi^\varphi \partial_x u^\varphi \quad (2.158)$$

However, many modern models consider that the internal energy depends on the local density ρ^φ rather than the partial density $[\alpha\rho]^\varphi$.

Once they wrote their evolution equation, they express the second principle of thermodynamic which in our case reduces to

$$\sum_\phi [\alpha\rho]^\phi d_t^\phi s^\phi \geq 0 \quad (2.159)$$

After that, they proceed to a change of variable and write this inequality with the Helmholtz free energy $\psi = e^\varphi - s^\varphi T$ instead of the entropy s . The equation (2.159) is restated as

$$\sum_\phi \frac{[\alpha\rho]^\varphi}{T^\phi} [-d_t^\phi \psi^\phi + d_t^\phi e^\phi - s^\phi d_t^\phi T^\phi] \geq 0 \quad (2.160)$$

They assumed after some computation that in order to respect the second principle, the free energy must depend on the density, the volume fraction and the temperature only.

$$\psi^\varphi = \psi(\rho^\varphi, \alpha^\varphi, T^\varphi) \quad (2.161)$$

This leads to the inequality

$$\sum_\phi \frac{[\alpha\rho]^\varphi}{T^\phi} \left[-\frac{\partial \psi^\phi}{\partial \alpha^\phi} d_t^\phi \alpha^\phi - \frac{\partial \psi^\phi}{\partial \rho^\phi} d_t^\phi \rho^\phi - \frac{\partial \psi^\phi}{\partial T^\phi} d_t^\phi T^\phi + d_t^\phi e^\phi - s^\phi d_t^\phi T^\phi \right] \geq 0 \quad (2.162)$$

which is expressed as follows with the mass conservation

$$\sum_{\phi} \frac{[\alpha\rho]^{\varphi}}{T^{\phi}} \left[-\frac{\partial\psi^{\phi}}{\partial\alpha^{\phi}} + \frac{\partial\psi^{\phi}}{\partial\rho^{\phi}} \frac{\rho^{\phi}}{\alpha^{\phi}} \right] d_t^{\phi}\alpha^{\phi} + \frac{[\alpha\rho]^{\varphi}}{T^{\phi}} \left[\frac{\partial\psi^{\phi}}{\partial T^{\phi}} + s^{\phi} \right] d_t^{\phi}T^{\phi} + \left[-\frac{\pi^{\phi}}{T^{\phi}} + \frac{\partial\psi^{\phi}}{\partial\rho^{\phi}} \frac{[\alpha\rho]^{\phi}\rho^{\phi}}{T^{\phi}} \right] \partial_x u^{\phi} \geq 0 \quad (2.163)$$

They defined then the following quantities

$$p^{\varphi} = (\rho^{\varphi})^2 \frac{\partial\psi^{\varphi}}{\partial\rho^{\varphi}} \qquad \beta^{\varphi} = \alpha^{\varphi} \rho^{\varphi} \frac{\partial\psi^{\varphi}}{\partial\alpha^{\varphi}}, \quad (2.164)$$

which leads to

$$\sum_{\phi} \frac{1}{T^{\phi}} \left[-\beta^{\phi} + p^{\phi} \right] d_t^{\phi}\alpha^{\phi} + \frac{[\alpha\rho]^{\varphi}}{T^{\phi}} \left[\frac{\partial\psi^{\phi}}{\partial T^{\phi}} + s^{\phi} \right] d_t^{\phi}T^{\phi} + \left[-\pi^{\phi} + \alpha^{\phi} p^{\phi} \right] \frac{\partial_x u^{\phi}}{T^{\phi}} \geq 0. \quad (2.165)$$

Now, the aim is to close the undetermined form in order to respect the second principle. They set then

$$\pi^{\phi} = \alpha^{\phi} p^{\phi} \qquad \text{and by definition } \frac{\partial\psi^{\phi}}{\partial T^{\phi}} = -s^{\phi} \quad (2.166)$$

The only problem comes now from the volume fraction. Using the volume filling constraint, the inequality becomes

$$d_t^+ \alpha^+ [p^+ - p^- - (\beta^+ - \beta^-)] + \Delta u [p^- - \beta^-] \partial_x \alpha^+ \geq 0 \quad (2.167)$$

This inequality has no reason to be satisfied, in [Baer & Nunziato \(1986\)](#), the last form goes in other groups of terms and helps to close mass transfer. However, the first form is written exactly the same. To be sure of its sign, [Baer & Nunziato \(1986\)](#) postulated the existence of a function μ which satisfies

$$\alpha^+ \alpha^- [p^+ - p^- - (\beta^+ - \beta^-)] = \mu d_t^+ \alpha^+ \quad (2.168)$$

Therefore, dissipation and thus the respect of the second principle of thermodynamic are insured. However, dissipation occurs nearly everywhere in the flow. Indeed, at each change of volume ($d_t^{\varphi}\alpha^{\varphi}$ or $d_t^{\varphi}\rho^{\varphi} \neq 0$), the model dissipates, even in expansions which are supposed to be isentropic. It must be stressed that when dealing with dissipation, an infinity of closures are possible because the condition to fulfill is an inequality. However, isentropic closures are unique (for a given set of energies). Here, the only physically tenable isentropic closure is to set the pressure equality which leads to the 6 equation model.

Another way to obtain the volume fraction equation

Another way to obtain a volume fraction equation is to follow the work of [Drew \(1983\)](#). In this work the author uses volume averaging. Therefore, the function of presence of a fluid

φ called χ^φ varies only at the interface between two phases. The natural evolution of this quantity is

$$\partial_t \chi^\varphi + u_i \partial_x \chi^\varphi = 0. \quad (2.169)$$

This means that the function of presence is transported by the velocity of the interface u_i . More generally

$$\partial_t \chi^\varphi + u \partial_x \chi^\varphi = 0 \quad (2.170)$$

with u the local velocity of the flow.

The question is then, how to average this quantity ?

$$\partial_t \overline{\chi^\varphi} + \overline{u \partial_x \chi^\varphi} = 0 \quad (2.171)$$

In the classical averaging,

$$\alpha^\varphi = \overline{\chi^\varphi}, \quad \rho^\varphi = \frac{\overline{\rho \chi^\varphi}}{\alpha^\varphi}, \quad a^\varphi = \frac{\overline{a \rho \chi^\varphi}}{[\alpha \rho]^\varphi} \quad (2.172)$$

which leads to

$$\partial_t \alpha^\varphi + u^\varphi \partial_x \alpha^\varphi + \overline{(u^\varphi)' \partial_x \chi^\varphi} = 0 \quad (2.173)$$

however, the variation $(u^\varphi)'$ is such that

$$\overline{(u^\varphi)' \rho \chi^\varphi} = 0 \quad (2.174)$$

therefore, it is not possible to remove the last form. The variation of velocity around the interface can be closed by assuming that it is proportional to the pressure variation at the interface which leads to the B.N. type model.

2.A Appendix: computation of the new pressure gradient (2.3.3)

The total pressure gradient is obtained by summation over all the fluids.

$$[\nabla P]_c^n = \sum_{\phi, d} \alpha_c^{\phi n} \sigma_{cd}^{\phi n - 1/2} \mathbf{s}_{cd}^{n-1/2} (p_d^n - p_c^n) \quad (2.175)$$

To modify this total gradient, the form in σ is symmetrized and using the identity on the of centering factor $\sigma_{cd}^{\phi n - 1/2} + \sigma_{dc}^{\phi n - 1/2} = 1$ (which indicates that the fluid either goes from c to d or from d to c).

$$\frac{1}{2} \sum_{\phi, d} [\alpha_c^{\phi n} + \alpha_c^{\phi n} (\sigma_{cd}^{\phi n - 1/2} - \sigma_{dc}^{\phi n - 1/2})] \mathbf{s}_{cd}^{n-1/2} (P_d^n - P_c^n) \quad (2.176)$$

Then, the second occurrence of the volume fraction is symmetrized.

$$\begin{aligned} & \frac{1}{2} \sum_{\phi,d} \left[\alpha_c^{\phi n} + \frac{1}{2}(\alpha_c^{\phi n} + \alpha_d^{\phi n})(\sigma_{cd}^{\phi n-1/2} - \sigma_{dc}^{\phi n-1/2}) \right] \mathbf{s}_{cd}^{n-1/2} (P_d^n - P_c^n) \\ & + \frac{1}{4} \sum_{\phi,d} \left[(\alpha_c^{\phi n} - \alpha_d^{\phi n})(\sigma_{cd}^{\phi n-1/2} - \sigma_{dc}^{\phi n-1/2}) \right] \mathbf{s}_{cd}^{n-1/2} (P_d^n - P_c^n) \end{aligned} \quad (2.177)$$

The last term is of order 3 and therefore is neglected. The first term can be transformed (using the identity on the centering factor) into

$$\begin{aligned} & \frac{1}{2} \sum_{\phi,d} \left[\alpha_c^{\phi n} + \frac{1}{2}(\alpha_c^{\phi n} + \alpha_d^{\phi n})(2\sigma_{cd}^{\phi n-1/2} - 1) \right] \mathbf{s}_{cd}^{n-1/2} (P_d^n - P_c^n) \\ = & \frac{1}{2} \sum_{\phi,d} (\alpha_c^{\phi n} + \alpha_d^{\phi n}) \sigma_{cd}^{\phi n-1/2} \mathbf{s}_{cd}^{n-1/2} (P_d^n - P_c^n) + \frac{1}{2} \sum_{\phi,d} (\alpha_c^{\phi n} - \alpha_d^{\phi n}) \mathbf{s}_{cd}^{n-1/2} (P_d^n - P_c^n) \end{aligned} \quad (2.178)$$

The last term of the expression vanishes because the sum of the volume fraction is equal to one. Then, the final gradient is obtained by factorizing the volume fraction in the cell c of the fluid φ

$$\alpha^\varphi \nabla^\varphi P = \alpha_c^{\varphi n} \sum_d \bar{\sigma}_{cd}^{\varphi n-1/2} \mathbf{s}_{cd}^{n-1/2} (P_d^n - P_c^n) \quad (2.179)$$

with

$$\bar{\sigma}_{cd}^{\varphi n-1/2} = \frac{1}{2} \sigma_{cd}^{\varphi n-1/2} + \frac{1}{2} \sum_\phi \alpha_d^{\phi n} \sigma_{cd}^{\phi n-1/2} \quad (2.180)$$

CHAPTER 3

Taming the “stiff stiffness” of pressure work and relaxation in numerical schemes for compressible multi-fluid flows ¹

Contents

3.1	Aim: pressure in multi-fluid models and schemes	73
3.2	Background: multi-fluid models and schemes	75
3.3	Explicit backbone evolution equations; stiffness	80
3.4	Single time-step integration of pressure work	85
3.5	One-dimensional numerical tests	92
3.6	Conclusion	105
3.A	Other pressure issues in compressible multi-fluid models and schemes	106
3.B	The backbone model	108
3.C	The GEEC scheme for the backbone model	112
3.D	Semi-analytical solution of isentropic two-fluid expansion	115
3.E	Noh’s test for ideal–stiffened gas mixtures	117

Designing models and schemes for compressible multi-fluid flow is often considered as challenging when dealing with contrasted equations of state, low volume fractions, or high compression or expansion ratios. This is due to the potentially severe stiffness of pressure couplings, aggravated by (i) their quadratic multiplicity as they connect all energy reservoirs (ii) the entropy conditions to be preserved on each fluid, (iii) their potentially unknown signs, and (iv) their potential “stiff stiffness,” defined in the present work. Whether captured under pressure-equilibration or pressure-relaxation models—where fluids respectively share a common pressure or undergo a damped evolution towards a common pressure—the stiff terms of the evolution equations have always required dedicated numerical approaches, with sometimes mixed results depending on specific applications.

Some broad general guidelines are here proposed to tame the stiff stiffness issues of the pressure terms. The framework is that of pressure-equilibrated average-field (or Euler–

¹submitted to Int J Multiph Flow, 22nd December 2021

Euler) models, discretized with a splitting of momentum and internal energy equations: this makes the stiff terms behave locally as simple ODEs, amenable to integration by simple schemes. The present approach resorts to (partly) exponential integrators to provide explicit estimations of implicit pressures. The final explicit scheme, though not as robust as would its fully implicit version, displays a vastly improved resilience to stiffness.

Numerical tests were carried out on strenuous versions of usual 1D shock tubes on two-fluid mixtures of air and water (described by ideal and stiffened gases). In view of the excellent results, further 1D test in more extreme conditions were considered: free expansions, and shocks on zero pressure state (Noh’s test). At usual acoustic CFL values, expansions were robustly simulated for air volume fractions from less than 10^{-12} to up to nearly 1. Similarly, shocks on zero pressure states were simulated to different final states for air volume fractions as low as 10^{-8} , with air density factors across shocks ranging between a few hundreds and hundredths depending on the choice of dissipation in each fluid. All tests were carried out on a previously developed Geometry, Energy, and Entropy Consistent (GEEC) scheme [IJMF, 132, 103324 (2020)].

3.1 Aim: pressure in multi-fluid models and schemes

The modeling and computation of multi-fluid flows appears as a never ending endeavor: there were over 7000 articles in the field published during year 2020 according to Google Scholar,² up about two and five fold from 2010 and 2000 respectively. A superficial inspection of the query results shows that about a tenth involve at least some model discussion, adaptation, comparison, etc. and about a fourth deal with compressible systems—as defined by the non-vanishing presence of at least one compressible phase, a case of high relevance in numerous applications.

This exuberance comes from the enormous variety of systems found in nature and industry which require the development of correspondingly specific models and schemes: beyond fundamental conservation laws (mass, momentum, etc. which are sufficient for detailed direct numerical simulation approaches) and basic numerical tools (finite volumes, Riemann solvers, particles-in-cell, etc.), all sorts of system-specific averaging assumptions and closures must be invoked (fluctuations, turbulence, drag...), making models very specific and different from each other. The present work will deal with the specific but very broad class of averaged-field models, also known as Euler–Euler.

A critical ingredient in all Euler–Euler compressible multi-fluid models is *mean pressure*. In such systems, terms involving mean pressure appear primarily in momentum fluxes, buoyancy forces, pressure work on internal energy, and EOS (Equations Of State): although seldom acknowledged, this produces numerous, intricate, and stiff couplings between *all* the fluids’ energy reservoirs which can severely strain numerical schemes (Vazquez-Gonzalez *et al.*, 2020, §§ 1.3 & 3.6, note 4). The extreme stiffening potential of pressure couplings

²as returned by query: "multiphase flow" model scheme.

in common systems is illustrated by air–water mixtures where hydrodynamic time scales can be stiffened by factors in excess of 10^4 , as highlighted in previous publications (see for instance [Vazquez-Gonzalez *et al.*, 2020](#), § 3.6) and illustrated in Section 3.2.2.

Somewhat surprisingly however, most of the available strategies for model closures and scheme discretizations appear to dilute the pressure stiffness issue among broader concerns of physical relevance, model well-posedness, and adaptation of standard numerical methods: a dominant controversy in the field is the ill-posedness of many multi-fluid models, still active after over half a century and which has sometimes motivated inconsistent “corrected pressure closures” in the models (see for instance [Vazquez-Gonzalez *et al.*, 2020](#), §§ 1.2 & A, & refs therein). A brief overview and discussion on pressure closures is provided in 3.A for modeling strategies in common use.

The central issue of the present work is the proper *physical* and *numerical* treatment of EOS pressure couplings as deduced from first principles. The aim is to provide building blocks for closures and schemes adapted to their specific potential stiffness and yet as “universal” as possible, i.e. applicable to most schemes up to minor adaptations. The rationale for demanding this universality hinges on the fact that, pressure being the derivative of a well defined potential (here internal energies given by EOS), mean pressure terms should be expected to be *uniquely defined by first principles of mechanics and thermodynamics* ([Vazquez-Gonzalez *et al.*, 2020](#), § 3 & refs therein). Although this general principle (applicable in both physical and numerical settings) constrains simple multi-fluid systems to *equal fluid pressures*, the guidelines provided here will remain applicable to approaches with non-equal (but algebraically related) fluid pressures. In this spirit, the present study will be restrained to a single-pressure multi-fluid model stripped of all dissipation and fluctuation terms, here designated as the “backbone” model as introduced in Section 3.2.1.

The main results, i.e. the discretization approaches of the pressure terms of the backbone model, are derived in Section 3.4. As prerequisites, Section 3.2 reminds the specific background of relevant concepts and Section 3.3 lists the basic physical equations to be dealt with. For readers familiar with compressible multi-fluid flows, these sections can be skipped and just referred to for notations. Section 3.5 provides results of numerical test which have been deliberately designed to severely strain the numerical schemes, well beyond the usual two-fluid Riemann problems: free expansion in vacuum and strong “Noh” shocks ([Noh, 1987](#)), both on a stiff two-fluid system with velocity equilibration. All tests were carried out in a 1D setting on ideal-gas–stiffened-gas mixtures tuned to mimic air and water. Results show robust, stable, and consistent behavior at reasonable CFL values, independently of (even extreme) volume fraction values. Since the pressure stiffness issues are weakly coupled to transport and appear as equations formally equivalent to ODEs, the 1D results readily extend to higher dimensions.

3.2 Background: multi-fluid models and schemes

3.2.1 Derivation of multi-fluid models; backbone model

The (to-be-closed) statistical equations of multi-fluid models are most commonly deduced from the single-time-and-point single-fluid equations (usually Euler or Navier–Stokes) by application of an *averaging procedure*. The specificities of this averaging step (order of correlations, averaging set, etc.) must be adapted to the type of the flow and to the quantities of interest. The approach was first applied to some (not all) conservation equations (for instance [van Deemter & van der Laan, 1961](#); [Hinze, 1963](#)), and full sets of volume-averaged two-fluid equations were eventually produced (for instance [Nigmatulin, 1967](#); [Delhaye, 1968](#); [Drew, 1971](#); [Ishii & Ibiki, 2011](#))—for more modern discussions and references see for instance [Wörner \(2003, § 3\)](#), [Morel \(2005, § 3\)](#), or [Brennen \(2005, § 1\)](#). The ensuing equations describe the evolution of per-fluid average quantities but involve second- and higher-order correlations of the fluctuations: these correlation terms are produced by the a-priori-unknown non-linear effects and require supplementary closure laws.

The correlation terms are intrinsically dissipative and system dependent, whereas *the general structure of the equations with their non-dissipative terms alone is system independent and thus universal*. Following [Vazquez-Gonzalez et al. \(2016, 2020\)](#), the dissipation-stripped multi-fluid model will be designated here as the backbone model—here given in Section 3.3.1 and derived in 3.B. It only involves transport and pressure terms, with external source terms of momentum and internal energy when required.

The absence of any dissipation in the backbone model has two noticeable consequences ([Vazquez-Gonzalez et al., 2020, § 3](#)): (i) its equations can be obtained in a unique way from a *least action principle* where the Lagrangian density of the system involves the mean kinetic and internal energies of the fluids, and (ii) the ensuing Euler–Lagrange equations constrain *all fluids at any given time and point to share the same common average pressure*, i.e. the backbone model is a so-called “single-pressure” model—also designated as “pressure equilibrated” or “isobaric.” This last property is a major motivation to build corresponding schemes with pressure equilibration, which can ensure low-dissipation and quasi-isentropic character (to scheme order). Naturally, numerical scheme design always involves all sorts of trade-offs and partial but controlled pressure equilibration may turn out to be acceptable in some cases.

Backbone-based derivations of multi-fluid models and schemes thus follow the general route represented in Fig. 3.1 where dissipation terms are deliberately removed and brought back. This strategy was recently applied to develop the “GEEC” scheme ([Vazquez-Gonzalez et al., 2020](#)) which will be used here to benchmark the stiffness-capturing techniques in Section 3.5.

An important side property of the backbone model as derived from the above averaging approach is that it also describes the evolution of interface cells in numeric schemes—when cells intersect boundaries between fluids of different properties or states ([Saurel & Abgrall,](#)

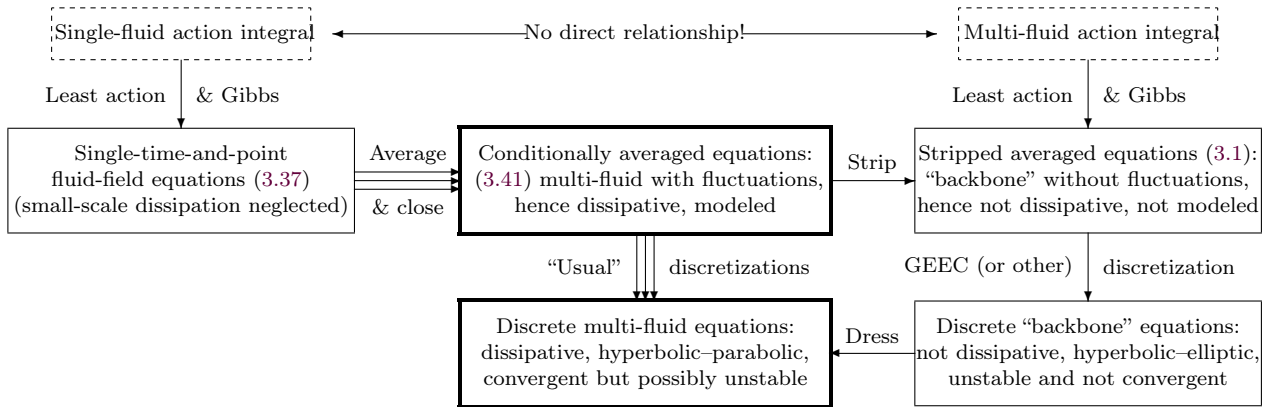


Figure 3.1: Representation of modeling and discretization procedures of multi-fluid equations. The usual direct approaches (triple arrows) produce modeled average equations and corresponding numerical schemes (thick middle frames) with good stability, convergence, and dissipation properties, but most often with poor behavior on isentropic flows. In contrast, an intermediate discretization procedure of the so-called “backbone” dissipation-free equations (right hand side frames) can simply recover isentropic behavior (to the scheme’s order). Following this approach, the GEEC scheme used here (Vazquez-Gonzalez *et al.*, 2020) is derived by a mimicking procedure of the least action principle and Gibbs’ thermodynamic relationship. The non-averaged equations (left hand side frames) are represented for reference to stress their difference with the backbone model: despite formal analogies in evolution equations, the multi-fluid action cannot be obtained from the single-fluid action. The averaging and stripping procedures are detailed in 3.B for a simplified case.

1999a,b; Saurel & Le Métayer, 2001; Chang & Liou, 2007, and references therein). This is due to the formal identity between the physical statistical averaging and the numerical cell averaging. As expected, controversies on the proper discrete equations for evolving interface cells have practically mirrored those on multi-fluid models although with emphasis on somewhat different aspects. The present work will fully apply to both situations and will consider corresponding backgrounds indifferently.

3.2.2 Present issue: “stiff stiffness” of pressure work and equilibration

A common feature to all multi-fluid models is their potential pressure-related *stiffness* and moreover, their potential *stiff stiffness*. These properties will be rigorously defined and quantified in Section 3.3, but it is useful to introduce now a qualitative and intuitive example to facilitate understanding.

A system of water containing a low volume fraction of air bubbles—say 1%—can be viewed as numerically friendly: as known for decades, the effective speed of sound of the mixture c is low (down to a minimum of about 30 m/s in standard conditions) because of both the high compressibility of the bubbles and the high inertia of the surrounding water. According to usual wisdom, an explicit numerical scheme would thus have its time step limited by a weak CFL condition $\Delta t \lesssim \Delta x/c$. Now, within this time step limit, global volume changes in excess of merely 1% could appear and thus collapse the air bubbles: the

effective speed of sound of the mixture would then approach that of water thus inducing *stiffness*. But moreover, this change of stiffness would appear over a small volume change thus making *stiffness stiff*. Stiffness is related to a high first derivative of pressure (low compressibility or high speed of sound), whereas *stiff stiffness* is related to a high *second derivative of pressure* (high fundamental derivative).

The issues of pressure-related stiffness appear to have been mentioned but seldom stressed in previous works despite being potentially present in all forms of the multi-fluid equations. They are mostly eliminated in pure isentropic models, not considered here, where the internal energies and pressures are given by (non-differential) functions of the densities—as in classical two-fluid four-equation models compared by [Vazquez-Gonzalez *et al.* \(2016\)](#). Now, this requires that isentropic curves be provided by the EOS, a situation almost never encountered in practical situations. In contrast, most hydro-schemes perform approximate integration of pressure work in the energy equations under assumptions that scheme residues be small and entropic. However, in stiff systems such as multi-fluid, the time-step constraints can make residues large or even dominant, while their entropic character has still to be preserved.

In previous works involving one of the authors (this chapter is an article submitted to IJMF and written by E.Heulhard de Montigny and A. Llor) ([Vazquez-Gonzalez *et al.*, 2016, 2020](#)), the stiffness issues were clearly identified on the backbone model (though not tackled) when expressed with the explicit form of the internal energy equations. In this form—here given in Section 3.3.2, derived in 3.B.3, and previously obtained by [Munkejord *et al.* \(2009\)](#); [Kreeft & Koren \(2010\)](#)—the pressure work on the various (possibly numerous) fluids is separated in individual and fluid-to-fluid exchange contributions, making accessible the analysis of stiffness effects and the design of adapted numerical schemes.

3.2.3 Present hydrodynamic scheme: GEEC

The pressure-related stiffness issues mentioned in Section 3.2.2 are made even more challenging by the sheer number of convoluted pressure couplings between all energy reservoirs: for instance a 10-fluids system involves 10 entropy constraints and 20 energy reservoirs (kinetic and internal), with 20 flux terms and $20 \times 19/2 = 190$ one-to-one exchange terms! Now, the possible stiffness of this exchange network is marginally affected by the flux terms which are usually under control of shallower CFL conditions: pressure couplings are basically in-cell ODE-like problems.

Unsurprisingly, many numerical approaches have resorted to varied forms of splitting strategies with the expectation that stiffness be isolated and captured in well controlled sub-steps of the evolution cycle. However, this must be achieved while also controlling the numerical residues on entropy and the sign of their final balance: it makes pressure contributions difficult to split from each other, while still being more easily split from other terms. For instance, it appears somewhat overoptimistic to follow the approach of many Riemann-based schemes whereby pressure terms in momentum and energy equations are split into flux and source parts which are discretized separately in different sub-steps: ensuring

the final entropic consistency of the global time step on each fluid is then barely tractable, if at all.

A counterexample of a proper Riemann-based strategy—though on a velocity-equilibrated model—was provided by [Despres & Lagoutiere \(2007\)](#) with a Lagrange-plus-remap scheme: all the pressure effects are computed at once in the Lagrangian sub-step. Through proper implicit centering of pressure in the thermodynamic integration path, entropic behavior was then proved. The present work follows this one-step course and pays scrupulous attention to possible collateral effects detrimental to entropy consistency.

For all illustrative purposes in Section 3.5, stiffness-resilient pressure schemes will here be adapted to the “Geometry, Energy, and Entropy Consistent (GEEC)” scheme ([Vazquez-Gonzalez et al., 2020](#))—summarized in 3.C. This scheme performs an explicit one-step discretization of the general multi-fluid backbone model with an order-one geometry- and entropy-consistent approach. Shocks are captured through an explicit artificial viscosity stress ([Mattsson & Rider, 2015](#), & refs therein) whose dissipation can be distributed on the fluids according to coefficients freely defined by the user. However, its explicit character makes it non-entropic (to scheme order) and fragile in stiff situations. This was a motivation of the present study.

3.2.4 Present approach: explicit estimates of implicit pressures

Regardless of details on background algorithms discussed in Section 3.2.3, every time step of an hydro-scheme performs a thermodynamic transformation of the fluids in the system. This evolution is actually a *jump* between initial and final states, between which an actual *path* of continuous states may or may not be defined and may or may not be effectively computed: examples of pure jumps and computed paths can be respectively found in [Despres & Lagoutiere \(2007\)](#) and [Miller & Puckett \(1996\)](#). In any case, entropic behavior is then ensured if the final states lies above the isentropic curves defined by the fluids’ initial states and the eventual irreversible energy sources. In that respect, computing isentropic curves may be regarded as most reassuring but appears computationally demanding ([Miller & Puckett, 1996](#)) and superfluous as only the final pressure and irreversible works along the path need to be known.

An important property stemming from thermodynamic principles is that reversible pressure work over isentropes are always above their various *order-one implicit* approximations, regardless of EOS stiffness. This was exploited by [Despres & Lagoutiere \(2007\)](#) and is more closely examined in Section 3.4 as it provides *universal recipes* to produce entropic evolution in hydro-schemes. Now, this comes at the expense of implicit calculations of final states, which may be particularly convoluted in the presence of numerous couplings between all the energy reservoirs (including kinetic). Moreover, adapting implicit techniques to fully explicit schemes such as the multi-fluid GEEC can introduce unexpected difficulties. Also noticeable is the fact that under-estimation of pressure work induces some dissipation whose distribution over the different fluids is not defined by first principles and thus not unique:

discrepant results can be produced by even the same hydro-scheme when fitted with different pressure equilibration algorithms, as only in the isentropic limit are all evolution paths necessarily identical.

In order to overcome the issues and complexities brought by the calculation of implicit final pressures to obtain entropic pressure work, the present study explores a somewhat less robust but much less demanding approach of *explicit estimates of implicit pressures* (or EEIP, see Section 3.4.4). Such estimations are accessible because an explicit evolution equation (possibly stiff) can be exhibited for the equilibrated pressure in the backbone model—similarly to internal energies as mentioned in Section 3.2.2. Standard numerical schemes for stiff equations can then be selected and simply embedded in an explicit scheme such as the multi-fluid GEEC, as shown in Section 3.5.1.

3.2.5 Some previous approaches

As will appear in Section 3.4, multi-fluid pressure equilibration or relaxation comes in countless types and forms because it cannot be defined in a unique way from first principles: it is an intrinsically dissipative process whose irreversible production can be distributed over the fluids in completely arbitrary ways, possibly justified by model- or scheme-specific criteria. Below is a short list of some important landmarks in the field.

Pressure equilibration in multi-fluid schemes happens to be a special case of “equilibrium with internal adiabatic constraints,” an old problem examined in classical textbooks of thermodynamics (Callen, 1960, 1985, resp. App. C & pb. 2.7-3). Its solution—defined by the distribution of entropy production—is indeterminate or not unique, a finding then perceived as counter-intuitive which stirred controversies (Curzon & Leff, 1979; Chardin, 1986; Gruber, 1999; Khalil, 2019, & refs therein).

Early numerical schemes treated multi-fluid mixtures under the “equal strain” assumption Benson (1992, § 3.11 & refs therein), a physically inconsistent closure but numerically simple and not so fragile in many cases.

Miller & Puckett (1996, § 5 & ref. 15) proposed a quasi-isentropic equilibration approach similar to the present “coupled exact isentropes” in Section 3.4.3, based on a fractional-step algorithm and embedded in a Eulerian second-order Godunov scheme.

Despres & Lagoutiere (2007, § 5 & ref. 15) proposed an implicit equilibration approach similar to the present “coupled implicit shocks” in Section 3.4.3, embedded in a Lagrangian second-order Godunov scheme.

Chang & Liou (2007) proposed an implicit equilibration approach similar to the present “coupled iso-energies” in Section 3.4.3, embedded in an AUSM⁺-up second-order scheme.

Yanilkin *et al.* (2013); François *et al.* (2013) reviewed and tested various *relaxation* schemes in respectively ALE and Lagrangian-or-Eulerian settings. Lallemand *et al.* (2005); Saurel *et al.* (2009); Le Métayer *et al.* (2013) introduced various schemes for the pressure relaxation model of Baer & Nunziato (1986).

Recently, Hantke *et al.* (2021) considered the pressure equilibrated limit of the model

of Baer & Nunziato (1986), and Chiochetti & Müller (2020) introduced an exponential integrator to capture its stiff pressure relaxation. An exponential scheme is also proposed and tested here in Sections 3.4.3 and 3.5. No previous occurrence of this stiffness compliant approach was found for pressure relaxation or equilibration.

3.3 Explicit backbone evolution equations; stiffness

3.3.1 Backbone model with explicit pressure work

The complete set of equations of the backbone model—whose derivation along the usual conditional averaging approach is provided for reference in 3.B—can be written as

$$D_t^\varphi(\alpha^\varphi \rho^\varphi) = 0, \quad (3.1a)$$

$$D_t^\varphi(\alpha^\varphi \rho^\varphi u_i^\varphi) + \alpha^\varphi p_{,i} = \alpha^\varphi \rho^\varphi g_i, \quad (3.1b)$$

$$D_t^\varphi(\alpha^\varphi \rho^\varphi e^\varphi) - \alpha^\varphi p \frac{d_t^\varphi \rho^\varphi}{\rho^\varphi} = \alpha^\varphi \rho^\varphi \dot{w}^\varphi, \quad (3.1c)$$

$$p = \mathcal{P}^\varphi(\rho^\varphi, e^\varphi), \quad (3.1d)$$

$$1 = \sum_\varphi \alpha^\varphi, \quad (3.1e)$$

for mass conservation (3.1a), evolution equations of momenta and internal energies (3.1b) and (3.1c), completed with the single-pressure and volume-filling conditions (3.1d) and (3.1e). α^φ , ρ^φ , \mathbf{u}^φ , e^φ , \dot{w}^φ , and \mathcal{P}^φ are respectively the mean volume fractions, densities, velocities, internal energies, external (irreversible) energy sources, and half-EOS of fluids φ . p and \mathbf{g} are the common pressure field and gravity (momentum source). The Eulerian and Lagrangian derivative operators along fluid velocities are respectively defined as

$$D_t^\varphi \cdot = \partial_t^\varphi \cdot + (\cdot u_i^\varphi)_{,i}. \quad (3.2a)$$

$$d_t^\varphi \cdot = \partial_t^\varphi \cdot + \cdot_{,i} u_i^\varphi, \quad (3.2b)$$

with Einstein's rule of summation on repeated coordinate indices ($i, j = 1, 2, 3$) without covariant–contravariant separation—thus $p_{,i} \hat{\mathbf{e}}_i = \nabla p$ and $u_{j,j} = \nabla \cdot \mathbf{u}$. Energy equations are here provided for the fluids' *internal* energies, bearing in mind that fluids' *total* energies can be recovered in the standard form by the following combination

$$\begin{aligned} (3.1c) + \frac{p}{\rho^\varphi} \times (3.1a) + u_i^\varphi \times (3.1b)_i - \left(\frac{1}{2} u_i^\varphi u_i^\varphi\right) \times (3.1a) \\ \Rightarrow D_t^\varphi \left(\alpha^\varphi \rho^\varphi \left(e^\varphi + \frac{1}{2} u_i^\varphi u_i^\varphi \right) \right) + (\alpha^\varphi p u_i^\varphi)_{,i} + p \partial_t \alpha^\varphi \\ = \alpha^\varphi \rho^\varphi \dot{w}^\varphi, \quad (3.3) \end{aligned}$$

which conserves the system's total energy as $\sum_\varphi \partial_t \alpha^\varphi = 0$. This notation for combining equations will be used in all the following, taking care that it represents the application of the linear combination identically to both left and right hand sides exactly as given in the referred equations.

For two fluids φ , the system is known as the single-pressure six-equations two-fluid model. It is also applicable to the numerical computation of cell-averaged quantities in mixed cells at interfaces between fluids (see for instance Saurel & Abgrall, 1999a,b; Lallemand *et al.*, 2005; Chang & Liou, 2007, & refs therein). Assuming addition of an infinitely strong drag force to induce velocity equilibration, the per-fluid momentum equations (3.1b) degenerate into the usual total momentum equation

$$\partial_t(\rho u_i) + (\rho u_i u_j)_{,j} + p_{,i} = \rho g_i, \quad (3.4)$$

where $\rho = \sum_{\varphi} \alpha^{\varphi} \rho^{\varphi}$ and $\rho \mathbf{u} = \sum_{\varphi} \alpha^{\varphi} \rho^{\varphi} \mathbf{u}^{\varphi}$ are the mean total density and momentum with $\mathbf{u}^{\varphi} = \mathbf{u}$. As the stiffness related issues are weakly dependent on relative drift velocities (low Mach number) all the tests reported here were carried out on equilibrated-velocity systems.

3.3.2 Explicit pressure work in energy equations; stiffness

As extensively discussed in a previous work (Vazquez-Gonzalez *et al.*, 2020, §§ 3.5 & 3.6) the analysis and discretization of the internal energy equations (3.1c) is much more conveniently carried out on the following alternative form

$$D_t^{\varphi}(\alpha^{\varphi} \rho^{\varphi} e^{\varphi}) = - \underbrace{\beta^{\varphi} p \bar{u}_{i,i}}_V + \underbrace{\sum_{\phi} \mu^{\varphi\phi} p_{,i} (u_i^{\varphi} - u_i^{\phi})}_D - \underbrace{\sum_{\phi} \mu^{\varphi\phi} (\Gamma^{\varphi} \rho^{\varphi} \dot{w}^{\varphi} - \Gamma^{\phi} \rho^{\phi} \dot{w}^{\phi})}_R + \underbrace{\alpha^{\varphi} \rho^{\varphi} \dot{w}^{\varphi}}_I. \quad (3.5)$$

where

$$\bar{\mathbf{u}} = \sum_{\phi} \alpha^{\phi} \mathbf{u}^{\phi} \quad (\text{volume weighed velocity, } \neq \mathbf{u}), \quad (3.6a)$$

$$\begin{aligned} \beta^{\varphi} &= (\alpha^{\varphi} / \gamma^{\varphi}) / \sum_{\phi} (\alpha^{\phi} / \gamma^{\phi}) \\ &= (\alpha^{\varphi} / (\rho^{\varphi} c^{2\varphi})) / \sum_{\phi} (\alpha^{\phi} / (\rho^{\phi} c^{2\phi})), \end{aligned} \quad (3.6b)$$

$$\mu^{\varphi\phi} = (\alpha^{\varphi} / \gamma^{\varphi}) \beta^{\phi} = \beta^{\varphi} (\alpha^{\phi} / \gamma^{\phi}) = \mu^{\phi\varphi}, \quad (3.6c)$$

with

$$\gamma^{\varphi} = \left[\frac{\rho \partial p}{p \partial \rho} \Big|_s \right]^{\varphi} = \rho c^{2\varphi} / p \quad (\text{adiabatic exponent of } \varphi), \quad (3.6d)$$

$$\Gamma^{\varphi} = \left[\frac{\partial p}{\rho T \partial s} \Big|_{\rho} \right]^{\varphi} \quad (\text{Grüneisen coefficient of } \varphi), \quad (3.6e)$$

$c^{2\varphi}$ being the squared speeds of sound. It must be stressed that (3.5) is rigorously equivalent to (3.1c), but is *explicit*, i.e. without time derivatives of ρ^{φ} . The derivation of (3.5) was provided for instance by Vazquez-Gonzalez *et al.* (2020, § 3.5 & refs therein) and is summarized in 3.B.3. Terms similar to V in (3.5) also appear in the context of mixed-cell pressure relaxation algorithms, as for instance in Benson (1992, eq. 3.11.2.2 & refs cited) or Yanilkin *et al.* (2013, eq. 23 & refs cited).

The decomposition of pressure work on the right-hand side of form (3.5) provides important insight by separating the contributions of the different physical processes (Vazquez-Gonzalez *et al.*, 2020, § 3.6):

V: is the *fraction* of the *reversible* pressure work on fluid φ due to changes in *total Volume* $\bar{u}_{i,i}$, as given by coefficients β^φ ;

D: is the *exchange* of *reversible* pressure work between fluids φ and ϕ due to their *relative Drift* $\mathbf{u}^\varphi - \mathbf{u}^\phi$ along the pressure gradient;

R: is the *exchange* of *Reversible* pressure work between fluids φ and ϕ due to their *differential response* to their respective irreversible energy sources \dot{w}^φ and \dot{w}^ϕ ;

I: is the usual direct Irreversible energy source on fluid φ .

From now on, the evolution equations of the fluids' internal energies will always be considered in their explicit form (3.5) only. Evolution equations of densities and pressure, possibly required at some points, will also be considered in corresponding explicit forms, as obtained for instance in 3.B.3.

3.3.3 Stiffness of contrasted systems; air–water example

The backbone evolution equations (3.1a), (3.1b), and (3.5)—as any other general multi-fluid equations—involve terms which all contain factor α^φ : this ensures that singular behaviors are avoided in the $\alpha^\varphi \rightarrow 0$ limits. However, the *relative amplitudes* of these terms can still be quite different and may induce unexpected stiff behaviors.

The basic yardstick of stiffness for a system of compressible fluids is its global compressibility—related to its speed of sound which defines the numeric CFL stability condition. This total compressibility appears on the evolution equation of the total energy, which in isentropic conditions is given by

$$\sum_\varphi (3.5) \quad \Rightarrow \quad \sum_\varphi D_t^\varphi (\alpha^\varphi \rho^\varphi e^\varphi) = -p \bar{u}_{i,i}. \quad (3.7)$$

Compared to the total pressure work $p \bar{u}_{i,i}$, the per-fluid pressure work on fluid φ , term V in (3.5), thus scales as

$$\beta^\varphi / \alpha^\varphi = 1 / (\alpha^\varphi + \gamma^\varphi \sum_{\phi \neq \varphi} \alpha^\phi / \gamma^\phi). \quad (3.8)$$

As already noticed by Vazquez-Gonzalez *et al.* (2016, 2020, resp. §§ “Explicit pressure...” & 3.6), this ratio can take very high values for $\alpha^\varphi \rightarrow 0$ if $\gamma^\phi \gg \gamma^\varphi$ and $\alpha^\phi \lesssim 1$ for some $\phi \neq \varphi$.

A particularly important case of stiff mixture is provided by the air–water two-fluid system. It will be used for bench-marking purposes in all the following and will be described by half-EOS of stiffened gas type

$$p^\varphi = \Gamma^\varphi \rho^\varphi e^\varphi - (\Gamma^\varphi + 1) \Pi^\varphi, \quad (3.9)$$

which reduce to ideal gas for $\Pi^\varphi = 0$ and yield $c^{2\varphi} = (\Gamma^\varphi + 1)(p^\varphi + \Pi^\varphi) / \rho^\varphi$. Parameters for air and water in standard conditions are listed in Table 3.1 and it is thus found that $\gamma^w / \gamma^a = (\rho c^2)^w / (\rho c^2)^a \approx 15,500$. Therefore, for small volume fractions of air below 10^{-5} , mixture volume changes are transferred to air inclusions with this strenuous amplification factor.

ρ^a (kg/m ³)	ρ^w (kg/m ³)	c^{2a} (m ² /s ²)	c^{2w} (m ² /s ²)
1.2	1000	(343) ²	(1480) ²

Table 3.1: Approximate stiffened gas parameters for air (a) and water (w) in standard conditions.

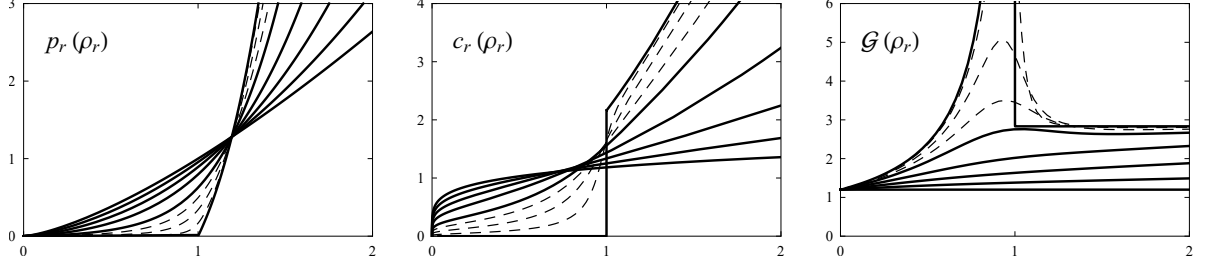


Figure 3.2: Representations of isentropic curves $p_r(\rho_r)$ in reduced coordinates deduced from (3.12) with EOS parameters in last row of Table 3.2, with their first and second normalized derivatives for $\alpha_r^a = 0$ to 1 in 0.2 increments (thick solid lines) and 0.05, 0.1, and 0.15 (thin dashed lines). Noticeably, a discontinuity in the speed of sound and a divergence of the fundamental derivative appear at $\alpha_r^a = 0$ and $\rho_r = 1$, thus inducing the stiff stiffness of the system near this singularity.

3.3.4 Isentropic binary mixture of ideal–stiffened gases

A more systematic exploration of the stiffness issues in mixtures of contrasted fluids—approximated as ideal and stiffened gases and formally labeled here as $\varphi = a$ and w —can be carried out under the doubly isentropic assumption (adiabatic or no heat exchange between fluids).

Isentropic relations $p^\varphi = \mathcal{P}^\varphi(\rho^\varphi)$ can be integrated from (3.9) using arbitrary reference states as origins. These reference states will be chosen here as (i) pressure Π^w with density ρ_π^a for ideal gas and (ii) vanishing pressure with density ρ_0^w for stiffened gas. Elementary calculations eventually yield

$$\mathcal{P}^a(\rho^a) = \Pi^w \left(\rho^a / \rho_\pi^a \right)^{1+\Gamma^a}, \quad (3.10a)$$

$$\mathcal{P}^w(\rho^w) = \Pi^w \left(\left(\rho^w / \rho_0^w \right)^{1+\Gamma^w} - 1 \right), \quad (3.10b)$$

with the usual relationship between fluid densities and global density

$$1/\rho = c^a/\rho^a + c^w/\rho^w, \quad (3.11)$$

where c^φ are the (constant) mixture-defining mass fractions. Substituting ρ^φ from (3.10), the isentropic relation between p and ρ for the mixture is obtained in reduced form as

$$1/\rho_r = \alpha_r^a p_r^{-1/(1+\Gamma^a)} + \alpha_r^w (p_r + 1)^{-1/(1+\Gamma^w)}, \quad (3.12)$$

where the reduced pressure, density, and effective volume fractions are defined as

$$p_r = p/\Pi^w, \quad (3.13a)$$

$$\rho_r = \rho (c^a/\rho_\pi^a + c^w/\rho_0^w), \quad (3.13b)$$

$$\alpha_r^a = (c^a/\rho_\pi^a) / (c^a/\rho_\pi^a + c^w/\rho_0^w), \quad (3.13c)$$

$$\alpha_r^w = (c^w/\rho_0^w) / (c^a/\rho_\pi^a + c^w/\rho_0^w). \quad (3.13d)$$

The reduced isentrope (3.12) is thus completely defined by the three dimensionless parameters Γ^a , Γ^w , and $\alpha_r^w = 1 - \alpha_r^a$. At fixed EOS or Γ^φ , isentropes make a one-parameter bundle of paths, as illustrated in Fig. 3.2 for the Γ^φ values in last row of Table 3.2. Speeds of sound and fundamental derivatives (Menikoff & Plohr, 1989, § II.B) can be obtained as simple algebraic expressions when expressed as derivatives with respect to pressure

$$c_r^2(p_r) = \left(\frac{\partial \rho_r}{\partial p_r} \right)^{-1}, \quad \mathcal{G}_r(p_r) = 1 - \frac{\rho_r}{2} \frac{\partial^2 \rho_r}{\partial^2 p_r} \left(\frac{\partial \rho_r}{\partial p_r} \right)^{-2}. \quad (3.14)$$

Interestingly, at low α_r^a stiffness and stiff stiffness appear around $\rho_r = 1$ as visible on the speed of sound and fundamental derivative in Fig. 3.2. Numerical tests of free isentropic expansions, which follow these reduced isentropes, are presented in Section 3.5.5.

3.3.5 Deluding speed of sound; fundamental derivative

The impact of stiff stiffness can go, in indirect ways, beyond equations of internal energy and pressure equilibration, respectively examined in Sections 3.3.2 and 3.4. Here, impact on wave propagation will affect the CFL condition, of prime importance for compressible hydro-schemes.

Numerous references have explored the speed of sound in mixtures under various equilibration assumptions (Wijngaarden, 2007; Flåtten & Lund, 2011, & refs therein) but apparently none have dealt with the fundamental derivative. Only the case of the pressure- and velocity-equilibrated mixtures will be considered here because it is stiffer and thus more constraining, and also because it is more easily tractable (no wave analysis coupled to multiple momentum equations).

In the case of zero and infinite drag forces—the later yielding full velocity equilibration—the respective speeds of sound with the present notations are (see for instance Ferrer *et al.*, 2012, eqs 3.4 & 3.7)

$$c_0^2 = \sum_\varphi \beta^\varphi c^{2\varphi}, \quad (3.15a)$$

$$c_\infty^2 = \sum_\varphi \frac{\rho^\varphi}{\rho} \beta^\varphi c^{2\varphi}. \quad (3.15b)$$

The former is a convex combination of the fluids' speeds of sound, whereas the later, because of the ρ^φ/ρ factors, can produce sometimes severe reductions below the lowest of the fluids' speeds of sound. For instance in the air–water mixture in normal conditions c_∞ can be as low as 30 m/s, making erroneously believe that time steps can increase at given CFL value.

Lengthy but straightforward calculations can also provide the fundamental derivative of the mixture as

$$\mathcal{G}_\infty = \sum_\varphi \frac{\beta^\varphi}{\alpha^\varphi} \beta^\varphi \mathcal{G}^\varphi. \quad (3.16)$$

This again is not a convex combination of the fluids' fundamental derivatives, with corresponding amplification of \mathcal{G}_∞ values as observed in Section 3.3.4. Artificial viscosity techniques for shock capture could be significantly affected (Mattsson & Rider, 2015).

Amplification of the fundamental derivative can be so large as to affect the CFL condition. This can be estimated by a simple model of wave propagation in a Lagrangian cell experiencing volume change at a constant rate $u_{i,i}$. The speed of sound in the cell varies as

$$\frac{dc}{dt} = \frac{\partial c}{\partial \rho} \frac{d\rho}{dt} = -(\mathcal{G} - 1)cu_{i,i}, \quad (3.17a)$$

which is integrated as

$$c(t) = c(0) \exp[-(\mathcal{G} - 1)u_{i,i}t]. \quad (3.17b)$$

An acoustic perturbation departing from an edge of the cell will thus propagate at variable velocity and reach position

$$\int_0^t c(t') dt' = c(0) \frac{\exp[-(\mathcal{G} - 1)u_{i,i}t] - 1}{-(\mathcal{G} - 1)u_{i,i}}, \quad (3.18a)$$

at time t while the other edge will be at position

$$\Delta x(t) = \Delta x(0) \exp[u_{i,i}t]. \quad (3.18b)$$

The CFL ratio η identifies how far the perturbation has moved within the cell width, and thus

$$\eta = \frac{\exp[-(\mathcal{G} - 1)u_{i,i}\Delta t] - 1}{-(\mathcal{G} - 1)u_{i,i}\Delta t} \frac{c(0)\Delta t}{\Delta x(0)}, \quad (3.19a)$$

which yields when expanded at vanishing Δt

$$\Delta t = \left(1 - \frac{1}{2}(1 + \mathcal{G})u_{i,i} \frac{\eta \Delta x}{c}\right)^{-1} \frac{\eta \Delta x}{c}. \quad (3.19b)$$

This last expression shows the correction factor with respect to the usual CFL definition $\Delta t = \eta \Delta x / c$, which can be severely restrictive for compression $u_{i,i} < 0$ if \mathcal{G} is high. Symmetrically, the condition can be strongly relaxed for expansion. A CFL constraint may not always benefit from the reduction in speed of sound if the fundamental derivative increases concurrently.

3.4 Single time-step integration of pressure work

3.4.1 An important building block: the ‘‘implicit shock’’

Consider a general integration scheme of internal energy over the isentropic evolution of a single fluid. Regardless of scheme details, a single time step can be reduced to

$$e^1 - e^0 = -[(1 - \lambda)p^1 + \lambda p^0](v^1 - v^0), \quad (3.20a)$$

$$p^n = \mathcal{P}(v^n, e^n) \quad \text{for } n = 1, 2, \quad (3.20b)$$

which is consistent with the isentropic transform for $v^1 \rightarrow v^0$. In all this section, upper indices 0 and 1 label states at two given initial and final times, $v = 1/\rho$ is the per mass volume, \mathcal{P} is the (half-)EOS, and fluid index φ is omitted for readability. Weighing factor λ is in principle between 0 and 1 depending on the scheme details, at which bounds it yields respectively explicit and implicit schemes.

The entropic character of schemes similar to (3.20) was previously analyzed by Lagoutière (2000, § III.1.5.1) using Taylor–Lagrange expansions of entropy around state 1—assumed to be accessible. A different constructive method is followed here (expanded from Bethe, 1942, § II.6), in which entropy changes are analyzed along the locus of accessible states 1.

Using v^1 to parameterize the locus of states 1, differentiation of (3.20a) and the basic thermodynamic relations between de^1 , dp^1 , dv^1 , and entropy ds^1 yield (see also Bethe, 1942, eq. 31)

$$\begin{aligned} de^1 &= -(1-\lambda)(v^1 - v^0)dp^1 - [(1-\lambda)p^1 + \lambda p^0]dv^1, \\ \Leftrightarrow & [1 + (1-\lambda)\Gamma^1(1 - v^0/v^1)]T^1 ds^1 \\ &= [(1-\lambda)(1 - v^0/v^1)(c^1)^2/v^1 + \lambda(p^1 - p^0)]dv^1. \end{aligned} \quad (3.21)$$

For $v^1 = v^0$ where $s^1 = s^0$, this relation yields $ds^1/dv^1 = 0$: $s^1(v^1)$ is thus tangent to the isentrope—just as the Hugoniot curve which is also osculator. The factor on $T^1 ds^1$ is positive under condition

$$v^0/v^1 = \rho^1/\rho^0 \leq 1 + \frac{1}{(1-\lambda)\Gamma^1} = v^0/v_\infty^1, \quad (3.22)$$

which represents the upper admissible bound for compression—higher compression ratios are excluded as discussed below. The factor on dv^1 has two contributions of opposite sign, each of different signs depending on volume changes

$$\text{expansion:} \quad 1 - v^0/v^1 \geq 0 \quad p^1 - p^0 \leq 0, \quad (3.23a)$$

$$\text{compression:} \quad 1 - v^0/v^1 \leq 0 \quad p^1 - p^0 \geq 0. \quad (3.23b)$$

Thus, for $\lambda = 0$ the sign of the factor is well defined, yielding

$$\text{expansion:} \quad ds^1/dv^1 \geq 0, \quad (3.24a)$$

$$\text{compression:} \quad ds^1/dv^1 \leq 0, \quad (3.24b)$$

and (3.20) is always entropic—i.e. $s^1(v^1) \geq s^0$ for any admissible $v^1 > v_\infty^1$. For $\lambda = 1$, the situation is opposite and (3.20) always destroys entropy. For intermediate values of λ , the balance between the two contributions is highly dependent on the details of the EOS and will not be analyzed here.

An important feature of the $s^1(v^1)$ relationship is its divergence to infinity as $v^1 \rightarrow v_\infty^1$, with corresponding divergence of pressure p^1 and energy e^1 . All pressures are thus accessible but higher compression factors are not, with $v^0/v_\infty^1 = 1 + 1/\Gamma^1$ for $\lambda = 0$. Remarkably, for $\lambda = 1/2$, (3.20) represents the energy integration under the Rayleigh line with the

well known result that the compression limit on the Hugoniot curve (or shock adiabat) is $v^0/v_\infty^1 = 1 + 2/\Gamma^1$ with the ensuing condition $\Gamma > -2$ (Bethe, 1942, eq. II)—but the Hugoniot is not entropic for expansion when the fundamental derivative is positive (Bethe, 1942, eq. I & refs therein). By analogy, the transform defined by (3.20) for $\lambda = 0$ will thus be designated here as an “implicit shock.”

The universal entropic character of the implicit shock—regardless of EOS, step size, and the possible addition of external entropy sources—was recognized by Despres & Lagoutiere (2007) as an important ingredient in order to ensure the stability of multi-fluid thermodynamic evolution with pressure-equilibration, especially when embedded into complex algorithms.

3.4.2 Another building block: the “implicit isentrope”

Despite its universal entropic character, the implicit shock presented in Section 3.4.1 has two significant drawbacks: (i) it can be highly over-dissipative in compression, so much so that an asymptotically divergent pressure is obtained at finite volume and (ii) simple numerical estimates of implicitly shocked states can thus be of low accuracy. This motivates the introduction of other one-step schemes in order to better approximate the isentropic curve even for significant volume changes.

The implicit isentrope is here defined by approximating the pressure work over the isentrope with the *pressure on the isentrope at same final volume*. Keeping the same notations of Section 3.4.1, the final state (v^1, e^1, p^1) is thus obtained as

$$e^1 - e^0 = -p^*(v^1 - v^0), \quad (3.25a)$$

$$p^* = \mathcal{P}^*(v^1, s^0), \quad (3.25b)$$

$$p^1 = \mathcal{P}(v^1, e^1), \quad (3.25c)$$

where \mathcal{P}^* is the (half-)EOS expressed in volume–entropy variables and s^0 is the entropy of the initial state. In contrast to (3.20a), no intermediate pressures between p^0 and p^* will be considered for the pressure work in (3.25a) as they would again introduce a here irrelevant dependence on EOS details.

The entropic character can be analyzed from pressure work bounding. Denoting e^* the energy on the isentrope at volume v^1 , it is found

$$e^* = e^0 - \int_0^1 \mathcal{P}^*(v, s^0) dv \leq e^0 - p^*(v^1 - v^0) = e^1, \quad (3.26)$$

which holds because $\partial p/\partial v|_s < 0$ from the second principle of thermodynamics (the speed of sound is real). Thus $s^1 > s^0$ since $\partial e/\partial s|_v = T > 0$, and the implicit isentrope is entropic.

Now, the implicit shock being always entropic and assuming $\partial p/\partial s|_v > 0$ (positive Grüneisen coefficient, valid for most materials), its pressure at final state p_{IS}^1 verifies $p_{IS}^1 \geq$

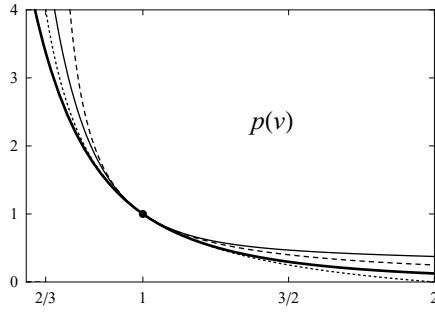


Figure 3.3: Illustration of the relative positions of the implicit isentrope (solid thin), implicit shock (dashed thin), Hugoniot (dotted thin), and isentrope (solid thick) in $p(v)$ representation from point $(1, 1)$ for an ideal gas with $\Gamma = 2$. Implicit isentrope and implicit shock are always entropic whereas Hugoniot is entropic in compression only. The implicit shock displays a vertical asymptote at $v = 1 + 1/\Gamma = 2/3$, not represented here.

p^* . Therefore

$$e_{IS}^1 = e^0 - p_{IS}^1(v^1 - v^0) \quad \left| \begin{array}{l} \leq e^0 - p^*(v^1 - v^0) = e^1 \quad \text{if } v^1 \geq v^0, \\ \geq e^0 - p^*(v^1 - v^0) = e^1 \quad \text{if } v^1 \leq v^0, \end{array} \right. \quad (3.27)$$

and the implicit isentrope is more entropic than the implicit shock for expansion, but less entropic for compression. This last property is useful as the implicit shock can be excessively over dissipative when approaching its asymptote at v_∞^1 .

The relative positions of the implicit shock, implicit isentrope, Hugoniot, and isentrope locus are illustrated in Fig. 3.3. As expected, the implicit isentrope and shock being tangent at v^0 , their entropy residues are of order two (order three for the Hugoniot).

3.4.3 Multi-fluid pressure equilibration

All single-pressure multi-fluid schemes include a pressure equilibration procedure, either embedded within the general evolution step or carried out in a separate sub-step after a (possibly) quasi-equilibrated evolution sub-step. Regardless of scheme details, equilibration consists in finding a common pressure for a final state and at given total volume and energy changes—or no changes if equilibration is carried out separately at constant total volume and energy. Obviously, an ideal scheme would be able to capture isentropic flows to the scheme order while remaining entropic: this is precisely the key feature of the step processes given in Sections 3.4.1 and 3.4.2.

Without loss of generality, pressure equilibration is here considered only in the case of constant total volume and energy. Extending notations of Section 3.4.1, this amounts to solving the implicit set of $2\Phi + 2$ equations on the $2\Phi + 1$ variables $(v^{\varphi 1}, e^{\varphi 1}, p^1)$ (Φ being

the number of fluids φ)

$$e^{\varphi 1} - e^{\varphi 0} = -\langle p \rangle^{\varphi} (v^{\varphi 1} - v^{\varphi 0}), \quad (3.28a)$$

$$p^1 = \mathcal{P}^{\varphi}(v^{\varphi 1}, e^{\varphi 1}), \quad (3.28b)$$

$$0 = \sum_{\varphi} c^{\varphi} (v^{\varphi 1} - v^{\varphi 0}), \quad (3.28c)$$

$$0 = \sum_{\varphi} c^{\varphi} (e^{\varphi 1} - e^{\varphi 0}), \quad (3.28d)$$

where c^{φ} are the (constant) fluid mass fractions. Effective pressures $\langle p \rangle^{\varphi}$ do not represent actual thermodynamic pressures but merely let factorize the volume changes in the energy changes, regardless of actual path and irreversible contributions. $\langle p \rangle^{\varphi}$ must be closed with the existing variables in order to make the system well defined. A simple constraint is a common pressure $\langle p \rangle^{\varphi} = \langle p \rangle$, thus energy conservation follows from volume conservation—this constraint is actually mandatory for two fluids $\Phi = 2$. Four closures will be considered here, three classical and one specific to the multi-fluid GEEC scheme.

Coupled implicit shocks This is the straightforward closure $\langle p \rangle^{\varphi} = p^1$ which reduces the system to coupled implicit shocks on each fluid. This procedure, apparently pioneered under somewhat different assumptions by [Lagoutière \(2000, § III.1.5.1\)](#) and [Despres & Lagoutière \(2007, § 4.1\)](#), is obviously entropic on each fluid according to Section 3.4.1. It is also rather simple, the equations being generally solved by iterative Newton–Raphson-like algorithms with EOS calls on each fluid at each iteration. However, for large initial imbalances it is limited by the $1 + 1/\Gamma^{\varphi}$ maximal per-fluid compression (3.22).

Coupled implicit isentropes In order to reduce the impact of over-dissipation with implicit shocks, it appears natural to use implicit isentropes and set now $\langle p \rangle^{\varphi} = p^*$. This procedure is akin to full isentropic path reconstructions ([Miller & Puckett, 1996](#)). However, it is not compatible with an exact equilibration of fluid pressures and a final equilibration sub-step must be added. Using for this purpose the implicit shock, the final equilibration scheme becomes

$$e^{\varphi*} - e^{\varphi 0} = -p^* (v^{\varphi*} - v^{\varphi 0}), \quad (3.29a)$$

$$p^* = \mathcal{P}^{\varphi*}(v^{\varphi*}, s^{\varphi 0}), \quad (3.29b)$$

$$0 = \sum_{\varphi} c^{\varphi} (v^{\varphi*} - v^{\varphi 0}), \quad (3.29c)$$

$$e^{\varphi 1} - e^{\varphi*} = -p^1 (v^{\varphi 1} - v^{\varphi*}), \quad (3.29d)$$

$$p^1 = \mathcal{P}^{\varphi}(v^{\varphi 1}, e^{\varphi 1}), \quad (3.29e)$$

$$0 = \sum_{\varphi} c^{\varphi} (v^{\varphi 1} - v^{\varphi 0}), \quad (3.29f)$$

(these are two successive systems of $2\Phi + 1$ equations on $2\Phi + 1$ variables, respectively $(v^{\varphi*}, e^{\varphi*}, p^*)$ and $(v^{\varphi 1}, e^{\varphi 1}, p^1)$). Now, this procedure comes at a significant price as, on top of iterative solution for the final implicit-shock procedure, the isentropic (half-)EOS $\mathcal{P}^{\varphi*}$ must be either known or reconstructed from integration of \mathcal{P}^{φ} .

Coupled exact isentropes If isentropes are known or reconstructed from integration, it appears possible to explicitly introduce dissipation and solve the $2\Phi + 2$ equations on the $2\Phi + 2$ variables $(v^{\varphi 1}, e^{\varphi 1}, p^1, \delta Q)$

$$e^{\varphi 1} = \mathcal{E}^{\varphi*}(v^{\varphi 1}, s^{\varphi 0}) + \theta^{\varphi} \delta Q, \quad (3.30a)$$

$$p^1 = \mathcal{P}^{\varphi}(v^{\varphi 1}, e^{\varphi 1}), \quad (3.30b)$$

$$0 = \sum_{\varphi} c^{\varphi} (v^{\varphi 1} - v^{\varphi 0}), \quad (3.30c)$$

$$0 = \sum_{\varphi} c^{\varphi} (e^{\varphi 1} - e^{\varphi 0}), \quad (3.30d)$$

where δQ is the total irreversible energy and θ^{φ} are fixed positive weighing coefficients such that $\sum_{\varphi} \theta^{\varphi} c^{\varphi} = 1$. The choice of θ^{φ} values can here be dictated by other considerations—for instance completely arbitrary or closely related to the physical processes in the system—which reflect the intrinsically underdeterminate distribution of entropy production (Callen, 1960, 1985, resp. App. C & pb. 2.7-3). It thus provides access to all the possible entropic solutions of the pressure equilibration problem—including the coupled implicit shocks and isentropes although the determination of corresponding θ^{φ} could be complex.

Coupled iso-energies The GEEC scheme—as various others (for instance Chang & Liou, 2007, § 2.8)—has the peculiarity of using explicit evolution equations to generate $e^{\varphi 1}$ from known pressure works on each fluid without previous knowledge of their volume changes. Per-fluid pressure works are built from estimates to the scheme order of the common pressure and the per-fluid volume changes. The scheme must then be complemented with a final thermodynamic closure with exact pressure equilibration, adapted from (3.28) into an implicit set of $\Phi + 1$ equations on the $\Phi + 1$ variables $(v^{\varphi 1}, p^1)$

$$p^1 = \mathcal{P}^{\varphi}(v^{\varphi 1}, e^{\varphi 1}), \quad (3.31a)$$

$$0 = \sum_{\varphi} c^{\varphi} (v^{\varphi 1} - v^{\varphi 0}). \quad (3.31b)$$

This closure is not associated with an integration path. The scheme quality thus hinges primarily on the entropic character of the pressure work estimates, embedded in the energies $e^{\varphi 1}$ provided by (3.28a). The native GEEC scheme, as visible on (3.53), formally involved an *explicit* pressure p^0 in (3.28a), thus making the scheme non-entropic according to Section 3.4.1.

3.4.4 EEIP: Explicit estimates of implicit pressures

According to Section 3.4.3, the basic principles of thermodynamics make pressure equilibration achievable: (i) always (it is entropic), (ii) regardless of EOS stiffness or contrasts, (iii) with implicit pressure closures (explicit closures may be entropic but are not universal), (iv) yielding non-unique results (distribution of dissipation must be specified by external conditions included into the implicit pressure closures), and (v) with some simple closures suited to numerical schemes. However, implicit pressure closures can make implementation

complex and computation expensive in practical applications: this is aggravated by the fact that pressure couples *all the kinetic and internal energies* in multi-fluid flows, thus making implicit pressure schemes especially convoluted and expensive (see for instance [Despres & Lagoutiere, 2007](#)).

Now, as also appeared in Section 3.4.3, there is a significant margin of freedom to select implicit pressure closures for universal entropic equilibration. Differences do appear in how the entropy production is distributed among the fluids, but if robustness alone is sought, this freedom may be exploited to resort to *estimates* of implicit pressures, and moreover to *explicit* estimates. Of course, some loss of universality may be expected but may be considered as acceptable if kept under control on (somewhat) restricted classes of systems and EOS and if inducing (big) gains on implementation complexity and computational resources.

The approximate prediction of pressure within multi-fluid hydro-schemes requires solving its evolution equation which, for the backbone model, is derived in 3.B.3 as

$$\partial_t p + \underbrace{\left(\sum_{\phi} \beta^{\phi} u_i^{\phi}\right) p_{,i}}_{\text{T}} = - \underbrace{\bar{\gamma} \bar{u}_{i,i} p}_{\text{V}} + \underbrace{\sum_{\phi} \beta^{\phi} \Gamma^{\phi} \rho^{\phi} \dot{w}^{\phi}}_{\text{I}}, \quad (3.32)$$

where $\bar{\gamma}$ is the mixture adiabatic exponent given by

$$1/\bar{\gamma} = \sum_{\phi} \alpha^{\phi} / \gamma^{\phi}, \quad (3.33)$$

and all other quantities are defined by (3.6). Factor $\bar{\gamma}$ can make this equation extremely stiff as discussed in Section 3.3.3 but moreover, p being the derivative of energy, it carries the *stiffness of the energy stiffness*. Also to be noticed, the sign of the stiffness carried by $\bar{u}_{i,i}$ may not be constant depending on compression or expansion. All this makes usual explicit or implicit integration schemes unacceptable for (3.32) in general, as their time step constraints could be incompatible with usual CFL limitations.

Equation (3.32) displays three very different contributions to be time integrated:

T is a Lagrangian transport term with a velocity given by a convex combination of fluid velocities: it is thus taken into account by underlying hydro-schemes under CFL-like conditions of time step and can be taken care of through splitting strategies;

I is an irreversible source term which can be significant (or even dominant) but which will generally *increase* the estimated pressure: This increase leads to a higher estimation of the pressure work in expansion (in absolute value) and thus destructs entropy. Thus, this term is ignored.

V is the main stiff term analyzed in this section: it must be time integrated to provide the EEIP at each time step.

When only retaining term V, (3.32) takes the particularly simple structure of a local scalar ODE, possibly stiff. In this case, a universally stable and positive integration scheme is the “exponential scheme” which can be viewed as intermediate between the first order

explicit and implicit schemes. Denoting $\tau = -\bar{\gamma}\bar{u}_{i,i}\Delta t$, all these schemes can be written in the common form at time step n

$$p^* = \begin{cases} p^n(1 + k\tau^n)^{1/k} & \text{General,} \\ p^n(1 + \tau^n) & \text{Expl. } k = 1, \quad -1 < \tau^n < +\infty, \\ p^n \exp \tau^n & \text{Expn. } k \rightarrow 0, \quad -\infty < \tau^n < +\infty, \\ p^n(1 - \tau^n)^{-1} & \text{Impl. } k = -1, \quad -\infty < \tau^n < +1, \\ p^n & \text{Unit. } k \rightarrow \pm\infty, \quad -\infty < \tau^n < +\infty, \end{cases} \quad (3.34)$$

where the restriction intervals on τ^n for stable positive behavior are appended.

The exponential scheme at $k = 0$ is especially appealing for its widest range of stability, and for its faster than algebraic character with correspondingly higher dissipation—in particular during expansions $\tau^n < 0$ where energies diminish. It was originally introduced by [Certaine \(1960\)](#) for stiff problems ([Curtiss & Hirschfelder, 1952](#)) and was reviewed recently ([Minchev & W. Wrig, 2005](#); [Eichwald, 2013](#), § III).

Combinations of schemes such as (3.34), depending for instance on the sign of τ^n , could also be considered as shown in Section 3.5 in the case of the GEEC scheme. It must be stressed that (3.34) is not intended to be a prediction of time-evolved pressures such as $p^{n+1/2}$ or p^{n+1} , hence notation p^* .

3.5 One-dimensional numerical tests

3.5.1 EEIP in the GEEC scheme

The general method of EEIP described in Section 3.4 was tested within the GEEC ALE (Arbitrary Lagrange–Euler) multi-fluid scheme—developed by [Vazquez-Gonzalez *et al.* \(2020\)](#), briefly introduced in Section 3.2.3, and fully described here for reference in 3.C. It is here used in its purely Eulerian mode by setting to zero the user-defined grid velocity.

The “native” GEEC scheme appears especially appealing in the present study thanks to some of its convenient features:

1. consistent isentropic behavior (to the scheme order) stemming from a mimetic derivation of the least action principle and the Gibbs equation, for the respective momentum and energy equations ([Vazquez-Gonzalez *et al.*, 2020](#), § 3);
2. specific velocity discretization (see Fig. 3.9), whereby transport does not induce volume changes of individual fluids—which in turn are fully taken into account by thermodynamic closures at the end of the cycle;
3. simple option for velocity equilibration within the cycle after momentum calculations (3.50c);
4. explicit user-tunable dissipation terms for shock capture, generally reduced to artificial viscosity stresses (3.49) and (3.53d);

5. fully explicit algorithm, including for pressure integration (3.48)—which is thus not fully entropic and potentially fragile for stiff contrasted mixtures.

The introduction of an EEIP p^* appears straightforward: (i) a simple sub-step (3.48) involving one or a combination of options in (3.34) is introduced to compute p^* and (ii) p^* is substituted for the explicit pressure p^n in all the increment equations of momenta (3.50) and internal energies (3.53) thus preserving consistency and energy conservation. The final pressure equilibration sub-step (3.54a) remains unchanged to generate p^{n+1} .

Preliminary explorations of the tests presented in the next sections provided some further hints to upgrade the native scheme into an EEIP version:

1. As already mentioned in Section 3.4.4, transport appeared controlled by a CFL condition and was never stiff. It can thus be safely discarded from the pressure equation (3.48) which is then local to each cell.
2. The native scheme robustly captured strong compression phases, whereas an exponential EEIP could then be fragile with respect to *floating point overflow*. The entropy deficit of the native scheme seems to be hidden here by the increase of internal energy and by the numerical dissipation sources.
3. In contrast, the native scheme performed dismally under strong expansion phases, whereas an exponential EEIP appeared particularly robust.

These elements inspired a simple hybrid closure for the EEIP (3.48), adapted from (3.34)

$$p^* = p^n \exp(\min[\tau^n, 0]), \quad (3.35)$$

which was used in all the present tests. This approach will be designated as Hybrid-EEIP or H-EEIP in all the following.

The most significant disruption of the dissipative character of EEIP in the scheme appears from the mismatch between time centerings of the volume rates of change $\langle \dot{V} \rangle_c^{n-1/2}$ and $\langle \dot{V} \rangle_c^n$ respectively in pressure and artificial viscosity (3.48) and (3.49a), and their works (3.53a) and (3.53d). This can lead to a loss of robustness for large time steps with possible sign reversal of these volume rates of change, i.e. nonphysical entropy destruction. A simple but efficient improvement, which was not experimented here, could consist in a prediction-correction approach of $\mathbf{u}_c^{n-1/2}$ and $\langle \dot{V} \rangle_c^{n-1/2}$ (akin to Llor *et al.*, 2016, § 2.5).

3.5.2 Selection and design of test cases

Shock tube description	Γ^w	Left initial state $x < 0$										Final time	Domain	Cells	CFL
		Right initial state $x > 0$					Final time								
		ρ^a	α^w	ρ^w	$p^{a,w}$	$u^{a,w}$	ρ^a	α^w	ρ^w	$p^{a,w}$	$u^{a,w}$				
Water-to-air, cross-contaminated (Saurel & Abgrall, 1999a, Figs 6 & 7)	$(\Gamma^a = 2/5)$ 3.4	10^{-14}	$1 - \alpha^a$	10^3	10^9	-490	$2 \cdot 10^{-4}$	$[-\frac{3}{4}, \frac{1}{4}]$	1000	0.2					
Water-to-air, cross-contaminated, enhanced stiffness	3.4	10^{-14}	$1 - \alpha^a$	10^3	10^{12}	0	$7 \cdot 10^{-6}$	$[-\frac{3}{5}, \frac{2}{5}]$	4000	0.4*					
Air-to-water, cross-contaminated (Liou & Chang, 2005, Fig. 17.11)	1.8	10^{-14}	$1 - \alpha^a$	2231†	10^9	0	$4 \cdot 10^{-4}$	$[-\frac{1}{4}, \frac{3}{4}]$	1000	0.2					
Water double expansion to vacuum, air contaminated	4 1	10^{-12}	$1 - \alpha^a$	$\approx 1.2^\ddagger$	$\approx 1.3^\ddagger$	$\approx -0.4^\ddagger$ $\approx 0.4^\ddagger$	1/4	$[-1, 1]$	2000	0.7					
Water double shock, air contaminated, low, medium, and high air dissipation	4 1	10^{-8}	$1 - \alpha^a$	1	10^{-14}	4/3 -4/3	5/22	$[-1, 1]$	500	0.3					

* First ten time steps computed with reduced CFL = 0.04. † Densities here adjusted in order to set initial temperature at 308 K.

‡ Actual initial density, pressure, and velocity to 10^{-16} accuracy: $\rho = 1.176686050042247$, $p = 1.255812630489673$, $u = 0.4299853856289317 + 0.00375$.

Table 3.2: Physical initial states and numerical conditions for the seven air-water shock tube tests carried out in the present work. Definition of CFL and closure of artificial viscosity are discussed in Section 3.5.3.

Numerical schemes for multi-fluid pressure equilibration can be conveniently benchmarked with 1D test cases on velocity-equilibrated air–water mixtures at very low volume fractions of either fluid. This is generally sufficient because of four important features:

1. pressure equilibration is essentially a local ODE (in Lagrangian coordinates);
2. which is weakly coupled to fluid-velocity differences;
3. whose stiffness is enhanced by fluid contrasts, as for air and water which are of prime practical importance; and
4. with maximal stiffness at low air volume fractions, where one-way coupling of the contaminant fluids holds.

As a premium, the one-way coupling condition makes the system behave as single-fluid, for which solutions of the evolution equations are often tractable analytically and independently of shock dissipation details. Tests with non-vanishing velocity differences or at non-negligible volume fractions have also been performed (see for instance Toumi, 1996; Toumi & Kumbaro, 1996), but they appear less constraining on accuracy (there is not a unique solution to Riemann problems) and robustness (stiffness appears at low volume fractions).

Previous robustness tests have thus privileged near-pure shock tubes, with air and water on each side of an initial pressure discontinuity and with slight cross-contamination of air by water and water by air. The dominant fluids evolve according to the Riemann problem solution, whereas the contaminant fluids merely sample the surrounding pressure and evolve isentropically unless submitted to shocks. In principle, the volume fractions of contaminant fluids could be arbitrarily small, but in practice, robustness and stability are generally lost over positivity or entropy violations below some volume-fraction threshold in the order of 10^{-7} at best.

For the present work, two tests among the most commonly reproduced so far were retained: the water-to-air and air-to-water shock tubes of respectively Saurel & Abgrall (1999a, Figs 6 & 7) and Liou & Chang (2005, Fig. 17.11) summarized in Table 3.2. Both of these shock tubes have been tested in the present work, but with initial volume fractions of contaminant fluids at 10^{-14} , significantly below usual levels and about two orders of magnitude above round-off level (see Table 3.2).

The water-to-air test was re-explored in its basic form by Saurel & Abgrall (1999b, § 4.1) and Saurel & Le Métayer (2001, § 4.1.1) among others. Some significant variations were also introduced: Kitamura *et al.* (2014, § 3.3.3), Chang & Liou (2007, § 3.4), Pandare *et al.* (2019, § 5.3), Luo *et al.* (2021, § 4.1) kept initial pressures but corrected initial densities so that temperature was uniform at 308 K; Sun (2013), Allaire *et al.* (2002, § 8.3), Saurel *et al.* (2003), and Saurel *et al.* (2008, § 7.1 & 7.2) modified the EOS, respectively with Tait EOS for water, Van der Waals EOS for the gas, plasmas instead of water and air, and dodecane liquid–vapor EOS; La Spina & de’ Michieli Vitturi (2012, § 5.2) explored the vanishing drag

between fluids; and Murrone & Guillard (2005, §§ 5.2.1 & 5.2.2) tested non negligible volume fractions.

To the authors' knowledge, the most strenuous variations on the water-to-air shock tube were presented by Saurel *et al.* (2009, § 4.3.2) and Saurel *et al.* (2007, 2009, §§ 5 & 4.3.1) with respectively a thousand-fold-increased initial high pressure (at 10^7 Pa) and a fifty-fold-reduced initial air density (at 1 kg/m^3). In the present work, these challenges have been combined into a new configuration with initial density and pressure ratios of respectively 10^3 and 10^7 (see Table 3.2).

The less common dual case of air-to-water shock tube was re-explored mostly by Liou *et al.* (2008, § V.B), Kitamura *et al.* (2014, § 3.3.1), and Pandare *et al.* (2019, § 5.2). Chang & Liou (2007, § 3.3), Li (2020, § 5.2), and Denner *et al.* (2018, § 7.5.2) considered the test with modified water EOS, with respectively $\Gamma^w = 0.932$, 0.9276 , and 3.1 . This test being less demanding than the water-to-air shock tubes, no enhanced configurations are proposed here.

Because robustness is mostly challenged by zones of air-contaminated water (see Section 3.3.4), two specific configurations were also designed to separately test expansions fans and shocks on this mixture (see Table 3.2): a free expansion to zero-pressure final state, and a shock on zero-pressure initial state—an extension of the classical test of Noh (1987) (see Table 3.2).

Expansion to low pressures were explored as idealized cavitation tests by Saurel & Abgrall (1999a, § 6.1, Fig. 20), Saurel & Le Métayer (2001, § 4.2.1), or Kitamura *et al.* (2014, § 3.4). A critical element here for preserving robustness of computations is the initial volume fraction of air which is usually set *above* 10^{-3} . In the present work, the initial volume fraction is again set at 10^{-12} , far below usual levels (see Table 3.2). Further details are presented in Section 3.5.5 with the derivation of a semi-analytical solution in 3.D.

The extension of Noh's test to stiffened gas EOS was considered by Burnett *et al.* (2018). 3.E further considers the case of an ideal–stiffened gas mixture assuming that fluids are adiabatic and that shock dissipation can be distributed at will over the fluids. Again, strenuous conditions are defined by low air volume fractions, here set at 10^{-8} (see Table 3.2). Further details are presented in Section 3.5.6.

3.5.3 General numerical conditions, shock dissipation

Thermodynamic closure Although the pressure equilibration algorithm of the present work intends to be stiffness compliant, it may still be *ill-conditioned*, i.e. sensitive to small numerical perturbations induced for instance by round-off. This important element was already noticed by Chang & Liou (2007, § 2.8)—whose thermodynamic closure is very similar to that of the present GEEC scheme in (3.54a)—and becomes especially critical at very low volume fractions close to round-off limits. Some standard numerical precautions were thus taken in solving equations for the final state at the end of a cycle, similar to those of Chang & Liou (2007, § 2.8). These will not be elaborated here as they fall off the scope of the

present study.

CFL definition It is common practice to define the (variable) time step at each iteration with respect to some maximum CFL value over the calculation domain. This makes comparison of different tests less objective as speeds of sound in numerically singular cells can be significantly above consistent values. As all the test cases in the present work have quasi-analytical solutions, analytical speeds of sound can be computed and, combined with cell sizes and fluid velocity in (3.47), provide a reference CFL for time steps. The reported CFL values in Table 3.2 follow this definition and were chosen to be the highest “no-crash” tenths. No corrections with the fundamental derivative were included (see Section 3.3.5) so as to facilitate comparisons with other existing results.

Artificial dissipation As mentioned in Section 3.4.3 and previously discussed by Vazquez-Gonzalez *et al.* (2020, § 3.7), shock dissipation in a multi-fluid system must be specified on a case-by-case analysis to mimic the actual physical dissipation processes in the system: just as for dissipation from pressure equilibration (see Section 3.4.3), thermodynamic principles alone cannot define shock dissipation in full. Therefore, in the absence of universal physical rationales, numerical tests can be carried out with dissipation weights which are either: (i) selected by some “common sense” argument or (ii) pushed to extreme values, possibly nonphysical but strenuous enough to test robustness limits. In the present work, all the test cases were carried out with a standard linear–quadratic artificial viscosity closure of the mixture as defined by common practice (Mattsson & Rider, 2015, & refs therein)—including a linear component in expansion phases (3.49),—but the associated dissipation was distributed with different weighing λ^φ in (3.53d). λ^φ were defined as Grüneisen scaled coefficients for shock-tube tests (Vazquez-Gonzalez *et al.*, 2020, eq. 27), or as ad hoc (possibly extreme) user-predefined coefficients for Noh’s tests. Naturally, the intrinsic dissipation of the scheme—i.e. per fluid numerical residues on transport, pressure work, and pressure equilibration—are fixed once and for all in the GEEC scheme and are not affected by λ^φ .

3.5.4 Shock tube tests

Results from the three shock-tube tests of Table 3.2 are summarized in Fig. 3.4.

Some general features can be observed:

1. For legibility and scheme testing consistency, the initial values of α^a and α^w in the three shock-tube tests were chosen equal. The robustness was thus limited by the weakest of the cells in the weakest of the tests. Some of the reported volume fractions could thus be somewhat reduced without affecting robustness.
2. The three tests were computed without any major difficulty with CFL values in usual ranges for hydro-schemes and regardless of α^a values down to 10^{-14} , well below the lowest of previously reported values around 10^{-7} .

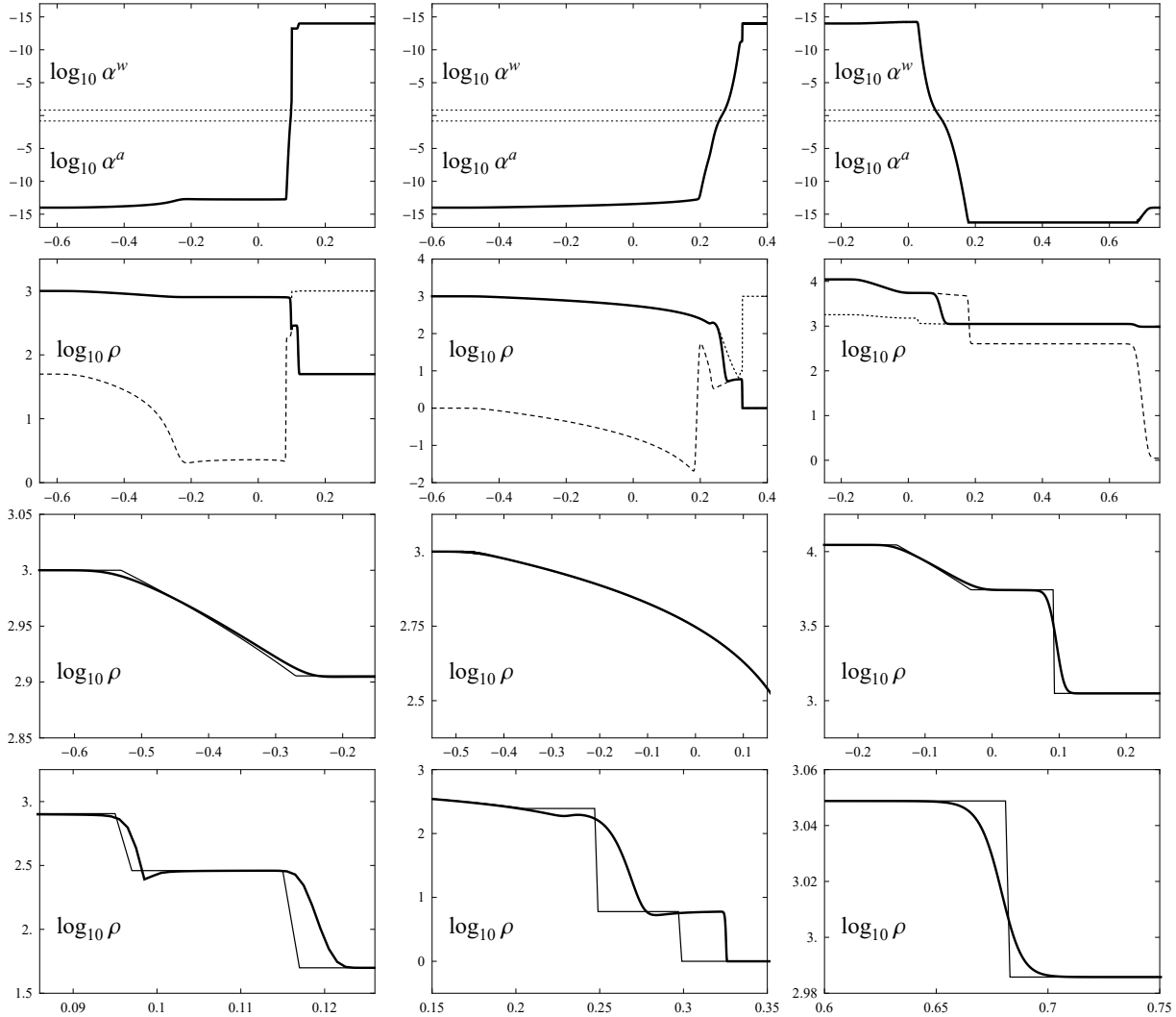


Figure 3.4: Final simulated profiles for the three “cross-contaminated” shock-tube numerical tests discussed in text: air-to-water (first column), enhanced air-to-water (second column), and water-to-air (third column). In each column from top to bottom (log scales): combined air and water volume fractions (first row); mixture, air, and water densities (respectively thick solid, dashed and dotted lines, second row); left expanded views on computed and analytical mixture density (respectively thick and thin lines, third row); right expanded views on computed and analytical mixture density (respectively thick and thin lines, fourth row). Notice the wide dynamical ranges on volume fractions and the shifts on shocks positions. See numerical conditions in Table 3.2.

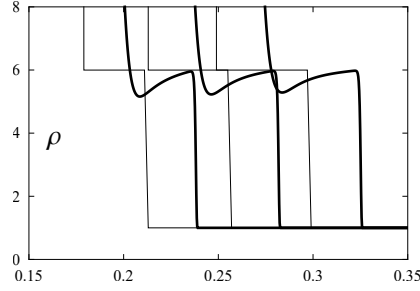


Figure 3.5: Computed and analytical density profiles (respectively thick and thin lines) around the shock wave at three different times for the enhanced water-to-air shock tube. The constant shift between computed and analytical profiles signals the presence of an initial time shift due to numerical effects.

3. Large swings of air densities over three orders of magnitude on short distances can be observed close to contacts and shocks (second row in Fig. 3.4).
4. In the enhanced-stiffness water-to-air case it was necessary to perform ten time steps at a tenth of the nominal CFL value in order to pass the initial transients. This is attributed to the very extreme conditions which are generated as the three waves start separating (expansion, contact, and shock) and where air and water densities experience over- and under-shoots by an order of magnitude (see Fig. 3.4).
5. For all tests, the native GEEC scheme provided very similar results as its H-EEIP modified version, possibly with some slight reductions of maximum “no-crash” CFL values which were not specifically measured here.
6. Numerical diffusion is observed as the present GEEC scheme was developed to first order. The initial state for the standard water-to-air shock tube was thus set into a uniform motion (see Table 3.2) adjusted to compensate the displacement of the contact discontinuity and reduce its spreading (first column in Fig. 3.4).
7. Matching to the analytical solutions is observed in all cases (see last two rows in Fig. 3.4) except for numerical diffusion effects and time shifts on contacts and shocks for the water-to-air cases.
8. The mismatch observed on shock position in the enhanced water-to-air test appears to be due to the initial transient where the three coincident waves separate slowly and experience numerical diffusion. However, after full separation, shocks do propagate according to theory up to a time shift at origin. This is visible on computed and analytical profiles at different times (see Fig. 3.5).

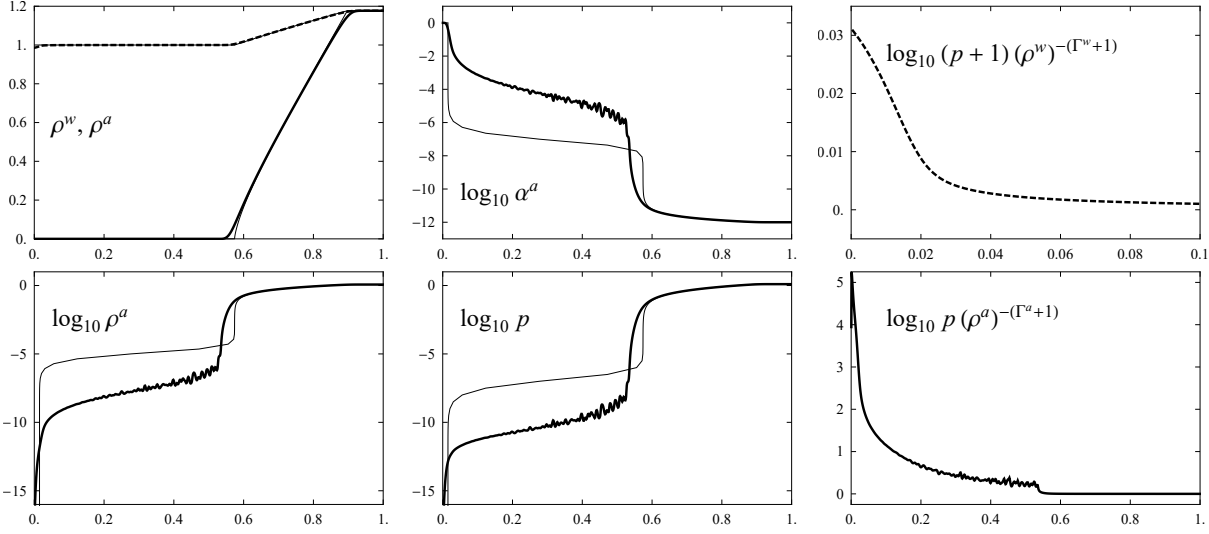


Figure 3.6: Final simulated half-profiles of double expansion initiated as in Table 3.2: air and water densities (respectively solid and dashed lines, left column), air volume fraction and pressure (respectively top and bottom, middle column), and emulated entropy change from initial state for air and water (respectively top and bottom, right column). Corresponding semi-analytical solutions provided in 3.D are given in thin lines.

3.5.5 Isentropic two-fluid expansion test

The isotropic expansion of air-contaminated water can be described by a semi-analytical self-similar solution which is derived in 3.D. The profiles connecting high pressure and vacuum for varying reduced volume fractions of air α_r^a are illustrated in Fig. 3.10. At low α_r^a , expansion proceeds in two phases: (i) at pressures comparable to Π^w , both water and air expand, whereas (ii) at vanishing pressures, water evolves practically at constant volume while air expands and eventually reaches unit volume fraction. In between, a fast transition occurs with an increase of air density by possibly many orders of magnitude. This is the stiffest moment during expansion, with the occurrence of stiff stiffness according to the analysis of Section 3.3.4 and Fig. 3.2.

With the initial conditions of the water double expansion in Table 3.2, the two step expansion are well separated in the simulations carried out with the H-EEIP corrected scheme, as illustrated in Fig. 3.6. The test in Table 3.2 is ideally defined assuming that pressure falls to zero at the center of the domain without opening a vacuum cavity. This is desirable because a Eulerian scheme cannot drain completely the central cells. Now, numerical dissipation actually makes air expand more than isentropically and in order to reach air volume fractions close to unity at origin, it is necessary to increase slightly the initial velocity. As specified in Table 3.2, it is here increased in order that the exact solution would leave a void of fifteen cells on each side of origin as visible in Fig. 3.6.

Some general features can be observed:

1. Simulations are robustly carried out with the H-EEIP-corrected scheme at an initial

air volume fraction of $\alpha_r^a = 10^{-12}$ and a constant CFL value of 0.7. For this CFL value the native scheme could not handle volume fractions below 10^{-3} without crashing. This is consistent with the analysis of Section 3.4.1 whereby explicit schemes destroy entropy—which here cannot be offset by isentropic heating during compression phases, in contrast for instance with Noh’s test in Section 3.5.6.

2. Artificial viscosity was set to zero, $a_1 = 0$, in order to better capture the isentropic evolution. Usual non-zero values would further increase entropy production, without impacting the scheme robustness.
3. The scheme robustness allows to reach final pressures well below 10^{-20} at origin.
4. The steep central transition near $x = 0.6$ is smeared and delayed by numerical diffusion.
5. Large errors on air density and volume fraction, as well as mixture pressure, appear during the air expansion phase between $x = 0$ and ≈ 0.5 (see left two columns in Fig. 3.6). These errors can be attributed to numerical dissipation which impacts primarily air, as visible on the pseudo-entropy profiles (see right column in Fig. 3.6). Formally, the implicit pressure in H-EEIP amounts to adding a linear artificial viscosity with a coefficient locked onto the pressure stiffness τ in (3.34)—instead of being user defined.
6. Slight oscillations on pressure are observed at the beginning of the air expansion phase, between $x \approx 0.2$ and 0.5. These oscillations, which appear “frozen” and do not impact stability, are probably produced by the combination of very low pressure (below 10^{-10}), absence of artificial viscous stress, vanishing numerical diffusion due to low velocity in this phase, and coupling to round-off errors.
7. Entropy production on the mixture is very mild even near the origin (see upper right in Fig. 3.6). It is much more modest than that produced with Godunov type schemes (for instance Shen *et al.*, 2010, fig. 9).

3.5.6 Two-fluid extension of Noh’s test

The initial state of the original test of Noh (1987) consists of an ideal gas at unit density, zero pressure (hence zero temperature and speed of sound), and with uniform unit velocity towards a wall at the origin. An infinitely strong shock thus propagates from the wall, inducing the theoretical maximum shock compression. This is obviously a final horizon of stiffness for CFD and makes a mandatory test for most shock-physics codes. It is thus appealing to extend this model flow to more complex EOS and to multi-fluid systems.

For stiffened gas, the zero pressure condition does not make a vanishing speed of sound. But if contaminated by an ideal-gas, *however small its volume fraction*, the speed of sound vanishes (see Section 3.3.4 and Fig. 3.2). Paradoxically, this does not define the shock from

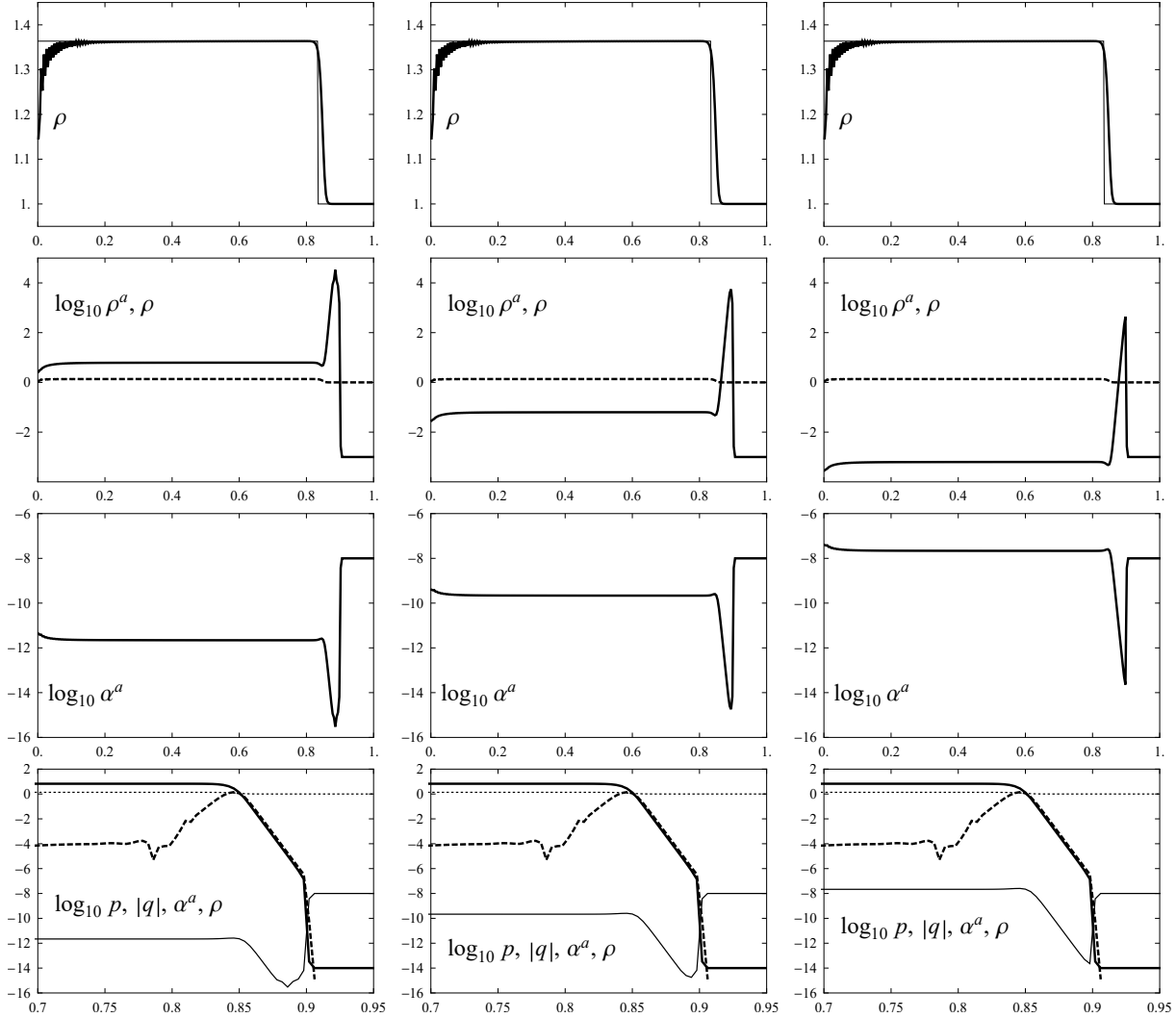


Figure 3.7: Final simulated half-profiles for the extended Noh numerical test on “air-contaminated” water (normalized stiffened gas) for three shock dissipation levels on air as defined in text: low, medium, and high (respectively first, second, and third columns at $\kappa^a = 10^{-2}$, 1, and 10^2). In each column from top to bottom: computed and analytical mixture density (respectively thick and thin lines, first row); air volume fractions (second row, log scale); mixture and air densities (respectively thick solid and dashed lines, third row, log scale); expanded views on air pressure, artificial viscosity stress, volume fractions, and mixture density in shock region (respectively thick, thick dashed, thin, and thin dotted lines, fourth row). Notice the wide dynamical ranges on volume fractions, the high air densities at rising edges of shocks, and the air *expansion* under shock for high shock dissipation (third column). See numerical conditions in Table 3.2.

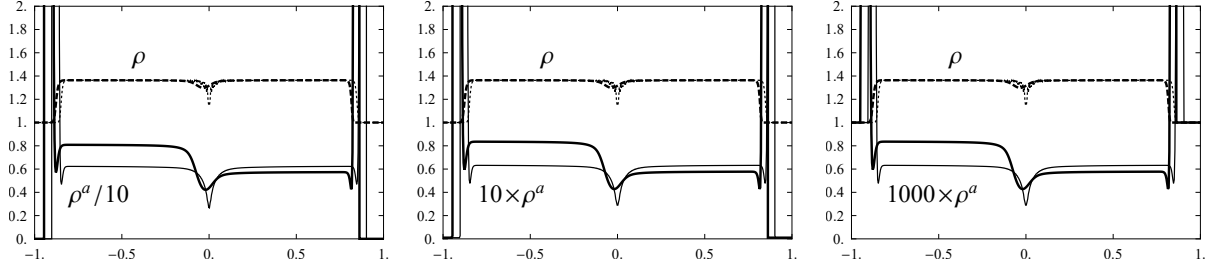


Figure 3.8: Final simulated profiles of air and mixture densities (resp. solid and dashed lines) for the multi-fluid Noh numerical test on normalized “air-contaminated” water with and without added initial uniform velocity of $u = 6/5$ (resp. thick and thin lines) for $\kappa^a = 10^{-2}$, 1, and 10^2 (resp. from left to right). The physically identical shocks on each side are perturbed by the asymmetry of the transport-induced dissipation, thus producing different air shocked densities in a $\approx 3/2$ ratio despite exact jump conditions on the mixture density.

κ^a	10^{-2}	1	10^2
α_0^a	Weak	Medium	Strong
10^{-8}	5,500	55	0.55
$1/3$	1,200	17	NA
$2/3$	300	8.5	NA
$1 - 10^{-8}$	9.4	6	NA

Table 3.3: Air-density ratios ρ_1^a/ρ_0^a across shock as observed in simulated flows on ideal-stiffened gas mixtures at initial zero pressure for selected air volume fractions α^a and air weighing factors of dissipation κ^a in (3.36). NA: non-accessible tests as dissipation weights on water would be negative. As expected, for vanishing volume fraction of air and even dissipation on fluids, the air compression ratio matches the theoretical maximum $1 + 2/\Gamma^a = 6$.

the wall in a unique way because the initial amount of internal energy in water (of any possible magnitude) impacts the energy jump across the shock. Furthermore, the shock behavior also depends on how the dissipated energy is shared between the fluids (see Section 3.5.3).

A general analysis of shocks in adiabatic mixtures of ideal and stiffened gases at zero pressure is provided in 3.E. It shows that for given EOS and with proper scaling, the system behavior can be fully described in an algebraically explicit way by three independent non-dimensional parameters: the initial volume fractions and the volume ratios across shock for each of the two fluids. Not all combinations of parameters are accessible for adiabatic fluid mixtures as visible on the representation of admissible parameters in Fig. 3.11. Analytical formulas in the limit of vanishing ideal gas and for water-consistent Grüneisen coefficients let define the test involving simple fractions of Table 3.2—with final water density of $15/11 \approx 1.36$, close to the theoretical maximum of $3/2$ for $\Gamma^w = 4$.

Preliminary simulations of two-fluid-adapted Noh tests for various air–water volume fractions confirmed the general results of 3.E. Initial pressures were set to 10^{-14} because at exact zero, round-off errors would inevitably bring the system to nonphysical states of

negative densities or temperatures. The fluids' weighing coefficients of dissipation were expressed as

$$\lambda^a = \kappa^a \alpha_0^a, \quad \text{and} \quad \lambda^w = 1 - \lambda^a, \quad (3.36)$$

where κ^a was a predefined constant representing an amplifying factor of dissipation on air and α_0^a was the initial air volume fraction. Observed air density ratios across shock are reported in Table 3.3 showing the strong impact of κ^a , especially in the one way coupling limit at low α^a .

As expected, the most fragile of the preliminary tests appeared at low α^a . These were thus retained in Table 3.2 for the three values $\kappa^a = 10^{-2}$, 1, and 10^2 . Results are summarized in Fig. 3.4.

Some general features can be observed:

1. For legibility and scheme testing consistency, the initial α^a and CFL values in the three two-fluid Noh tests were chosen equal. The robustness was thus limited by the weakest of the tests. These values could thus be somewhat optimized on specific cases without affecting robustness.
2. As expected in this one-way coupling limit for air, results match the analytical solution for water irrespective of dissipation on air (first row in Fig. 3.4).
3. As for the standard test of Noh (1987), typical ‘‘wall heating’’ effects close to the origin are observed on all quantities for water and air in all cases, with some ‘‘frozen’’ oscillations of no impact on the robustness and stability of the calculations.
4. Consistently with findings in 3.E, the post-shock air density can be well above or well below the initial density (second row in Fig. 3.4), when dissipation level on air is respectively low or high as defined by κ^a .
5. Within the shock layer, a strong overshoot of air density is always observed (second row in Fig. 3.4). This is due to the virtually infinite compressibility of the gas in the initial state of vanishing pressure.
6. Concomitant with density overshoot, air volume fractions undershoot by up to seven orders of magnitude, thus approaching round-off floor (third row in Fig. 3.4). This is the main factor which limits initial volume fractions to $\alpha^a \gtrsim 10^{-8}$.
7. Because of the air density overshoot, the shock layer takes a peculiar three stage structure (fourth row in Fig. 3.4): (i) a very fast air compression around $x = 0.9$, (ii) a slower air expansion between $x = 0.9$ and 0.85 induced by the progressive build up of dissipation, and (iii) a quick water compression around $x = 0.85$ where the bulk of shock dissipation occurs (see artificial viscosity profiles).

8. Despite the combination of very strong compression and expansion phases, the native GEEC scheme provided very similar results as its H-EEIP modified version, possibly with some slight reductions of maximum “no-crash” CFL values which were not specifically measured here.

Although the dissipation level on air, here controlled by κ^a , dominantly affects the final state of the contaminant, all other sources also contribute, notably the intrinsic dissipation of the scheme. It must thus be kept in mind that, within the simplistic multi-fluid dissipation retained here, κ^a does not define dissipation in an univocal way. This is exemplified for instance when carrying a multi-fluid Noh test with an added uniform velocity to the initial condition of $u = 6/5$: the left and right velocities are then $12/5$ and 0 thus enhancing or reducing numerical diffusion. Resulting density profiles in Fig. 3.8 show post-shock air densities in a 3:2 ratio between left and right, while no differences are observed on the mixture density as expected. Somewhat surprisingly, this 3:2 ratio is practically constant for all dissipation levels on air κ^a . A tentative explanation could be that numerical dissipation is here mostly in the form of numerical diffusion.

The present study does not intend to provide methods to ensure well defined shock dissipation irrespective of scheme contributions. It merely shows that a significant control can be exerted to make shock capture less scheme dependent and more physics relevant through adapted closures of artificial viscosity.

3.6 Conclusion

The present work was devoted to the specific but ubiquitous issue of potential stiffness of pressure work couplings in simulations of contrasted compressible multi-fluid flow. The main findings are:

1. An appropriate general formalism was introduced in order to recast pressure terms in an explicit way amenable to a stiffness quantitative analysis. Stiffness and “stiff stiffness” of pressure terms then appear naturally (Section 3.3)—these designate respectively strong time derivatives and strong second derivatives. The analysis was applied here to the “backbone” model—also known as the pressure-equilibrated six-equations model in the case of two fluids,—which is common to most multi-fluid models when canceling dissipative correlations. This was illustrated on the simple air-water mixture of high practical importance.
2. Universal numerical solutions based on implicit pressure calculations were then proposed to preserve robustness for all coupling strengths (Section 3.4). Thermodynamic consistency warrants the per-fluid entropic character of such schemes.
3. A slightly degraded but significantly simpler approach was then determined based on a hybrid explicit estimate of implicit pressure (H-EEIP, Section 3.4.4). It was directly

adapted to a “GEEC” scheme previously proposed by [Vazquez-Gonzalez *et al.* \(2020\)](#) for compressible multi-fluid flows (3.C), here restricted by velocity equilibration.

4. The ensuing modified scheme was found to perform very successfully on two standard tests of the literature and three new tests specifically designed for being extremely strenuous, involving strong shocks and expansions in vacuum (Section 3.5). CFL conditions were not affected despite contrasts between fluids by orders of magnitude on volume fractions, densities, speeds of sound, or dissipation strengths.

Other pressure related issues have often been blamed for observed fragility in multi-fluid models and schemes, notably their possibly non-hyperbolic and ill-posed character sometimes related to pressure equilibration (3.A). Now, it must be stressed that, whatever modifications are introduced to recover hyperbolic behavior or other ailments, the possible stiffness of pressure couplings is always present and requires specific care. The option of mollifying the pressure stiffness was not retained here: not only can it seriously distort physical behavior, but it appears especially convoluted in the presence of highly variable multi-fluid conditions such as EOS singularities and contrasts, or number of fluids and energy reservoirs. Although all tests were here carried out on a two-fluid air–water system, the present techniques apply readily to any number of fluids with minimal intrusion in existing schemes. As an example, a 20-fluid system presents 40 basic energy reservoirs (kinetic and internal, excluding others for the sake of example), 20 entropy conditions, and $40 \times (40 - 1) / 2 = 780$ pressure couplings all of which must be properly and consistently discretized.

Further developments are presently being considered: (i) equilibrated pressure approximations in systems actually involving physically motivated pressure imbalances, (ii) adaptation of present robustness prescriptions to second and higher order schemes, (iii) scheme-independent approaches to physical shock dissipation, (iv) inclusion of fundamental derivatives in the schemes.

Acknowledgments

The authors are particularly grateful towards S. Guisset, R. Chauvin, and B. Manach-Pérennou for very helpful and creative discussions.

3.A Other pressure issues in compressible multi-fluid models and schemes

Various authors have objected the relevance of the backbone model (3.1), often blaming the single-pressure constraint for its observed ailments and recommending the introduction of non-equal pressure assumptions. They generally justify preservation of non-equal pressures by at least one of the following main reasons: (i) their significant and persistent physical existence, (ii) their significant but transient physical or numerical existence, (iii) their presumed

necessity in order to restore the well-posedness of the multi-fluid equations, and (iv) their convenience in order to reduce the numerical stiffness of inter-fluid pressure equilibration by finite-rate relaxation equations. These will be briefly commented below, but the ensuing approaches to modeling and discretization will not be detailed: their wide diversity reflects that of underlying dissipation assumptions which, in contrast to isentropic behavior, are not unique.

i) Persistent non-equal physical pressures These reflect the presence of supplementary potential energy reservoirs such as surface tension between fluids (Laplace pressure as in [Ramshaw, 1978](#)) or kinetic energies of velocity fluctuations due to added mass, turbulence, granular agitation pressure, etc. (Bernoulli-like effects as in [Geurst, 1985](#)). Dissipation-free evolution equations (backbone models) can again be obtained from variational principles ([Gavrilyuk & Saurel, 2002](#); [Heulhard de Montigny *et al.*, 2021](#), & refs therein) and complemented with dissipation terms. If these energies are small enough however, models can still be constrained by pressure equilibration ([Heulhard de Montigny *et al.*, 2021](#)).

ii) Transient non-equal physical pressures These reflect the presence of supplementary kinetic and potential energy reservoirs on internal degrees of freedom, as found for bubble dynamics. Effects at macroscopic scales are observable when “in-phase” coherent pulsing motions are present, for instance under shock excitation ([Wijngaarden, 2007](#), & refs therein). Theoretical and experimental estimations were provided for instance by [Beylich & Gülhan \(1990, fig. 3\)](#) or [Kapila *et al.* \(2001, § B\)](#). When “out-of-phase” incoherent, these can be treated as second-order correlations or even neglected. Dissipation-free evolution equations with non-equal pressures (backbone model) can also be obtained from variational principles ([Bedford & Drumheller, 1978](#); [Gavrilyuk & Saurel, 2002](#), & refs therein) and complemented with dissipation terms (as found in [Baer & Nunziato, 1986](#); [Chang & Ramshaw, 2008](#)).

iii) Well-posedness of multi-fluid models with non-equal pressures The demand by numerous authors for well-posed hyperbolic multi-fluid models has lead to developing numerous correction strategies to the backbone model. A widespread belief is that well-posedness requires non-equal pressures: for instance, the algebraic and popular momentum exchange term of [Stuhmiller \(1977\)](#) can be interpreted as a pressure imbalance, and the model variants considered in points (i) and (ii) above also have impact. More intrusive is the addition of a volume fraction equation driven by pressure imbalance for detonating systems by [Baer & Nunziato \(1986\)](#). It was later extended to all types of systems ([Saurel & Abgrall, 1999a](#)) for which, however, its physical relevance appears questionable ([Bdzil *et al.*, 1999](#); [Kapila *et al.*, 2001](#); [Dinh *et al.*, 2004](#); [Theofanous & Chang, 2008](#); [Lhuillier *et al.*, 2013](#), & refs therein) and its asymptotic limit yields a backbone model with added terms of cryptic interpretation ([Hantke *et al.*, 2021](#), eq. 2.16).

iv) Stiffness reduction of non-equal pressure relaxation This is the most pragmatic reason for accepting non-equal pressures although a numerically acceptable relaxation time may not be always easily found. As already mentioned in Section 3.2.1, these pressure relaxation schemes can also be easily adapted to mixed interface cells in order to either damp the stiffness of the pressure equilibration (Kamm *et al.*, 2011; Yanilkin *et al.*, 2013, & refs therein) or to describe fine sub-cell Riemann-like problems at interfaces (Loubère *et al.*, 2012; François *et al.*, 2013; Sun, 2013; Barlow *et al.*, 2014). Some of the pressure relaxation approaches considered in point (iii) above can also reduce the stiffness of pressure equilibration, although in some cases they merely displace the stiffness issues to other equations (Chiocchetti & Müller, 2020).

Most of the corrections or extensions of the backbone model considered in points (i) to (iii) have marginal impact on the stiffness issues related to pressure terms. Only in point (iv) are these issues tackled by reducing stiffness through pressure relaxation, but on somewhat questionable premises. For instance, pressure equilibration within an interface cell can be viewed as inconsistent with a low CFL-constrained time step and motivates pressure relaxation: pressure changes are mediated by acoustic waves which have to propagate various times across the cell to reach equilibration (see for instance Barlow *et al.*, 2014, § I). Now, this argument should also apply to pure cells, within which details of uneven pressure fields are actually never taken into account (except maybe in shock fitting techniques) as discretization generally assumes homogeneous field values in each cell—thus contributing to numerical diffusion.

At this point it is worthwhile citing Miller & Zimmerman (2009, Conclusions): “... *making a model for the behavior of mixed zones is treacherously close to devising epicycles. It is possible to spend limitless amounts of time trying to get a single zone to reproduce ‘physically reasonable’ behavior. One should not attempt to do too much. Sub-zonal models are only intended to keep a calculation running with believable physical results, not to accurately solve the details of what happens inside a small volume. If those details are needed, then more zones must be spent on the problem. If, however, a code is crashing because mixed zones are producing physically unreasonable solutions, then an improved sub-zonal model for mixed material behavior may be the answer.*”

The issue of pressure stiffness is essential and common to all the model variants discussed above and it is always amenable to implementation of the present numerical techniques. Switching between the stripped backbone model and dressed versions only affects terms other than pressure as illustrated in Fig. 3.1.

3.B The backbone model

3.B.1 Statistical multi-fluid evolution equations

The present appendix is a brief reminder on the derivation of average multi-fluid equations, highlighting the separation of pressure contributions (mean, inter-fluid imbalance, and fluc-

tuations). More details can be found in [Wörner \(2003, § 3\)](#), [Morel \(2005, § 3\)](#), or [Brennen \(2005, § 1\)](#).

The instantaneous and local evolution equations for mass conservation of each fluid, total momentum (Euler, no surface tension, no viscosity), total internal energy (no heat flux), and pressure closure (EOS) are

$$\partial_t(c^\varphi \rho) + (c^\varphi \rho u_j)_{,j} = 0, \quad (3.37a)$$

$$\partial_t(\rho u_i) + (\rho u_i u_j)_{,j} + p_{,i} = \rho g_i, \quad (3.37b)$$

$$\partial_t(\rho e) + (\rho e u_j)_{,j} + p u_{j,j} = \rho \dot{w}, \quad (3.37c)$$

$$p = \mathcal{P}(\{c^\varphi\}, \rho, e, \boldsymbol{\sigma}). \quad (3.37d)$$

In contrast to the rest of this chapter all symbols in the present appendix stand for the one-point one-time non-averaged quantities, and $\boldsymbol{\sigma}$ stands for supplementary thermodynamic variables (such as entropies) which fully define the state of the fluids. As represented in [Fig. 3.1](#), this set of equations can be obtained from a least action principle and from Gibbs' identity.

The mixture is represented by the *mass fractions* of fluids φ , $\{c^\varphi\}$ with $\sum_\varphi c^\varphi = 1$, whose evolution equations are given by mass conservation. All the following is thus applicable irrespective of the nature and affinity of the fluids. For immiscible fluids, $c^\varphi(t, x)$ only take values 0 or 1 and coincide with the fluids' presence functions.

Conditional ensemble averages, denoted by an over-bar, are now applied to the following combinations of [\(3.37\)](#)

$$\overline{(3.37a)}, \quad (3.38a)$$

$$\overline{c^\varphi \times (3.37b) + u_i \times (3.37a) - c^\varphi u_i \times \sum_\phi (3.37a)^\phi}, \quad (3.38b)$$

$$\overline{c^\varphi \times (3.37c) + e \times (3.37a) - c^\varphi e \times \sum_\phi (3.37a)^\phi}, \quad (3.38c)$$

$$\overline{(3.37d)}. \quad (3.38d)$$

Assuming commutation of the averaging operator with derivations—which is rigorously true for the ensemble average—elementary transformations yield

$$\partial_t(\overline{c^\varphi \rho}) + (\overline{c^\varphi \rho u_j})_{,j} = 0, \quad (3.39a)$$

$$\partial_t(\overline{c^\varphi \rho u_i}) + (\overline{c^\varphi \rho u_i u_j})_{,j} + \overline{c^\varphi p_{,i}} = \overline{c^\varphi \rho g_i}, \quad (3.39b)$$

$$\partial_t(\overline{c^\varphi \rho e}) + (\overline{c^\varphi \rho e u_j})_{,j} + \overline{c^\varphi p u_{j,j}} = \overline{c^\varphi \rho \dot{w}}, \quad (3.39c)$$

$$\overline{p} = \overline{\mathcal{P}(c^\varphi, \rho, e, \boldsymbol{\sigma})}. \quad (3.39d)$$

Defining means and fluctuations as

$$\alpha^\varphi = \overline{c^\varphi}, \quad \alpha^\varphi \rho^\varphi = \overline{c^\varphi \rho}, \quad (3.40a)$$

$$\alpha^\varphi \rho^\varphi u_i^\varphi = \overline{c^\varphi \rho u_i}, \quad u_i^{\varphi'} = u_i - u_i^\varphi, \quad (3.40b)$$

$$\alpha^\varphi p^\varphi = \overline{c^\varphi p}, \quad p^{\varphi'} = p - p^\varphi, \quad (3.40c)$$

$$\alpha^\varphi \rho^\varphi e^\varphi = \overline{c^\varphi \rho e}, \quad \alpha^\varphi \rho^\varphi \dot{w}^\varphi = \overline{c^\varphi \rho \dot{w}}, \quad (3.40d)$$

where $\sum_{\varphi} \alpha^{\varphi} = 1$, the averaged evolution equations are recast into their usual form

$$\partial_t(\alpha^{\varphi} \rho^{\varphi}) + (\alpha^{\varphi} \rho^{\varphi} u_j^{\varphi})_{,j} = 0, \quad (3.41a)$$

$$\begin{aligned} \partial_t(\alpha^{\varphi} \rho^{\varphi} u_i^{\varphi}) + (\alpha^{\varphi} \rho^{\varphi} u_i^{\varphi} u_j^{\varphi})_{,j} + \overline{(c^{\varphi} \rho^{\varphi} u_i^{\varphi'} u_j^{\varphi'})}_{,j} \\ + \underbrace{\alpha^{\varphi} \bar{p}}_B + \underbrace{(\alpha^{\varphi} (p^{\varphi} - \bar{p}))}_{F_1} + \underbrace{\overline{c^{\varphi} p^{\varphi'}}}_{F_2} + \underbrace{\overline{c_{,i}^{\varphi} p'}}_D = \alpha^{\varphi} \rho^{\varphi} g_i, \end{aligned} \quad (3.41b)$$

$$\begin{aligned} \partial_t(\alpha^{\varphi} \rho^{\varphi} e^{\varphi}) + (\alpha^{\varphi} \rho^{\varphi} e^{\varphi} u_j^{\varphi})_{,j} + \overline{(c^{\varphi} \rho^{\varphi} e^{\varphi'} u_j^{\varphi'})}_{,j} \\ + \underbrace{\bar{p} \overline{c^{\varphi} u_{j,j}}}_V + \underbrace{\overline{c^{\varphi} p' u_{j,j}}}_I = \alpha^{\varphi} \rho^{\varphi} \dot{w}^{\varphi}, \end{aligned} \quad (3.41c)$$

$$\bar{p} = \sum_{\phi} \alpha^{\phi} p^{\phi}, \quad (3.41d)$$

$$p^{\varphi} = \mathcal{P}^{\varphi}(\rho^{\varphi}, e^{\varphi}, \boldsymbol{\sigma}^{\varphi}) + \underbrace{\sum_{xy} \frac{\partial^2 \mathcal{P}^{\varphi}}{\partial x \partial y} \cdot \overline{x' y'}}_H + \dots \quad (3.41e)$$

Strictly speaking α^{φ} is the *presence probability* of fluid φ , but it is designated here as the *volume fraction* according to common accepted usage—since first derivations used volume averaging. Notice that, following [Kataoka \(1986\)](#), mass fraction gradients $c_{,i}^{\varphi}$ appear and produce sheets of Dirac functions for discontinuous c^{φ} —as found in the important case of immiscible fluids (see also [Llor, 2005](#), § 3.1).

All the fluctuation-containing terms in (3.41) must be closed in order to solve the equations, usually from the mean quantities through system- and situation-dependent expressions. The pressure related terms have been separated into different contributions corresponding to various effects:

B: Buoyancy force, proportional to fluid volume;

F₁: momentum Flux from inter-fluid pressure differences;

F₂: momentum Flux from intra-fluid pressure fluctuations;

D: Drag from pressure fluctuations at interfaces, mostly due to turbulence and added mass;

V: reversible work of mean pressure into internal energy or $-pdV$;

I: Irreversible work of pressure fluctuations into internal energy;

H: contribution of thermodynamic state fluctuations to EOS of fluids to second-order (Hessian);

all of which except B and V require closure assumptions.

3.B.2 Backbone evolution equations

Equations (3.41) by themselves cannot provide total energy conservation as the kinetic energy of velocity fluctuations is not included. These equations could be derived and also complemented if applicable with added mass, surface tension effects, and internal volume exchanges (bubble vibrations). These effects will not be explored here as they marginally affect the mean pressure couplings, the only effects retained in the backbone model.

Cancellation of all fluctuation-containing terms in (3.41) *including* F_1 yields the non-dissipative backbone model in (3.1)—with notations (3.2a). The work of the pressure forces in the momentum equations can now be balanced with internal energies according to substitution

$$\overline{c^\varphi u_{j,j}} = -\overline{c^\varphi \frac{d_t \rho}{\rho}} \approx -\alpha^\varphi \frac{d_t^\varphi \rho^\varphi}{\rho^\varphi} = D_t^\varphi \alpha^\varphi, \quad (3.42)$$

which thus ensures conservation of total energy. The cancellation of term F_1 in (3.41) may not appear as a requirement to generate the backbone model. Several objections have been raised as commented in 3.A and have led to unequal pressure models.

The backbone model can be obtained independently of this averaging-and-closure procedure by applying the least action principle to a Lagrangian involving only the mean kinetic and internal energies of the fluids as noted in Fig. 3.1 (see for instance [Vazquez-Gonzalez et al., 2020](#), § 3 & refs therein). *This procedure forces fluid pressures to be equal.* The only possibility for a least action approach to yield unequal pressures is to add to the Lagrangian the missing kinetic and potential energy reservoirs. For instance, bubble oscillations derive from a Lagrangian containing the gas and liquid internal energies and the kinetic energy of the bubbles' volume variations ([Bedford & Drumheller, 1978](#); [Gavrilyuk & Saurel, 2002](#)).

3.B.3 Derivation of evolution equations in explicit form

At various points in the present work, explicit evolution equations are required for stiffness and prediction issues, notably in Section 3.3.2 for the multi-fluid equations of internal energies. These were already provided by [Vazquez-Gonzalez et al. \(2020, § 3.5\)](#) and are reproduced here for reference.

The starting point is the fundamental thermodynamic identity on the (common) pressure along the fluid trajectories

$$d_t^\varphi p = c^{2\varphi} d_t^\varphi \rho^\varphi + \Gamma^\varphi \rho^\varphi T^\varphi d^\varphi s^\varphi, \quad (3.43)$$

where $T^\varphi d^\varphi s^\varphi = \dot{w}^\phi$ are the per-mass irreversible energy sources on fluid φ . When combined with the mass conservation equations as

$$\sum_\varphi \left[(\alpha^\varphi / (\rho^\varphi c^{2\varphi})) \times (3.43) + (1/\rho^\varphi) \times (3.1a) \right], \quad (3.44)$$

it readily yields the explicit evolution equation of pressure (3.32).

The pressure evolution equation (3.32) can then be combined with (3.43) as

$$(\alpha^\varphi / (\rho^\varphi c^{2\varphi})) \times ((3.32) - (3.43)), \quad (3.45)$$

to yield the explicit evolution equations of the fluid densities (and also of their volume fractions)

$$\alpha^\varphi \frac{d_t^\varphi \rho^\varphi}{\rho^\varphi} = -D_t^\varphi \alpha^\varphi = \beta^\varphi \left[-\bar{u}_{i,i} + \sum_\phi \frac{\alpha^\phi}{\rho^\phi c^{2\phi}} \times \left((u_i^\varphi - u_i^\phi) p_{,i} - \Gamma^\varphi \rho^\varphi \dot{w}^\varphi + \Gamma^\phi \rho^\phi \dot{w}^\phi \right) \right]. \quad (3.46)$$

Substituted into the implicit evolution equations of internal energies (3.1c), this expression yields the energy equation in explicit form (3.5).

3.C The GEEC scheme for the backbone model

The multi-fluid GEEC scheme used in all the present numerical tests was first obtained and described by *Vazquez-Gonzalez et al. (2020)*. It displays the following main features:

1. arbitrary number of fluids;
2. arbitrary mesh dimension, structure, and motion—prescribed by the user or adjusted on-the-fly to the flow’s evolution;
3. continuity with the workhorse space- and-time-staggered schemes of in-house legacy codes;
4. explicit mass, momentum, and internal energy increment equations for each fluid, coupled by a single common pressure field;
5. exact conservation to round-off errors of each fluid’s mass, total momentum, and total energy;
6. second-order accuracy in the Lagrangian limit and first-order accuracy of fluid transport relative to the grid;
7. proper capture to second-order accuracy of isentropic flows—or quasi-symplectic behavior;

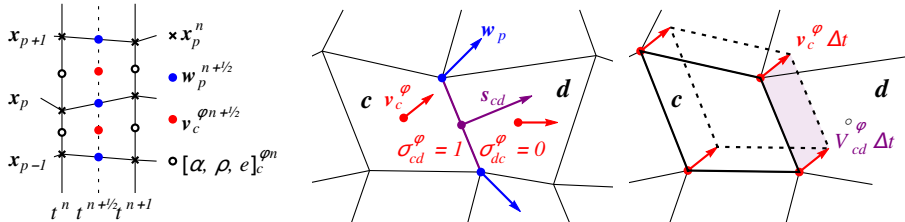


Figure 3.9: Graphical representations of mesh and discretized quantities in space–time (left) and 2D-space (center), with the swept-flux cell-to-cell transfers (right). Notice the respective node and cell centering of grid and per-fluid relative-to-grid velocities, $\vec{w}_p^{n+1/2}$ and $\vec{v}_c^{\varphi n+1/2}$.

8. shock capture and scheme stabilization ensured by a proper multi-fluid extension of usual single-fluid closures of artificial viscosity;
9. stable and robust behavior with high CFL condition on usual stiff test cases—devoid of common distortions such as hourglassing, DeBar artifacts, fragility to small volume fractions or large density ratios, etc.

The scheme is fully described below. For the present study, it is adapted to an EEIP by addition of sub-step 2.

All quantities are defined at integer- or half-integer-labeled times t^n or $t^{n-1/2} = (t^n + t^{n-1})/2$. As illustrated in Fig. 3.9 the system is defined at time t^n by quantities:

- $\Delta t^{n-1/2}$ time increment from t^{n-1} to t^n ,
- $\vec{u}_c^{\varphi n-1/2}$ absolute velocity of fluid φ ,
- $\vec{w}_p^{n-1/2}$ grid velocity,
- \vec{x}_p^n grid position,
- $\vec{v}_c^{\varphi n-1/2}$ grid-relative velocity of fluid φ ,
- $\sigma_{cd}^{\varphi n-1/2}$ upwind factor of fluid φ from cell c to cell d ($= 0$ or 1),
- $[\alpha\rho]_c^{\varphi n}$ apparent density of fluid φ ,
- $e_c^{\varphi n}$ per mass internal energy of fluid φ ,
- $\alpha_c^{\varphi n}$ volume fraction of fluid φ ,
- $\rho_c^{\varphi n}$ density of fluid φ ,
- p_c^n pressure (common to fluids),
- $q_c^{\varphi n}$ artificial viscosity stress of fluid φ .

The scheme evolves these quantities to time t^{n+1} by applying the seven sub-steps to follow. V_c^n , $\vec{s}_{cd}^{n+1/2}$, and $\mathring{V}_{cd}^{\varphi n-1/2}$ are respectively cell volumes, face vectors from cell c to cell d , and volume transport rate from c to d for fluid φ . All transport operators follow a swept-flux approach defined by the $\mathring{V}_{cd}^{\varphi n-1/2}$.

1. Time step determination from given CFL

$$\Delta t^{n+1/2} = \text{CFL} \times \min_{\varphi,c} \left\{ h_c^n / (c_c^n + |\vec{v}_c^{\varphi n-1/2}|) \right\}, \quad (3.47)$$

where c_c^n is the effective speed of sound of the mixture.

2. Explicit estimation of implicit pressure (IIEP), if selected

$$p_c^* = p_c^n \min[1, \exp(\tau_c^n)], \quad (3.48a)$$

where

$$\tau_c^n = -\bar{\gamma}_c^n \langle \mathring{V} \rangle_c^{n-1/2} / V_c^n. \quad (3.48b)$$

For the native GEEC scheme, $p_c^* = p_c^n$ is fully explicit.

3. Artificial viscosity, following common practice (Mattsson & Rider, 2015, & refs therein)

$$q_c^n = \rho_c^n \mathcal{Q}[\langle \mathring{V} \rangle_c^{n-1/2} / V_c^n, c_c^n] \quad (3.49a)$$

where

$$\langle \mathring{V} \rangle_c^{n-1/2} = \sum_{\varphi, d} \bar{s}_{cd}^{n-1/2} \cdot \left(\alpha_c^{\varphi n} \bar{\sigma}_{cd}^{\varphi n-1/2} \vec{u}_c^{\varphi n-1/2} + \alpha_d^{\varphi n} \bar{\sigma}_{dc}^{\varphi n-1/2} \vec{u}_d^{\varphi n-1/2} \right), \quad (3.49b)$$

$$\rho_c^n = \sum_{\phi} [\alpha \rho]_c^{\phi n}, \quad (3.49c)$$

$$\mathcal{Q}[S, C] = a_2 (\min[0, S] h)^2 - a_1 C S h, \quad (3.49d)$$

h being the characteristic cell size, and a_2 and a_1 being the respective quadratic and linear artificial-viscosity coefficients, here set to $a_2 = a_1 = 0.5$ in all the present work.

4. Momentum increments

$$\begin{aligned} & V_c^n [\alpha \rho]_c^{\varphi n} \vec{u}_c^{\varphi n+1/2} - V_c^{n-1} [\alpha \rho]_c^{\varphi n-1} \vec{u}_c^{\varphi n-1/2} \\ & + \Delta t^{n-1/2} \sum_d (\mathring{V}_{cd}^{\varphi n-1/2} [\alpha \rho]_c^{\varphi n-1} \vec{u}_c^{\varphi n-1/2} - \mathring{V}_{dc}^{\varphi n-1/2} [\alpha \rho]_d^{\varphi n-1} \vec{u}_d^{\varphi n-1/2}) \\ & = -\Delta t^n \alpha_c^{\varphi n} \sum_d \bar{\sigma}_{cd}^{\varphi n-1/2} \bar{s}_{cd}^{n-1/2} (p_d^* - p_c^* + q_d^n - q_c^n), \end{aligned} \quad (3.50a)$$

where the corrected upwinding factors are

$$\bar{\sigma}_{cd}^{\varphi n-1/2} = \frac{1}{2} \sigma_{cd}^{\varphi n-1/2} + \frac{1}{2} \sum_{\phi} \alpha_d^{\phi n} \sigma_{cd}^{\phi n-1/2}. \quad (3.50b)$$

Equilibration of fluid velocities (infinite drag), if selected

$$u_c^{\varphi n+1/2} = u_c^{n+1/2} = \sum_{\phi} [\alpha \rho]_c^{\phi n} u_c^{\phi n+1/2} / \sum_{\phi} [\alpha \rho]_c^{\phi n}. \quad (3.50c)$$

5. Grid velocity for ALE calculations

$$\vec{w}_p^{n+1/2} = \mathcal{W}(\{\vec{u}_c^{\varphi n+1/2}\}), \quad (3.51a)$$

$$\vec{v}_c^{\varphi n+1/2} = \vec{u}_c^{\varphi n+1/2} - \vec{w}_c^{n+1/2}, \quad (3.51b)$$

$$\mathring{V}_{cd}^{\varphi n+1/2} = \sigma_{cd}^{\varphi n+1/2} \bar{s}_{cd}^{n+1/2} \cdot \vec{v}_c^{\varphi n+1/2}, \quad (3.51c)$$

$$\sigma_{cd}^{\varphi n+1/2} = H(\bar{s}_{cd}^{n+1/2} \cdot \vec{v}_c^{\varphi n+1/2}), \quad (3.51d)$$

where H is the Heaviside function.

For Eulerian grid, $\vec{w}_p^{n+1/2} = \vec{0}$ as in present numerical tests.

6. Mass transport

$$\begin{aligned} & V_c^{n+1} [\alpha \rho]_c^{\varphi n+1} - V_c^n [\alpha \rho]_c^{\varphi n} \\ & + \Delta t^{n+1/2} \sum_d (\mathring{V}_{cd}^{\varphi n+1/2} [\alpha \rho]_c^{\varphi n} - \mathring{V}_{dc}^{\varphi n+1/2} [\alpha \rho]_d^{\varphi n}) = 0. \end{aligned} \quad (3.52)$$

7. Internal energy increments

$$\begin{aligned}
& V_c^{n+1}[\alpha\rho]_c^{\varphi n+1} e_c^{\varphi n+1} - V_c^n[\alpha\rho]_c^{\varphi n} e_c^{\varphi n} \\
& \quad + \Delta t^{n+1/2} \sum_d (\overset{\circ}{V}_{cd}^{\varphi n+1/2} [\alpha\rho]_c^{\varphi n} e_c^{\varphi n} - \overset{\circ}{V}_{dc}^{\varphi n+1/2} [\alpha\rho]_d^{\varphi n} e_d^{\varphi n}) \\
& = -\Delta t^n \beta_c^{\varphi n} p_c^* \langle \overset{\circ}{V} \rangle_c^n \\
& \quad + \Delta t^n \sum_\phi \mu_c^{\varphi\phi n} (\langle \vec{u}^\varphi \cdot \vec{\nabla} p \rangle_c^n - \langle \vec{u}^\phi \cdot \vec{\nabla} p \rangle_c^n) \\
& \quad - \sum_\phi \mu_c^{\varphi\phi n} (\Gamma_c^{\varphi n} \langle \rho^\varphi \delta W^\varphi \rangle_c^n - \Gamma_c^{\phi n} \langle \rho^\phi \delta W^\phi \rangle_c^n) \\
& \quad \quad \quad + \alpha_c^{\varphi n} \langle \rho^\varphi \delta W^\varphi \rangle_c^n, \quad (3.53a)
\end{aligned}$$

where $\beta_c^{\varphi n}$, $\mu_c^{\varphi\phi n}$, and $\Gamma_c^{\varphi n}$ are given by (3.6), mean drift work on fluid φ is

$$\begin{aligned}
\langle \vec{u}^\varphi \cdot \vec{\nabla} p \rangle_c^n & = \frac{1}{2} \sum_d \bar{\sigma}_{cd}^{\varphi n-1/2} (\vec{u}_c^{\varphi n+1/2} + \vec{u}_c^{\varphi n-1/2}) \cdot \bar{s}_{cd}^{n-1/2} \\
& \quad \quad \quad \times (p_d^* - p_c^*), \quad (3.53b)
\end{aligned}$$

and mean global volume change rate is

$$\begin{aligned}
\langle \overset{\circ}{V} \rangle_c^n & = \frac{1}{2} \sum_{\varphi,d} \bar{s}_{cd}^{n-1/2} \cdot [\alpha_c^{\varphi n} \bar{\sigma}_{cd}^{\varphi n-1/2} (\vec{u}_c^{\varphi n+1/2} + \vec{u}_c^{\varphi n-1/2}) \\
& \quad \quad \quad + \alpha_d^{\varphi n} \bar{\sigma}_{dc}^{\varphi n-1/2} (\vec{u}_d^{\varphi n+1/2} + \vec{u}_d^{\varphi n-1/2})]. \quad (3.53c)
\end{aligned}$$

The dissipation is estimated as follow,

$$\begin{aligned}
\alpha_c^{\varphi n} \langle \rho^\varphi \delta W^\varphi \rangle_c^n & = -\Delta t^n \lambda_c^{\varphi n} q_c^n \langle \overset{\circ}{V} \rangle_c^n \\
& \quad + \Delta t^{n-1/2} \sum_d \overset{\circ}{V}_{dc}^{\varphi n-1/2} \frac{1}{2} [\alpha\rho]_d^{\varphi n-1} \\
& \quad \quad \quad \times (\vec{u}_c^{\varphi n+1/2} - \vec{u}_d^{\varphi n-1/2}) \cdot (\vec{u}_c^{\varphi n-1/2} - \vec{u}_d^{\varphi n-1/2}), \quad (3.53d)
\end{aligned}$$

The coefficient $\lambda_c^{\varphi n}$ weighs the total dissipation sources on fluid φ (other than numerical residues). It is set here to $\lambda_c^{\varphi n} = [(\alpha^\varphi/\Gamma^\varphi)/\sum_\phi(\alpha^\phi/\Gamma^\phi)]_c^n$ unless specified otherwise.

8. Volume fractions, densities and pressure, given as solutions to the implicit set of equations

$$\mathcal{P}^\varphi(\rho_c^{\varphi n+1}, e_c^{\varphi n+1}) = p_c^{n+1}, \quad (3.54a)$$

$$[\alpha\rho]_c^{\varphi n+1}/\rho_c^{\varphi n+1} = \alpha_c^{\varphi n+1}, \quad (3.54b)$$

$$\sum_\varphi \alpha_c^{\varphi n+1} = 1, \quad (3.54c)$$

where \mathcal{P}^φ is the (half-)EOS of fluid φ .

3.D Semi-analytical solution of isentropic two-fluid expansion

Isentropic free expansion is described by the mass and momentum equations (3.1a) and (3.1b) with the mixture EOS (3.12). In reduced quantities and expressing all fields as functions of

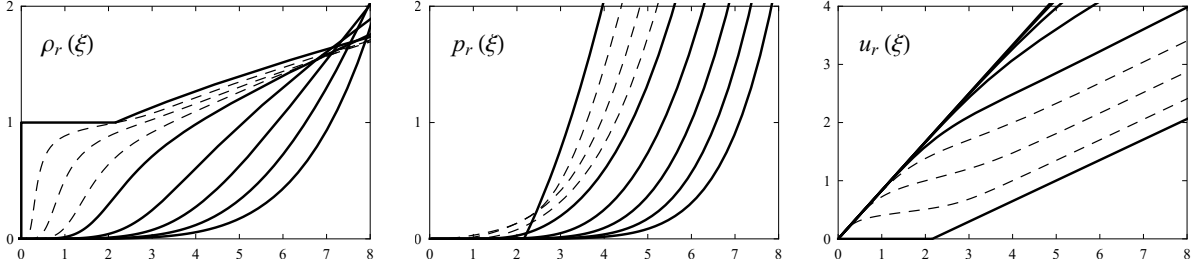


Figure 3.10: Non-dimensional semi-analytical profiles of expansion to vacuum of ideal-stiffened gas mixtures of varying compositions as given in Fig. 3.2: pressure, density, and velocity (from left to right).

α^a	u	c	t^{Final}
10^{-12}	0.4299853856289317	3.096037495936114	1/4
1/20	1.530201240096114	2.746459432810063	1/5
1/2	4.356034272582599	1.607886811203803	1/6
19/20	5.959547847799742	1.248993348739162	1/8
$1 - 10^{-12}$	6.111757952493628	1.222351581614179	1/8

Table 3.4: Velocity and speed of sound at the point where density and pressure conditions of the double-expansion of air-contaminated water match values in Table 3.2 for different air volume fractions α^a . Final simulation times are defined to keep the profile within the $[0, 1]$ interval. Expansion profiles for similar α^a values are illustrated in Fig. 3.10.

the reduced quantity $\xi = x/t$, the equations become (subscript r is implicit in this appendix)

$$0 = -\xi \frac{\partial}{\partial \xi} \rho + \frac{\partial}{\partial \xi} (\rho u), \quad (3.55a)$$

$$0 = -\xi \frac{\partial}{\partial \xi} (\rho u) + \frac{\partial}{\partial \xi} (\rho u^2) + c^2 \frac{\partial}{\partial \xi} \rho. \quad (3.55b)$$

This homogeneous system of ODEs has a non zero solution only if its determinant does not cancel or

$$(u - \xi)^2 - c^2 = 0. \quad (3.56)$$

Selecting the positive velocity branch to eliminate u in (3.55a) yields the ODE for ρ

$$\left(\rho \frac{\partial c}{\partial \rho} + c\right) \frac{\partial}{\partial \xi} \rho = \rho. \quad (3.57)$$

As isentropic curves takes a particularly simple form as functions of pressure, it appears simpler to express the expansion wave as $\xi(p)$, taking p as a parametric variable. It is thus found

$$\frac{\partial}{\partial p} \xi = (\rho c)^{-1} + \frac{\partial}{\partial p} c, \quad (3.58)$$

which is solved from point $p = 0$ where $\xi = 0$ and $c = 0$ by the simple quadrature

$$\xi(p) = \int_0^p \frac{dp}{\rho c} + c. \quad (3.59)$$

Closed with EOS (3.12), numerical integration of this last quadrature provides semi-analytical solutions for any initial air volume fraction. Various such resulting expansion profiles are illustrated in Fig. 3.10 for EOS coefficients of Table 3.2. Table 3.4 lists some velocities and speeds of sound at the canonical point where $\rho^a = \rho^w$ with the same coefficients. These provide simple initial conditions for test cases.

As visible in Fig. 3.10, the solutions display a strong gradient of pressure and air density for small initial air volume fractions.

3.E Noh’s test for ideal–stiffened gas mixtures

Since its inception, the numerical test of Noh (1987) has become a mandatory benchmark for compressible hydro-schemes. Despite a simple setting (ideal gas, 1D, fixed wall condition, uniform unit initial density and velocity) its initial pressure and temperature are null, thus making an infinitely strong shock propagate from the wall. This challenges two critical features of an hydro-scheme: (i) its entropic character, as any errors of wrong sign on a zero pressure state can be fatal (in practice initial pressure is set just above round-off level, i.e. 10^{-15} for double precision) and (ii) its CFL limitations, especially during initial transients which can generate singular states (known as wall heating).

This test is extended here to the contrasted two-fluid velocity-equilibrated mixture of ideal and stiffened gases—for convenience here designated as “air” and “water,” and labeled “a” and “w.” Now, this cannot be achieved without giving up the important feature of infinitely strong shock: it is impossible to find a non trivial pressure-equilibrated ideal–stiffened gas mixture where both fluids have vanishing speed of sound. It is thus assumed here that the initial condition is merely at zero pressure, thus ensuring zero speed of sound on the ideal gas only.

Another important feature of any extension of Noh’s test is that dissipation details now impact the jump conditions and propagation velocity of the shock. It is however possible to determine the set of all shock-accessible states of the mixture as shown below.

In the reference frame of the shock front, jump conditions on the mixture’s total mass, momentum, and energy are

$$0 = \llbracket \rho u \rrbracket_0^1, \quad (3.60a)$$

$$0 = \llbracket \rho u^2 + p \rrbracket_0^1, \quad (3.60b)$$

$$0 = \llbracket \rho(e + u^2/2) + pu \rrbracket_0^1, \quad (3.60c)$$

where subscripts 0 and 1 label respectively the up- and downstream states and $\llbracket \times \rrbracket_0^1$ denote jumps across the shock layer. Assuming vanishing initial upstream pressure $p_0 = 0$, these

conditions define the velocities and a thermodynamic relationship

$$u_0 = -\left(e_1 - e_0 + \frac{1}{2}p_1(\rho_1^{-1} + \rho_0^{-1})\right) / \sqrt{2(e_1 - e_0)}, \quad (3.61a)$$

$$u_1 = -\left(e_0 - e_1 + \frac{1}{2}p_1(\rho_1^{-1} + \rho_0^{-1})\right) / \sqrt{2(e_1 - e_0)}, \quad (3.61b)$$

$$0 = \rho_1^{-1} - \rho_0^{-1} + 2(e_1 - e_0)/p_1. \quad (3.61c)$$

It is thus sufficient to provide up- and downstream states of the mixture compatible with (3.61c) to fully define the shock.

For the single-pressure air–water mixture with (constant) mass fractions c^a and c^w , densities and energies are

$$1/\rho_{\{0,1\}} = c^w/\rho_{\{0,1\}}^w + c^a/\rho_{\{0,1\}}^a, \quad (3.62a)$$

$$e_{\{0,1\}} = c^w e_{\{0,1\}}^w + c^a e_{\{0,1\}}^a, \quad (3.62b)$$

$$p_0 = 0 = \Gamma^w \rho_0^w e_0^w - (\Gamma^w + 1)\Pi^w = \Gamma^a \rho_0^a e_0^a, \quad (3.62c)$$

$$p_1 = \Gamma^w \rho_1^w e_1^w - (\Gamma^w + 1)\Pi^w = \Gamma^a \rho_1^a e_1^a. \quad (3.62d)$$

Mass fractions, final densities and final pressure can be scaled into reduced quantities $\alpha_0^{\{a,w\}}$, $v_r^{\{a,w\}}$, and p_r , respectively initial volume fractions, Hugoniot-scaled volume ratios across shock, and stiffened-gas-scaled final pressure, defined as

$$c^{\{a,w\}} = \alpha_0^{\{a,w\}} \rho_0^{\{a,w\}} / \rho_0, \quad (3.63a)$$

$$\rho_1^{\{a,w\}} = \rho_0^{\{a,w\}} (1 + 2/\Gamma^{\{a,w\}}) / v_r^{\{a,w\}}, \quad (3.63b)$$

$$p_1 = p_r \Pi^w (\Gamma^w + 1) / (1 + \Gamma^w/2), \quad (3.63c)$$

with realizability constraints $\alpha_0^w + \alpha_0^a = 1$, $v_r^{\{a,w\}} > 0$, and $p_r > 0$. Substitution of energies and scaled quantities in (3.61c) yields after some algebra

$$0 = \alpha_0^w \left(v_r^w - 1 - \frac{1 + 2/\Gamma^w - v_r^w}{p_r} \right) + \alpha_0^a (v_r^a - 1), \quad (3.64)$$

hence

$$p_r = \frac{\alpha_0^w (1 + 2/\Gamma^w - v_r^w)}{\alpha_0^w v_r^w + \alpha_0^a v_r^a - 1}. \quad (3.65)$$

In this form and for given initial composition and EOS (here appearing as $\alpha_0^{\{a,w\}}$ and Γ^w), the thermodynamic condition (3.61c) reduces to an algebraic relationship between the three independent scaled variables $v_r^{\{a,w\}}$ and p_r . The set of accessible shocks is thus two dimensional but is bounded by realizability constraints. Shock conditions are selected within this domain by the strength of the shock and the balance of entropy production between fluids.

With condition (3.65), the realizability constraint $p_r > 0$ now limits the acceptable $v_r^{\{a,w\}}$ values to

$$v_r^w < 1 + 2/\Gamma^w \quad \text{and} \quad \alpha_0^w v_r^w + \alpha_0^a v_r^a > 1, \quad (3.66a)$$

or

$$v_r^w > 1 + 2/\Gamma^w \quad \text{and} \quad \alpha_0^w v_r^w + \alpha_0^a v_r^a < 1, \quad (3.66b)$$

This last condition is specific of multi-fluid behavior as it allows water to *expand* through shock. It is accessible only if $\alpha_0^w/\alpha_0^a < (1 - v_r^a)\Gamma^w/2$. Air expansion is also accessible, but simultaneous expansion of air and water is forbidden.

Total entropy must increase through shock but expliciting this condition on a two-fluid system requires knowledge of the individual fluid entropies, not contained in the half-EOS. It is permissible for instance that the entropy of *one* of the fluids *decreases* through a shock provided that the *total entropy increases*—though actual physical dissipation processes in such cases could be highly complex and specific.

Accessible from the half-EOS of the present study is the more restrictive condition of *entropy increase on each of the fluids*, a situation designated here as “doubly entropic.” For ideal gas at zero pressure, this is already fulfilled by the realizability condition $p_1 > 0$. For the stiffened gas, inserting (3.10b) into (3.65), it is found

$$\frac{\alpha_0^w(1 + 2/\Gamma^w - v_r^w)}{\alpha_0^w v_r^w + \alpha_0^a v_r^a - 1} > \frac{1 + \Gamma^w/2}{1 + \Gamma^w} \left[\left(\frac{1 + 2/\Gamma^w}{v_r^w} \right)^{1+\Gamma^w} - 1 \right], \quad (3.67)$$

or

$$\alpha_0^a v_r^a < 1 - \alpha_0^w v_r^w \left(1 - \frac{(1 + \Gamma^w) \left[\frac{1+2/\Gamma^w}{v_r^w} - 1 \right]}{(1 + \Gamma^w/2) \left[\left(\frac{1+2/\Gamma^w}{v_r^w} \right)^{1+\Gamma^w} - 1 \right]} \right), \quad (3.68)$$

In the (v_r^a, v_r^w) planes at fixed $\alpha_0^{\{a,w\}}$ values, this limit can be shown to connect points $(v_r^a, v_r^w) = (1, 1 + 2/\Gamma^w)$ and $(1/\alpha_0^a, 0)$ where it is tangent respectively to the Hugoniot line of water and to the $p_r = \infty$ limit. This is illustrated in Fig. 3.11 for the $\Gamma_0^{\{a,w\}}$ values in last row of Table 3.2.

Compared to the single-fluid test, the doubly-entropic two-fluid Noh test can produce densities beyond the Hugoniot limits $1 + 2/\Gamma^{\{a,w\}}$, for either of the fluids (but not both at once) and for any initial volume fractions as visible in Fig. 3.11. It can also produce *lower* densities for water or air respectively if $\alpha_0^w < 1/(1 + 2/\Gamma^w)$ or $\alpha_0^a < 1/(1 + 2/\Gamma^a)$.

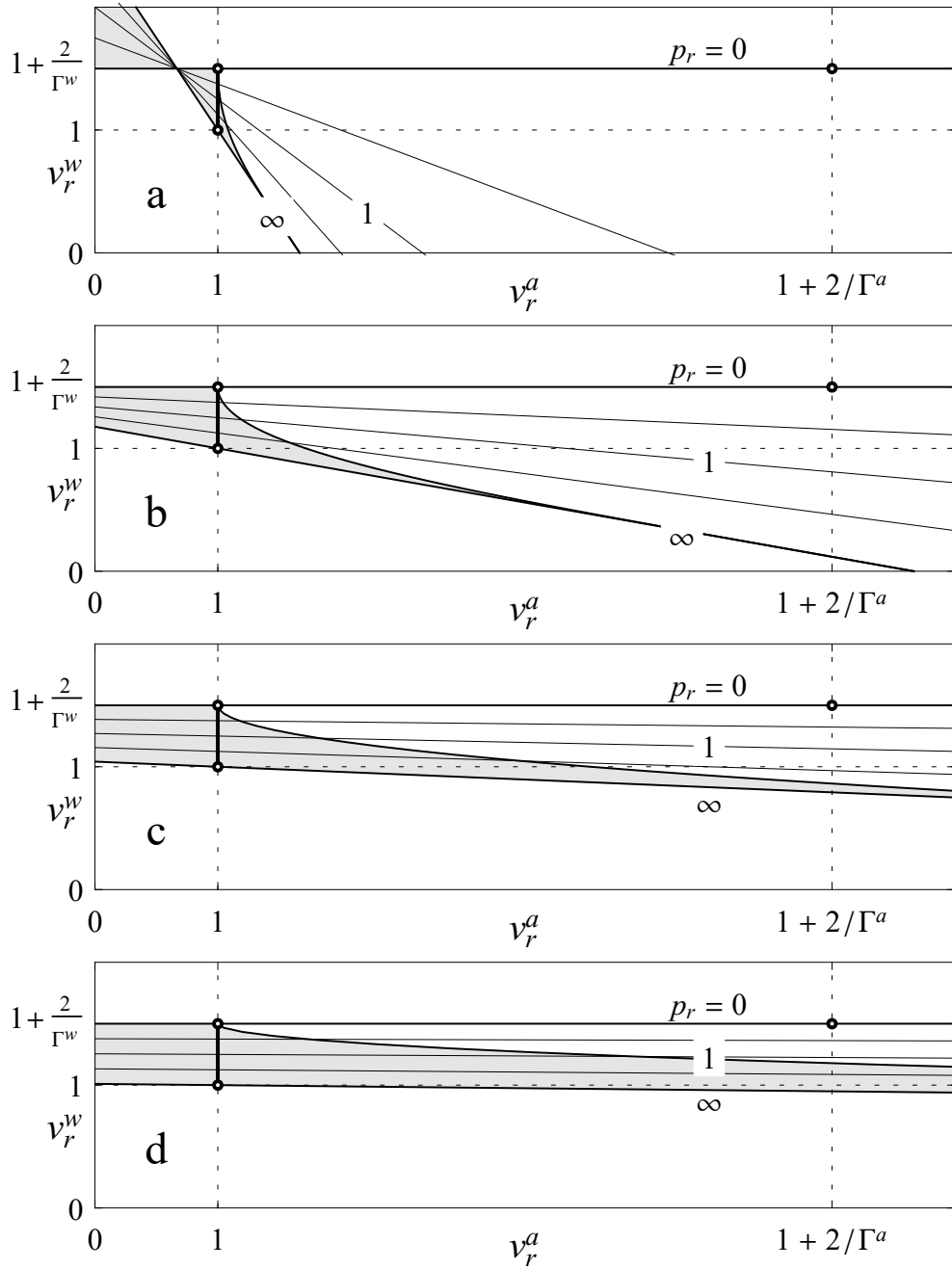


Figure 3.11: Representation of accessible shocked states in the adiabatic two-fluid extension of Noh’s test illustrated on an air–water mixture: for varying initial volume fractions of air $\alpha_0^a = 60\%$, 15% , 4% , and 1% (from top to bottom), states accessible by all combinations of adiabatic irreversible energy productions span the gray zones in the planes of reduced coordinates (v_r^a, v_r^w) (3.63b). The corresponding reduced shock pressures p_r (3.63c) are represented by their contour lines at values 0 and ∞ (medium thick lines), and $\frac{1}{3}$, 1, and 3 (thin lines). Independent shock adiabats on each of the fluids would connect the pole (white point) with different shocked states for varying shock pressures (thick line joining white points). The forbidden zone (white area) is defined by negative final pressure or negative entropy production on water (respectively out or within of the $p_r = 0$ and $p_r = \infty$ lines).

CHAPTER 4

Preserving isentropic behavior in multi-fluid systems through fundamental energy closures and first principle

Contents

4.1 Introduction	122
4.1.1 Thermodynamic consistency in multiphase flows	122
4.1.2 Isentropy through variational approaches and first principles	124
4.1.3 Explicit formalization in anticipation of future numerical schemes	126
4.2 Fundamental modeling of some energy reservoirs	127
4.2.1 Energy reservoirs at the cornerstone of non relaxed multiphase models	127
4.2.2 Energies of fluctuations lost by averaging process	129
4.3 Dissipation free models with added fluctuations	136
4.3.1 Lagrangian and momentum equation	136
4.3.2 Forcing pressure equality	139
4.3.3 Kinetic energy equations, conservation of the total energy	141
4.3.4 Explicit internal energy equations	143
4.A Appendix: pressure evolution equation with added mass and without pressure constraint	147

4.1 Introduction

4.1.1 Thermodynamic consistency in multiphase flows

General overview of entropy issues in fluid models and schemes

Entropy is a polymorphic concept of physics, first introduced to understand cycles in steam engines (Clausius, Carnot, etc...) where its link with irreversibly was established. It was soon applied to fluid mechanics in the shock theory (Rankine, Hugoniot, etc...) (Salas,

2007) and the phase transition (Joseph Black). It is at the root of powerful postulates in mechanics of equilibrium such as the maximum entropy principle used by Callen (1985). Now, entropy should be preserved in absence of dissipative effects such as viscosity, heat conduction, etc. . . in fluid mechanics. Once a system is characterized by potentials and constraints, its isentropic evolution is unique. A discrepancy from it leads to either entropy production in the best-case scenario or entropy destruction which corresponds to a violation of the second principle.

If continuous models may preserve exactly this property, numerical schemes produce errors at the scheme order which deviate the computed thermodynamic path from the isentropic one. This is why capturing isentropic evolution by numerical schemes is said to be especially fragile by Asher & McLachlan (2005). However, it has been recognized that entropy production stabilizes schemes. In this spirit, correction of Godunov schemes aiming to solve the Euler equations are made (Harten, 1983) to ensure enough dissipation at each time step and artificial viscosity is introduced to stabilize Lagrangian schemes (VonNeumann & Richtmyer, 1950) in shocks. However, if artificial viscosity stands for mesoscopic viscous mechanisms that occur in shocks and are not taken into account at model scale, correction of Godunov like schemes dissipate everywhere, i.e. even outside shocks (Shen *et al.*, 2010). Thus isentropy cannot be preserved exactly in numerical computations but can be approximated *as much as possible*.

On the other hand, preserving exact isentropy in fluid models is always possible. Dissipation free constitutive equations of the simple single fluid system are the Euler equations, known since several centuries. The entropy evolution is straightforward to extract and shows the exact isentropic character of this set of equations. Still, entropy criteria is necessary to select the right solution in discontinuous data. However, more complex fluid systems which integrate radiation, turbulence, . . . are tough to model because they involve several internal interactions between various potentials. Many dissipation mechanisms exist inside these systems which produce irreversible energy transfers between potentials. These mechanisms occur at sub-scale and depend on microscopic description. Thus, several possibilities exist to close these dissipations depending on various a priori choices about microscopic physics inside systems. However, once all the potentials have been set, the non dissipative macroscopic physics becomes unique. This involves that there is a unique expression for each interaction inside the system.

Zoom on multi-fluid Euler-Euler modeling

Among complex fluid systems, multiphase flows represent a large domain of research that has been developed to predict many industrial and academical flows. One of the most popular way to model them is the Eulerian-Eulerian approach. It consists on considering that all fluids may coexist on the same time-space point. All fluids are described by a set of fields standing for various quantities of interest such as velocity, pressure, etc. . . . These fields are linked through a system of partial differential equation (PDE) similar to the Euler equations

(containing transport, pressure gradient, etc. . .). To obtain this set of PDE, the single fluid equations (Euler or Navier–Stokes) are conditionally averaged with the function of presence of a given fluid of the mixture. The ensuing equations described the evolution of mean fluid quantities and contains also high order terms whose closures are needed. These closures depend on residual interpretations, themselves resulting of the type of flows studied and the averaging operator used.

First applications of averaging approaches were made by [van Deemter & van der Laan \(1961\)](#) and [Hinze \(1963\)](#), they were soon popularized by [Ishii \(1975\)](#) and [Drew \(1983\)](#). The modern form of models issued from this approach consists on three equations per fluid representing the evolution of their mass, momentum and energy. These equations are complemented by constraint on the sum of averaged presence functions, denoted (sometimes misleadingly) volume fractions and the state equation (EOS) of each phase. To complete the system, more equations are needed ¹. Generally, these missing equations are relations between phase pressures which may be algebraic ([Toumi, 1996](#)), static ([Ramshaw, 1978](#)) or dynamic ([Baer & Nunziato, 1986](#)). This last set of equations has been extensively discussed for two reasons. First, it does not comes directly from the averaging process, thus, similarly to the fluctuation terms, its validity depends on the type of flow considered and the averaging operator used. Secondly, its choice impact the well-posedness of the model ([Gidaspow *et al.*, 1973](#); [Ramshaw, 1978](#); [Saurel & Abgrall, 1999a](#)) and thus its applicability to be used for real flows’ simulation.

Closure choices are not unique and lead to a great variety of models specific to a given flow type. However, once the energy reservoirs of the system are specified, there is only one isentropic evolution. The cornerstone reservoirs are specified by the mean evolution equations and are formed by the mean kinetic and mean internal energy of each fluid. Therefore, among the various possible closures only one allows to follow the isentropic evolution corresponding to the averaged equations. Nevertheless, other closures are possible as long as they do not lead to violation of the second principle ([Arnold *et al.*, 1990](#)).

4.1.2 Isentropy through variational approaches and first principles

Structure of isentropic systems

According to [Berdichevsky \(2009\)](#), equations that derived from a variational method possess a variational structure whose major feature is the reciprocity of physical interactions. From him: ‘*All equations of microphysics possess such a structure*’ and this property can be extended to reversible macroscopic systems because they derive from microscopic ones. When systems are simple enough, variational approach is not necessary to find motions possessing the variational structure. A famous example are the Euler equations which derive from a least action principle but were found in 1757 by Euler without using the Lagrange formal-

¹for N phases: $4 \times N + 1$ equations (N mass, N momentum, N energy, N EOS + volume fraction) for $5 \times N$ unknowns ($\alpha^\varphi, u^\varphi, \rho^\varphi, e^\varphi, p^\varphi$)

ism of 1756. However, when systems become more complex with non trivial interactions, variational methods are powerful to obtain reversible equations because the consistency between the PDEs and the energy reservoirs, possibly tedious, is provided by straightforward differentiations.

Compressible multiphase flow systems are made of several fluids who possess at least two energy reservoirs (the internal and kinetic energy). These fluids are coupled through the volume filling condition and are constrained by their mass conservation. All reservoirs may exchange energy which gives potentially $N \times (N - 1)$ coupling terms that must be modeled. Thus, these systems fall into the category of complex systems where variational methods are very competitive in order to predict their isentropic evolution.

One particular variational method is the least action principle (LAP) formulated by Lagrange. The functional which is minimized in this method corresponds to the integral over time of the difference between the kinetic and potential energies of the system. This principle may appear odd because of its non locality and the peculiarity of the functional (Berdichevsky, 2009). However, it has successfully survived many physical revolutions from quantum mechanics to general relativity.

Least action principle in fluid mechanics

The use of the LAP in fluid mechanics appeared relatively lately compared to other domains of physics. It can be traced back to Clebsch (1859) for incompressible flows and to Bateman (1929) for irrotational compressible flows. However, using variational methods in optics started with Fermat in 1657. Because fluid mechanics may be described with two different coordinate systems (Euler and Lagrange), two different options have been pursued to apply the LAP. However, because this principle is independent of the choice of coordinates, these two options were found to be equivalent (Herivel, 1955) and clarified by Seliger & Whitham (1968). The first option is to work with Lagrangian coordinates and has been developed by Eckart (1938), Eckart (1960). Using the Eulerian coordinates was less straightforward because constraints had to be introduced in the functional. It was Lin (1959) who introduced is famous one which keeps trace of the particles' Lagrangian coordinates. A last formulation of the LAP was developed by Bretherton (1970) using the concept of virtual motion.

Because multiphase flows may obey to complex motion, the LAP was used to add micro phenomena in models. The precursors of this method are Bedford & Drumheller (1978) who developed a model for the kinetic energy of bubbles. This new kinetic energy was also taken into account by Saurel & Abgrall (1999a) and Sciarra *et al.* (2003) within LAP. All of these authors used the virtual motion approach to derive their functional. LAP in Eulerian coordinates was also used to predict superfluid behavior (Geurst, 1980) and to take into account added mass effects in multiphase models (Geurst, 1985).

4.1.3 Explicit formalization in anticipation of future numerical schemes

Numerical schemes crafting relies on specific PDE structures to be formulated. For instance, finite element methods are preferably applied to elliptic PDE. In fluid dynamics computation, finite volume schemes based on fluxes are extensively used because they apply to conservative PDE. This is why Euler equations are often formalized in total energy. In multiphase flows, models may rarely be written in fully conservative forms. A well known example is the one pressure model (or six equations model) (Toumi, 1996; Munkejord *et al.*, 2009; Vazquez-Gonzalez *et al.*, 2020), where volume fraction is outside pressure derivative (or inversely which is the so called nozzling term) in the momentum equation. However, models always possess one conservative part (at least the transport), which can be discretized with finite volume schemes. Furthermore, convection part of the model may be hyperbolic and thus discretized by Godunov like schemes (Saurel & Abgrall, 1999a). This is the case for the Baer & Nunziato (1986) (BN) like models.

Now, discretization of non conservative terms must be carefully crafted in order to respect conservations and thermodynamic consistency². One way to achieve this is the use of variational methods leading to symplectic schemes preserving the geometric structure of numerical flows (Marx, 2008; Hairer *et al.*, 2006). However, energy equations do not derive from variational methods but from first principles (Gibbs equations). Thus, their discretization is not provided with standard recipes. Yet, as shown by Vazquez-Gonzalez *et al.* (2020), continuous forms may be mimicked to build conservative and consistent discretizations. However, respecting conservation involve explicit dynamics to avoid complex studies of high dimensional non linear systems.

In multiphase flows Eulerian-Eulerian models, all fluids are coupled through the volume filling constraint. Thus, explicit formulation of energies is not straightforward to obtain. BN like models impose explicit dynamics of volume fractions through their specific pressure relation and thus explicit dynamics of energies. However, pressure equality in the six equations model does not lead immediately to explicit dynamics. To the knowledge of the authors, explicit formulation of energy equations in this model are only written by Vazquez-Gonzalez *et al.* (2020) and nearly by Munkejord *et al.* (2009) where the explicit volume fraction dynamics is deduced. Though, explicit formulations also reveals stiffness due to contrasted EOS which is inherent to all multiphase models, even in the BN types models (Chiocchetti & Müller, 2020). Thus, explicit forms allows to adapt numerical schemes to capture it. In two-phase flow modeling with single pressure models, only two potentials are implicitly coupled. These are the internal energies of both fluid whose dynamics contain time derivative of volume fraction (Munkejord *et al.*, 2009; Vazquez-Gonzalez *et al.*, 2020). However, when other energies are added to the system (bubbles inertia, added mass, surface tension, etc. . .), more potentials are coupled and thus explicit formulations are harder to obtain. We derive here consistent explicit energies equations in multiphase systems containing various energy reservoirs issued from literature.

²thermodynamic consistency is also an issue in full conservative PDE system discretization

4.2 Fundamental modeling of some energy reservoirs

4.2.1 Energy reservoirs at the cornerstone of non relaxed multiphase models

Averaging procedure to obtain multiphase models

As explained above, multiphase models are obtained through averaging processes of single phase systems. This averaging is conditioned by the mass fraction of the fluid φ denoted here c^φ . This function is equal to 1 when only the fluid φ is present and 0 when it disappears. Because the aim is to obtain dissipation free multiphase equation, dissipation free single fluid equations are averaged. Their simplest form is the Euler equations. Conditional averaging resumes to multiply them by c^φ and apply the averaging operator denoted over-bar. This yields:

$$\overline{c^\varphi \partial_t(\rho)} + \overline{c^\varphi \partial_x(\rho u)} = 0, \quad (4.1a)$$

$$\overline{c^\varphi \partial_t(\rho u)} + \overline{c^\varphi \partial_x(\rho u^2)} + \overline{\partial_x(c^\varphi p)} = 0, \quad (4.1b)$$

$$\overline{c^\varphi \partial_t(\rho e)} + \overline{c^\varphi \partial_x(\rho e u)} + \overline{c^\varphi p \partial_x(u)} = 0, \quad (4.1c)$$

$$\bar{p} = \overline{\sqrt{(c^\varphi, \rho, e, \boldsymbol{\sigma})}}. \quad (4.1d)$$

In contrast to the rest of this chapter, p stands here for the one-point one-time non-averaged pressure. $\boldsymbol{\sigma}$ stands for supplementary thermodynamic variables (such as entropies) which fully define the state of the fluids. The mass fraction is transported with the fluid velocity in order to ensure the mass conservation of each fluid. Now, assuming that averaging and derivative operations commute, this set of equations leads to:

$$\partial_t(\overline{c^\varphi \rho}) + (\overline{c^\varphi \rho u_j})_{,j} = 0, \quad (4.2a)$$

$$\partial_t(\overline{c^\varphi \rho u_i}) + (\overline{c^\varphi \rho u_i u_j})_{,j} + \overline{c^\varphi p_{,i}} = 0, \quad (4.2b)$$

$$\partial_t(\overline{c^\varphi \rho e}) + (\overline{c^\varphi \rho e u_j})_{,j} + \overline{c^\varphi p u_{j,j}} = 0, \quad (4.2c)$$

$$\bar{p} = \overline{\sqrt{(c^\varphi, \rho, e, \boldsymbol{\sigma})}}. \quad (4.2d)$$

Defining means and fluctuations as

$$\alpha^\varphi = \overline{c^\varphi}, \quad \alpha^\varphi \rho^\varphi = \overline{c^\varphi \rho}, \quad (4.3a)$$

$$\alpha^\varphi \rho^\varphi u_i^\varphi = \overline{c^\varphi \rho u_i}, \quad u_i^{\varphi'} = u_i - u_i^\varphi, \quad (4.3b)$$

$$\alpha^\varphi p^\varphi = \overline{c^\varphi p}, \quad p^{\varphi'} = p - p^\varphi, \quad (4.3c)$$

$$\alpha^\varphi \rho^\varphi e^\varphi = \overline{c^\varphi \rho e}, \quad \alpha^\varphi \rho^\varphi \dot{w}^\varphi = \overline{c^\varphi \rho \dot{w}}, \quad (4.3d)$$

where $\sum_{\varphi} \alpha^{\varphi} = 1$, the averaged evolution equations are restated into usual form

$$\partial_t(\alpha^{\varphi} \rho^{\varphi}) + (\alpha^{\varphi} \rho^{\varphi} u_j^{\varphi})_{,j} = 0, \quad (4.4a)$$

$$\begin{aligned} \partial_t(\alpha^{\varphi} \rho^{\varphi} u_i^{\varphi}) + (\alpha^{\varphi} \rho^{\varphi} u_i^{\varphi} u_j^{\varphi})_{,j} + \underbrace{(\overline{c^{\varphi} \rho^{\varphi} u_i^{\varphi'} u_j^{\varphi'}})_{,j}}_A \\ + \underbrace{\alpha^{\varphi} \bar{p}_{,i}}_B + \underbrace{(\overline{c^{\varphi} p^{\varphi'}} + \alpha^{\varphi} (p^{\varphi} - \bar{p}))_{,i}}_F + \underbrace{\overline{c_{,i}^{\varphi} p'}}_D = 0, \end{aligned} \quad (4.4b)$$

$$+ \underbrace{\alpha^{\varphi} p_{,i}^{\varphi} + \alpha_{,i}^{\varphi} (p^{\varphi} - \bar{p}) - \overline{c_{,i}^{\varphi} p'}}_{+ \alpha^{\varphi} p_{,i}^{\varphi} + \alpha_{,i}^{\varphi} (p^{\varphi} - \bar{p}) - \overline{c_{,i}^{\varphi} p'}}$$

$$\begin{aligned} \partial_t(\alpha^{\varphi} \rho^{\varphi} e^{\varphi}) + (\alpha^{\varphi} \rho^{\varphi} e^{\varphi} u_j^{\varphi})_{,j} + \underbrace{(\overline{c^{\varphi} \rho^{\varphi} e^{\varphi'} u_j^{\varphi'}})_{,j}} \\ + \underbrace{\bar{p} \overline{c^{\varphi} u_{j,j}}}_W + \underbrace{\overline{c^{\varphi} p' u_{j,j}}}_S = 0, \end{aligned} \quad (4.4c)$$

$$\bar{p} = \sqrt{(\alpha^{\varphi}, \bar{\rho}, \tilde{e}, \bar{\sigma}) + \underbrace{\sum_{xy} \frac{\partial^2}{\partial x \partial y} \cdot \overline{x' y'}}_H + \dots}. \quad (4.4d)$$

Now, this system of PDE has been obtain in a strictly formal way. No precision has been presumed about the averaging operator ³ or the type of flow studied to proceed to the computation. However, if the mean quantities have clear meanings, the residual terms denoted by a capital letters are subject to interpretation depending on these two definitions. As an example, with ensemble averaging in bubbly flows, this terms may be interpreted as:

A: Turbulent transport.

B: Buoyancy forces.

F: Flux of momentum from intra-fluid and inter-fluid pressure fluctuations.

D: Drag.

W: Reversible work of pressure into internal energy.

S: Irreversible work of pressure fluctuations into internal energy.

H: Second-order corrections to EOS from fluids' state fluctuations.

Because they represent fluctuations in macroscopic evolution, they contain all the system dissipation. Thus, setting them to zero stripped all entropy production from the model. The ensuing set of equations is known as the six equations model. Because setting different expressions of residuals only add more terms to the equation, it is at the roots of all other multiphase models. This is why it has been called *backbone* model by [Vazquez-Gonzalez](#)

³except commutation with the derivatives which are rigorously true for ensemble averaging

et al. (2020). This model yields:

$$D_t^\varphi(\alpha^\varphi \rho^\varphi) = 0, \quad (4.5a)$$

$$D_t^\varphi(\alpha^\varphi \rho^\varphi u_i^\varphi) + \alpha^\varphi p_{,i} = 0, \quad (4.5b)$$

$$D_t^\varphi(\alpha^\varphi \rho^\varphi e^\varphi) - \alpha^\varphi p \frac{d_t^\varphi \rho^\varphi}{\rho^\varphi} = 0, \quad (4.5c)$$

$$p = \sqrt{\rho^\varphi, e^\varphi}, \quad (4.5d)$$

$$1 = \sum_\varphi \alpha^\varphi. \quad (4.5e)$$

Variational derivation of the backbone model

Due to its isentropic character, this set of equations possesses a variational structure. To build the functional from which it derives, one needs to find the system's energy reservoirs. In the light of (4.5c) and (4.5b), these reservoirs are the kinetic and potential energies of each fluid which yields respectively $\frac{1}{2}[\alpha\rho]^\varphi(u^\varphi)^2$ and $[\alpha\rho]^\varphi e^\varphi$. Also, each fluid is constrained by its mass conservation and the Lin constraint and is coupled with the others through the volume filling constraint. Also, examination of the equation (4.5c) combined with the mass conservation (4.5a) suggests that internal energies are function of ρ^φ . However, the model being isentropic, entropy dependency is not visible but must be still considered. The functional yields (Vazquez-Gonzalez *et al.*, 2020):

$$\begin{aligned} \mathcal{A} = \int_T \int_\Omega \sum_\phi \left[\frac{1}{2}[\alpha\rho]^\phi (u^\phi)^2 - [\alpha\rho]^\phi e(\rho^\phi, s(\xi^\phi)) + \Phi^\varphi D_t^\phi([\alpha\rho]^\phi) \right. \\ \left. + \Psi^\phi d_t^\phi(\xi^\phi) \right] + \Pi \left[\sum_\phi \alpha^\phi - 1 \right] dxdt \end{aligned} \quad (4.6)$$

The derivation of the action is made in (Vazquez-Gonzalez *et al.*, 2020) and is not repeated here. It is shown that a combination of the ensuing Euler–Lagrange equations leads to the backbone model (4.5). Also, the variation with respect to the volume fraction leads to

$$0 = \Pi + \underbrace{(\rho^\varphi)^2 \frac{\partial e^\varphi}{\partial \rho^\varphi}}_{p^\varphi} \quad (4.7)$$

which corresponds the single pressure model. Thus, equal pressure closure is not only an assumption in the backbone model but a necessary condition to obtain a dissipation free model with energy reservoirs reduced to the kinetic and internal energies.

4.2.2 Energies of fluctuations lost by averaging process

The set of equations (4.5) represents ideal situations where all fluctuation terms which contain dissipation and short scale potentials are negligible. Therefore, only few situations

can be reasonably predicted with this rough modeling approach. However, because it is at the roots of all other models, its discretization must be carefully crafted to be able to add other building blocks. These blocks are higher order effects but may be crucial to predict correctly real multiphase flows.

Effects	Description	Closure
External turbulence	Agitation of dispersed particles	(4.18)
Internal turbulence	Turbulence inside a phase	(4.36)
Surface tension	Interfacial effect opposed to inclusions' deformation	(4.44)
Added mass	Effective inertial mass of a structure drifting in a surrounding phase	(4.45)

External turbulence

One of the most higher order effects studied is the turbulence contained inside [A] in (4.4b). In suspension flows, this term stands for chaotic motion of particles due to interactions or direct collisions (Lhuillier *et al.* (2013)). The kinetic energy associated to this turbulent motion has been inspected by de Bertonado (1992), Saurel *et al.* (2003) and Herard (2005). Its dynamics may be derived by several approaches presented here.

Kinetic approach The kinetic theory has been used in Gidaspow (1994) to study this motion (called granular temperature in this book) through Boltzmann description. A simpler approach is presented here, based on an idealized system. Particles' agitation is defined as

$$k_e = \frac{1}{2}[(u'_x)^2 + (u'_y)^2 + (u'_z)^2]. \quad (4.8)$$

With the isotropic hypothesis, this expression simplifies to

$$k_e = \frac{3}{2}(u'_n)^2 \text{ with } n = x, y \text{ or } z. \quad (4.9)$$

The system studied is a fictive volume of fluid filled with particles. In the reference frame of the mean particle velocity, walls are affected by particle collisions. These collisions lead to an effective pressure called granular pressure. To estimate this pressure, a momentum balance is made on the wall. The number of particles hitting a wall area $\Delta y \Delta z$ of normal e_x by unit of time yields

$$N = \frac{1}{2} \frac{\alpha_{\text{particle}}}{v_{\text{particle}}} u'_x \Delta y \Delta z \quad (4.10)$$

with v_{particle} being the particles' volume. The momentum transmitted to the wall by unit of time is then

$$\begin{aligned} \Delta(mv) &= 2Nm_{\text{particle}}u'_x = \alpha_{\text{particle}} \frac{m_{\text{particle}}}{v_{\text{particle}}} (u'_x)^2 \Delta y \Delta z \\ &= \frac{2}{3}[\alpha\rho]_{\text{particle}} k_e \Delta y \Delta z. \end{aligned} \quad (4.11)$$

Ensuing pressure is then obtained as

$$p_{ke} = \frac{\Delta(mv)}{\Delta y \Delta z} = \frac{2}{3}[\alpha\rho]_{\text{particle}}ke. \quad (4.12)$$

A thermodynamic relation is needed to relate this pressure to the other variables of the system. This relation mimics Gibbs equation

$$dK_e = -p_{ke}dV + T_e dS_e. \quad (4.13)$$

K_e is defined as the turbulent energy associated to particles agitation

$$K_e = V[\alpha\rho]ke. \quad (4.14)$$

The mass of particle inside the volume V is constant. In isentropic evolution, the thermodynamic relation 4.13 yields

$$dK_e = -p_{ke}dV. \quad (4.15)$$

With the equation (4.14) and (4.15), the Gibbs equation (4.13) is restated to

$$\begin{aligned} V[\alpha\rho]dke &= -p_{ke}dV - Vked[\alpha\rho] - [\alpha\rho]kedV. \\ &= p_{ke}V \frac{d[\alpha\rho]}{[\alpha\rho]} - Vked[\alpha\rho] + [\alpha\rho]keV \frac{d[\alpha\rho]}{[\alpha\rho]} \\ \Rightarrow dke &= p_{ke} \frac{d[\alpha\rho]}{[\alpha\rho]^2}. \end{aligned} \quad (4.16)$$

The entropy of the external turbulent energy depends only on the Lagrangian coordinates in the isentropic case. Thus, to mimic the internal energy, the following closure is used for the turbulent external energy

$$ke^\varphi = ke^\varphi([\alpha\rho]^\varphi, \xi^\varphi) \text{ mimics } e^\varphi = e^\varphi(\rho^\varphi, \xi^\varphi), \quad (4.17)$$

$$\frac{\partial ke^\varphi}{\partial [\alpha\rho]^\varphi} = \frac{pke^\varphi}{([\alpha\rho]^\varphi)^2} \text{ mimics } \frac{\partial e^\varphi}{\partial \rho^\varphi} = \frac{p^\varphi}{(\rho^\varphi)^2}. \quad (4.18)$$

Averaging approach Obtaining evolution equations of the particles' agitation by averaging process has been studied by [Lhuillier & Raviart \(2020\)](#). The procedure is similar the multiphase flow models derivation by averaging. The agitation is defined by the variation of the mean kinetic energy per fluid to the kinetic energy per fluid formed by the mean quantities (4.19).

$$[\alpha\rho]^\varphi ke^\varphi = \frac{1}{2} \overline{c^\varphi \rho (u^\varphi)'_i (u^\varphi)'_i} = \overline{c^\varphi \frac{1}{2} \rho u_i^2} - \frac{1}{2} [\alpha\rho]^\varphi (u_i^\varphi)^2 \quad (4.19)$$

To obtain the evolution of this residuals, dynamics of both terms must be computed. The equation on the average kinetic energy is derived by multiplying the equation (4.4b) by u_i^φ and using the equation (4.5a)

$$\partial_t \left(\frac{1}{2} [\alpha\rho]^\varphi (u_i^\varphi)^2 \right) + \left(\frac{1}{2} [\alpha\rho]^\varphi (u_i^\varphi)^2 u_j^\varphi \right)_{,j} = -\alpha^\varphi p_{,i}^\varphi u_i^\varphi + \text{Res } u_i^\varphi. \quad (4.20)$$

The non averaged kinetic energy yields simply

$$\partial_t(\frac{1}{2}\rho u_i^2) + (\frac{1}{2}\rho(u_i)^2 u_j)_{,j} = -p_{,i} u_i. \quad (4.21)$$

The agitation dynamics is obtained through

$$\overline{c^\varphi \times (4.21)} - (4.20). \quad (4.22)$$

The temporal derivative is

$$\begin{aligned} & \overline{c^\varphi \partial_t(\frac{1}{2}\rho u_i^2)} - \partial_t(\frac{1}{2}[\alpha\rho]^\varphi (u_i^\varphi)^2) \\ \text{with } d_t c^\varphi = 0 : & = \partial_t(\overline{c^\varphi \frac{1}{2}\rho u_i^2}) + \overline{\frac{1}{2}\rho u_i^2 c_{,j}^\varphi u_j} - \partial_t(\frac{1}{2}[\alpha\rho]^\varphi (u_i^\varphi)^2) \\ & = \partial_t(\overline{c^\varphi \frac{1}{2}\rho (u_i^\varphi + (u_i^\varphi)')^2}) + \overline{\frac{1}{2}\rho u_i^2 c_{,j}^\varphi u_j} \\ & \quad - \partial_t(\frac{1}{2}[\alpha\rho]^\varphi (u_i^\varphi)^2) \\ & = \partial_t([\alpha\rho]^\varphi \text{ke}^\varphi) + \underbrace{\partial_t(\overline{c^\varphi \rho u_i^\varphi (u_i^\varphi)'})}_{=0} + \overline{\frac{1}{2}\rho u_i^2 c_{,j}^\varphi u_j}. \end{aligned} \quad (4.23)$$

The advection part is

$$\begin{aligned} & \overline{c^\varphi (\frac{1}{2}\rho u_i^2 u_j)_{,j}} - (\frac{1}{2}[\alpha\rho]^\varphi (u_i^\varphi)^2 u_j^\varphi)_{,j} \\ & = (\overline{c^\varphi \frac{1}{2}\rho u_i^2 u_j})_{,j} - \overline{c_{,j}^\varphi \frac{1}{2}\rho u_i^2 u_j} - (\frac{1}{2}[\alpha\rho]^\varphi (u_i^\varphi)^2 u_j^\varphi)_{,j} \\ & = (\overline{c^\varphi \frac{1}{2}\rho (u_i^\varphi + (u_i^\varphi)')^2 (u_j^\varphi + (u_j^\varphi)')})_{,j} - \overline{c_{,j}^\varphi \frac{1}{2}\rho u_i^2 u_j} - (\frac{1}{2}[\alpha\rho]^\varphi (u_i^\varphi)^2 u_j^\varphi)_{,j} \\ & = \underbrace{(\overline{c^\varphi \frac{1}{2}\rho (u_i^\varphi)^2 (u_j^\varphi)'})_{,j}}_{=0} + \underbrace{(\overline{c^\varphi \rho u_i^\varphi (u_i^\varphi)' u_j^\varphi})_{,j}}_{=0} + \underbrace{(\overline{c^\varphi \rho u_i^\varphi (u_i^\varphi)' (u_j^\varphi)'})_{,j}}_{u_i^\varphi R_{ij,j} + R_{ij} u_{i,j}^\varphi} \\ & \quad + ([\alpha\rho]^\varphi \text{ke}^\varphi u_j^\varphi)_{,j} + \underbrace{(\overline{c^\varphi \frac{1}{2}\rho (u_i^\varphi)' (u_i^\varphi)' (u_j^\varphi)'})_{,j}}_{\text{neglected}} - \overline{c_{,j}^\varphi \frac{1}{2}\rho u_i^2 u_j}. \end{aligned} \quad (4.24)$$

The right part is

$$-\overline{c^\varphi p_{,i} u_i} + \alpha^\varphi p_{,i}^\varphi u_i^\varphi + R_{ij,j} u_i^\varphi - (p^\varphi - \bar{p})\alpha_{,i}^\varphi u_i^\varphi + \overline{p' c_{,i}^\varphi u_i^\varphi}. \quad (4.25)$$

The evolution of the kinetic turbulent energy yields then

$$D_t^\varphi([\alpha\rho]^\varphi \text{ke}^\varphi) = -R_{ij} u_{i,j}^\varphi + \underbrace{\text{Res}}_{\overline{c^\varphi p_{,i} (u_i^\varphi - u_i)}}. \quad (4.26)$$

With an isotropic hypothesis, the Reynolds tensor R_{ij} is modeled as

$$R_{ij} = \frac{2}{3}[\alpha\rho]^\varphi \text{ke}^\varphi \delta_{ij} = \text{pke}^\varphi \delta_{ij}. \quad (4.27)$$

By neglecting residuals and using the continuity relation (4.5a), the equation (4.26) is re-stated as

$$d_t^\varphi(\text{ke}^\varphi) = \text{pke}^\varphi \frac{d_t^\varphi([\alpha\rho]^\varphi)}{([\alpha\rho]^\varphi)^2}. \quad (4.28)$$

The equation over the external turbulent pressure can be derived from (4.28)

$$d_t^\varphi(\text{pke}^\varphi) = \frac{5}{3}\text{pke}^\varphi \frac{d_t^\varphi[\alpha\rho]^\varphi}{([\alpha\rho]^\varphi)^2}. \quad (4.29)$$

Internal turbulence

In addition to the chaotic motion of particles, carrier fluid may experience turbulence as in single fluid flows. Models to capture this turbulence are purely single fluid models. One example of closure is proposed in this section. The kinetic turbulent energy is defined as

$$k = \frac{\overline{\rho u_i'' u_i''}}{\bar{\rho}}. \quad (4.30)$$

With computation on the Favre average equations (details in Galera (2005) p 30), the evolution equation of this energy is obtained as

$$\partial_t(\bar{\rho}k) + \partial_{x_i}(\bar{\rho}k\tilde{u}_i) = -\bar{\rho}\widetilde{u_j'' u_i''} \partial_{x_j}\tilde{u}_i + \text{neglected terms}. \quad (4.31)$$

To simplify the model, all the terms called *neglected terms* are neglected (2 to 5 in Galera (2005)). The Reynolds tensor may be modeled as

$$\tilde{R}_{ij} = -\bar{\rho}\widetilde{u_j'' u_i''} = \mu_t [(\partial_{x_j}\tilde{u}_i + \partial_{x_i}\tilde{u}_j) - \frac{2}{3}\delta_{ij}\partial_{x_k}\tilde{u}_k] - \frac{2}{3}\bar{\rho}k\delta_{ij}. \quad (4.32)$$

The shear part is neglected, the evolution equation of the internal turbulent energy is restated then as

$$\partial_t(\bar{\rho}k) + \partial_{x_i}(\bar{\rho}k\tilde{u}_i) = -\frac{2}{3}\bar{\rho}k\partial_{x_i}(\tilde{u}_i). \quad (4.33)$$

With the Favre averaged mass conservation equation (for a single fluid), the evolution yields

$$d_t(k) = \frac{2}{3}k \frac{d_t\bar{\rho}}{\bar{\rho}}. \quad (4.34)$$

With the definition of $d_t(a) = \partial_t(a) + \tilde{u}_i\partial_{x_i}(a)$. The entropy of the turbulent energy is not easy to define, however, for an isentropic flow, it depends only of the Lagrangian coordinates. Thus, by setting the following pressure $p_k = \frac{2}{3}\bar{\rho}k$, a closure mimicking the internal energy yields then

$$k = k(\rho, \xi) \text{ mimics } e = e(\rho, \xi), \quad (4.35)$$

$$\frac{\partial k}{\partial \rho} = \frac{p_k}{\rho^2} \text{ mimics } \frac{\partial e}{\partial \rho} = \frac{P}{\rho^2}. \quad (4.36)$$

Therefore, inside each structure, an internal mass turbulence k^φ may be defined which is ruled by the Gibbs equation $k^\varphi(\rho^\varphi, \xi^\varphi)$ with $\partial_{\rho^\varphi}k^\varphi = \frac{pk^\varphi}{(\rho^\varphi)^2}$ and $pk^\varphi = \frac{2}{3}\rho^\varphi k^\varphi$. Dynamics of the internal turbulent pressure can be computed as

$$d_t^\varphi(pk^\varphi) = \frac{5}{3}pk^\varphi \frac{d_t^\varphi(\rho^\varphi)}{\rho^\varphi}. \quad (4.37)$$

Surface tension

Deviation of pressure fluid to the mean pressure expressed in the form [F] in (4.4b) may be interpreted in bubbly flows as surface tension. The surface tension represents the resistance of structures (such as bubbles) to be deformed. Its origin lies at molecular scale which is the scale of the interfaces between the constituents. The resulting pressure is often modeled by the Young and Laplace law (Chung, 2007; Ramshaw, 1978) involving the curvature of the interface. Therefore, the surface tension effect is purely geometric, i.e. it depends only on the position of the fluid particles. Thus, it falls into the variational formalism. Several options are explored here to close this effect.

First model The first model is a simple example of how to take into account this phenomenon in a flow with spherical inclusions (ie bubbles in a water air flow). With the Laplace formula, the surface tension energy of a bubble is

$$E_{tens} = \sigma 4\pi r^2, \quad (4.38)$$

with r the radius of a bubble and σ the surface tension (considered here as constant). The per volume energy associated to this model is then

$$e_{tens} = 3\sigma\alpha\frac{1}{r}, \quad (4.39)$$

with r the mean radius. This expression represents the potential in the flow due to the surface tension contained at the interfaces. As the mass of the bubble is constant (if there are no mass exchanges), the radius is directly linked to the density of inclusions as $m_b = \frac{4}{3}\pi r^3\rho$.

Second model Surface tension in a water air flow is studied by Ramshaw (1978). In this paper, the authors aimed to predict the evolution of a separated flow in a pipe. The two fluids are denoted here by the signs + and -. To model surface tension, a relation between pressure (4.41) is proposed where the curvature is modeled by the second derivative of the void fraction. It is very difficult to use a 'backward' procedure to find the corresponding energy. However, it happens that the potential proposed by Gavriluk & Saurel (2002) which yields

$$\frac{1}{2}\sigma|\nabla\alpha|^2 \quad (4.40)$$

leads to this relation between the pressures

$$p^+ - p^- = \sigma\partial_x^2\alpha^+ \quad (4.41)$$

which is exactly the relation proposed in (Ramshaw, 1978).

Third model The third model is inspired of [Lhuillier *et al.* \(2010\)](#), but it is added here with a variational method that leads notably to a pressure relation not present in their model. Two main variables are introduced, the surface energy ei^φ and the interfacial density ai^φ of the fluid φ . The two quantities follow the evolution equations (4.42) and (4.43)

$$D_t^i(ei^\varphi) = \sigma D_t^i(ai^\varphi), \quad (4.42)$$

$$D_t^i(ai^\varphi) = \frac{2}{3} ai^\varphi \frac{D_t^\varphi \alpha^\varphi}{\alpha^\varphi}, \quad (4.43)$$

with the operator $D_t^I(a) = \partial_t(a) + (u_j^I a)_{,j}$ and σ the surface tension of the dispersed phase. The relation (4.43) is just a transcription of the power law between a surface and a volume. To close this, the velocity of energy transport needs to be modeled. One choice done by [Lhuillier *et al.* \(2010\)](#) is $u^I = u^\varphi$ with φ referring to the fluid associated with the inclusion. The model is simplified here by using the following relation between the interfacial area and the interfacial energy $ei^\phi = \sigma ai^\phi$. With the mass conservation (4.5a), this yields

$$D_t^\varphi(ei^\varphi) = -pi^\varphi \alpha^\varphi \frac{d_t^\varphi \rho^\varphi}{\rho^\varphi}, \quad (4.44a)$$

$$d_t^\varphi(pi^\varphi) = \frac{1}{3} pi^\varphi \frac{d_t^\varphi \rho^\varphi}{\rho^\varphi}, \quad (4.44b)$$

with $pi^\varphi = \frac{2}{3} \sigma \frac{ai^\varphi}{\alpha^\varphi}$.

Added mass

The added mass effect or virtual mass effect is a turbulent effect that occurs when there is a drift between two fluids, especially when inclusions (bubbles, grain, etc. . .) of a light fluid are moving in a heavier one. Its introduction is needed because the classical hydrodynamic mass of the inclusions (their volume times their density) does not correspond to their inertial mass. A common example is a bubble into a flow of water at rest. To set the bubble into motion, not only the air inside needs to be accelerated but also all the surrounding water which is much heavier. When the flow around the bubble is totally resolved, this effect is naturally taken into account. However, after an averaging process, information on the behavior of water around the bubble is lost. The mean velocity of the water is equal to the instantaneous velocity far away from the bubble. Thus, the kinetic energy associated is null in the case of a water at rest. But the kinetic energy is not the square of the average velocity (which is zero here) but the average of the square. As a consequence, the added mass can be considered as a turbulent effect because it represents a kinetic energy due to the perturbation of the carrier phase velocity around the particle. More explanations about meaning of added mass and computation for single structure are made by [Clause \(2003\)](#). In the light of this definition, added mass depends on the mass of the fluid displaced and the relative velocity of the two phases. An averaged energy would then depend on the void fraction of the particles and the density of the carrier phase. However, as shown in

Zhang & VanderHeyden (2002), the mesoscale effects of the added mass need to be taken into account in a two fluid flow by considering the average density surrounding the particle which is $\rho = [\alpha\rho]^+ + [\alpha\rho]^-$. Thus, the added mass energy is written in a general way as

$$E_{add} = \frac{1}{2}A\left(\frac{\alpha^+ - \alpha^-}{2}, [\alpha\rho]^+, [\alpha\rho]^-\right)|\mathbf{u}^+ - \mathbf{u}^-|^2. \quad (4.45)$$

Because the coefficient A is a density formed by a combination of both fluids, it must verifies the homogeneity condition

$$A = [\alpha\rho]^+ A_{, [\alpha\rho]^+} + [\alpha\rho]^- A_{, [\alpha\rho]^-}. \quad (4.46)$$

A last condition is that the added mass coefficient must vanish as one of the void fraction tends to zero. A closure that satisfies these properties is the closure of Youngs (1989)

$$A = \alpha^+ \alpha^- \rho. \quad (4.47)$$

4.3 Dissipation free models with added fluctuations

4.3.1 Lagrangian and momentum equation

Construction of the Lagrangian

To complete the backbone model with the effects above, their corresponding energies are added in the Lagrangian (4.6). However, when new fields are introduced such as the interfacial density, constraints that link them to the previous fields must be added in the action. Those on turbulent energies are not necessary because these potentials depend explicitly on the density and Lagrangian coordinates. The new Lagrangian of the system becomes therefore

$$\begin{aligned} L = \sum_{\phi} \left(\right. & \underbrace{\frac{1}{2}[\alpha\rho]^{\phi}(u_j^{\phi})^2 - [\alpha\rho]^{\phi}e^{\phi}(\rho^{\phi}, \xi^{\phi}) - [\alpha\rho]^{\phi}k^{\phi}(\rho^{\phi}, \xi^{\phi})}_{(1)} \\ & - \underbrace{[\alpha\rho]^{\phi}ke^{\phi}([\alpha\rho]^{\phi}, \xi^{\phi})}_{(2)} - \underbrace{ei^{\phi}(ai^{\phi})}_{(3)} + \Phi^{\phi}D_t^{\phi}([\alpha\rho]^{\phi}) \\ & \left. + \underbrace{\eta^{\phi}(\rho^{\phi}D_t^{\phi}(ai^{\phi}) + \frac{2}{3}ai^{\phi}d_t^{\phi}(\rho^{\phi}))}_{(4)} + \Psi^{\phi}d_t^{\phi}(\xi^{\phi}) \right) \\ & + \underbrace{\frac{1}{2}A([\alpha\rho]^+, [\alpha\rho]^-, \Delta\alpha)(\Delta u_j)^2}_{(5)} - \Pi\left(\sum_{\phi}\alpha^{\phi} - 1\right). \end{aligned} \quad (4.48)$$

In the new Lagrangian (5.22), the following forms have been thus added:

- (1) the internal turbulent energy
- (2) the external turbulent energy,

- (3) the interfacial energy,
- (4) the constraint that links the interfacial area density to the density,
- (5) the added mass kinetic energy.

For all the added effects except the added mass, the number of fluids is arbitrary. However, it is restricted to two with added mass for simplicity which are called in that case + and -. Variations of the action $\tilde{A} = \int_T \int_\Omega L dt dx$ with respect to the degrees of freedom $[\alpha\rho]^\phi$, u_i^ϕ , α^ϕ , ξ^ϕ , ai^ϕ and all the Lagrangian multipliers lead to the Euler-Lagrange equations

$$\begin{aligned} \delta[\alpha\rho]^\phi : 0 = & \frac{1}{2}(u_j^\phi)^2 - e^\phi - \rho^\phi e_{,\rho^\phi}^\phi - k^\phi - \rho^\phi k_{,\rho^\phi}^\phi - \text{ke}^\phi \\ & - [\alpha\rho]^\phi \text{ke}_{, [\alpha\rho]^\phi}^\phi - \text{d}_t^\phi(\Phi^\phi) + \frac{\eta^\phi}{\alpha^\phi} \text{D}_t^\phi(\text{ai}^\phi) \\ & - \frac{2}{3} \frac{1}{\alpha^\phi} \text{D}_t^\phi(\eta^\phi \text{ai}^\phi) + \frac{1}{2} A_\pm (\Delta u_j)^2 \end{aligned} \quad (4.49a)$$

$$\begin{aligned} \delta\alpha^\phi : 0 = & (\rho^\phi)^2 e_{,\rho^\phi}^\phi + (\rho^\phi)^2 k_{,\rho^\phi}^\phi - \frac{\rho^\phi \eta^\phi}{\alpha^\phi} \text{D}_t^\phi(\text{ai}^\phi) \\ & + \frac{2}{3} \frac{\rho^\phi}{\alpha^\phi} \text{D}_t^\phi(\text{ai}^\phi \eta^\phi) \pm \frac{1}{4} A_\alpha (\Delta u_j)^2 - \Pi \end{aligned} \quad (4.49b)$$

$$\begin{aligned} \delta u_i^\phi : 0 = & [\alpha\rho]^\phi u_i^\phi - [\alpha\rho]^\phi \Phi_{,i} - \text{ai}^\phi (\eta^\phi \rho^\phi)_{,i} \\ & + \frac{2}{3} \eta^\phi \text{ai}^\phi \rho_{,i}^\phi + \Psi^\phi \xi_{,i}^\phi \pm A \Delta u_i \end{aligned} \quad (4.49c)$$

$$\delta\xi^\phi : 0 = -[\alpha\rho]^\phi e_{,\xi^\phi}^\phi - [\alpha\rho]^\phi k_{,\xi^\phi}^\phi - [\alpha\rho]^\phi \text{ke}_{,\xi^\phi}^\phi - \text{D}_t^\phi(\Psi^\phi) \quad (4.49d)$$

$$\delta\text{ai}^\phi : 0 = -\text{ei}_{,\text{ai}^\phi}^\phi - \text{d}_t^\phi(\eta^\phi \rho^\phi) + \frac{2}{3} \eta^\phi \text{d}_t^\phi(\rho^\phi) \quad (4.49e)$$

$$\delta\Phi^\phi : 0 = \text{D}_t^\phi([\alpha\rho]^\phi) \quad (4.49f)$$

$$\delta\eta^\phi : 0 = \rho^\phi \text{D}_t^\phi(\text{ai}^\phi) + \frac{2}{3} \text{ai}^\phi \text{d}_t^\phi(\rho^\phi) \quad (4.49g)$$

$$\delta\Psi^\phi : 0 = \text{d}_t^\phi(\xi^\phi) \quad (4.49h)$$

$$\delta\Pi : 0 = \sum_\phi \alpha^\phi - 1 \quad (4.49i)$$

With the equation (4.49e) and the constraint (4.49g), the equation (4.49b) can be simplified as

$$\Pi = p^\phi + \text{pk}^\phi - \underbrace{\frac{2}{3} \frac{\text{ai}^\phi}{\alpha^\phi} \text{ei}_{,\text{ai}^\phi}^\phi}_{\text{pi}^\phi = \frac{2}{3} \frac{\text{ai}^\phi}{\alpha^\phi} \sigma} \pm \frac{1}{4} A_{,\alpha} (\Delta u_j)^2. \quad (4.50)$$

The equation (4.50) is an algebraic relation between pressures. It shows that the total pressures per fluid are equal. This total pressure is the sum of contributions from internal energy, internal turbulence, surface tension and added mass (through the added mass coefficient). Thus, this relation involves all the energy reservoirs with the exception of the kinetic energy and the turbulent *external* energy which do not depend on the thermodynamic variables

(density or void fraction) but on the local mass ($[\alpha\rho]^\phi$) and the local velocity (u_i^ϕ). However, the kinetic energy reservoirs are still coupled through the added mass contribution $\pm\frac{1}{4}A_{,\alpha}\Delta^2u_j$ due to the drift.

Momentum equations

The relation (4.49c) shows that added mass contributes to the momentum quantity with the term $\pm A\Delta u_i$. The Clebsch decomposition of this momentum contains Lagrange multipliers that must be eliminated to derive the momentum equation.

This is achieved by the following computation $D_t^\phi(4.49c)$.

$$\begin{aligned} D_t^\phi([\alpha\rho]^\phi u_i^\phi \pm A\Delta u_i) &= [\alpha\rho]^\phi d_t^\phi(\Phi_{,i}) + D_t^\phi(\text{ai}^\phi(\eta^\phi \rho^\phi)_{,i}) \\ &\quad - \frac{2}{3}D_t^\phi(\eta^\phi \text{ai}^\phi \rho^\phi_{,i}) - D_t^\phi(\Psi^\phi \xi^\phi_{,i}) \end{aligned} \quad (4.51)$$

Using (4.43) and (4.49g), the form corresponding to surface tension is restated as

$$\begin{aligned} D_t^\phi(\text{ai}^\phi(\eta^\phi \rho^\phi)_{,i}) - \frac{2}{3}D_t^\phi(\eta^\phi \text{ai}^\phi \rho^\phi_{,i}) &= -\frac{2}{3}\frac{\text{ai}^\phi}{\rho^\phi}\rho^\phi_{,i}\text{ei}^\phi_{,\text{ai}^\phi} + \text{ai}^\phi(\eta^\phi \rho^\phi)_{,i}u_{j,i}^\phi \\ &\quad - \frac{2}{3}\text{ai}^\phi\eta^\phi\rho^\phi_{,i}u_{j,i}^\phi \end{aligned} \quad (4.52)$$

With (4.5a), (4.49d), (4.49h) contributions of the other forms are

$$\begin{aligned} [\alpha\rho]^\phi d_t^\phi(\Phi_{,i}) - D_t^\phi(\Psi^\phi \xi^\phi_{,i}) &= [\alpha\rho]^\phi (d_t^\phi(\Phi))_{,i} \\ -[\alpha\rho]^\phi \Phi_{,i}u_{j,i}^\phi + \Psi^\phi \xi^\phi_{,i}u_{j,i}^\phi + [\alpha\rho]^\phi \xi^\phi_{,i}(e_{,\xi^\phi}^\phi + k_{,\xi^\phi}^\phi + ke_{,\xi^\phi}^\phi). \end{aligned} \quad (4.53)$$

With (4.49a) and (4.5a) this can be simplified as

$$\begin{aligned} [\alpha\rho]^\phi d_t^\phi(\Phi_{,i}) - D_t^\phi(\Psi^\phi \xi^\phi_{,i}) &= -\alpha^\phi [p^\phi + \text{pk}^\phi]_{,i} - (\text{pke}^\phi)_{,i} \\ &\quad + [\alpha\rho]^\phi \left(\frac{\text{pi}^\phi}{\rho^\phi}\right)_{,i} + [\alpha\rho]^\pm \frac{1}{2}(A_{,\pm}(\Delta u_j)^2)_{,i} \\ &\quad + [\alpha\rho]^\phi u_j^\phi u_{j,i}^\phi + [\alpha\rho]^\phi \Phi_{,i}u_{j,i}^\phi - \Psi^\phi \xi^\phi_{,i}u_{j,i}^\phi. \end{aligned} \quad (4.54)$$

Using the equation (4.49c) to eliminate the multipliers form the combination, the final momentum equation is obtained as

$$\begin{aligned} \underbrace{D_t^\phi([\alpha\rho]^\phi u_i^\phi \pm A\Delta u_i)}_{(1)} &= -\underbrace{\alpha^\phi (p^\phi + \text{pk}^\phi - \text{pi}^\phi)_{,i}}_{(2)} - \underbrace{(\text{pke}^\phi)_{,i}}_{(3)} \\ &\quad + \underbrace{\frac{1}{2}[\alpha\rho]^\pm (A_{,\pm}(\Delta u_j)^2)_{,i} \mp u_{j,i}^\pm A\Delta u_j}_{(4)} \end{aligned} \quad (4.55)$$

This momentum equation is composed by a series of distinct terms. On the left part is written the transport of the total momentum quantity (1) which now takes into account the added mass. On the right part, there are: (2) the gradient of the pressures derived from potentials depending on volume fraction (or density) weighted by the volume fraction, (3) the gradient of external turbulent pressure depending only of the local mass of the fluid, (4) complex terms issued from the added mass.

4.3.2 Forcing pressure equality

Justification of equal pressure constraint

Experiments in multiphase flows sometimes reveal variations between pressures of the different phases. For instance, when a shock propagates into a bubbly flow, bubbles oscillate during a short period after the shock impact (Beylich & Gülhan, 1990), (Brennen, 2005, chap 4.4). The relaxation time of these oscillations is at the *ms* order. Therefore, the pressure relaxation is much faster than the velocity and temperature one. Also, this relaxation is a transitory effect damped by viscosity. In bubbly flows, it is ruled by the Rayleigh–Plesset equation whose non dissipative part may be obtained with a least action principle (Saurel & Abgrall, 1999a; Sciarra *et al.*, 2003). The potential introduced corresponds to the bubbles’ kinetic energy. Added mass effects also lead to non pressure relaxation as shown by the equation (4.50). Added mass is also a transitory effect but lasts as long as the fluids’ velocities are not relaxed which means that pressure relaxation can not be considered as instantaneous. However, it is possible to evaluate the impact of neglecting the added mass pressure in the relation between pressures.

To evaluate this impact, a single bubble a volume V^b , density ρ^b and pressure p^b inside a water flow is considered. The added mass pressure is roughly equal to the dynamic pressure. The volume variation can be then estimated as

$$\frac{dV}{V} = \frac{1}{2} \frac{\rho^w}{\rho^b} M^2 \quad (4.56)$$

with $M = \frac{|\Delta u_i|}{c_s}$. Two effects are then in competition, the ratio of density between the bubbles and the surrounding fluid versus the Mach number of the drift. In usual bubbly flows, the drift is of the m.s^{-1} order whereas the sound speed is of $3 \times 10^2 \text{ m.s}^{-1}$. Thus the volume variation is about one per cent. Therefore, added mass contribution to pressure may be neglected. However, the other forms may not be discarded. As an example, the inertia in the momentum quantity $A\Delta u_i$ may be dominant before the classic inertia of the fluid.

In addition to these physical based arguments, practical issues to build usable models involve to conserve pressure equality. As explained in (4.1.3), explicit energy evolutions are necessary to build numerical schemes able to insure conservations without solving complex systems and to capture internal stiffness. These equations are obtained by using the pressure relation issued from the LAP. Therefore, this relation reflects the coupling between the energy reservoirs and thus determine the degree of complexity of the equations. Because relation (4.50) couples all the energy reservoirs, the ensuing energy equations are extremely complex (4.A). Crafting a consistent and conservative numerical scheme solving these equations seems unrealistic. This is why pressure relaxation is now imposed in the model.

New Lagrangian, cost of the constraint

The equation (4.49b) shows that the relation between pressures is imposed by the potentials depending on the thermodynamic quantities (the volume fraction or the density). Nev-

ertheless, it is possible to impose a relation between pressures by the mean of a Lagrange multiplier in the Lagrangian. This relation imposes a constant equilibrium between pressures issued from internal energies. With addition of this constraints, the Lagrangian becomes

$$L = (5.22) + \theta(p^+ - p^-) \quad (4.57)$$

As the derivation is a linear operator, the new Euler-Lagrange equations are restated as

$$\delta[\alpha\rho]^\phi : (4.49a) \pm \frac{\theta}{\alpha^\pm} p_{,\rho^\pm}^\pm \quad (4.58a)$$

$$\delta\alpha^\phi : \Pi = p^\phi + pk^\phi + pi^\phi \pm \frac{1}{4}A_{,\alpha}\Delta^2u_j \pm \frac{\rho^\pm\theta}{\alpha^\pm} p_{,\rho^\pm}^\pm \quad (4.58b)$$

$$\delta u_i^\phi : (4.49c) \quad (4.58c)$$

$$\delta\xi^\phi : (4.49d) \pm \theta s_{,\xi^\pm}^\pm p_{,s^\pm}^\pm \quad (4.58d)$$

$$\delta ai^\phi : (4.49e) \quad (4.58e)$$

$$\delta\theta^\phi : (4.5a) \quad (4.58f)$$

$$\delta\eta^\phi : (4.49g) \quad (4.58g)$$

$$\delta\Psi^\phi : 0 = (4.49h) \quad (4.58h)$$

$$\delta\Pi : 0 = \sum_{\phi} \alpha^\phi - 1 \quad (4.58i)$$

$$\delta\theta : 0 = p^+ - p^- \quad (4.58j)$$

There are now two relations over pressures, the relation (4.58b) and the relation (4.58j). These two relations lead to the expression of the Lagrangian multiplier θ in function of the other pressures as

$$\theta = \frac{-\Delta(pk^\phi + pi^\phi) - \frac{1}{2}A_{,\alpha}\Delta^2u_j}{(\frac{\gamma^+}{\alpha^+} + \frac{\gamma^-}{\alpha^-})p}. \quad (4.59)$$

The Lagrange multiplier can be then interpreted as the ratio between variations to the equilibrium $p^+ - p^-$ without constraint and the common pressure itself p . It is the cost to return to the equilibrium. This cost may be restated as

$$\theta = \alpha^+\alpha^- \frac{-\Delta(pk^\phi + pi^\phi) - \frac{1}{2}A_{,\alpha}\Delta^2u_j}{\rho_{\text{eq}}c_{\text{eq}}^2} \quad (4.60)$$

with $\rho_{\text{eq}}c_{\text{eq}}^2 = (\alpha^-\rho^+(c_s^+)^2 + \alpha^+\rho^-(c_s^-)^2)$. If the other effects are neglected, it may be expressed with a Mach number and a density ratio as in (4.56). This cost is found to be negligible in many industrial fluid flows.

The new momentum quantity yields

$$\begin{aligned} D_t^\phi([\alpha\rho]^\phi u_i^\phi \pm A\Delta u_i) &= -\alpha^\phi(p^\phi + pk^\phi + pi^\phi)_{,i} - (pke^\phi)_{,i} \\ &+ \frac{1}{2}[\alpha\rho]^\pm (A_{,\pm}\Delta^2u_j)_{,i} \mp u_{j,i}^\pm A\Delta u_j \\ &\mp \alpha^\pm \left(\frac{\theta}{\alpha^\pm} \gamma^\pm p\right)_{,i} \pm \theta_{,i} p. \end{aligned} \quad (4.61)$$

The momentum quantity now involves gradients of the pressure relaxation cost.

4.3.3 Kinetic energy equations, conservation of the total energy

Without added mass, there is only one kinetic energy per fluid which is classically $\frac{1}{2}[\alpha\rho]^\varphi(u^\varphi)^2$. This kinetic energy involves only the mass of the phase and its velocity. Thus it does not couple phases with each other. The equation of the kinetic energy of each phase is obtained by multiplying the momentum equation of a phase by its velocity and using the mass conservation. Without pressure constraint, it yields then

$$D_t^\phi(\frac{1}{2}[\alpha\rho]^\phi(u_i^\phi)^2) = -\alpha^\phi \underbrace{(p^\phi + pk^\phi - pi^\phi)_{,i}u_i^\phi}_{(1)} - \underbrace{(pke^\phi)_{,i}u_i^\phi}_{(2)}. \quad (4.62)$$

Therefore, the kinetic energy equation per fluid is explicit with two distinct contributions. The contribution (1) is the action of the total pressure weighted by the volume fraction which ultimately couples all the fluids together with the relation $\sum_\phi \alpha^\phi = 1$. It means that the action of the total pressure is distributed on the kinetic energy of a phase according to its volume fraction, itself coupled to the internal energy through the density. However, the form (2) does not depend on volume fraction and therefore couples only the reservoir of external turbulence of the fluid to its kinetic energy. As it will be seen in the next part, this difference has a strong impact on the internal energies' computation.

Now if added mass is considered, the combination above leads to another time derivative which can not be simplified.

$$D_t^\phi(\underbrace{\frac{1}{2}[\alpha\rho]^\phi(u_i^\phi)^2}_{E_c^\phi}) \pm u_i^\phi D_t^\phi(A\Delta u_i) = -f^\phi u_i^\phi. \quad (4.63)$$

By summing all the equations (4.63) over the fluids, the total kinetic energy evolution is obtained on the LHS but there is still a time derivative on the RHS.

$$\sum_\phi E_c^\phi + \partial_t(\underbrace{\frac{1}{2}A(\Delta u_i)^2}_{\text{added mass energy}}) = -\frac{1}{2}\Delta u_i \underbrace{\partial_t A}_{(a)} + \text{transport} - f^\phi u_i^\phi. \quad (4.64)$$

The coupling due to added mass is seen in (4.64) with two observations. Added mass energy appears only if all the fluid momentum equations multiplied by their velocity are summed which means that the added mass energy and the kinetic energy of all fluids are coupled. The term (a) involves derivatives of the void fraction which itself involves derivatives of the density, and ultimately the internal energies. This shows that added mass couples all the system's energy reservoirs and therefore that explicit energy equations will be very complex. However, adding the pressure equality constraint simplifies the procedure as it will be shown in the next part.

Still, even without pressure constraint, Noether's theorem guarantees that total energy is conserved and gives directly the flux with the following computation.

$$\begin{aligned}
H &= \sum_{\phi} \left(\frac{\partial L}{\partial [\alpha \dot{\rho}]^{\phi}} [\alpha \dot{\rho}]^{\phi} + \frac{\partial L}{\partial \dot{\xi}^{\phi}} \dot{\xi}^{\phi} + \frac{\partial L}{\partial \dot{\text{ai}}^{\phi}} \dot{\text{ai}}^{\phi} + \frac{\partial L}{\partial \dot{\rho}^{\phi}} \dot{\rho}^{\phi} \right) - L \\
&= \sum_{\phi} \left(\Phi^{\phi} [\alpha \dot{\rho}]^{\phi} + \psi^{\phi} \dot{\xi}^{\phi} + \eta^{\phi} (\rho^{\phi} \dot{\text{ai}}^{\phi} + \frac{2}{3} \text{ai}^{\phi} \dot{\rho}^{\phi}) \right) - L \\
&= - \sum_{\phi} \left[\frac{1}{2} [\alpha \rho]^{\phi} (u_j^{\phi})^2 - [\alpha \rho]^{\phi} (e^{\phi} + k^{\phi} + \text{ke}^{\phi}) - \text{ei}^{\phi} \right. \\
&\quad \left. + \Phi^{\phi} ([\alpha \rho]^{\phi} u_j^{\phi})_{,j} + \psi^{\phi} u_j^{\phi} (\xi^{\phi})_{,j} + \eta^{\phi} (\rho^{\phi} (\text{ai}^{\phi} u_j^{\phi})_{,j} + \frac{2}{3} \text{ai}^{\phi} \rho_{,j}^{\phi} u_j^{\phi}) \right] \\
&\quad + \Pi \left(\sum_{\phi} \alpha^{\phi} - 1 \right) - \frac{1}{2} A \Delta^2 u_j.
\end{aligned} \tag{4.65}$$

With the Euler-Lagrange equation (4.49c)

$$\begin{aligned}
[\alpha \rho]^{\phi} u_i^{\phi} \pm A \Delta u_i &= [\alpha \rho]^{\phi} \Phi_{,i}^{\phi} - \psi^{\phi} \xi_{,i}^{\phi} \\
&\quad + \text{ai}^{\phi} (\eta^{\phi} \rho^{\phi})_{,i} - \frac{2}{3} \eta^{\phi} \text{ai}^{\phi} \rho_{,i}^{\phi}, \\
\sum_{\phi} ([\alpha \rho]^{\phi} (u_i^{\phi})^2) + A \Delta^2 u_i &= \sum_{\phi} ([\alpha \rho]^{\phi} u_i^{\phi} \Phi_{,i}^{\phi} - \psi^{\phi} u_i^{\phi} \xi_{,i}^{\phi} \\
&\quad + u_i^{\phi} \text{ai}^{\phi} (\eta^{\phi} \rho^{\phi})_{,i} - u_i^{\phi} \frac{2}{3} \eta^{\phi} \text{ai}^{\phi} \rho_{,i}^{\phi}).
\end{aligned} \tag{4.66}$$

The final form of the Hamiltonian is then (using the constraint volume filling constraint):

$$\begin{aligned}
H &= \sum_{\phi} \left(E_c^{\phi} + [\alpha \rho]^{\phi} (e^{\phi} + k^{\phi} + \text{ke}^{\phi}) + \text{ei}^{\phi} + (\Phi^{\phi} [\alpha \rho]^{\phi} u_j^{\phi} \right. \\
&\quad \left. + \eta^{\phi} \rho^{\phi} \text{ai}^{\phi} u_j^{\phi})_{,j} \right) + \frac{1}{2} A \Delta^2 u_i.
\end{aligned} \tag{4.67}$$

The flux derived from the Noether theorem are then

$$\begin{aligned}
F_j &= \frac{\delta L}{\delta [\alpha \dot{\rho}]_{,j}^{\phi}} [\alpha \dot{\rho}]^{\phi} + \frac{\delta L}{\delta \dot{\xi}_{,j}^{\phi}} \dot{\xi}^{\phi} + \frac{\delta L}{\delta (u_j^{\phi})_{,j}} \dot{u}_j^{\phi} + \frac{\delta L}{\delta (\text{ai}^{\phi})_{,j}} \dot{\text{ai}}^{\phi} + \frac{\delta L}{\delta (\rho^{\phi})_{,j}} \dot{\rho}^{\phi} \\
&= \Phi^{\phi} u_j^{\phi} [\alpha \dot{\rho}]^{\phi} + \psi^{\phi} u_j^{\phi} \dot{\xi}^{\phi} + (\Phi^{\phi} [\alpha \rho]^{\phi} + \eta^{\phi} \rho^{\phi} \text{ai}^{\phi}) \dot{u}_j^{\phi} + \eta^{\phi} \rho^{\phi} u_j^{\phi} \dot{\text{ai}}^{\phi} \\
&\quad + \frac{2}{3} \eta^{\phi} \text{ai}^{\phi} u_j^{\phi} \dot{\rho}^{\phi} \\
&= \Phi^{\phi} (u_j^{\phi} [\alpha \dot{\rho}]^{\phi}) + \psi^{\phi} u_j^{\phi} \dot{\xi}^{\phi} + \eta^{\phi} \rho^{\phi} (\text{ai}^{\phi} \dot{u}_j^{\phi}) + \frac{2}{3} \eta^{\phi} \text{ai}^{\phi} u_j^{\phi} \dot{\rho}^{\phi}
\end{aligned} \tag{4.68}$$

The derivative of the Hamiltonian is equal to the flux and thus the total energy evolution

equation is

$$\begin{aligned}
\partial_t(E_{tot}) &= \sum_{\phi} \left[\partial_t(\Phi^{\phi}[\alpha\rho]^{\phi}u_j^{\phi} + \eta^{\phi}\rho^{\phi}\text{ai}^{\phi}u_j^{\phi})_{,j} - \right. \\
&\quad \left. (\Phi^{\phi}(u_j^{\phi}[\alpha\rho]^{\phi}) + \psi^{\phi}u_j^{\phi}\xi^{\phi} + \eta^{\phi}\rho^{\phi}(\text{ai}^{\phi}u_j^{\phi}) + \frac{2}{3}\eta^{\phi}\text{ai}^{\phi}u_j^{\phi}\rho^{\phi})_{,j} \right] \\
&= \sum_{\phi} \left(\Phi^{\phi}[\alpha\rho]^{\phi}u_j^{\phi} + (\eta^{\phi}\rho^{\phi})\text{ai}^{\phi}u_j^{\phi} + \psi^{\phi}u_j^{\phi}u_i^{\phi}\xi_{,i}^{\phi} \right. \\
&\quad \left. - \frac{2}{3}\eta^{\phi}\text{ai}^{\phi}u_j^{\phi}\rho^{\phi} \right)_{,j}.
\end{aligned} \tag{4.69}$$

The equation (4.49a), combined with (4.49e) and the constraint (4.49g), removes the temporal derivative on the right part on the Lagrangian multiplier Φ^{ϕ}

$$\begin{aligned}
[\alpha\rho]^{\phi}u_j^{\phi}\dot{\Phi} &= -[\alpha\rho]^{\phi}u_j^{\phi}u_i^{\phi}\Phi_{,i}^{\phi} + \frac{1}{2}[\alpha\rho]^{\phi}u_j^{\phi}(u_i^{\phi})^2 \\
&\quad - [\alpha\rho]^{\phi}u_j^{\phi}(e^{\phi} + k^{\phi} + \text{ke}^{\phi}) \\
&\quad - \alpha^{\phi}u_j^{\phi}(p^{\phi} + \text{pk}^{\phi} + \text{pi}^{\phi}) - u_j^{\phi}\text{pke}^{\phi} + \frac{1}{2}[\alpha\rho]^{\pm}u_j^{\pm}A_{,\pm}\Delta^2u_i.
\end{aligned} \tag{4.70}$$

The equation (4.49g) removes the other temporal derivatives

$$\text{ai}^{\phi}u_j^{\phi} \left((\eta^{\phi}\rho^{\phi}) - \frac{2}{3}u_j^{\phi}\rho^{\phi} \right) = -\text{ai}^{\phi}u_j^{\phi}u_i^{\phi} \left((\eta^{\phi}\rho^{\phi})_{,i} - \frac{2}{3}\eta^{\phi}\rho_{,i}^{\phi} \right) - u_j^{\phi}\text{ai}^{\phi}\text{ei}_{,\text{ai}^{\phi}}^{\phi} \tag{4.71}$$

With the equation (4.49c), the final form of the conservative total energy equation yields

$$\begin{aligned}
&\sum_{\phi} \left[D_t^{\phi} \left([\alpha\rho]^{\phi} \left(\frac{1}{2}(u_i^{\phi})^2 + e^{\phi} + k^{\phi} + \text{ke}^{\phi} \right) + D_t^{\phi}(\text{ei}^{\phi}) \right) + \partial_t \left(\frac{1}{2}A\Delta^2u_i \right) \right] \\
&= - \sum_{\phi} \left[\alpha^{\phi}u_j^{\phi}(p^{\phi} + \text{pk}^{\phi} + \text{pi}^{\phi}) + u_j^{\phi}\text{pke}^{\phi} \right]_{,j} \\
&\quad - \frac{1}{2} \left[(u_j^+[\alpha\rho]^+A_{,+} + u_j^-[\alpha\rho]^-A_{,-})\Delta^2u_i \right]_{,j} \left(\Rightarrow -(E_{\text{add}}\frac{1}{2}(u_j^+ + u_j^-))_{,j} - \frac{1}{4}((u_j^+ - u_j^-)([\alpha\rho]^+A_{,+} - [\alpha\rho]^-A_{,-}))_{,j} \right) \\
&\quad - \left[A\Delta u_i(u_j^+u_i^+ - u_j^-u_i^-) \right]_{,j}
\end{aligned} \tag{4.72}$$

The equation over the total energy is composed by transport on the left part and flux issued from interaction between the energy reservoirs on the right part. The added mass flux are the two last terms of the equation (4.72). The first of these may be restated to form a convective term transporting the added mass energy with the average velocity of the two fluids. The rest of the flux is the work of the pressures issued from the different potential reservoirs. However, the Noether theorem does not give the distribution of total flux over the different fluids and the different reservoirs. The next section explain how to obtain this.

4.3.4 Explicit internal energy equations

Only with turbulence and physical surface tension

Potential energy equations of the model are directly derived from first principle considering that the evolution of *each* phase is isentropic. First, the procedure is applied without added

mass and pressure constraint.

As seen in (4.3.3), two categories of potential can be distinguished. The first category contains the potentials that depend only of the mass of the phases. These potentials do not couple the fluids together because they are not impacted by the volume filling constraint. In the examples taken, the external agitation is in this category as seen in (4.3.1). Its isentropic energy evolution is written explicitly thanks to the mass conservation as

$$D_t^\phi([\alpha\rho]^\phi ke^\phi) = pke^\phi \frac{d_t^\phi([\alpha\rho]^\phi)}{[\alpha\rho]^\phi} = \underbrace{-pke^\phi u_{j,j}^\phi}_{(1)}. \quad (4.73)$$

The term (1) of this equation combines with the term (2) of the equation (4.63).

The other category regroupes potentials that depend on the volume fraction (or the density). The internal energy, internal turbulent energy and surface tension are in this category. All of these potentials are coupled through the void fraction relation which is translated in the Euler Lagrange equations by the relation between pressure (4.50). The isentropic Gibbs like equation can be written for each fluid as

$$D_t^\phi(\text{energy}) = \text{pressure} \frac{D_t^\phi \rho^\phi}{(\rho^\phi)^2} \quad (4.74)$$

(even if the surface tension is not exactly written like this). To obtain explicit energy equations, the temporal derivative over the density must be removed. This is achieved by using the relation over volume fractions and its dual relation over the pressures. Each pressure is linked to the density by a relation similar to

$$d_t^\phi(\text{pressure}) = g^\phi \text{pressure} \frac{d_t^\phi(\rho^\phi)}{\rho^\phi} = -g^\phi \frac{\text{pressure}}{\alpha^\phi} dD_t^\phi(\alpha^\phi). \quad (4.75)$$

To obtain an explicit equation, all the pressure Gibbs equations (4.75) are summed and combined with (4.50) (with no added mass contribution here).

$$d_t^\phi(\Pi) = -\frac{\gamma^\phi p^\phi + \frac{5}{3}pk^\phi + \frac{1}{3}pi^\phi}{\alpha^\phi} D_t^\phi(\alpha^\phi). \quad (4.76)$$

The sum of the volume fraction allows to remove the temporal derivative on the right part.

$$\nu \partial_t \Pi + \Pi_{,j} \sum_\phi \frac{\alpha^\phi}{\tilde{p}^\phi} u_j^\phi = -\bar{u}_{j,j} + \sum_\phi \frac{\alpha^\phi}{\tilde{p}^\phi} pi^\phi u_{j,j}^\phi \quad (4.77)$$

with, $\bar{u}_{j,j} = \sum_\phi D_t^\phi(\alpha^\phi) = \sum_\phi (\alpha^\phi u_{j,j}^\phi)_{,j}$, $\tilde{p}^\phi = \gamma^\phi p^\phi + \frac{5}{3}pk^\phi + \frac{1}{3}pi^\phi$ and $\nu = \sum_\phi \frac{\alpha^\phi}{\tilde{p}^\phi}$.

This expression makes the temporal derivative of the total pressure appear explicitly which leads to the explicit equation of the density of each phase.

$$\alpha^\varphi \frac{d_t^\varphi \rho^\varphi}{\rho^\varphi} = -\beta^\varphi \bar{u}_{j,j} + \Pi_{,j} \sum_\phi \mu^{\varphi\phi} (u_j^\varphi - u_j^\phi) \quad (4.78)$$

with $\mu^{\varphi\phi} = \frac{\alpha^\phi}{\bar{p}^\phi} \frac{\alpha^\varphi}{\bar{p}^\varphi} \frac{1}{\nu}$ and $\beta^\varphi = \frac{\alpha^\varphi}{\bar{p}^\varphi \nu}$.

With this explicit equation, all the energies can be computed with the Gibbs like equation (4.74).

$$D_t^\varphi([\alpha\rho]^\varphi e^\varphi) = -\beta^\varphi p^\varphi \bar{u}_{j,j} + p^\varphi \sum_{\phi} \mu^{\varphi\phi} (d_t^\varphi(\Pi) - d_t^\phi(\Pi)) \quad (4.79)$$

$$D_t^\varphi([\alpha\rho]^\varphi k^\varphi) = -\beta^\varphi \text{pk}^\varphi \bar{u}_{j,j} + \text{pk}^\varphi \sum_{\phi} \mu^{\varphi\phi} (d_t^\varphi(\Pi) - d_t^\phi(\Pi)) \quad (4.80)$$

$$D_t^\varphi(\text{ei}^\varphi) = \beta^\varphi \text{pi}^\varphi \bar{u}_{j,j} - \text{pi}^\varphi \sum_{\phi} \mu^{\varphi\phi} (d_t^\varphi(\Pi) - d_t^\phi(\Pi)) \quad (4.81)$$

The conservation of energy is satisfied because the sum of the coefficient β^φ is equal to one, the total pressure $p^\varphi + \text{pk}^\varphi - \text{pi}^\varphi$ is equal for each fluid and the last term in each energy equation vanish by summing over the all the fluids.

$$\begin{aligned} & \sum_{\phi} D_t^\phi([\alpha\rho]^\phi (e^\phi + k^\phi + \text{ke}^\phi) + \text{ei}^\phi + \frac{1}{2}[\alpha\rho]^\phi (u_j^\phi)^2) \\ &= - \sum_{\phi} \text{pke}^\phi u_{j,j}^\phi - \sum_{\phi} u_j^\phi (\text{pke}^\phi)_{,j} \\ & \quad - \underbrace{\sum_{\phi} \beta^\phi}_{=1} \underbrace{(p^\phi + \text{pk}^\phi - \text{pi}^\phi)}_{\Pi} \underbrace{\bar{u}_{j,j}}_{\sum_{\phi} (\alpha^\phi u_j^\phi)_{,j}} - \sum_{\phi} \alpha^\phi u_j^\phi \underbrace{(p^\phi + \text{pk}^\phi - \text{pi}^\phi)_{,j}}_{\Pi_{,j}} \end{aligned} \quad (4.82)$$

The different behavior between the potentials depending on the mass and those depending on the void fraction (or density) appears in the energy equations. In the first category, potentials are not coupled together. Each one forms a distinct flux which is only composed of mass and velocity. In the second category, the effects are coupled and their pressure work conjointly. For each of these potential, the associated pressure contributes linearly to the total work of pressure ($(\Pi \bar{u}_i)_{,i}$ in equation 4.82). However, the distribution of the total work of pressure to a given fluid through the coefficient β^φ contains *all* the potentials effect of this category. As an example, the pressure work in the internal energy equation of the fluid φ is the work of the associated pressure p^φ but this work is weighted by a coefficient β^φ which depends on the pressure p^φ but also on the pressure pk^φ and pi^φ .

Only added mass

Until now, the added mass was not introduced in energy computations because this effect couples all energy reservoirs as seen in the section (4.3.3). Therefore, the computation done in (4.3.4) is very tedious. For simplicity, only two fluids denoted + and - are considered with the three following energy reservoirs: internal energy, kinetic energy and added mass. In the previous section, only potentials depending on the void fraction where coupled together through the volume filling constraint. Thus, this relation completed by its dual relation over pressures was enough to uncoupled the evolution equations. But added mass pressure is built

with velocities and volume fraction $\frac{1}{2}A_{,\alpha}\Delta^2u_i$. Therefore, it is not possible to write directly a relation similar to (4.75) due to the velocity derivatives. However, after long combinations of equations which involve all the momentum equations, it is possible to obtain this type of relation with additional terms composed by gradients. Computational details are provided in annex. In the end, the internal energy dynamics contains few dozens of terms that can not be simplified. Therefore, it seems impossible to build a scheme which consistently discretizes the full model while respecting the conservation of energy. To tackle this issue, the internal pressures are forced to be equal, $p^+ = p^- = p$. This constraint allows to use directly the computation done in (4.3.4). The energy equations yields then

$$D_t^\varphi([\alpha\rho]^\varphi e^\varphi) = -\beta^\varphi p \bar{u}_{j,j} + \sum_{\phi} \mu^{\phi\varphi} (d_t^\varphi(p) - d_t^\phi(p)). \quad (4.83)$$

The total kinetic energy equation is obtain by the combination of the momentum quantity (4.61) multiplied by the phase velocity $\sum(4.61)^{\phi}u^\phi$ and the total internal energy equation is obtained by using the Gibbs relation and the relation over the void fraction.

$$\begin{aligned} D_t^+(E_c^+) + D_t^-(E_c^-) + D_t^+(E_{int}^+) + D_t^-(E_{int}^-) + \partial_t(E_{add}) = \\ - \sum_{\phi} (\alpha^\phi u_i^\phi p^\phi)_{,i} - [A\Delta u_j (u_i^+ u_j^+ - u_i^- u_j^-)]_{,i} \\ - \frac{1}{2} [\Delta^2 u_j (A_{,+}[\alpha\rho]^+ u_i^+ + A_{,-}[\alpha\rho]^- u_i^-)]_{,i} \\ - \frac{1}{4} A_{,\alpha} \Delta^2 u_i \partial_t(\Delta\alpha) - \alpha^+ u_i^+ (\frac{\theta}{\alpha^+} \gamma^+ p)_{,i} + \alpha^- u_i^- (\frac{\theta}{\alpha^-} \gamma^- p)_{,i} + \theta \Delta u_i p_{,i} \end{aligned} \quad (4.84)$$

The last line of this equation is not conservative, however, explicit volume fraction dynamic may be extracted from explicit internal energy equations and Gibbs equations.

$$p\partial_t(\Delta\alpha) = -2p[(u_i^+ \alpha^+)_{,i} \beta^- - \beta^+ (u_i^- \alpha^-)_{,i}] - 2\mu p_{,i} \Delta u_i \quad (4.85)$$

with the expression of θ (4.59) (without turbulence and surface tension), the last line can be written as a conservative flux which leads to the conservative total energy evolution

$$\begin{aligned} \sum_{\phi} D_t^\phi \left([\alpha\rho]^\phi (\frac{1}{2}(u_i^\phi)^2 + e^\phi) \right) + \partial_t(E_{add}) = - \sum_{\phi} (\alpha^\phi u_i^\phi p^\phi)_{,i} \\ - \frac{1}{2} [\Delta^2 u_j (A_{,+}[\alpha\rho]^+ u_i^+ + A_{,-}[\alpha\rho]^- u_i^-)]_{,i} - [A\Delta u_j (u_i^+ u_j^+ - u_i^- u_j^-)]_{,i} \\ + [p_{add} (u_i^+ \alpha^+ \beta^- - u_i^- \alpha^- \beta^+)]_{,i} \end{aligned} \quad (4.86)$$

The added mass is taken into account in a fully conservative and explicit model at the price of a correction θ . Without this correction, it is not possible to obtain a consistent model toward thermodynamics that can be fully explicit and simple enough to be implemented in a numerical code.

4.A Appendix: pressure evolution equation with added mass and without pressure constraint

The system studied here is composed of two fluids + and -. The potentials of the system are the internal energies, the kinetic energies and the added mass energy $\frac{1}{2}A\Delta^2u_i$. Added mass pressure is denoted $\tilde{p} = \frac{1}{2}A, \alpha\Delta^2u_i$

By summing the equation over each fluid $\sum_{\pm}(4.55)$ (without turbulence and surface tension), the total momentum evolution is

$$\begin{aligned}
\sum_{\pm} D_t^{\pm}([\alpha\rho]^{\pm}u_i^{\pm} \pm A\Delta u_i) &= -\alpha^+p^+ - \alpha^-p^- \\
&+ \frac{1}{2}([\alpha\rho]^+(A,+)_{,i} + [\alpha\rho]^-(A,-)_{,i})\Delta^2u_j \\
&\text{(using 4.46 and the derivative of } A) \\
&= -p_{,i} + \alpha^+_{,i} \underbrace{(p^+ + \frac{1}{2}\tilde{p})}_{=\Pi} + \alpha^-_{,i} \underbrace{(p^- - \frac{1}{2}\tilde{p})}_{=\Pi} \\
&\text{(using 4.58b and the volume fraction constraint)} \\
&= -p_{,i}.
\end{aligned} \tag{4.87}$$

The total flux momentum p is the average mass pressure, each mass pressure can be expressed in function of this flux.

$$p = \alpha^+p^+ + \alpha^-p^-, \tag{4.88}$$

$$p^{\pm} = p \pm \alpha^{\mp}\frac{1}{2}A, \alpha\Delta^2u_j. \tag{4.89}$$

By introducing it into the momentum equations, they can be written in the following conservative form

$$\begin{aligned}
D_t^{\pm}([\alpha\rho]^{\pm}u_i^{\pm} \pm A\Delta u_i) &= -\alpha^{\pm}p_{,i} \mp (A, +[\alpha\rho]^+u_{j,i}^- + A, -[\alpha\rho]^-u_{j,i}^+) \Delta u_j \\
&\pm \frac{1}{2}\alpha^+ \alpha^- [(A, \alpha\Delta^2u_j)_{,i} + \rho^+(A, +)_{,i}\Delta^2u_j - \rho^-(A, -)_{,i}\Delta^2u_j].
\end{aligned} \tag{4.90}$$

The pseudo ‘Gibbs’ equation over the dynamic pressure $\tilde{p} = \frac{1}{2}A, \alpha\Delta^2u_i$ is coupled with the added mass kinetic energy due do the drift. The following combination leads to the evolution of the directed energy $\frac{1}{2}K\Delta^2u_i$, with $K = \frac{[\alpha\rho]^+[\alpha\rho]^-}{\rho} + A$,

$$\left(\sum_{\pm} \pm 4.90_i \times \frac{[\alpha\rho]^{\mp}}{\rho} \right) \times \Delta u_i. \tag{4.91}$$

After long but direct computations, the directed energy evolution is

$$\begin{aligned}
D_t^0(K)\Delta^2u_i + \frac{1}{2}Kd_t^0(\Delta^2u_i) - K\Delta^2u_i \left[u_j^+ \left(\frac{[\alpha\rho]^-}{\rho} \right)_{,j} + u_j^- \left(\frac{[\alpha\rho]^+}{\rho} \right)_{,j} \right] \\
= \alpha^+ \alpha^- \frac{\rho^+ - \rho^-}{\rho} p_{,i} \Delta u_i - (A, +[\alpha\rho]^+u_{j,i}^- + A, -[\alpha\rho]^-u_{j,i}^+) \Delta u_i \Delta u_j \\
+ \frac{1}{2}\alpha^+ \alpha^- [(A, \alpha\Delta^2u_j)_{,i} + \rho^+(A, +)_{,i}\Delta^2u_j - \rho^-(A, -)_{,i}\Delta^2u_j] \Delta u_i
\end{aligned} \tag{4.92}$$

with $u_i^0 = \frac{[\alpha\rho]^- u_i^+ + [\alpha\rho]^+ u_i^-}{\rho}$ and d_t^0 its Lagrangian transport operator associated. The drift $\Delta^2 u_i$ and the coefficient K has been separated to be introduced into the derivative of the dynamic pressure \tilde{p} . After long but simple computations, the following expression of the dynamic pressure evolution is

$$d_t^0(\tilde{p}) = \pm g d_t^0(\alpha^\pm) + G \quad (4.93)$$

with

$$g = \Delta^2 u_i \left[\frac{1}{2} A_{,\alpha\alpha} - \frac{A_{,\alpha}^2}{K} \right] \quad (4.94)$$

and

$$\begin{aligned} \frac{K}{A_{,\alpha}} G = & K \Delta^2 u_i \left[u_j^+ \left(\frac{[\alpha\rho]^-}{\rho} \right)_{,j} + u_j^- \left(\frac{[\alpha\rho]^+}{\rho} \right)_{,j} \right] \\ & - \left(\left(\frac{[\alpha\rho]^{+2}}{\rho^2} + A_{,-} \right) D_t^0([\alpha\rho]^+) + \left(\frac{[\alpha\rho]^{-2}}{\rho^2} + A_{,+} \right) D_t^0([\alpha\rho]^-) \right. \\ & \quad \left. - \frac{1}{2} \frac{K}{A_{,\alpha}} [A_{,\alpha+} d_t^0([\alpha\rho]^+) + A_{,\alpha-} d_t^0([\alpha\rho]^-)] \right) \Delta^2 u_i \\ & + \alpha^+ \alpha^- \frac{\rho^+ - \rho^-}{\rho} p_{,i} \Delta u_i - (A_{,+} [\alpha\rho]^+ u_{j,i}^- + A_{,-} [\alpha\rho]^- u_{j,i}^+) \Delta u_j \Delta u_i \\ & + \frac{1}{2} \alpha^+ \alpha^- [(A_{,\alpha} \Delta^2 u_j)_{,i} + \rho^+ (A_{,+})_{,i} \Delta^2 u_j - \rho^- (A_{,-})_{,i} \Delta^2 u_j] \Delta u_i. \end{aligned} \quad (4.95)$$

Thanks to the mass conservation, the transport of $[\alpha\rho]^\phi$ can be expressed without time derivative. Thus, the evolution of \tilde{p} is completely explicit, the equation 4.93 can be then modified to match the usual Gibbs equation.

$$\begin{aligned} d_t^\pm(\pm \alpha^\mp \tilde{p}) = & - \frac{\alpha^\pm}{\rho^\pm} (\alpha^\mp g \pm \tilde{p}) d_t^\pm(\rho^\pm) - \frac{\alpha^\pm}{\rho^\pm} (\alpha^\mp g \pm \tilde{p}) u_{j,j}^\pm [\alpha\rho]^\pm \\ & \pm \alpha^\mp G + \alpha^\mp (u_j^0 - u_j^\pm) (g \alpha_{,j}^\pm \mp \tilde{p}_{,j}). \end{aligned} \quad (4.96)$$

Then, the mass pressure equation and the added mass pressure equations can be combined similarly as the geometric density effects.

$$d_t^\pm(\pm \alpha^\mp \tilde{p}) = \tilde{\gamma}^\pm \tilde{p}_{add}^\pm \frac{d_t^\pm \rho^\pm}{\rho^\pm} + G^\pm, \quad (4.97)$$

$$d_t^\pm(p^\pm) = \gamma^\pm p^\pm \frac{d_t^\pm \rho^\pm}{\rho^\pm} + \Gamma^\pm \rho^\pm W^\pm \quad (4.98)$$

with

$$\tilde{\gamma}^\pm \tilde{p}_{add}^\pm = -\alpha^\pm (\alpha^\mp g \pm \tilde{p}), \quad (4.99)$$

$$G^\pm = -\frac{\alpha^\pm}{\rho^\pm} (\alpha^\mp g \pm \tilde{p}) u_{j,j}^\pm [\alpha\rho]^\pm \pm \alpha^\mp G + \alpha^\mp (u_j^0 - u_j^\pm) (g \alpha_{,j}^\pm \mp \tilde{p}_{,j}). \quad (4.100)$$

The same procedure can be then applied and the internal energy equations are similar to (4.79) with

$$\tilde{p}^\pm = \tilde{\gamma}^\pm \tilde{p}_{add}^\pm + \gamma^\pm p^\pm, \quad \tilde{W}^\pm = \Gamma^\pm W^\pm + \frac{G^\pm}{\rho^\pm}. \quad (4.101)$$

CHAPTER 5

Collisions in Eulerian-Eulerian modeling of dispersed multiphase flows

Contents

5.1	Introduction	151
5.1.1	The coupling challenge	151
5.1.2	Modeling of collisions	151
5.1.3	Collisions' challenging aspects	152
5.1.4	The present approaches	153
5.2	The interior collisions	154
5.2.1	Turbulent agitation	154
5.2.2	Energy closure	155
5.2.3	Lagrangian and momentum equation	159
5.2.4	Energy equations	160
5.2.5	Pressure equilibrium	161
5.3	Exterior collisions	161
5.3.1	The main principle	161
5.3.2	Collision model	162
5.3.3	Mass, momentum and energy exchange	163
5.3.4	Closing the model	164
5.4	The final model	165
5.5	Numerical tests	166
5.5.1	Interior collisions tests	166
5.5.2	Exterior collisions tests	168
5.5.3	Complete collision	168
5.6	An extension of the model	170
5.A	Appendix	173

5.1 Introduction

5.1.1 The coupling challenge

As explained in chapter (2), prediction of multiphase flows is crucial in many industrial and academical areas. Many different types of such flows exist following the nature of the constituting structures (molecule, inclusions, large zone with pure components. . .). Among them, dispersed flows are flows with small inclusions (compared to the scale of the flow) of various materials inside a continuous medium. The inclusions form the dispersed phases and the continuous medium the carrier phase. However, whatever the type of flow, three main challenges must be faced to predict accurately its evolution: i) the capture of the couplings between phases, ii) the stability of the flow and iii) the thermodynamic consistency.

The present chapter addresses the first challenge in the case of dispersed multi-phase flows. This challenge consists in taking into account the variety of interactions between phases. These interactions can be classified in three types (Balachandar, 2010): i) one-way coupling where the carrier phase influences the dispersed phase, ii) two-way coupling where there is a backward coupling from the dispersed phase to the carrier phase and iii) four-way coupling when there are interactions inside the dispersed phase. In very dilute regimes, one way coupling is enough to accurately predict the flow. When the mass of the dispersed phase becomes significant compared to the mass of the carrier phase, two way coupling is needed. In dense regimes, four way couplings are needed because collisions of the inclusions impact the flow.

Dispersed multi-phase flows are present in industrial applications such as sediment transport, fuel extraction, combustion, fluidized bed, etc. In such applications, the particles' volume fraction may be very high and four-way coupling becomes necessary. Therefore, various effects must be considered between carrier phase and dispersed phase such as drag, possibly added mass and collisions between the inclusions.

5.1.2 Modeling of collisions

The main approaches to describe the dispersed phase are the Lagrangian methods, the kinetic approaches and the Eulerian approaches. In the Lagrangian approaches, collisions are described by explicit interactions between the particles or parcels (computational particles). These interactions can be modeled by short distance potentials (Coulomb) or contact forces (friction, etc..) (Tsuji *et al.*, 1993). In the kinetic approaches, collisions are captured by modeling the collision operator (Liu *et al.*, 2012). In the Eulerian approaches, many authors use the concept of granular pressure (Gevrin *et al.*, 2008) in dense regimes. This granular pressure goes to infinity when the dispersed phase volume fraction approaches the compaction limit and depends on the agitation of the particles around the average velocity. The high energy associated to agitation is modeled with a continuous field whose evolution equation is added to the usual two-fluid model. It must be stressed that granular pressure models collisions between mesoscopic particles whereas the thermodynamic pressure models micro-

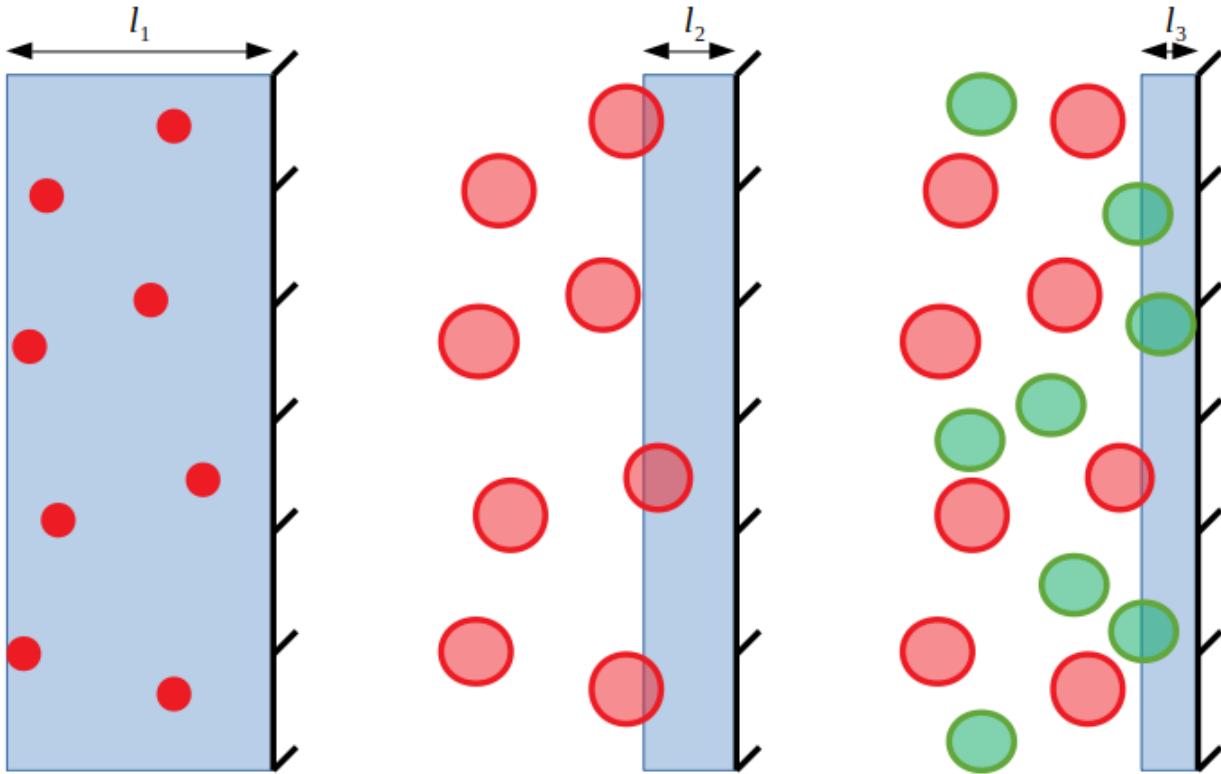


Figure 5.1: Collisions of a) point sphere, b) hard spheres and c) two groups of hard spheres against a wall, the distance l_i define the area where particles are likely to hit the wall.

scopic phenomena. Building and adjusting the correct form of the granular pressure relies on experimental data (Aguilar-Corona *et al.*, 2011), derivation from Boltzmann equations (Ding & Gidaspow, 1990) and macroscopic description.

5.1.3 Collisions' challenging aspects

The granular pressure comes from the collisions of particles. One way to define this pressure is to consider the transfer of momentum by unit of surface and time to a fictive wall (4) hit by them. Now, the difficulties lie in the estimation of this transfer. In dilute regimes, particles can be approximated by points. Thus, they do not collide with each other before hitting the wall and thus the closure of external agitation as made in (4) is relevant. However, in dense regimes, this assumption is not accurate. Their mean free path depends on their density and volume. Thus, the wall layer which contains particles susceptible to collide with the wall shrinks. Also, when several groups of particles are hitting the walls, a given particle interacts with all of them and not only the ones in its group.

The three situations are illustrated on figure (figure 5.1). In the first situation, point particles hit the wall (figure 5.1 left). In that case, particles cannot collide with each other. Identification of particles susceptible to collide with the wall during a given time step is straightforward (blue domain) and so is the wall pressure. In the second case (figure 5.1

middle), particles are not point like and they are then likely to collide with each other as well as hitting the wall. Given a time interval Δt , it is more convoluted to predict which particles are going to reach the wall. In addition, because particles interact together, the same particle may hit the wall several times during the time interval. Therefore, closure of the granular pressure has to take into account the mass, mean velocity and mean free path of particles. This becomes even more complex when several groups of particles coexist (figure 5.1 right). In that case, the granular pressure is the sum of the total impulse impacts on the wall. Also, the mean free path of a given particles depends on the volume and density of all particles which involves a coupling with all groups.

The granular pressure and the associated potential may be derived by mesoscopic scale analyses. However, in macroscopic scale described by Eulerian methods, granular agitation possesses some artifacts due to the average process inherent of the method. This is illustrated here by showing the impact of a dispersed phase split in several groups. Originally, the Lagrangian of the dispersed phase is

$$L = \frac{1}{2}Nm\bar{u}^2 - mke \quad (5.1)$$

with $\bar{u} = \sum_p u_p/N$ and $ke = \frac{1}{2} \sum_p (u_p - \bar{u})^2$. Now the dispersed phase is divided in two groups. The Lagrangian of the system becomes

$$L_{\text{groups}} = \sum_i \frac{1}{2}N_i m \bar{u}_i^2 - mke_i \quad (5.2)$$

with $\bar{u}_i = \sum_{p \in i} u_p/N_i$ and $ke_i = \frac{1}{2} \sum_{p \in i} (u_p - \bar{u}_i)^2$. The old Lagrangian may be written again (computation details are provided in (5.A)) as

$$L = L_{\text{groups}} - \sum_i N_i m (\bar{u} - \bar{u}_i)^2. \quad (5.3)$$

Thus, the Lagrangian is not invariant by splitting into groups (in contrast with the total energy). Therefore, the ensuing Euler–Lagrange and the momentum equations will differ.

5.1.4 The present approaches

In Eulerian description, the PDF of the dispersed phase may be divided in several groups or phases in order to capture non Maxwellian distributions. Particles are distributed in these phases following criteria such as their size, mean velocity, etc... Yet, as explained above, a given particle is likely to interact with *all* particles whatever the phase they come from. However, the Eulerian formalism does not identify each particles, it only identifies groups of particles into different phases. Therefore, collisional effects which are mesoscopic effects have to be translated in macroscopic ones. In this chapter, these are divided in two categories. The first category contains the average effects of collisions inside a phase, it will be called here interior collisions. The second part represents the effects of collisions between two different phases, it will be referred here to exterior collisions. For a single particle, this

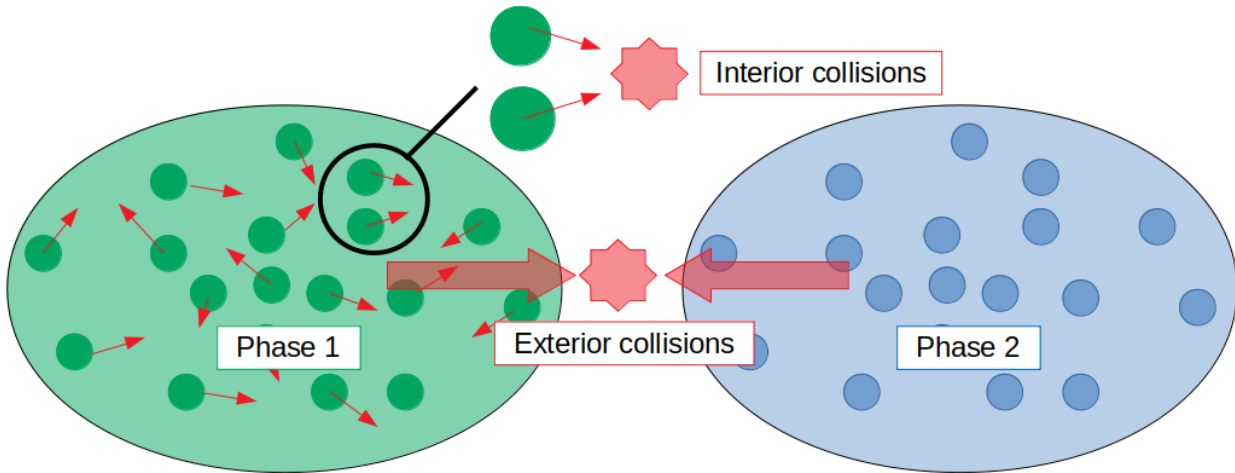


Figure 5.2: Illustration of the two different types of collision

approach means that collisions with particles of its group will be treated differently (with interior collisions formalism) than collision with particles of other groups (with exterior collision formalism).

The interior collisions are taken into account by a potential depending on the kinetic turbulent agitation and on the compaction limit. The isentropic equations of this model are deduced with a least action principle and the procedure described in chapter (4). The exterior collisions (collisions between different phases) are taken into account by the addition of new phases which collect the particles that have collided. These new phases will be called *collector* phases. They are introduced to identify particles that have collided from the others inside the same group. Indeed, as there is only one value of velocity, energy, etc. . . per phase in Eulerian description, non Maxwellian distribution are not captured. Thus, a collision between two structures inside a cell affect *all* the particles in this cell. However, introducing new phases allows non Maxwellian distribution to be reproduced. It is then possible to give new values for collided particles with mass, energy and momentum different to the structure from which they come without affecting the particles that have not collided.

5.2 The interior collisions

5.2.1 Turbulent agitation

In two-fluid models, equations of conservation derive from an averaging process of the local hydrodynamic fields (u , ρ , etc. . .) weighted by a presence function of each constituent (Drew, 1983; Ishii, 1975). This procedure leads to fluctuation terms that represent various effects specific to the multi-fluid flows such as surface tension and virtual mass. Among them, the velocity fluctuations issued from transport averaging appear in a term called the Reynolds Tensor. In the RANS literature, these velocity fluctuations are modeled with a new field called turbulent agitation. Various evolution equations of this field and its dissi-

pation exist in literature leading to a great amount of RANS models. This evolution can be postulated or found with computation based on the existing PDEs representing momentum conservation or even found with the kinetic theory. In chapter (4) it has been introduced in the Lagrangian to obtain evolution equations with a variational method coupled with a Gibbs like relation. The ensuing equations are consistent and furthermore improve the system stability as noted by Youngs (1989); Lhuillier *et al.* (2013). In the dilute regimes, the closure by the kinetic approach leads to similar results as those obtained by the averaging approach in (4) where only the diagonal part of the Reynolds tensor is kept.

However, in these regimes, influence of the particles' volume is not considered. In the kinetic approach, collisions between particles are neglected by the point particles approximation. In the averaging approach, the punctual particle hypothesis is present in the local equations averaged. These equations are fluid equations where the stress tensor is reduced to pressure. However, the validity of this modeling is wrong when two particles collide with each other. In such situations, the stress tensor should contain elastic effect, young modulus, etc. . . of the materials. Thus, because the local equations do not consider collisions between particles, the ensuing averaged equation do not contain this effect either.

In the literature, closures are usually applied to the granular pressure (Gevrin *et al.*, 2008; Kamenetsky *et al.*, 2000; Wachem *et al.*, 2001) that takes into account the compaction limit by an increasing function of particles' volume fraction. In this chapter, we propose a closure for granular pressure in (5.2.2) and we obtain its associated potential by integration. On the contrary of the punctual hypothesis made in (4), the particles' volume is taken into account. Therefore, the potential depends on the dispersed phase's volume fraction.

5.2.2 Energy closure

The closure of the potential embodying the turbulent effect with collisions between particles is based on two facts: i) the compaction limit effect is a consequence of an infinite frequency collision limit and i) hard collisions between particles is non dissipative. The point i) involves that turbulence and compaction limit must be taken into account jointly. The point ii) involves that it is possible to use the LAP to compute the trajectory of the system.

Because the potential should depends on the volume of the particles, we propose a potential that depends on the volume fraction of the dispersed phase. Furthermore, the momentum quantity transferred to the wall depends on the mass of the particles. Therefore, the potential depends also of the partial density of the particles.

$$[\alpha\rho]^\varphi ke^\varphi(\alpha^\varphi, \rho^\varphi \xi^\varphi), \quad (5.4)$$

Now, this potential must be coupled to the other fields. With the kinetic theory for point particle or with a conditional averaging with local fluid equations, the following isentropic closure is obtained (4),

$$\partial ke^\varphi = pke^\varphi \frac{\partial[\alpha\rho]^\varphi}{([\alpha\rho]^\varphi)^2}, \quad (5.5a)$$

$$pke^\varphi = \frac{2}{3}[\alpha\rho]^\varphi ke^\varphi. \quad (5.5b)$$

This expresses that the kinetic turbulent agitation depends only of the Lagrangian coordinates of the fluid particle and the number of particles per unit volume (which is directly linked to the averaged mass of the particles).

$$ke^\varphi = ke^\varphi([\alpha\rho]^\varphi, \xi^\varphi). \quad (5.6)$$

The kinetic theory used to obtain this closure considers only points particles. Thus the compaction limit and volume fraction dependency does not appear.

It must be stressed here that this potential models only interior collisions inside a structure, this is why it depends only on the volume fraction of the given structure. However, when several dispersed phases coexist, this potential is not able to take into account the total volume occupied by the dispersed phase with its actual compaction limit as explained in (5.2.2).

An example of mesoscopic derivation of closure for granular pressure

An example of closure's derivation is presented here. The system considered is made of particles inside a box. Particles are ideally spread in the box in a simple Cartesian grid (figure 5.3). They are considered to move only along horizontal parallel lines (the black dotted line in figure 5.3).

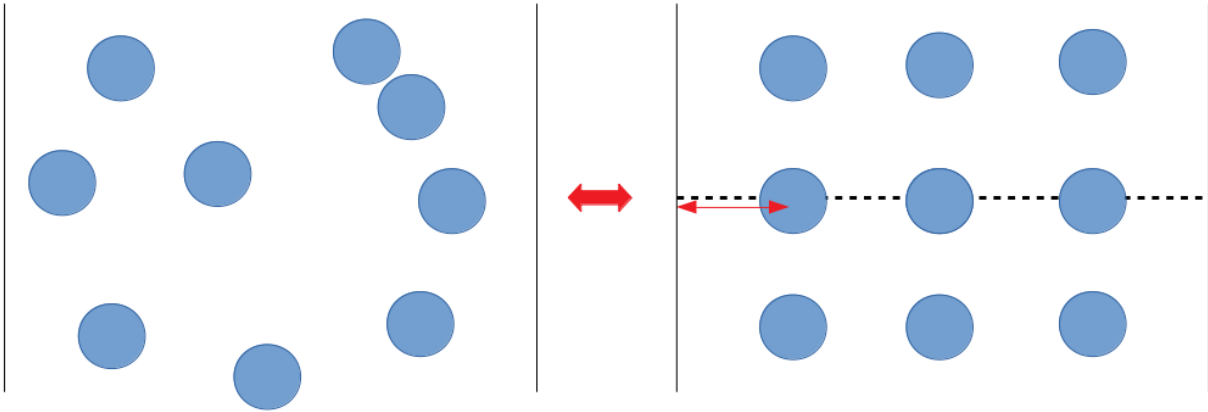


Figure 5.3: Ideal particles' distribution inside a box

To compute the granular pressure, an estimation of the number of collisions by unit of time is needed. Only particles close to the wall are susceptible to collide. Therefore, the frequency of collisions with the wall depends only on the average distance between particles and their mean velocity. During a long enough time interval (before the mean time between collision), an estimate of the number of collisions with a single particle in the dotted black

line is

$$N = \frac{1}{2} \frac{u}{d} \Delta t \quad (5.7)$$

where d is the mean free path of the particles. The total number of collisions in a section ΔS is then evaluated as

$$N_{\text{tot}} = Nn(d + r_{\text{particle}})\Delta S \quad (5.8)$$

The granular pressure is deduced

$$p_{\text{granular}} = nm u^2 \left(1 + \frac{r_{\text{particle}}}{d}\right) \quad (5.9)$$

with n the density of particle and m their mass. The mean distance between particles may be estimated as the cubic square of the volume left.

$$d = \frac{1}{N_p} V_c^{\frac{1}{3}} = \frac{1}{N_p} (V_{\text{max}} - N_p V_{\text{part}})^{\frac{1}{3}} = \frac{1}{N_p} (\alpha_c V_{\text{tot}} - N_p V_{\text{part}})^{\frac{1}{3}} = \frac{1}{N_p} V_{\text{tot}}^{\frac{1}{3}} (\alpha_c - \alpha)^{\frac{1}{3}} \quad (5.10)$$

with α_c the compaction limit and N_p the number of particles. The ratio between the characteristic dimension of the box and the number of particles can be estimated as

$$\frac{V_{\text{tot}}^{\frac{1}{3}}}{N_p} = r_{\text{particle}} + d. \quad (5.11)$$

Thus, the mean distance becomes

$$d = r_{\text{particle}} \frac{(\alpha_c - \alpha)^{\frac{1}{3}}}{1 - (\alpha_c - \alpha)^{\frac{1}{3}}}. \quad (5.12)$$

The closure sought depends then only on the relative mean velocity, the volume fraction and the compaction limit.

$$p_{\text{granular}} = \frac{1}{2} [\alpha \rho] u^2 \frac{1}{(\alpha_c - \alpha)^{\frac{1}{3}}} \quad (5.13)$$

Now that the granular pressure is closed, the ensuing turbulent agitation is determined with a Gibbs' relation.

The first principle, the mass conservation and the definition of mass energy lead to the following relations

$$dK_e = -p_{\text{granular}} dV \quad K_e = V[\alpha \rho] k_e \quad m = V[\alpha \rho] \quad (5.14)$$

In the light of the pressure's closure, the variables of interest for the compaction potential are $[\alpha \rho]^\varphi$ and α^φ . When the partial density varies, the same differential form than the one presented in the chapter (4) is obtained.

$$dk_e^\varphi = p_{\text{granular}} \frac{d[\alpha \rho]^\varphi}{([\alpha \rho]^\varphi)^2} \quad (5.15)$$

Now, the thermodynamics imposes that the energy must be an exact form. According to the Schwartz's theorem, this involves that the cross derivatives must be equal. The derivative of the agitation with respect to α is postulated with some functional f as

$$dke^\varphi = f(\alpha^\varphi, [\alpha\rho]^\varphi)ke^\varphi d\alpha^\varphi \quad (5.16)$$

To insure the equality between the cross derivatives, the following identity must be satisfied

$$f_{, [\alpha\rho]^\varphi \alpha^\varphi} = \frac{1}{2} \frac{1}{[\alpha\rho]^\varphi} \frac{1}{3} \frac{1}{(\alpha_c - \alpha^\varphi)^{\frac{4}{3}}} \quad (5.17)$$

which means that the partial derivative with respect to α^φ is

$$f_{, \alpha^\varphi} = \frac{1}{6} \frac{\ln([\alpha\rho]^\varphi)}{(\alpha_c - \alpha^\varphi)^{\frac{4}{3}}}. \quad (5.18)$$

A potential $ke^\varphi(\alpha^\varphi, [\alpha\rho]^\varphi)$ that satisfies these differential relations is

$$ke^\varphi(\alpha^\varphi, [\alpha\rho]^\varphi) = ([\alpha\rho]^\varphi)^{\frac{1}{2}} \frac{1}{(\alpha_c - \alpha^\varphi)^{1/3}} \quad (5.19)$$

Even if it comes from a coherent derivation, this potential seems far too complex. Therefore, we will use in what follows a simpler form

$$ke^\varphi = ([\alpha\rho]^\varphi)^{\frac{2}{3}} f(\alpha^\varphi) \quad (5.20)$$

with f a function which goes to infinity when the volume fraction reaches the compaction limit and unity when it goes to zero. With this simple closure, the same agitation potential without compaction effect is found again in dilute regimes. The differential relations are then

$$ke_{, [\alpha\rho]^\varphi}^\varphi = \frac{2}{3} \frac{ke^\varphi}{[\alpha\rho]^\varphi} \quad ke_{, \alpha^\varphi}^\varphi = \frac{f'(\alpha^\varphi)}{f(\alpha^\varphi)} ke^\varphi \quad (5.21)$$

For the function f , we use simply $f(\alpha^\varphi) = \frac{\alpha_c}{\alpha_c - \alpha^\varphi}$ in the numerical simulations presented in the bottom. However, the equations will be written formally, thus applicable to all closures.

It must be stressed that the present derivation is just an illustration of the capture of collisions by a potential and does not intent to be relevant to predict real dispersed flows. The set of equations derived in the following introduces the agitation potential in a pure formal way and thus any other potential's closure can be introduced providing that it depends on the same variables (i.e. the partial density and the volume fraction of the phase). Several equations of state for hard spheres exist (Carnahan–Starling, Kolafa correction...) which could be used to obtain different closures of the agitation potential.

5.2.3 Lagrangian and momentum equation

As in chapter (4), the isentropic momentum equations of the system are obtained with a variational method. The Lagrangian of the system is made with the kinetic energies (1), the internal energies (2), the interior collision potentials (3), the mass constraint (4), the Lin constraint (5) and the volume filling constraint (6).

$$L = \sum_{\phi} \left(\underbrace{\frac{1}{2}[\alpha\rho]^{\phi}(u_j^{\phi})^2}_{(1)} - \underbrace{[\alpha\rho]^{\phi}e^{\phi}(\rho^{\phi}, \xi^{\phi})}_{(2)} - \underbrace{[\alpha\rho]^{\phi}\text{ke}^{\phi}([\alpha\rho]^{\phi}, \alpha^{\phi}, \xi^{\phi})}_{(3)} \right. \\ \left. + \underbrace{\theta^{\phi}D_t^{\phi}([\alpha\rho]^{\phi})}_{(4)} + \underbrace{\Psi^{\phi}d_t^{\phi}(\xi^{\phi})}_{(5)} \right) - \Pi \left(\underbrace{\sum_{\phi} \alpha^{\phi} - 1}_{(6)} \right). \quad (5.22)$$

The resulting Euler Lagrange equations are obtained by derivation of the Lagrangian with respect to the degrees of freedom $[\alpha\rho]^{\varphi}$, α^{φ} , u_i^{φ} , ξ^{φ} and the Lagrangian multipliers θ^{φ} , Ψ^{φ} and Π .

$$\delta[\alpha\rho]^{\varphi} : 0 = \frac{1}{2}(u_j^{\varphi})^2 - e^{\varphi} - \rho^{\varphi}e_{,\rho^{\varphi}}^{\varphi} - \text{ke}^{\varphi} - [\alpha\rho]^{\varphi}\text{ke}_{,[\alpha\rho]^{\varphi}}^{\varphi} - d_t^{\varphi}(\theta^{\varphi}) \quad (5.23a)$$

$$\delta\alpha^{\varphi} : 0 = (\rho^{\varphi})^2 e_{,\rho^{\varphi}}^{\varphi} - \Pi - [\alpha\rho]^{\varphi}\text{ke}_{,\alpha^{\varphi}}^{\varphi} \quad (5.23b)$$

$$\delta u_i^{\varphi} : 0 = [\alpha\rho]^{\varphi}u_i^{\varphi} - [\alpha\rho]^{\varphi}\theta_{,i}^{\varphi} + \Psi^{\varphi}\xi_{,i}^{\varphi} \quad (5.23c)$$

$$\delta\xi^{\varphi} : 0 = -[\alpha\rho]^{\varphi}e_{,\xi^{\varphi}}^{\varphi} - [\alpha\rho]^{\varphi}\text{ke}_{,\xi^{\varphi}}^{\varphi} - D_t^{\varphi}(\Psi^{\varphi}) \quad (5.23d)$$

$$\delta\theta^{\varphi} : 0 = D_t^{\varphi}([\alpha\rho]^{\varphi}) \quad (5.23e)$$

$$\delta\Psi^{\varphi} : 0 = d_t^{\varphi}(\xi^{\varphi}) \quad (5.23f)$$

$$\delta\Pi : 0 = \sum_{\phi} \alpha^{\phi} - 1 \quad (5.23g)$$

with $p^{\varphi} = (\rho^{\varphi})^2 e_{,\rho^{\varphi}}^{\varphi}$. The equation (5.23b) shows that the total pressure is the sum of two contributions: the material pressure and the compaction pressure $p_c^{\varphi} = [\alpha\rho]^{\varphi}\text{ke}_{,\alpha^{\varphi}}^{\varphi}$. The equilibrium is now between the difference of material pressure and compaction pressure of each phases.

The computation of momentum equation is a bit lengthy but is straightforward (5.A).

$$D_t^{\varphi}([\alpha\rho]^{\varphi}u_i^{\varphi}) = -\alpha^{\varphi}\Pi_{,i} - \underbrace{\left[([\alpha\rho]^{\varphi})^2 \text{ke}_{,[\alpha\rho]^{\varphi}}^{\varphi} + \alpha^{\varphi} [\alpha\rho]^{\varphi} \text{ke}_{,\alpha^{\varphi}}^{\varphi} \right]}_{p_{\text{ke}}^{\varphi}},_{,i} \quad (5.24) \\ = -\alpha^{\varphi}p_{,i}^{\varphi} - [\alpha\rho]^{\varphi}\text{ke}_{,\alpha^{\varphi}}^{\varphi}\alpha_{,i}^{\varphi} - \left[([\alpha\rho]^{\varphi})^2 \text{ke}_{,[\alpha\rho]^{\varphi}}^{\varphi} \right]_{,i}.$$

The momentum conservation is ensured and exhibits two fluxes: i) the total pressure flux formed by summation over the momentum quantities and ii) turbulent pressure flux composed with two contributions, a contribution from the pressure associated to a mass variation and a contribution from the compaction pressure associated to the volume fraction variation.

5.2.4 Energy equations

The energy equations are computed by the same procedure developed in (4). Manipulations of the pressure relation (5.23b) allow to explicit the total pressure derivative. With the procedure detailed in chapter (4), the explicit energy equations are obtained. Computational details (with addition of eventual dissipation) are provided in (5.A). The explicit dynamics of internal energies are

$$D_t^\varphi([\alpha\rho]^\varphi e^\varphi) = -\beta^\varphi p^\varphi \bar{u}_{j,j} - p^\varphi \sum_\phi \mu^{\varphi\phi} \Pi_{,j}(u_j^\phi - u_j^\varphi) + p^\varphi \sum_\phi \mu^{\varphi\phi} (p_{e1}^\phi u_{j,j}^\phi - p_{e1}^\varphi u_{j,j}^\varphi). \quad (5.25)$$

The explicit compaction potential equation is also deduced as

$$\begin{aligned} D_t^\varphi([\alpha\rho]^\varphi ke^\varphi) = & - \underbrace{p_{ke}^\varphi u_{j,j}^\varphi}_{[C]} + \underbrace{p_c^\varphi \beta^\varphi \bar{u}_{j,j}}_{[A]} \\ & + \underbrace{p_c^\varphi \sum_\phi \mu^{\varphi\phi} \Pi_{,j}(u_j^\phi - u_j^\varphi) - p_c^\varphi \sum_\phi \mu^{\varphi\phi} (p_{e1}^\phi u_{j,j}^\phi - p_{e1}^\varphi u_{j,j}^\varphi)}_{[B]}. \end{aligned} \quad (5.26)$$

with $\bar{u}_i = \sum_\phi \alpha^\phi u_i^\phi$, $\mu^{\varphi\phi} = \frac{\alpha^\varphi}{p_{e2}^\varphi} \beta^\phi$, $\beta^\varphi = \frac{\alpha^\varphi}{p_{e2}^\varphi \nu}$, $\nu = \sum_\phi \frac{\alpha^\phi}{p_{e2}^\phi}$,

$$p_{e1}^\varphi = [\text{ke}_{,\alpha^\varphi}^\varphi + [\alpha\rho]^\varphi \text{ke}_{,\alpha^\varphi[\alpha\rho]^\varphi}^\varphi + \text{ke}_{,\alpha^\varphi\alpha^\varphi}^\varphi \alpha^\varphi] [\alpha\rho]^\varphi,$$

$$p_{e2}^\phi = [\gamma^\varphi p^\varphi + \alpha^\varphi [\alpha\rho]^\varphi \text{ke}_{,\alpha^\varphi\alpha^\varphi}^\varphi],$$

$$\text{and } p_{ke}^\varphi = ([\alpha\rho]^\varphi)^2 \text{ke}_{,[\alpha\rho]^\varphi}^\varphi + \alpha^\varphi [\alpha\rho]^\varphi \text{ke}_{,\alpha^\varphi}^\varphi.$$

The evolution of the compaction potential is controlled by:

A The work of compaction pressure weighted by the relative compressibility of the fluid.

B Reversible energy exchanges made of a pressure gradient along the drift.

C A turbulent pressure multiplied by the rate of mass change ($p_{ke}^\varphi \frac{d_t^\varphi [\alpha\rho]^\varphi}{[\alpha\rho]^\varphi}$).

The equations (5.24), (5.25) and (5.26) conserve the total energy (as the Noether theorem would have proved because the Lagrangian is time invariant). Its evolution yields

$$\sum_\phi D_t^\phi([\alpha\rho]^\phi (e^\phi + \text{ke}^\phi + \frac{1}{2}(u_j^\phi)^2)) = -[\Pi \bar{u}_j + p_{ke}^\phi u_{j,j}^\phi]_{,j}. \quad (5.27)$$

Now that the isentropic equations are written, the dissipative part of the model is introduced. It is reduced here to a drag force between the air and the dispersed phase modeled as

$$f_s^\varphi = -\alpha^\varphi \rho^0 f(\text{Re}^\varphi) \Delta u^\varphi \quad (5.28)$$

with 0 the carrier phase, $\Delta^\varphi u = u^0 - u^\varphi$ and Re a function of $\Delta^\varphi u$. The sum of the reaction due to the drag force between the carrier phase and the disperses phase is added in the carrier phase momentum equation as

$$f_s^0 = - \sum_\phi f_s^\phi. \quad (5.29)$$

The drag force leads to kinetic energy dissipation. Some part of the dissipation will be converted in heat into the carrier and dispersed phase energy equation as source terms. The other part will be converted in agitation in the turbulent equation. The weight of the transfer to each energy reservoir is another modelization issue that we do not explore here.

5.2.5 Pressure equilibrium

The scheme used to solve the model is described by [Vazquez-Gonzalez *et al.* \(2020\)](#). In this algorithm, a system is solved to verify the EOS of each fluid, the volume filling condition and the pressure relation. In ([Vazquez-Gonzalez *et al.*, 2020](#))), the pressure of each phase were equal. Here, the pressure relation is

$$\Pi = p^\varphi - [\alpha\rho]^\varphi \text{ke}_{,\alpha^\varphi}^\varphi \quad (5.30)$$

Thus, the equilibrium is done accounting for the collision pressure. At the end of the first step of the algorithm, the internal energies e^φ , the collision potential ke^φ and the partial density $[\alpha\rho]^\varphi$ are computed. Now, the thermodynamic quantities that verify the equations cited above (which are already verified at the order of the scheme) must be obtained. To do so, the following system with independent variables $\{\rho^\varphi\}$ and Π is solved

$$\begin{aligned} \sum_{\phi} [\alpha\rho]^\phi / \rho^\phi &= 1, \\ \Pi &= p^\varphi - [\alpha\rho]^\varphi \text{ke}_{,\alpha^\varphi}^\varphi. \end{aligned} \quad (5.31)$$

This system is potentially stiff and may need adapted numerical methods.

5.3 Exterior collisions

5.3.1 The main principle

Exterior collisions are collisions between two structures. They occur at macroscopic scales. By structures we understand macroscopic collections of mesoscopic particles like jets, clouds, etc. The goal is to capture particles ensuing from a collision between two macroscopic structures. Inside these structures, there are particles that will collide and particles that won't. The aim is to capture the behavior of both groups. However, the Eulerian description is not able to capture both groups without the introduction of a new phase in the model. Indeed, there is only one averaged field per fluid. Thus, it is not possible to distinguish particles that have collided from the others inside a phase. The idea is therefore to introduce a new phase, initially empty (nearly no mass and no void fraction) that will collect the particles issued from the collisions between two structures by the mean of mass, momentum and energy exchanges. These phases will be called *collector* phases or fluids. We denote φ_b the *collector* of the fluid φ , ie, the fluid that will collect the particles of φ that have collided.

5.3.2 Collision model

The situation modeled is the crossing of two groups of particles φ and ϕ . We denote $A^{\varphi\phi}$ the probability of a particle p^φ from the fluid φ to collide with a particle p^ϕ from the fluid ϕ . The following hypothesis, reasonable if the time step is small compared to the mean time between two collisions, is used. *The probability of collision between a particle p^φ and some particles of the fluid ϕ is equal to the probability that the particle p^φ collide with only **one** particle of the fluid ϕ .* All the particles from one fluid are considered with the same radius and velocity (which is already assumed in a cell). The cross-section of a particle p^φ crossing a cloud of particles p^ϕ is defined as

$$\sigma^{\varphi\phi} = 4\pi(r^\varphi + r^\phi)^2. \quad (5.32)$$

In the reference frame of the particles p^ϕ , the volume of space covered by p^φ with the cross-section $\sigma^{\varphi\phi}$ during the time step Δt can be expressed as

$$V^{\varphi\phi} = \sigma^{\varphi\phi}|u^\varphi - u^\phi|\Delta t. \quad (5.33)$$

The average number of particles p^ϕ present in the volume $V^{\varphi\phi}$ is

$$N^{\varphi\phi} = V^{\varphi\phi}\alpha^\phi \frac{3}{4\pi r^{\phi 3}} \quad (5.34)$$

If the time step is small enough, $N^{\varphi\phi}$ is between 0 and 1 and represents the probability that a single particle p^φ collide with a a particle p^ϕ of the cloud ϕ during the step time Δt . The average number of collisions between the fluid ϕ and the fluid φ per unit of time and volume is then

$$n^{\varphi\phi} = N^{\varphi\phi} \frac{1}{\Delta t V} = N^{\varphi\phi} \alpha^\varphi \frac{3}{4\Delta t \pi r^{\varphi 3}} = |u^\varphi - u^\phi| \alpha^\phi \alpha^\varphi \frac{9(r^\varphi + r^\phi)^2}{4\pi r^{\varphi 3} r^{\phi 3}} \quad (5.35)$$

This number is symmetric with respect to φ and ϕ . The total mass of the fluid φ per unit of volume and time which collides with the fluid ϕ is then

$$\begin{aligned} \dot{m}^{\varphi|\phi} &= n^{\varphi\phi} \rho^\varphi \frac{4}{3} \pi r^{\varphi 3} \\ &= |u^\varphi - u^\phi| \alpha^\phi [\alpha\rho]^\varphi \frac{3(r^\phi + r^\varphi)^2}{r^{\phi 3}} \end{aligned} \quad (5.36)$$

In general way, the total mass colliding by unit of volume and time can be modeled as

$$\dot{m}^{\varphi|\phi} = \rho^\varphi |u^\varphi - u^\phi| \alpha^\phi \alpha^\varphi g(r^\varphi, r^\phi) \quad (5.37)$$

with $[g] = m^{-1}$.

5.3.3 Mass, momentum and energy exchange

The *collector* fluids recover all the particles that have collided, the exchange form $\Psi^{\varphi\varphi_b}$ is then

$$\Psi^{\varphi\varphi_b} = \sum_{\phi} \dot{m}^{\varphi|\phi} \quad (5.38)$$

In a general way, we denote $\Psi^{\varphi\rightarrow\phi}$ the transfer of mass from the fluid φ to the fluid ϕ . For any fluid φ , the mass conservation and the momentum conservation is then

$$D_t^\varphi([\alpha\rho]^\varphi) = \sum_{\phi} \Psi^{\phi\rightarrow\varphi} - \sum_{\phi} \Psi^{\varphi\rightarrow\phi}. \quad (5.39)$$

A new velocity must be associated to the particles that have collided. In a collision between spheres, this new velocity depends on the two post collision velocities, their mass, the direction of the contact and a coefficient of restitution (Jenkins & Savage, 1983). However, with the Eulerian description, there is no access to the detail of the contact direction. It will be modeled later. For now, the ensuing velocity is a function of incident velocities, densities and a coefficient of restitution.

$$D_t^\varphi([\alpha\rho]^\varphi u_i^\varphi) = \text{forces} + \sum_{\phi} \Psi^{\phi\rightarrow\varphi} h(u^\varphi, u^\phi, \rho^\varphi, \rho^\phi, e) - \sum_{\phi} \Psi^{\varphi\rightarrow\phi} u^\varphi. \quad (5.40)$$

The only condition required is the conservation of the momentum quantity which means that

$$\sum_{\phi} \sum_{\varphi} \Psi^{\phi\rightarrow\varphi} h(u^\varphi, u^\phi, \rho^\varphi, \rho^\phi, e) - \Psi^{\varphi\rightarrow\phi} u^\varphi = 0. \quad (5.41)$$

The kinetic equation obtained from the linear combination $u_i^\varphi \times 5.40^\varphi - \frac{1}{2}u_i^{\varphi^2} \times 5.39^\varphi$ is

$$\begin{aligned} D_t^\varphi\left(\frac{1}{2}[\alpha\rho]^\varphi u_i^{\varphi^2}\right) &= \text{other variations} \\ &+ \sum_{\phi} \Psi^{\phi\rightarrow\varphi} \left(h(u^\varphi, u^\phi, \rho^\varphi, \rho^\phi, e)u^\varphi - \frac{1}{2}u^{\varphi^2}\right) \\ &- \sum_{\phi} \Psi^{\varphi\rightarrow\phi} \left(h(u^\varphi, u^\phi, \rho^\varphi, \rho^\phi, e)u^\varphi - \frac{1}{2}u^{\varphi^2}\right) \end{aligned} \quad (5.42)$$

Collisions must respect the second law of thermodynamics, so the sum of the terms added in the kinetic energy equations must be negative (ie that the total collision effects destruct kinetic energy). The kinetic energy loss will be converted into heat and agitation in the internal and turbulent energy equations. We denote \dot{W} and \dot{W}_e the heat and the turbulent energy production. The dissipation is introduced in the equations in the spirit of (Vazquez-Gonzalez *et al.*, 2020).

$$d_t^\varphi(e^\varphi) = p^\varphi \frac{d_t^\varphi \rho^\varphi}{(\rho^\varphi)^2} + \dot{W}^\varphi \quad (5.43)$$

$$d_t^\varphi(\text{ke}^\varphi) = -[\alpha\rho]^\varphi \text{ke}_{, [\alpha\rho]^\varphi}^\varphi u_{j,j}^\varphi + \text{ke}_{, \alpha^\varphi}^\varphi d_t^\varphi(\alpha^\varphi) + \dot{W}_e \quad (5.44)$$

With the condition of energy conservation

$$\sum_{\varphi} [\alpha\rho]^{\varphi} \dot{W}^{\varphi} + [\alpha\rho]^{\varphi} \dot{W}_e^{\varphi} = \rho \dot{W} \quad (5.45)$$

with $\rho \dot{W}$ the total kinetic energy destruction due to entropic effects.

5.3.4 Closing the model

The model is closed by assigning the expression of the mass exchange, the velocity after collisions, the closure of the drag force and the distribution of the dissipation. Mass exchanges from the fluid φ to a fluid φ_b due to the collision with the fluid ϕ are modeled as

$$\Psi^{\varphi \rightarrow \varphi_b} = \kappa \rho^{\varphi} \alpha^{\varphi} \alpha^{\phi} |u^{\phi} - u^{\varphi}| \quad (5.46)$$

It is postulated here that the vector that links the center of two particles at the instant of contact is in the direction of the drift between the two particles (see 5.A).

$$\begin{aligned} h(u^{\varphi}, u^{\phi}, \rho^{\varphi}, \rho^{\phi}, e) &= \frac{\rho^{\varphi} u^{\varphi} + \rho^{\phi} u^{\phi}}{\rho^{\varphi} + \rho^{\phi}} - e \frac{\rho^{\phi}}{\rho^{\varphi} + \rho^{\phi}} (u^{\varphi} - u^{\phi}) \\ &= (1+e) \frac{\rho^{\phi}}{\rho^{\phi} + \rho^{\varphi}} u^{\phi} + \frac{\rho^{\varphi} - e\rho^{\phi}}{\rho^{\varphi} + \rho^{\phi}} u^{\varphi} \end{aligned} \quad (5.47)$$

The momentum conservation must be verified. The total momentum exchange yields

$$\kappa \sum_{\varphi} \sum_{\phi} \alpha^{\varphi} \alpha^{\phi} |u^{\varphi} - u^{\phi}| \underbrace{\left(\frac{\rho^{\varphi} \rho^{\varphi} u^{\varphi} + \rho^{\varphi} \rho^{\phi} u^{\phi}}{\rho^{\varphi} + \rho^{\phi}} - e \frac{\rho^{\varphi} \rho^{\phi}}{\rho^{\varphi} + \rho^{\phi}} (u^{\varphi} - u^{\phi}) - \rho^{\varphi} u^{\varphi} \right)}_{-\frac{\rho^{\varphi} \rho^{\phi}}{\rho^{\varphi} + \rho^{\phi}} (e+1)(u^{\varphi} - u^{\phi})}. \quad (5.48)$$

The form under brace is asymmetrical and thus vanish by summation. Therefore, the momentum conservation is verified. The last feature to verify is the respect of the second principle. The kinetic destruction due to the collision between φ and ϕ is distributed among the fluids φ and ϕ and the collector fluids φ_b and ϕ_b .

$$\begin{aligned} &\Delta E_c^{\varphi} + \Delta E_c^{\varphi_b} + \Delta E_c^{\phi} + \Delta E_c^{\phi_b} = \\ &+ \kappa \alpha^{\varphi} \alpha^{\phi} |u^{\varphi} - u^{\phi}| (\rho^{\varphi} h(u^{\varphi}, u^{\phi}, \rho^{\varphi}, \rho^{\phi}, e) u^{\varphi_b} + h(u^{\phi}, u^{\varphi}, \rho^{\phi}, \rho^{\varphi}, e) u^{\phi_b}) \\ &- \kappa \alpha^{\varphi} \alpha^{\phi} |u^{\varphi} - u^{\phi}| \left(\rho^{\varphi} [u^{\varphi} u^{\varphi} - \frac{1}{2}(u^{\varphi})^2 + \frac{1}{2}(u^{\varphi_b})^2] + \rho^{\phi} [u^{\phi} u^{\phi} - \frac{1}{2}(u^{\phi})^2 + \frac{1}{2}(u^{\phi_b})^2] \right) \end{aligned} \quad (5.49)$$

With the closure of h , it can be shown after lengthy computations (5.A) that the dissipation is

$$\begin{aligned} \dot{W}_{\text{coll}} &= -\kappa \alpha^{\varphi} \alpha^{\phi} |u^{\varphi} - u^{\phi}| \frac{1}{2} \\ &\quad \left[(\rho^{\varphi})^2 (u^{\varphi} - u^{\varphi_b})^2 + (\rho^{\phi})^2 (u^{\phi} - u^{\phi_b})^2 + 2e \rho^{\varphi} \rho^{\phi} (u^{\varphi} - u^{\varphi_b})(u^{\phi} - u^{\phi_b}) \right. \\ &\quad \left. + \rho^{\varphi} \rho^{\phi} ((u^{\phi_b} - u^{\varphi})^2 + (u^{\phi} - u^{\varphi_b})^2 + 2e(u^{\phi_b} - u^{\varphi})(u^{\phi} - u^{\varphi_b})) \right]. \end{aligned} \quad (5.50)$$

As the elasticity coefficient is between 0 and 1, the dissipation is always positive.

Now, this dissipation must be distributed among the potentials as source term. It is assumed here that the dissipation due to the drag is distributed in the air's internal energy and in the particles' agitation. The dissipation of the collisions is distributed in the internal and agitation energies of the collector fluids.

5.4 The final model

The final model may now be written. The equations for the original fluids are

$$D_t^\varphi([\alpha\rho]^\varphi) = - \sum_{\phi} \dot{m}^{\varphi|\phi} \quad (5.51)$$

$$D_t^\varphi([\alpha\rho]^\varphi u_i^\varphi) = - \alpha^\varphi \Pi_{,i} - (p_{\text{ke}}^\varphi)_{,i} - \sum_{\phi} \dot{m}^{\varphi|\phi} u^\varphi \quad (5.52)$$

$$\begin{aligned} D_t^\varphi([\alpha\rho]^\varphi e^\varphi) = & - \beta^\varphi p^\varphi \bar{u}_{j,j} - \sum_{\phi} \dot{m}^{\varphi|\phi} e^\varphi \\ & - p^\varphi \sum_{\phi} \mu^{\varphi\phi} [d_t^\phi(\Pi) - d_t^\varphi(\Pi)] + p^\varphi \sum_{\phi} \mu^{\varphi\phi} [p_{e1}^\phi u_{j,j}^\phi - p_{e1}^\varphi u_{j,j}^\varphi] \\ & - p^\varphi \sum_{\phi} \mu^{\varphi\phi} (\rho^\varphi \dot{W}^\varphi - \rho^\phi \dot{W}^\phi) + [\alpha\rho]^\varphi \dot{W}^\varphi \end{aligned} \quad (5.53)$$

$$\begin{aligned} D_t^\varphi([\alpha\rho]^\varphi \text{ke}^\varphi) = & \beta^\varphi p_c^\varphi \bar{u}_{j,j} - \sum_{\phi} \dot{m}^{\varphi|\phi} \text{ke}^\varphi - p_{\text{ke}}^\varphi u_{j,j}^\varphi \\ & + p_c^\varphi \sum_{\phi} \mu^{\varphi\phi} [d_t^\phi(\Pi) - d_t^\varphi(\Pi)] - p_c^\varphi \sum_{\phi} \mu^{\varphi\phi} [p_{e1}^\phi u_{j,j}^\phi - p_{e1}^\varphi u_{j,j}^\varphi] \\ & + p_c^\varphi \sum_{\phi} \mu^{\varphi\phi} (\rho^\varphi \dot{W}^\varphi - \rho^\phi \dot{W}^\phi) + [\alpha\rho]^\varphi \dot{W}_e^\varphi. \end{aligned} \quad (5.54)$$

and for the *collector* fluids

$$D_t^{\varphi b}([\alpha\rho]^{\varphi b}) = \sum_{\phi} \dot{m}^{\varphi|\phi} \quad (5.55)$$

$$\begin{aligned} D_t^{\varphi b}([\alpha\rho]^{\varphi b} u_i^{\varphi b}) = & - \alpha^{\varphi b} \Pi_{,i} - (P_{\text{ke}}^{\varphi b})_{,i} \\ & + \sum_{\phi} \dot{m}^{\varphi|\phi} h(u^\varphi, u^\phi, \rho^\varphi, \rho^\phi, e) \end{aligned} \quad (5.56)$$

$$\begin{aligned} D_t^{\varphi b}([\alpha\rho]^{\varphi b} e^{\varphi b}) = & - \beta^{\varphi b} p^{\varphi b} \bar{u}_{j,j} + \sum_{\phi} \dot{m}^{\varphi|\phi} e^{\varphi b} \\ & - p^{\varphi b} \sum_{\phi} \mu^{\varphi b\phi} [d_t^\phi(\Pi) - d_t^{\varphi b}(\Pi)] + p^{\varphi b} \sum_{\phi} \mu^{\varphi b\phi} [\bar{p}^\phi u_{j,j}^\phi - \bar{p}^{\varphi b} u_{j,j}^{\varphi b}] \\ & - p^{\varphi b} \sum_{\phi} \mu^{\varphi b\phi} (\rho^{\varphi b} \dot{W}^{\varphi b} - \rho^\phi \dot{W}^\phi) + [\alpha\rho]^{\varphi b} \dot{W}^{\varphi b} \end{aligned} \quad (5.57)$$

$$\begin{aligned} D_t^{\varphi b}([\alpha\rho]^{\varphi b} \text{ke}^{\varphi b}) = & \beta^{\varphi b} p_c^{\varphi b} \bar{u}_{j,j} + \sum_{\phi} \dot{m}^{\varphi|\phi} \text{ke}^\varphi - p_{\text{ke}}^{\varphi b} u_{j,j}^{\varphi b} \\ & + p_c^{\varphi b} \sum_{\phi} \mu^{\varphi b\phi} [d_t^\phi(\Pi) - d_t^{\varphi b}(\Pi)] - p_c^{\varphi b} \sum_{\phi} \mu^{\varphi b\phi} [p_{e1}^{\phi b} u_{j,j}^\phi - p_{e1}^{\varphi b} u_{j,j}^{\varphi b}] \\ & + p_c^{\varphi b} \sum_{\phi} \mu^{\varphi b\phi} (\rho^{\varphi b} \dot{W}^{\varphi b} - \rho^\phi \dot{W}^\phi) + [\alpha\rho]^{\varphi b} \dot{W}_e^{\varphi b}. \end{aligned} \quad (5.58)$$

with $\rho^\varphi \bar{W} = \Gamma^\varphi \rho^\varphi \dot{W}^\varphi - [\alpha\rho]^\varphi \dot{W}_e^\varphi$

Fluid	Γ^φ	Π^φ Pa	ρ^φ $\text{kg} \cdot \text{m}^{-3}$
Air	2/5	0	1.0
Particles	6	$2.1 \cdot 10^9$	1000

Table 5.1: Approximate stiffened gas parameters for air and particles in present study. Densities are given at normal pressure 10^5 Pa.

5.5 Numerical tests

In all tests done in this section, the air is controlled the perfect state EOS and the particles to the stiffened gas EOS (5.59) with the parameters set in table (5.1).

$$p = \Gamma \rho e - \pi \quad (5.59)$$

5.5.1 Interior collisions tests

The first numerical simulation tests only the interior collisions to see its effect on a single phase. Two tests are done, one in 1D and one 2D.

1D test The first test aims to visualize the 1D effect of the potential and the transfer of energy from the kinetic energy to agitation energy via drag's dissipation. This test consists on a cloud of particles moving into air. Particles velocity is initialized at 10 m.s^{-1} . The shape of the initial volume fraction is a Gaussian of amplitude 0.55 at 0.3 m. The air and the particles exchange momentum via a drag forces. The dissipation due to the drag force goes in two different energy reservoirs. One part goes to the air internal energy, scaled by the air volume fraction, and the other part goes to the particle agitation energy, scaled by the particles' volume fraction. The results are shown in figure (5.4). The cloud is dispersed by the potential asymmetrically. The asymmetry of the diffusion comes from the asymmetry of the production due to the drag dissipation.

2D test The second test case aims to visualize the 2D effects of the potential and its impact in a *real* industrial situation. It consists on the simulation of a jet of particles inside a pipe. At the entry, the flow is made of a particle cloud inside air. The pipe is originally filed with air. Particles inside the jet are initially turbulent which means that the dispersed phase in entry has a turbulent kinetic energy. Inflow velocity is 10 m.s^{-1} and the end the simulation corresponds to the arrival of the jet close to the pipe end (after 0.7s). The initial value of the turbulent agitation is 3 J.kg^{-1} . The dispersion of the jet is seen in (5.5) by comparing jets with or without agitation. The compaction limit disperses the jet more than the simple agitation (with $f = 1$). The fact that the jet is narrowed in the figure (5.5a) is due to the wall boundaries conditions in the top and bottom of the domain.

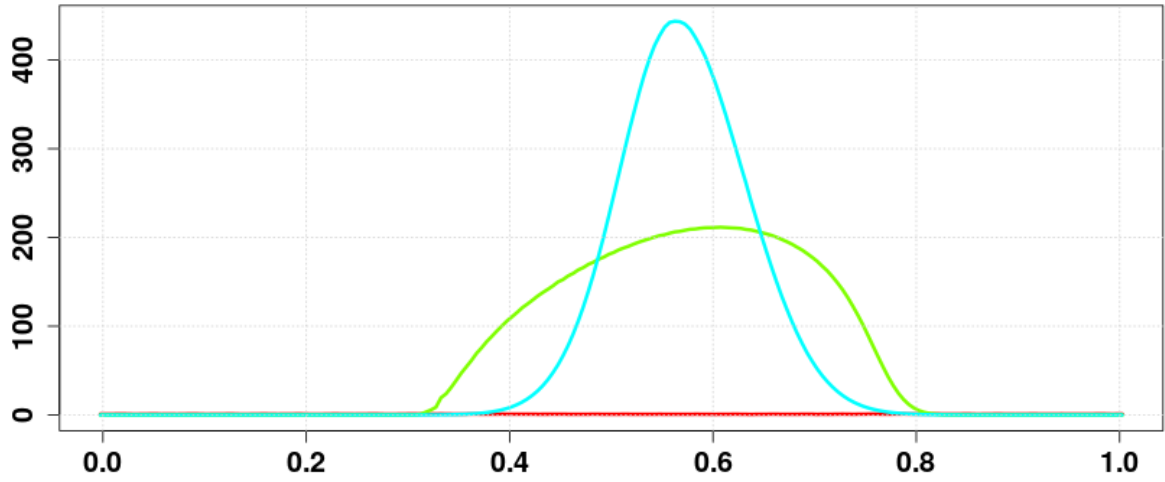
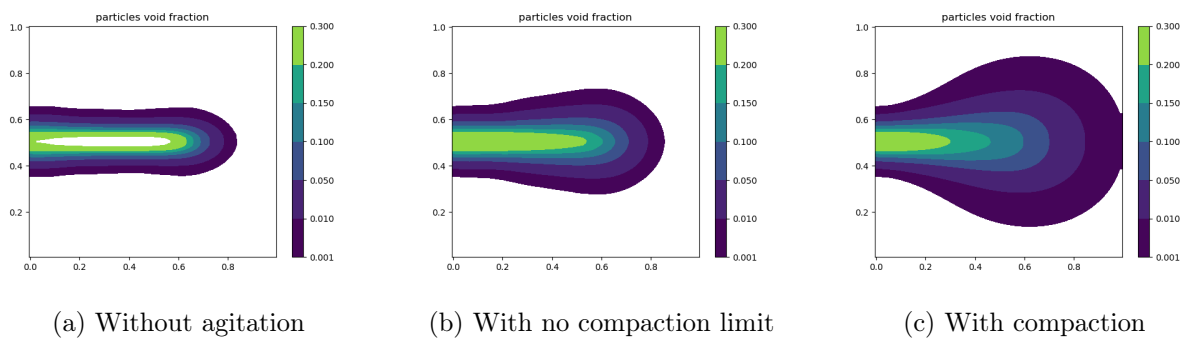


Figure 5.4: Partial densities of the different phases in the mixture in $kg.m^{-3}$. In green and blue, the dispersed phase with and without agitation, in red the air.



(a) Without agitation

(b) With no compaction limit

(c) With compaction

Figure 5.5: One particle jet inside a pipe

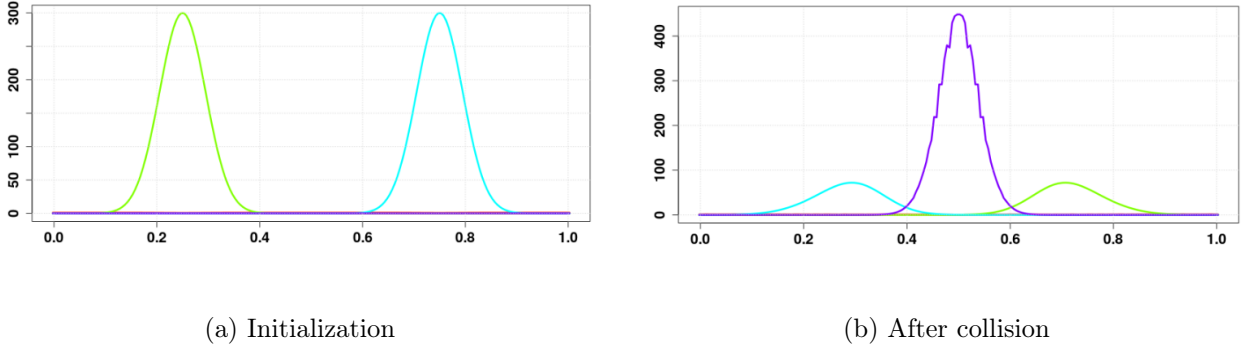


Figure 5.6: Partial densities of the different phases of the mixture in $kg.m^{-3}$. In green and blue, the dispersed phase without agitation, in red the air, in violet the *collector* fluid.

5.5.2 Exterior collisions tests

The effect of the exterior collisions without interior collisions (agitation) is tested here. The test aims to verify the correct behavior of the exchanges between the particle fluids and the *collector* fluids. Two clouds crossing into an air background are simulated, the results of their collision will feed the *collector* fluid in the middle of the domain. The dissipation due to the exchanges goes to the internal energy of the *collector* fluid because it is assumed that the collisions heat only the collided particles. The clouds and the *collector* fluid also exchange momentum with air through the drag force and the dissipation of the drag force goes to the internal energy of each fluid pondered by their volume fraction (see 5.A). Because the fluids are initialized with no agitation that is not feed by dissipation next, it stays null during all the computation. The results are presented in figure (5.6).

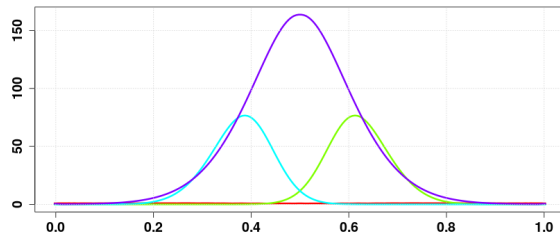
In the light of figure (5.6), the *collector* has been fed with the other clouds. Some irregularities on the void fraction profile appear which are hard to explain.

5.5.3 Complete collision

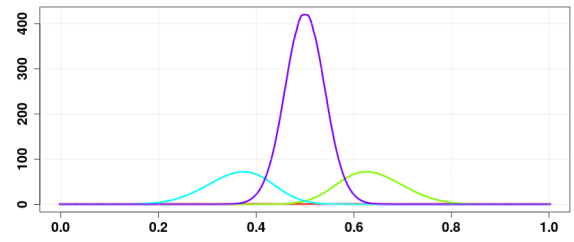
The last test cases combine both types of collisions. The first test is again the crossing of two clouds in an air background. However, this time the agitation energy is feed with the dissipation due to the drag force or to the exchange between the clouds and the *collector* fluid.

The *collector* clouds is diffused with regularized profile. In the first figure of (5.7), the dissipation due to exchanges is very strong and spread the collided particles. In the second figure, the dissipation due to the drag is weaker, the particles are less spread. However, the irregularities of the void fraction profile are still removed. Because the drag force also dissipates in the non collided clouds, they are also spread non uniformly (due to the asymmetry of the drag force).

The last test case is the collision of two jets inside an air tube. Their inlet velocity is $[10, \pm 10]$ $m.s^{-1}$. The collision gives birth to a collided jet that is going to spread due to the turbulent agitation. Two simulations has been done for this case. One simulation with



(a) Agitation feed with dissipation of collisions



(b) Agitation feed with drag dissipation

Figure 5.7: Partial densities of the different phases of the mixture in $kg.m^{-3}$. In green and blue, the dispersed phase, in red the air, in violet the *collector* fluid. (a) energy agitation only feed with dissipation due to exchange, (b) with dissipation due to drag.

only interior collisions and one simulation with also exterior collision. The collided jet is less dispersed with the exterior collision and a peak of volume fraction close to the compaction limit remains where the two jets cross. Also, the collisions impact the jets later in the simulation with the exterior collisions.

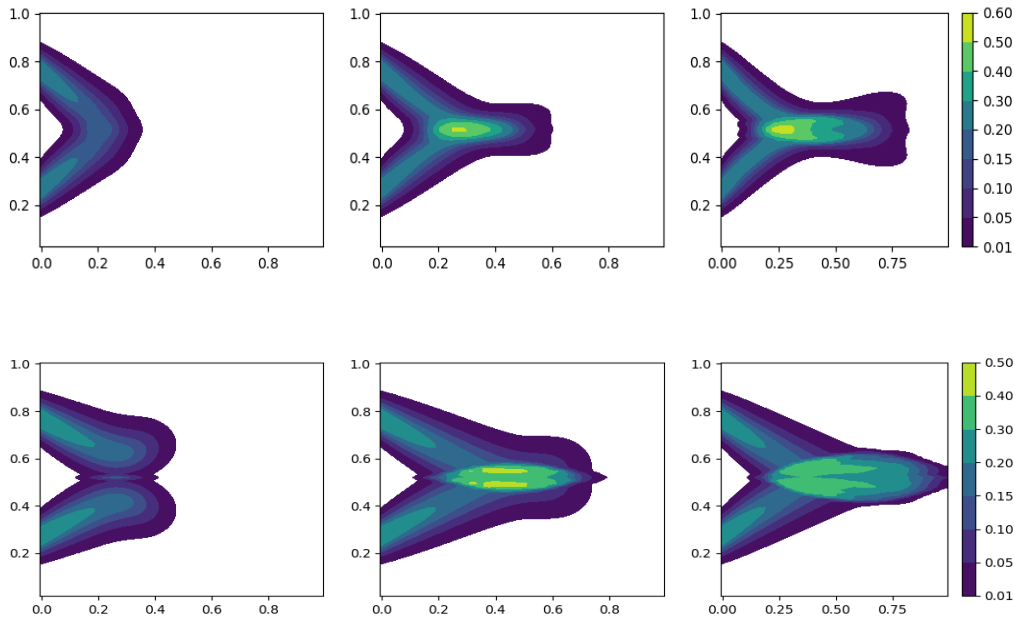


Figure 5.8: Crossing of two jets with exterior collisions above and compaction only (bottom): volume fraction of particles, contour level at different times of the simulation ($t = 0.03s, 0.045s, 0.6s$).

5.6 An extension of the model

In the current development, two types of collisions have been identified: collisions inside structures and between structures. The first type has been modeled with a potential and implemented in the model via a variational method to conserve its geometric character. The second type was taken into account by mass, momentum and energy exchanges between the different phases. If these exchanges can represent point collisions between spheres in the perfect elastic limit, they can not avoid dissipation here due to the average process of the Eulerian framework (see appendix 5.A). There are two major defects in this second way to deal with collisions:

- First, the collisions are no more a geometric process. They do not derive from a potential and are closed in the mass and momentum equations rather than by a potential approach. Therefore, we introduce dissipation due to mass and momentum exchanges that is purely an effect of the Eulerian (average) approach. This dissipation which feed the internal energy or the agitation has no clear meaning.
- Secondly, this type of collision needs to assign a phase for each macroscopic structure (here each jet). Therefore, the price to describe a collision is to introduce a new phase whose fields is going to be computed in all domain. In simulation with multiple structures, the cost of the method becomes unrealistic.

A possibility to remove the second type of collision is to take into account all the collisions with a potential that will eventually dissipate into internal energy by a further modeling. The simplest way to do this is to modify the potential of collision for each phase as follow

$$\text{ke}^\varphi([\alpha\rho]^\varphi, \alpha^\varphi, \xi^\varphi) \rightarrow \text{ke}^\varphi([\alpha\rho]^\varphi, \alpha_d, \xi^\varphi), \quad (5.60)$$

with α_d the sum over all the discrete phases susceptible to collide. However, by introducing this potential, all the internal energy equations become coupled together and the explicit equations are tedious to obtain. However, if there is only one carrier phase with many discrete species inside, the no volume filling allows to recast the potential as

$$\text{ke}^\varphi([\alpha\rho]^\varphi, \alpha^p, \xi^\varphi) \quad (5.61)$$

with α^p the carrier phase's volume fraction.

Introduction of these new potentials in the Lagrangian leads to the following momentum equations: (5.63) for the carrier phase, (5.64) for any dispersed phase and to the relation between pressures (5.62).

$$\begin{aligned} \Pi &= p^p - \sum_d [\alpha\rho]^d \text{ke}_{,\alpha^p}^d, \\ \Pi &= p^d \end{aligned} \quad (5.62)$$

$$\begin{aligned} D_t^p([\alpha\rho]^p u_i^p) &= -\alpha^p p_{,i}^p \\ &= -\alpha^p \Pi_{,i} - \alpha^p \left[\sum_d [\alpha\rho]^d \text{ke}_{,\alpha^p}^d \right]_{,i} \end{aligned} \quad (5.63)$$

$$D_t^d([\alpha\rho]^d u_i^d) = -\alpha^d \Pi_{,i} - \left[[\alpha\rho]^d ([\alpha\rho]^d \text{ke}_{,[\alpha\rho]^d}^d + \alpha^p \text{ke}_{,\alpha^p}^d) \right]_{,i} + \alpha^p \left[[\alpha\rho]^d \text{ke}_{,\alpha^p}^d \right]_{,i} \quad (5.64)$$

The momentum is conserved by summation and its equation yields

$$\sum_d D_t^d([\alpha\rho]^d u_i^d) + D_t^p([\alpha\rho]^p u_i^p) = -\Pi_{,i} - \left[[\alpha\rho]^d ([\alpha\rho]^d \text{ke}_{,[\alpha\rho]^d}^d + \alpha^p \text{ke}_{,\alpha^p}^d) \right]_{,i}. \quad (5.65)$$

As before, there are two fluxes: the first one is the total pressure gradient and the second one is a contribution from the kinetic turbulent pressure which is similar to the previous model except that the carrier phase's volume fraction replaces the dispersed phase's volume fraction.

The energy equations are obtained by the same procedure, first, the total pressure evolution is computed. The turbulent pressure evolution yields

$$\begin{aligned} d_t^p([\alpha\rho]^d \text{ke}_{,\alpha^p}^d) &= (\text{ke}_{,\alpha^p}^d + [\alpha\rho]^p \text{ke}_{,\alpha^p[\alpha\rho]^d}^d) d_t^p([\alpha\rho]^d) + [\alpha\rho]^d \text{ke}_{,\alpha^p\alpha^p}^d d_t^p(\alpha^p) \\ &= [\alpha\rho]^d \text{ke}_{,\alpha^p\alpha^p}^d D_t^p(\alpha^p) + (\text{ke}_{,\alpha^p}^d + [\alpha\rho]^d \text{ke}_{,\alpha^p[\alpha\rho]^p}^d - \text{ke}_{,\alpha^p\alpha^p}^d \alpha^p) [\alpha\rho]^d u_{j,j}^p \\ &\quad - (\text{ke}_{,\alpha^p}^d + [\alpha\rho]^p \text{ke}_{,\alpha^p[\alpha\rho]^p}^d) ([\alpha\rho]^d u_{j,j}^d) \end{aligned} \quad (5.66)$$

The internal and turbulent energies are then obtained by combining the total pressure evolution ensuing from Gibbs' relations and (5.66).

The internal energy's dynamics of the dispersed phases and carrier phase are

$$\begin{aligned} D_t^d([\alpha\rho]^d e^d) &= -\Pi\beta^d \bar{u}_{j,j} + \Pi \sum_{\phi} \mu^{\varphi\phi} \Pi_{,j}(u_j^{\varphi} - u_j^{\phi}) - \Pi\mu^{dp} p_{e1}^p u_{j,j}^p \\ &\quad - \Pi\mu^{dp} \sum_d k_e^d([\alpha\rho]^d u_{j,j}^d), \end{aligned} \quad (5.67)$$

$$\begin{aligned} D_t^p([\alpha\rho]^p e^p) &= -p^p \beta^p \bar{u}_{j,j} + p^p \sum_{\phi} \mu^{\varphi\phi} \Pi_{,j}(u_j^p - u_j^{\phi}) + p^p \sum_d \mu^{dp} p_{e1}^p u_{j,j}^p \\ &\quad + p^p \sum_d \mu^{dp} \sum_d k_e^d([\alpha\rho]^d u_{j,j}^d). \end{aligned} \quad (5.68)$$

Eventually, the turbulent energy of the dispersed phases are

$$\begin{aligned} D_t^d([\alpha\rho]^d ke^d) &= -([\alpha\rho]^d)^2 ke_{[\alpha\rho]^d}^d u_{j,j}^d + [\alpha\rho]^d ke_{,\alpha^p}^d \alpha_{,j}^p u_j^d - [\alpha\rho]^d ke_{,\alpha^p}^d (u_j^p \alpha^p)_{,j} \\ &\quad + [\alpha\rho]^d ke_{,\alpha^p}^d \left[\beta^p \bar{u}_{j,j} + \sum_{\phi} \Pi_{,j} \mu^{\phi p} (u_j^{\phi} - u_j^p) - \sum_d \mu^{pd} p_{e1}^p u_{j,j}^p \right] \\ &\quad - \sum_d \mu^{pd} \sum_d k_e^d([\alpha\rho]^d u_{j,j}^d), \end{aligned} \quad (5.69)$$

with $p_{e1}^p = \sum_d (ke_{,\alpha^p}^d + [\alpha\rho]^d ke_{,\alpha^p[\alpha\rho]^p}^d - ke_{,\alpha^p\alpha^p}^d \alpha^p)[\alpha\rho]^d$ for the carrier phase and $p_{e1}^d = \gamma^d p^d$ for a dispersed phase,

$$p_{e2}^p = \gamma^p p^p + \alpha^p \sum_d [\alpha\rho]^d ke_{,\alpha^p\alpha^p}^d,$$

$$k_e^d = ke_{,\alpha^p}^d + [\alpha\rho]^p ke_{,\alpha^p[\alpha\rho]^p}^d$$

The definition of the coefficient β and μ are identical to the first model.

This set of equation seems difficult to use in practice because the energy equations (5.68) and (5.69) are very complex. Therefore, will be difficult to discretize these equations while ensuring the energy conservation *and* the thermodynamic consistency.

5.A Appendix

Transformation of a Lagrangian by splitting

$$\begin{aligned}
L &= \sum_i \frac{1}{2} N_i m (\bar{u} - \bar{u}_i + \bar{u}_i)^2 - \frac{1}{2} \sum_i m \sum_{p \in i} (\bar{u} - \bar{u}_i + \bar{u}_i - u_p)^2 \\
&= \sum_i \frac{1}{2} N_i m \bar{u}_i^2 + \sum_i N_i m \bar{u}_i (\bar{u} - \bar{u}_i) + \sum_i \frac{1}{2} N_i m (\bar{u} - \bar{u}_i)^2 \\
&\quad - \frac{1}{2} \sum_i m \sum_{p \in i} (\bar{u} - \bar{u}_i)^2 - \underbrace{\sum_i m (\bar{u} - \bar{u}_i) \sum_{p \in i} (\bar{u}_i - u_p)}_{=0} - \frac{1}{2} \sum_i m \sum_{p \in i} (\bar{u}_i - u_p)^2 \\
&= \sum_i \frac{1}{2} N_i m \bar{u}_i^2 - m k e_i - \sum_i N_i m (\bar{u} - \bar{u}_i)^2 + \underbrace{\sum_i N_i m \bar{u} (\bar{u} - \bar{u}_i)}_{=0} \\
&= L_{\text{groups}} - \sum_i N_i m (\bar{u} - \bar{u}_i)^2
\end{aligned} \tag{5.70}$$

Momentum equation from Least Action principle

The computation of the momentum equation is a bit lengthy but straightforward.

$$\begin{aligned}
D_t^\varphi([\alpha\rho]^\varphi u_i^\varphi) &= -\alpha^\varphi p_{,i}^\varphi - [\alpha\rho]^\varphi [k e^\varphi + [\alpha\rho]^\varphi k e_{, [\alpha\rho]^\varphi}^\varphi]_{,i} + [\alpha\rho]^\varphi \xi_{,i}^\varphi k e_{,\xi}^\varphi \\
&= -\alpha^\varphi \Pi_{,i} - \alpha^\varphi [[\alpha\rho]^\varphi k e_{,\alpha}^\varphi]_{,i} \\
&\quad - [\alpha\rho]^\varphi \left([\alpha\rho]_{,i}^\varphi k e_{, [\alpha\rho]^\varphi}^\varphi + \alpha_{,i}^\varphi k e_{,\alpha^\varphi}^\varphi + \frac{([\alpha\rho]^\varphi)^2 k e_{, [\alpha\rho]^\varphi}^\varphi}{[\alpha\rho]^\varphi} \right)_{,i} - [\alpha\rho]_{,i}^\varphi k e_{, [\alpha\rho]^\varphi}^\varphi \\
&= -\alpha^\varphi \Pi_{,i} - \underbrace{\left[([\alpha\rho]^\varphi)^2 k e_{, [\alpha\rho]^\varphi}^\varphi + \alpha^\varphi [\alpha\rho]^\varphi k e_{,\alpha^\varphi}^\varphi \right]}_{p_e^\varphi}_{,i}
\end{aligned} \tag{5.71}$$

Explicit energy equations

The explicit equation over the turbulent pressure is

$$\begin{aligned}
d_t^\varphi(p^\varphi) &= -\frac{\gamma^\varphi}{\alpha^\varphi} p^\varphi D_t^\varphi(\alpha^\varphi) \\
d_t^\varphi([\alpha\rho]^\varphi k e_{,\alpha^\varphi}^\varphi) &= -k e_{,\alpha^\varphi}^\varphi [\alpha\rho]^\varphi u_{j,j}^\varphi + [\alpha\rho]^\varphi d_t^\varphi(k e_{,\alpha^\varphi}^\varphi) \\
&= -[k e_{,\alpha^\varphi}^\varphi + [\alpha\rho]^\varphi k e_{,\alpha^\varphi [\alpha\rho]^\varphi}^\varphi + k e_{,\alpha^\varphi \alpha^\varphi}^\varphi \alpha^\varphi] [\alpha\rho]^\varphi u_{j,j}^\varphi \\
&\quad + [\alpha\rho]^\varphi k e_{,\alpha^\varphi \alpha^\varphi}^\varphi D_t^\varphi(\alpha^\varphi)
\end{aligned} \tag{5.72}$$

The dynamics of the common pressure is then

$$d_t^\varphi(\Pi) = \underbrace{[\text{ke}_{,\alpha^\varphi}^\varphi + [\alpha\rho]^\varphi \text{ke}_{,\alpha^\varphi[\alpha\rho]^\varphi}^\varphi + \text{ke}_{,\alpha^\varphi\alpha^\varphi}^\varphi \alpha^\varphi]}_{p_{e1}^\varphi} [\alpha\rho]^\varphi u_{j,j}^\varphi - \underbrace{[\gamma^\varphi p^\varphi + \alpha^\varphi [\alpha\rho]^\varphi \text{ke}_{,\alpha^\varphi\alpha^\varphi}^\varphi]}_{p_{e2}^\varphi} \frac{D_t^\varphi(\alpha^\varphi)}{\alpha^\varphi}. \quad (5.73)$$

This equation becomes implicit by summation over all fluids

$$\nu \partial_t(\Pi) + \Pi_{,j} \sum_\phi \frac{\alpha^\phi}{p_{e2}^\phi} u_j^\phi = \sum_\phi \frac{p_{e1}^\phi}{p_{e2}^\phi} u_{j,j}^\phi - \bar{u}_{j,j}, \quad (5.74)$$

with $\nu = \sum_\phi \frac{\alpha^\phi}{p_{e2}^\phi}$, $\beta^\varphi = \frac{\alpha^\varphi/p_{e2}^\varphi}{\nu}$ to obtain

$$\partial_t(\Pi) = -\Pi_{,j} \sum_\phi \beta^\phi u_j^\phi + \sum_\phi \beta^\phi p_{e1}^\phi u_{j,j}^\phi - \frac{1}{\nu} \bar{u}_{j,j}. \quad (5.75)$$

The ensuing volume fraction's equation is

$$D_t^\varphi(\alpha^\varphi) = \sum_\phi \mu^{\varphi\phi} \Pi_{,j} (u_j^\phi - u_j^\varphi) - \sum_\phi \mu^{\varphi\phi} (p_{e1}^\phi u_{j,j}^\phi - p_{e1}^\varphi u_{j,j}^\varphi) + \beta^\varphi \bar{u}_{j,j}. \quad (5.76)$$

The explicit internal energy equations are then deduced.

Computation of the dissipation

With the closure used, the kinetic variations writes

$$\begin{aligned} \kappa \alpha^\varphi \alpha^\phi |u^\varphi - u^\phi| & \left(\rho^\varphi \frac{\rho^\varphi u^\varphi + \rho^\phi u^\phi}{\rho^\varphi + \rho^\phi} u^{\varphi b} - e \frac{\rho^\varphi \rho^\phi}{\rho^\varphi + \rho^\phi} (u^\varphi - u^\phi) u^{\varphi b} \rho^\phi \frac{\rho^\varphi u^\varphi + \rho^\phi u^\phi}{\rho^\varphi + \rho^\phi} u^{\phi b} \right. \\ & - e \frac{\rho^\varphi \rho^\phi}{\rho^\varphi + \rho^\phi} (u^\phi - u^\varphi) u^{\phi b} \left. - \kappa \alpha^\varphi \alpha^\phi |u^\varphi - u^\phi| \left(\rho^\varphi [u^\varphi u^\varphi - \frac{1}{2}(u^\varphi)^2 + \frac{1}{2}(u^{\varphi b})^2] \right. \right. \\ & \left. \left. + \rho^\phi [u^\phi u^\phi - \frac{1}{2}(u^\phi)^2 + \frac{1}{2}(u^{\phi b})^2] \right) \right). \end{aligned} \quad (5.77)$$

We regroup the terms factorized with the elasticity coefficient together as well as the terms without elasticity coefficient.

$$\begin{aligned} \frac{1}{2}(\rho^\varphi)^2 (u^\varphi - u^{\varphi b})^2 + \frac{1}{2}(\rho^\phi)^2 (u^\phi - u^{\phi b})^2 + \frac{1}{2}\rho^\varphi \rho^\phi (u^\varphi - u^{\phi b})^2 + \frac{1}{2}\rho^\varphi \rho^\phi (u^\phi - u^{\varphi b})^2 \\ + e \rho^\varphi \rho^\phi (u^\varphi - u^\phi) (u^{\varphi b} - u^{\phi b}). \end{aligned} \quad (5.78)$$

Then, we use the equality

$$(u^\varphi - u^\phi)(u^{\varphi b} - u^{\phi b}) = (u^\varphi - u^{\varphi b})(u^\phi - u^{\phi b}) + (u^{\phi b} - u^\varphi)(u^\phi - u^{\varphi b}) \quad (5.79)$$

and we have proven the result.

Dissipation due to the drag force

The dissipation due to the drag force between a fluid ϕ and a fluid φ express as

$$dW = \frac{1}{2}C^{\varphi\phi}(u^\varphi - u^\phi)^2. \quad (5.80)$$

We distribute this dissipation among the fluid φ and ϕ as

$$dW^{\varphi|\phi} = \frac{\alpha^{\varphi|\phi}}{\alpha^\phi + \alpha^\varphi}dW \quad (5.81)$$

Collision between two spheres

The dynamics of the head-on collision between two hard spheres is described in (Gidaspow (1994)). We call k^\pm the vector that goes from the center of the particle $+$ to the center of the particle $-$. The post collision velocity express

$$\begin{aligned} u_2^+ &= \frac{m^+u_1^+ + m^-u_1^-}{m^+ + m^-} - \frac{m^-}{m^+ + m^-}ek \cdot (u_1^+ - u_1^-)k \\ u_2^- &= \frac{m^+u_1^+ + m^-u_1^-}{m^+ + m^-} - \frac{m^+}{m^+ + m^-}ek \cdot (u_1^- - u_1^+)k \end{aligned} \quad (5.82)$$

If we suppose that the vector k is in the direction of the difference of velocity, we have

$$\begin{aligned} k &= u_1^+ - u_1^- \\ u_2^+ &= \frac{m^+u_1^+ + m^-u_1^-}{m^+ + m^-} - \frac{m^-}{m^+ + m^-}e(u_1^+ - u_1^-) \\ u_2^- &= \frac{m^+u_1^+ + m^-u_1^-}{m^+ + m^-} - \frac{m^+}{m^+ + m^-}e(u_1^- - u_1^+) \end{aligned} \quad (5.83)$$

which is the model used.

CHAPTER 6

Exploratory work on a new hybrid method to model dispersed phases in multiphase flows

Contents

6.1	Introduction	179
6.1.1	Physics and modeling of dispersed multiphase flows	179
6.1.2	First tracking of particles in Eulerian cell	180
6.2	A new thermodynamic consistent approach	181
6.2.1	Hybrid description of particles	181
6.2.2	Variational approaches in discrete and semi-discrete systems	183
6.3	Application of the method on various systems	184
6.3.1	Full particles systems	184
6.3.2	Dispersed multiphase flows	185
6.3.3	Model with fluid and particles both compressible	187
6.4	Consistent numerical schemes	188
6.4.1	System with only compressible particles	188
6.4.2	System with fluid and non compressible particles	189
6.4.3	System with fluid and compressible particles	191
6.5	Precisions on the numerical schemes	193
6.5.1	On the particle spreading	193
6.5.2	On the transport equation	194
6.5.3	Dissipation forms	195
6.6	Numerical results	195
6.6.1	Incompressible particles in compressible fluids	195
6.6.2	Dispersed curtains	196
6.6.3	Compressible particle in shock and expansion	198
6.A	Appendix	200
6.A.1	Continuous	200
6.A.2	Discrete	202

6.1 Introduction

6.1.1 Physics and modeling of dispersed multiphase flows

As explained in (2 and 5), dispersed multiphase flows are defined as flows where a dispersed phase is distributed within a carrier phase in the form of inclusions (Balachandar, 2010). Both phases may be of various kinds depending on the industrial or academic applications where they are encountered, bubbly flows in stirred tanks (Shi & Rzehak, 2018), solid gas in fluidized bed (Zhang & VanderHeyden, 2001) or liquid gas in combustion chambers (Murrone & Villedieu, 2011). Couplings between the dispersed phase and the carrier phase occur at the particles' scale and are transitory, non linear and turbulent. Especially, the turbulence of the carrier phase may be enhanced or damped by the dispersed inclusions (Balachandar, 2010). Forces applied to particles by the carrier phase are of several kinds, from dynamic effects including Basset force or virtual mass to static effects with pressure gradient and highly non linear with the drag force. Also, interactions between the inclusions themselves may be very complex due to potential inelastic collisions, fragmentations, coalescences, etc. In addition, chemical aspects must be sometimes taken into account as well as phase transition (evaporation of the droplets) (Murrone & Villedieu, 2011).

Due to the high number of interfaces involved, interface tracking or capturing methods are unable to deal with such flows. Their computational cost becomes rapidly unrealistic when the inclusions' size diminishes or their number increases. Diffuse interface models are workable but struggle to capture collision effects and the non Maxwellian character of the NDF. However, kinetic methods are very efficient to deal with dispersed flows. They provide a good balance between computing needs and precision. Inside kinetic models, several solutions exist, from the complete resolution of the Williams' equation to the Eulerian methods. Among them, the Lagrange-Euler methods (LE) have been very fruitful to predict dispersed multiphase flows (Padding *et al.*, 2015; Snider, 2007).

Theoretical grounds of the Lagrange Euler methods

The Lagrange-Euler methods (LE) are applied specifically to dispersed multiphase flows. They are divided in several categories following the nature of the flows encountered (Padding *et al.*, 2015; Subramaniam, 2013). In all of these methods, particles are monitored in the Lagrangian frame whereas the carrier phase is modeled in the Eulerian frame. Particles' trajectories aim to reconstitute the number density function (NDF) solution of the Williams equation (Williams (1958)). If LE approaches can be prohibitive due to their computational cost when the number of particles increases, they present several advantages over an Eulerian description of the dispersed phase.

- They are able to capture non Maxwellian distribution of particles.
- They describe more accurately collisions between particles.

- They capture interactions with carrier phase easily, especially dynamics effects such as added mass and basset forces.

On the mathematical point of view, particles constitute the following approximation of the (NDF):

$$f = \sum_k \omega_k(t) \delta_{x_k(t)} \delta_{v_k(t)} \dots \quad (6.1)$$

The dynamics of $\omega_k, x_k, v_k, \dots$ is obtained by introducing this approximation in the kinetic equation. The development of multiphase (LE) methods was inspired by the first methods to track particles in mesh.

6.1.2 First tracking of particles in Eulerian cell

The first method to track particles in Eulerian cells seems to be the particle in cell (PIC) approach by [Evans & Harlow \(1957\)](#). The authors described the basic principles of the PIC approach for hydrodynamic. It has been notably improved by [O'Rourke *et al.* \(1993\)](#) since. The main ingredient of this method is the coupling between numerical particles through cells. The particles p of mass m_p are distributed in the domain. However, these particles do not possess their own density, velocity and internal energy. All of these quantities will be reconstructed in the center of the cell (e.g. density by the formula $\rho_c^n = \sum_p \frac{m_p}{V_c^n}$). All of the particles in the same cell share the same velocity (the velocity of the cell). The algorithm is split in three steps: velocity and internal energy computation, transport of the particles, corrections due to the transport (if a particle has moved from one cell to another). The velocity and internal energy computations are made with usual numerical schemes (e.g. finite difference). The global formulation of the method is then based on the coupling between discrete particles and continuous fields discretized in cells.

Multiphase adaptation MP–PIC and other methods

The PIC method was adapted to the multiphase flow with the MP–PIC method developed by [Andrews & O'Rourke \(1996\)](#). This method was extended to two dimensions by [Snider *et al.* \(1997\)](#) and to three by [Snider \(2001\)](#). The forward coupling is computed as the sum of the drag force and the fluid pressure gradient. As in the PIC approach, the properties of the discrete particles are mapped back to the Eulerian grid in order to compute the backward coupling. Furthermore, four way coupling is taken into account by a particle stress, evaluated with the volume fraction mapped back. Similar approaches have been developed such as coupling between finite volume method for the Eulerian phase and material point method ([Bardenhagen *et al.*, 2000](#)) (extension of PIC method) for the dispersed phase ([Baumgarten *et al.*, 2021](#)). Notable works are made by [Capecelatro & Desjardins \(2013\)](#) where particles are spread over several cells. An comprehensive review of the models as well as the numerical methods is made by [Subramaniam \(2013\)](#).

Main difficulties encountered

The (LE) methods are challenged by several issues. First, the coupling between the dispersed phase and the carrier phase is transitory, non linear and turbulent. Even if the (LE) methods have more degrees of freedom to describe the flow than the diffuse interface ones, they still struggle to capture it. Secondly, in the numerical point of view, they involve interactions between two entities of very different natures, the particles' discrete one and the carrier phase's continuous one. To do so, interpolations map discrete quantities into fields and vice versa. They turn out to be very complex in 3-D simulations. Also, backward coupling may be very costly in case of dense particle flow if the detail of all particles' interaction is computed. Modeling it by continuous potential depending on fields mapped back in Eulerian grid, as the MP-PIC methods do, allows to get ride of this problem with a loss of precision. Eventually, if the particles' size is comparable to the mesh size, stability issues may appears when their localization brutally changes from one cell to another. In that case, the carrier phase is suddenly expanded, resp compressed, which may crash the computations.

6.2 A new thermodynamic consistent approach

6.2.1 Hybrid description of particles

In the exploratory work presented here, we propose a continuous model for the fluid and a Lagrangian tracking of the particles by the mean of *numerical* particles as in many other (LE) methods. A numerical particle is a numerical entity which embodies a group of physical particles. This numerical particle is tracked along the domain of computation and will move within the fluid. One specific property of our particles is that there is no sharp interface between them and the carrier phase. It means that one particle is likely to coexist with the carrier phase and/or other particles similarly to diffuse interface methods (see figure 6.1).

All the physical particles included in the same numerical particle are supposed to have the same velocity (the velocity of the center of the particle). One consequence of this is that the transport equation is reduced to an ordinary equation linking the mass center of the numerical particle to its velocity. The spreading of the physical particles around the mass center is prescribed with an analytic function. This reminds the kernel used in the smooth hydrodynamic particle (SPH) method (Lucy, 1977; Gingold & Monaghan, 1977; Monaghan, 1988)). However, our method differs from SPH because particles are not moving interpolation points of continuous fields but numerical entities whose trajectory is computed with different equations than the traditional Euler system.

The particles interact due to their coexistence in the same point. Each of them contributes to the pressure in this point which in return will act on their velocity. Therefore, this method is more similar to a continuous model with a geometric transport (the position of the elements depends uniquely of the center of the particle) than an SPH like approach where the particles are the degrees of freedom of an interpolation.

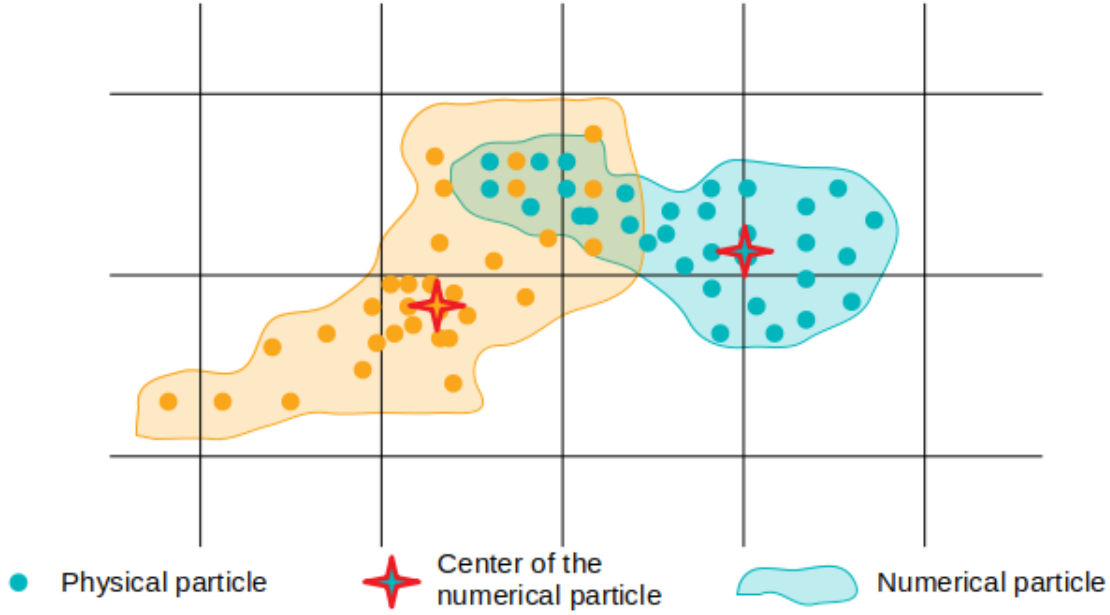


Figure 6.1: Numerical Particle

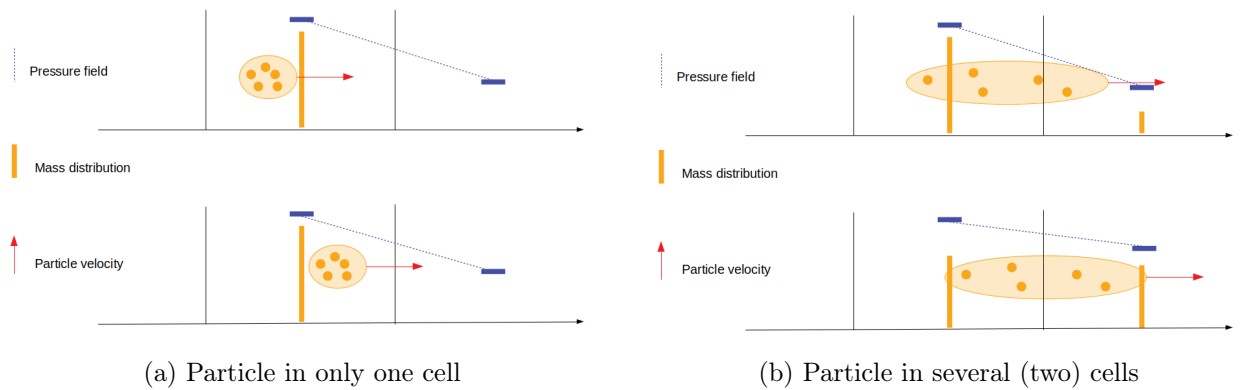
Continuous and discrete description The method we propose attributes the following properties to each numerical particle: a position, a velocity, a spreading, an internal energy, and a density (or specific volume) field. The pressure is more specific because it will be computed at each point (or in each cell after full discretization) in order to satisfy a local equilibrium. A continuous quantity a denoted $a_p(x, t)$ means the value of the field a associated to the particle p at (x, t) . A discrete quantity a denoted a_{pc}^n means the value of the quantity a at time t^n of the particle p in the cell c . It is stressed again that the particles are spread over several cells after full discretization.

field	position	velocity	distribution	internal energy	specific volume	pressure
continuous	$x_p(t)$	$u_p(t)$	$f_{m_p}(x_p, x, t)$	$e_p(x, t)$	$v_p(x, t)$	$p(x, t)$
discrete	x_p^n	$u_p^{n+1/2}$	$f_{m_{pc}}^n$	e_{pc}^n	v_{pc}^n	p_c^n

Table 6.1: degrees of freedom

It must be stressed that only the distribution function (and the velocity) depends on the position of the particles. The distribution plays the role of the transport of the particles (i.e. it assigns positions to the real particles in function of the mass center position of the numerical particles). The other quantities are thermodynamic ones which depend indirectly on the particles' positions.

On the necessity to distribute a particle In our scheme, a numerical particle is distributed in several cells. This can not be otherwise (only located in one cell) if we want to:



- avoid brutal variations of void fraction
- capture correctly the pressure gradient
- capture the right contribution of each particle to the pressure field

One option that has been discarded is to reconstruct the pressure field by interpolation of its values in the cell. With this choice, it is possible to use the derivative of this reconstruction to compute the pressure gradient applied on a given particle. However, by doing so, if the particle is located in one cell and stays in this cell during a time step, its move is *free* because it does not affect any potential and so the pressure field. Thus, the principle of reciprocity is violated. This is illustrated in the figure (6.2a). The particle distributed in one cell does not affect the pressure gradient during the time step because there is no mass variation (and thus density variation) in the cells where the pressure field is sampled. However, in the two cells distribution case (6.2b), the displacement makes the mass distribution changes and so the pressure gradient. This will be illustrated by using a variational method to derive a consistent numerical scheme. It will give evidence that a distribution of the particles among several cells is necessary to obtain a pressure gradient in the momentum equation of particle. This distribution over several cells also allow to have a smooth change in void fraction during a step time instead of a brutal one each time a particle crosses the boundary of the cell.

6.2.2 Variational approaches in discrete and semi-discrete systems

To find consistent trajectories of our hybrid particles, variational approaches are applied to a semi continuous system. Using these methods to obtain trajectories of material points is very efficient due to the system's complexity. Well known examples are the double pendulum, the multi spring-mass system, etc. Also, variational methods has been notably applied recently to derive a geometric discretization of the Vlasov-Maxwell system with a PIC method (Squire *et al.*, 2012; Kraus *et al.*, 2017). In hydrodynamic field, the LAP has been applied to smooth hydrodynamic particle (SPH) method (Price, 2012) developed by Gingold & Monaghan (1977) and Lucy (1977). Price (2012) uses also the first thermodynamics principle to compute his the equations. Our approach are very similar of those references because we aim to derive consistent trajectories of a discrete system.

6.3 Application of the method on various systems

Several systems has been studied to test the validity of this method. First, we have considered only particles moving in Eulerian grid similarly to the PIC approaches. Then, we have applied our method to a dispersed multiphase flow.

6.3.1 Full particles systems

In this system, we consider that there is no carrier phase and that the particles are compressible. The Lagrangian of the system contains the kinetic and internal energies of all particles. In addition, we constrain them to verify the no void condition.

$$L = \sum_p \frac{1}{2} m_p (u_p)^2 - \int_{\Omega} \left(\sum_p f_{m_p}(x_p) e(v_p) + \Pi \left(\sum_p f_{m_p} v_p - 1 \right) \right) dx \quad (6.2)$$

The derivation of the action with respect to the degrees of freedom x_p , v_p and Π leads to the Euler Lagrange equations

$$\delta x_p : 0 = -m_p \dot{u}_p - \int_{\Omega} \partial_{x_p} f_{m_p} [e_p + \Pi v_p] dx, \quad (6.3a)$$

$$\delta v_p : 0 = p_p - \Pi, \quad (6.3b)$$

$$\delta \Pi : 0 = \sum_p f_{m_p} v_p - 1. \quad (6.3c)$$

The momentum equation is derived from (6.3a and 6.3b)

$$m_p \dot{u}_p = - \int_{\Omega} [e_p + p v_p] \partial_{x_p} f_{m_p} dx \quad (6.4)$$

with $p = p_p$ the common pressure of each particles through (6.3b). This equation seems to inconsistent with the Euler equation where a pressure gradient appears. Here, the flux is formed by the enthalpy $H = E + pV$. However, it possible to show its consistency by using the thermodynamic relation between enthalpy and internal energy.

$$DH = DE + D(Vp) = -pDV + pDV + VDp = VDp. \quad (6.5)$$

The equation (6.4) is not conservative but can be restated using a property of the distribution function. The distribution function of the particle p has been written until now as function of x and x_p . However, to be relevant, the distribution must be homogeneous and decreases around x_p . Thus, the distribution is a function of the parameter $x_p - x$. Therefore, the derivative of f_{m_p} verifies $\partial_{x_p} f_{m_p} = -\partial_x f_{m_p}$. The ensuing developments made in annex (6.A.1) lead to the total momentum equation:

$$\sum_p m_p \dot{u}_p = \sum_p \int_{\Omega} \partial_x (f_{m_p} e_p) dx. \quad (6.6)$$

The total momentum flux is not formed by pressure but by the internal energy of all particles.

Particles are coupled through the volume filling condition and its dual relation over the pressure (6.3b). The internal energy reservoirs are then coupled together. To explicit this system, we use the same procedure developed by *Vazquez-Gonzalez et al. (2020)* and extended in (4). First, the thermodynamic identities over the pressure are formulated as

$$\partial_t(p) = -\gamma_p p \frac{\partial_t v_p}{v_p} = -p \frac{f_{m_p}}{\eta_p} \partial_t v_p \quad (6.7)$$

By summation and identifying total volume with the volume filling condition,

$$\partial_t(p) \sum_p \eta_p = p \sum_p v_p \partial_t(f_{m_p}) = p \sum_p v_p u_p \partial_{x_p}(f_{m_p}) \quad (6.8)$$

With this explicit equation over the common pressure, the specific volume equation may be deduced

$$p f_{m_p} \partial_t v_p = -\beta_p p \sum_q v_q u_q \partial_{x_q}(f_{m_q}) \quad (6.9)$$

with $\eta_p = \frac{f_{m_p} v_p}{\gamma_p}$, $\nu = \sum_p \eta_p$ and $\beta_p = \frac{\eta_p}{\nu}$.

The internal energy equation is then

$$\partial_t(f_{m_p} e_p) = e_p u_p \partial_{x_p}(f_{m_p}) + \beta_p P \sum_q v_q u_q \partial_{x_q}(f_{m_q}). \quad (6.10)$$

Summation over all particles (and using $\sum_q \beta_q = 1$) leads to the opposite term of kinetic energy production and shows the total energy conservation

$$\sum_p \partial_t [f_{m_p} e_p + \frac{1}{2} f_{m_p} u_p^2] = 0 \quad (6.11)$$

Now the internal energy equation (6.10) may be restated to

$$f_{m_p} \partial_t(e_p) = \beta_p p \underbrace{\sum_q v_q u_q \partial_{x_q}(f_{m_q})}_{[dV]}. \quad (6.12)$$

This expression makes makes appear the total volume variation $[dV]$ multiplied by the common pressure and a factor β . This corresponds to the pressure work weighted by the relative compressibility factor potentially stiff (3).

6.3.2 Dispersed multiphase flows

Model with fluid and non compressible particles

In this model, particles are rigid and move inside a compressible carrier phase. The Lagrangian of this system is now made with the kinetic energy of all particles plus the internal

and kinetic energies of the fluid. The volume filling constraint includes the presence of the carrier phase.

$$L = \sum_p \frac{1}{2} m_p u_p^2 + \int_{\Omega} \frac{1}{2} [\alpha \rho] u^2 - [\alpha \rho] e\left(\frac{[\alpha \rho]}{\alpha}, \xi\right) + \Psi d_t(\xi) + \Phi D_t([\alpha \rho]) - \Pi \left(\alpha + \sum_p v_p f_{m_p} - 1\right) dx \quad (6.13)$$

The particles' specific volume v_p is now a constant because they are considered to be rigid. The Euler–Lagrange equation that result from the action are thus:

$$\delta x_p : 0 = -m_p \dot{u}_p - \int_{\Omega} \Pi \partial_{x_p} f_p dx \quad (6.14a)$$

$$\delta \alpha : 0 = \underbrace{\rho^2 e_{,\rho}}_p - \Pi \quad (6.14b)$$

$$0 = : \text{Multi-fluid Euler–Lagrange equations} \quad (6.14c)$$

The other Euler–Lagrange equations are strictly the same than in the multi-continuous approach (4). We obtain then both momentum equations as

$$m_p \dot{u}_p = -v_p \int_{\Omega} p \partial_{x_p} f_{m_p} dx \quad (6.15)$$

$$D_t([\alpha \rho] u_i) = -\alpha p_{,i} \quad (6.16)$$

These equations are compatible with the Euler's system, the fluid experiments a pressure gradient and the particles are accelerated by the integral of the pressure around them. The energy equations are also straightforward to obtain as the particles are not compressible, thus, no coupling occurs between them and the fluid due to volume variations (the particles' transport imposes the variation of the fluid's volume).

$$D_t([\alpha \rho] e) = -p D_t(\alpha) = p [v_p \partial_t(f_{m_p}) - (\alpha u_i)_{,i}] = p [v_p u_p \partial_{x_p}(f_{m_p}) - (\alpha u_i)_{,i}] \quad (6.17)$$

Therefore, the energy equations of the fluid and particles are

$$\begin{aligned} D_t\left(\frac{1}{2}[\alpha \rho] u^2\right) &= -\alpha u_i p_{,i} \\ \frac{1}{2} m_p \dot{u}_p^2 &= -u_p v_p \int_{\Omega} P \partial_{x_p} f_{m_p} dx \\ D_t([\alpha \rho] e) &= -p \underbrace{[(\alpha u_i)_{,i} - u_p v_p \partial_{x_p} f_{m_p}]}_{dV} \end{aligned} \quad (6.18)$$

The energy is well conserved by integration over Ω and the the fluid is compressed according to the total volume change.

6.3.3 Model with fluid and particles both compressible

In this section, particles are no more rigid but compressible. The Lagrangian of the system is then complemented with the internal energies of the particles.

$$L = \sum_p \left(\frac{1}{2} m_p u_p^2 - \int_{\Omega} f_{m_p} e_p(v_p) dx \right) + \int_{\Omega} \frac{1}{2} [\alpha \rho] u^2 - [\alpha \rho] e\left(\frac{[\alpha \rho]}{\alpha}, \xi\right) + \Psi d_t(\xi) + \Phi D_t([\alpha \rho]) - \Pi(\alpha + \sum_p v_p f_{m_p} - 1) dx \quad (6.19)$$

The Euler Lagrange equations of this system are

$$\delta x_p : 0 = -m_p \dot{u}_p - \int_{\Omega} \partial_{x_p} f_{m_p} [e_p + \Pi v_p] dx \quad (6.20a)$$

$$\delta v_p : 0 = p_p - \Pi \quad (6.20b)$$

$$\delta \alpha : 0 = p - \Pi \quad (6.20c)$$

$$0 = \dot{\quad} : \text{Multi-fluid Euler-Lagrange equations} \quad (6.20d)$$

The Euler-Lagrange equations with only fluid's terms are still the same as in multi-continuous, thus the momentum equation will be unchanged. The momentum equation of the particles is also exactly the same as in the subsection 6.3.2. The LAP imposes also an instantaneous relaxation to the pressure of the particles and the fluid.

$$m_p \dot{u}_p = - \int_{\Omega} \partial_{x_p} (f_{m_p}) [e_p + p v_p] dx \quad (6.21)$$

$$D_t([\alpha \rho] u_i) = -\alpha p_{,i}$$

The conservation is not obvious yet, however, it is obtained by the same arguments developed in the subsection (6.3.1). It is demonstrated in annex (6.A.1) and yields

$$\sum_p m_p \dot{u}_p + \int_{\Omega} D_t([\alpha \rho] u) dx = - \int_{\partial \Omega} \sum_p f_{m_p} [e_p + p v_p] DS - \int_{\Omega} \partial_x(p) dx \quad (6.22)$$

Here, the energy equations are more complex to derive because the particles are compressible. However, the procedure developed in (Vazquez-Gonzalez *et al.* (2020)) can still be applied to recover the explicit equations because the pressure relaxation is instantaneous. After long but straightforward computations detailed in appendix (6.A.1), the internal energy equations yield

$$\partial_t(f_{m_p} e_p) = - \mu_p u_i p_{,i} - \beta_p P(\alpha u_i)_{,i} + \beta_p \sum_q u_q v_q p \partial_{x_q} (f_{m_q}) + u_p e_p \partial_{x_p} (f_{m_p}), \quad (6.23)$$

$$D_t([\alpha \rho] e) = + \sum_p \mu_p u_i p_{,i} - \beta P(\alpha u_i)_{,i} + \beta \sum_q u_q v_q p \partial_{x_q} (f_{m_q}). \quad (6.24)$$

with $\eta_p = \frac{f_{m_p} v_p}{\gamma_p}$, $\eta = \frac{\alpha}{\gamma}$, $\nu = \sum_p \eta_p + \eta$, $\beta = \eta/\nu$, $\beta_p = \eta_p/\nu$, $\mu_p = \eta \eta_p/\nu$.

Combined with the kinetic equations, the total energy is shown to be conserved

$$\int_{\Omega} D_t([\alpha\rho](\frac{1}{2}u_i^2 + e) + \sum_p \partial_t(\frac{1}{2}m_p u_p^2) = - \int_{\Omega} (\alpha u_i p)_{,i} dx. \quad (6.25)$$

6.4 Consistent numerical schemes

6.4.1 System with only compressible particles

The system is constituted with a collection of compressible hybrid particles that spread over fixed Eulerian cells. The discrete action is obtained by the following integration over time and space of the continuous one

$$A = \sum_n \left[\sum_p \left(\Delta t^{n+1/2} \frac{1}{2} m_p (u_p^{n+1/2})^2 - \Delta t^n \sum_c f_{m_{pc}}^n e_p(v_{pc}^n) \right) - \sum_c \Pi_c \left(\sum_p f_{m_{pc}}^n v_{pc} - V_c^n \right) \right]. \quad (6.26)$$

The derivation of the action leads to the discrete Euler–Lagrange relations.

$$\delta x_p : 0 = - m_p (u_p^{n+1/2} - u_p^{n-1/2}) - \Delta t^n \sum_c \frac{\partial f_{m_{pc}}^n}{\partial x_p} (e_{pc} + v_{pc}^n \Pi_c), \quad (6.27)$$

$$\delta v_{cp}^n : 0 = - \Delta t^n f_{m_{pc}}^n e'_{pc} - \Delta t^n m_{pc} \Pi_c. \quad (6.28)$$

The equation (6.28) shows the pressure equality between particles inside a cell. Thus, there is only one pressure per cell. The particles momentum equation yield

$$m_p (u_p^{n+1/2} - u_p^{n-1/2}) = - \Delta t^n \sum_c \frac{\partial f_{m_{pc}}^n}{\partial x_p} (e_{pc} + v_{pc}^n p_c^n). \quad (6.29)$$

This equation is not conservative. There is no reason that the sum of the enthalpies multiplied by the derivative of the mass cancels. To understand where does this fail comes, the Noether theorem is applied. It must be stressed that the distribution function depends on the particles' position and the cells' positions. Therefore, it yields: $f_{m_{pc}}^n = f_{m_{pc}}^n(x_p, x_c)$. The derivation of the Lagrangian with respect to space leads to:

$$\begin{aligned} L(x + dx) - L(x) &= dx \sum_p \sum_c \frac{\partial f_{m_{pc}}^n}{x_c} (v_{pc} \Pi + e_{pc}) \\ &= dx \sum_p \sum_c \frac{\partial f_{m_{pc}}^n}{\partial x_c} (v_{pc} p_c + e_{pc}) \end{aligned}$$

However, the function $f_{m_{pc}}^n$ is a function of the distance between x_p and x_c , therefore, we may restate this variation into

$$L(x + dx) - L(x) = - dx \sum_p \sum_c \frac{\partial f_{m_{pc}}^n}{\partial x_p} (v_{pc} p_c + e_{pc}) \quad (6.30)$$

which shows that the total momentum quantity is the translation of the Lagrangian. Therefore, the momentum conservation cannot be guaranteed when using fixed mesh because the Lagrangian is not space invariant. However, conservations are essentials to our schemes, therefore, this approach has not been explored further.

6.4.2 System with fluid and non compressible particles

In (6.4.1), it has been shown that an Eulerian mesh cannot not preserve the total momentum as it stands. Thus, the fluid is described now in a Lagrangian frame. The discrete action is built by the following approximation of the integral over space and time.

$$A = \sum_n \left[\sum_p \Delta t^{n+1/2} \frac{1}{2} m_p (u_p^{n+1/2})^2 + \sum_q \Delta t^{n+1/2} \frac{1}{2} m_q^n (u_q^{n+1/2})^2 - \sum_c \Delta t^n m_c e_c \left(\frac{V_c^n - \sum_p f_{v_{pc}}^n}{m_c} \right) \right] \quad (6.31)$$

There is no volume filling constraint in the Lagrangian because it is possible to express directly the fluid's density inside the cell thanks to the volume left by the particles and the mass of the cell.

The derivation of the action with respect to the particles and nodes' positions leads to the Euler–Lagrange equations.

$$\delta x_p : 0 = -m_p (u_p^{n+1/2} - u_p^{n-1/2}) - \Delta t^n \sum_c v_p \frac{\partial f_{m_{pc}}^n}{\partial x_p} p_c^n \quad (6.32)$$

$$\delta x_q : 0 = -m_q (u_q^{n+1/2} - u_q^{n-1/2}) - \Delta t^n \sum_{c,p} v_p \frac{\partial f_{m_{pc}}^n}{\partial x_q} p_c^n + \Delta t^n \sum_c \frac{\partial V_c^n}{\partial x_q} p_c^n \quad (6.33)$$

The ensuing momentum equations are compared to the continuous ones.

$$m_p \dot{u}_p = - \int_{\Omega} p \partial_{x_p} f_p dx \rightarrow m_p \frac{u_p^{n+1/2} - u_p^{n-1/2}}{\Delta t^n} = - \sum_c p_c^n v_p \partial_{x_p} f_{m_{pc}}^n \quad (6.34)$$

$$D_t([\alpha \rho] u_i) = -\alpha p_{,i} \rightarrow m_q \frac{u_q^{n+1/2} - u_q^{n-1/2}}{\Delta t^n} = \sum_c p_c^n \left[\partial_{x_q} V_c^n - \sum_p v_p \partial_{x_q} f_{m_{pc}}^n \right] \quad (6.35)$$

The momentum equation of particles is consistent with its continuous version. However, it is not obvious for the fluid because its description is Lagrangian. However, the volume filling conditions still applies.

$$V_c^n - \sum_p v_p f_{m_{pc}}^n = V_c^n \alpha_c^n \quad (6.36)$$

Then, the node's momentum equation may be restated as

$$m_q \frac{u_q^{n+1/2} - u_q^{n-1/2}}{\Delta t^n} = \sum_c p_c^n \partial_{x_q} (\alpha_c^n V_c^n) \quad (6.37)$$

This is similar to the CSTS scheme developed by Llor *et al.* (2016) with a modified corner vector

$$\partial_{x_q} V_c^n \rightarrow \partial_{x_q} V_c^n - \sum_p v_p \partial_{x_q} f_{m_{pc}}^n. \quad (6.38)$$

The cells' volume and the distribution function must be invariant by translation through space to guarantee the momentum's conservation. This condition leads to the following identities

$$\partial_{x_p} f_{v_{pc}}^n + \sum_q \partial_{x_q} f_{v_{pc}}^n = 0, \quad (6.39a)$$

$$\sum_q \partial_{x_q} V_c^n = 0. \quad (6.39b)$$

This is brought out by the total momentum equation

$$\begin{aligned} \sum_p m_p (u_p^{n+1/2} - u_p^{n-1/2}) + \sum_q m_q (u_q^{n+1/2} - u_q^{n-1/2}) \\ = \sum_c p_c^n \left[\sum_q \partial_{x_q} V_c^n - \sum_p (\partial_{x_p} f_{v_{pc}}^n + \sum_q \partial_{x_q} f_{v_{pc}}^n) \right]. \end{aligned} \quad (6.40)$$

The internal energy equation of the fluid is deduced directly from the Gibbs equation because particles are not compressible. Therefore, there is no coupling through pressure.

$$\begin{aligned} [\alpha \rho] d_t(e) &= \alpha p \frac{d_t \rho}{\rho} \\ &\Leftrightarrow \\ m_c (e_c^{n+1} - e_c^n) &= -p_c^n \underbrace{\left[u_q^{n+1/2} \sum_q \partial_{x_q} V_c^n - u_p^{n+1/2} \left(\sum_p \partial_{x_p} f_{v_{pc}}^n + \sum_q \partial_{x_q} f_{v_{pc}}^n \right) \right]}_{\approx D_t(\alpha_c^n V_c^n)} \end{aligned} \quad (6.41)$$

To insure the energy conservation, velocity terms in the expression (6.41) are modified. The final internal energy equation is then

$$\begin{aligned} m_c (e_c^{n+1} - e_c^n) &= -p_c^n \left[\frac{1}{2} (u_q^{n+1/2} + u_q^{n-1/2}) \left(\sum_q \partial_{x_q} V_c^n - \sum_{p,q} \partial_{x_q} f_{v_{pc}}^n \right) \right. \\ &\quad \left. - \frac{1}{2} (u_p^{n+1/2} + u_p^{n-1/2}) \sum_p \partial_{x_p} f_{v_{pc}}^n \right]. \end{aligned} \quad (6.42)$$

The fluid's density is simply determined with the knowledge of the cell's volume and its mass.

$$\rho_c^{n+1} = \frac{m_c}{V_c^{n+1} - \sum_p f_{v_{pc}}^{n+1}} \quad (6.43)$$

The pressure is computed with the fluid EOS.

6.4.3 System with fluid and compressible particles

Because particles are compressible, their discrete internal energy is added in the discrete action.

$$A = \sum_n \left[\sum_p \left(\Delta t^{n+1/2} \frac{1}{2} m_p (u_p^{n+1/2})^2 - \Delta t^n \sum_c f_{m_{pc}}^n e_p(v_{pc}^n) \right) + \sum_q \Delta t^{n+1/2} \frac{1}{2} m_q^n (u_q^{n+1/2})^2 - \sum_c \Delta t^n m_c e_c \left(\frac{V_c^n - \sum_p f_{m_{pc}}^n v_{pc}^n}{m_c} \right) \right] \quad (6.44)$$

The ensuing Euler–Lagrange equations are

$$\delta x_p : 0 = -m_p (u_p^{n+1/2} - u_p^{n-1/2}) - \Delta t^n \sum_c \frac{\partial f_{m_{pc}}^n}{\partial x_p} (e_{pc} - v_{pc}^n e'_c), \quad (6.45a)$$

$$\delta x_q : 0 = -m_q (u_q^{n+1/2} - u_q^{n-1/2}) - \Delta t^n \sum_{c,p} \frac{\partial f_{m_{pc}}^n}{\partial x_q} (e_{pc} - v_{pc}^n e'_c) - \Delta t^n \sum_c \frac{\partial V_c^n}{\partial x_q} e'_c, \quad (6.45b)$$

$$\delta v_{cp}^n : 0 = -\Delta t^n f_{m_{pc}}^n e'_{pc} + \Delta t^n f_{m_{pc}}^n e'_c. \quad (6.45c)$$

The equation (6.45c) shows again the pressure equality between the fluid and the particles. The momentum equations of nodes and particles yield

$$m_p (u_p^{n+1/2} - u_p^{n-1/2}) = -\Delta t^n \sum_c \frac{\partial f_{m_{pc}}^n}{\partial x_p} (e_{pc} + v_{pc}^n p_c^n) \quad (6.46a)$$

$$m_q (u_q^{n+1/2} - u_q^{n-1/2}) = \Delta t^n \sum_c \frac{\partial V_c^n}{\partial x_q} p_c^n - \Delta t^n \sum_{p,c} \frac{\partial f_{m_{pc}}^n}{\partial x_q} (e_{pc} + v_{pc}^n p_c^n) \quad (6.46b)$$

Manipulations of these momentum equation and the relations (6.39) bring out the total momentum preservation (6.A.2) .

Internal energy equations are deduced with the same procedure as the multi-fluid Eulerian system. The following equations take into account eventual dissipations. Computation details are provided in (6.A.1) The internal energy equations yield

$$m_{pc}^{n+1} e_{pc}^{n+1} - m_{pc}^n e_{pc}^n = - \underbrace{\Delta t^n \beta_{pc}^n p_c^n d_t \tilde{V}_{fc}^n}_{(1)} + \underbrace{\Delta t^n \langle \nabla f_{m_{pc}}^n \cdot u \rangle e_{pc}^n}_{(2)} + \underbrace{\sum_{\varphi} \mu_{\varphi p}^n (f_{m_{pc}}^n \Gamma_p^n W_p^n - m_{\varphi}^n \Gamma_{\varphi}^n W_{\varphi}^n)}_{(3)} + \underbrace{W_{pc}^n}_{(4)} \quad (6.47a)$$

$$m_c (e_c^{n+1} - e_c^n) = -\Delta t^n \beta_c^n p_c^n d_t \tilde{V}_{fc}^n + \sum_{\varphi} \mu_{\varphi c}^n (m_c \Gamma_c^n W_c^n - m_{\varphi}^n \Gamma_{\varphi}^n W_{\varphi}^n) + W_c^n \quad (6.47b)$$

with

$$\begin{aligned} \langle \nabla f_{m_{pc}}^n \cdot u \rangle &= \partial_{x_p} f_{m_{pc}}^n \frac{1}{2} (u_p^{n+1/2} + u_p^{n-1/2}) + \sum_q \partial_{x_q} f_{m_{pc}}^n \frac{1}{2} (u_q^{n+1/2} + u_q^{n-1/2}), \\ d_t \tilde{V}_c^n &= \frac{1}{2} \sum_q \frac{\partial V_c^n}{\partial x_q} (u_q^{n+1/2} + u_q^{n-1/2}) \\ &\quad - \frac{1}{2} \sum_p v_{pc}^{n+1} \left[\left(\frac{\partial f_{m_{pc}}^n}{\partial x_p} (u_p^{n+1/2} + u_p^{n-1/2}) + \sum_q \frac{\partial f_{m_{pc}}^n}{\partial x_q} (u_q^{n+1/2} + u_q^{n-1/2}) \right) \right] \end{aligned}$$

and $\nu = \sum_p \frac{f_{m_{pc}}^n v_{pc}^n}{\gamma_{pc}^n} + \frac{m_c v_c^n}{\gamma_c^n}$, $\beta_{pc}^n = \frac{f_{m_{pc}}^n v_{pc}^n}{\gamma_{pc}^n \nu}$, $\beta_c^n = \frac{m_c v_c^n}{\gamma_c^n \nu}$, $\mu_{\varphi c}^n = \beta_{\varphi c}^n \frac{m_c v_c^n}{\gamma_c^n}$.
The meaning of the constituting terms are

- (1) distribution of pressure work to the part of the particle p spread to the cell c .
- (2) transport of the internal energy
- (3) dissipation exchange
- (4) dissipation

(2) is called a transport term but corresponds to variation of internal energy in the cell due to the mass variation

$$e_p d_t (f_{m_p}) \approx e_{pc}^n (f_{m_{pc}}^{n+1} - f_{m_{pc}}^n) = \Delta t^n \langle \nabla f_{m_{pc}}^n \cdot u \rangle e_{pc}^n \quad (6.48)$$

Indeed, the real transport should be

$$- \sum_d \delta m_{cd} e_{pc}^n + \sum_d \delta m_{cd} e_{pd}^n \quad (6.49)$$

with δm_{cd} the transfer of mass from the distribution d to the distribution c . These mass transfers can be obtained by analysis of all mass variation in the cell where the particle spread. However, they will not match the form (2) at the order of the scheme. In fact, the deviation to the real transport may be huge in a shock where neighboring energies are very different.

Pressure relaxation Pressure relaxation is achieved with algebraic solver. The system to be solved is composed by the pressure equality, the state equations of each particle and the fluid and the no void constraint. Assuming that both phases obey to stiffened gas EOS and that particles share the same reference pressure, the pressure is solution of a second order polynomial. The EOS for the particles is

$$\begin{aligned} p_c^{n+1} &= \Gamma_p e_{pc}^{n+1} / v_{pc}^{n+1} - \pi_p \\ \frac{f_{m_{pc}}^{n+1} v_{pc}^{n+1}}{V_c^{n+1}} &= \frac{\Gamma_p f_{m_{pc}}^{n+1} e_{pc}^{n+1}}{V_c^{n+1} (p_c^{n+1} + \pi_p)} \end{aligned} \quad (6.50)$$

The EOS for the fluid is then

$$\begin{aligned} p_c^{n+1} &= \Gamma \rho_c^{n+1} e_c^{n+1} - \pi. \\ \alpha_c^{n+1} &= \frac{\Gamma [\alpha \rho]_c^{n+1} e_c^{n+1}}{p_c^{n+1} + \pi}. \end{aligned} \quad (6.51)$$

By summation,

$$1 = \frac{a_1}{p + \pi_1} + \frac{a_2}{p + \pi_2} \quad (6.52)$$

This is a second degree polynomial in p_c^{n+1} from which the solutions are known.

6.5 Precisions on the numerical schemes

6.5.1 On the particle spreading

The derivation of the evolution equations for the discrete systems are made in the previous parts. In these equations, the spreading of the particles among cells is written formally. One definition of the distribution that respect the relations (6.39) is proposed here. In addition to this preservation, physical consistency demands to preserve uniform acceleration in a uniform pressure gradient. One possibility is the barycentric coordinates, i.e. the spreading of the particle p on the cell c is equal to ξ_{pc} with ξ_{pc} the barycentric coordinate of the particles in with respect to the center of the cells c . If the number of spreading cells is higher than the number of dimensions plus one, there is an infinity of possible barycentric coordinates.

Let the pressure fields be

$$p_c^n = p_o^n - \nabla p \cdot (x_o - x_c). \quad (6.53)$$

The force applied on a given particle p is therefore

$$-p_o^n (x_o - x_p) \cdot \sum_c \partial_x \xi_{pc}^n + \sum_c \partial_x \xi_{pc}^n \nabla p \cdot (x_p - x_c). \quad (6.54)$$

The first form canceled because the spreading weights sum to unity. With the linearity of the derivation, the second form yields

$$\begin{aligned} & \partial_x \left[\sum_c \xi_{pc}^n \nabla p \cdot (x_p - x_c) \right] - \sum_c \xi_{pc}^n I \cdot \nabla p \\ &= \partial_x \left[\underbrace{\nabla p \cdot \sum_c \xi_{pc}^n (x_p - x_c)}_{=0} \right] - \underbrace{\sum_c \xi_{pc}^n I \cdot \nabla p}_{=1} \end{aligned} \quad (6.55)$$

Therefore, for any particles, the pressure gradient is $-\nabla p$.

Numerical simulations are presented in (6.3) to shows the impact of this choice.

It is clear that only the barycentric spreading preserves the respective position of the particles. Therefore, all the particles experiment well the same pressure gradient.

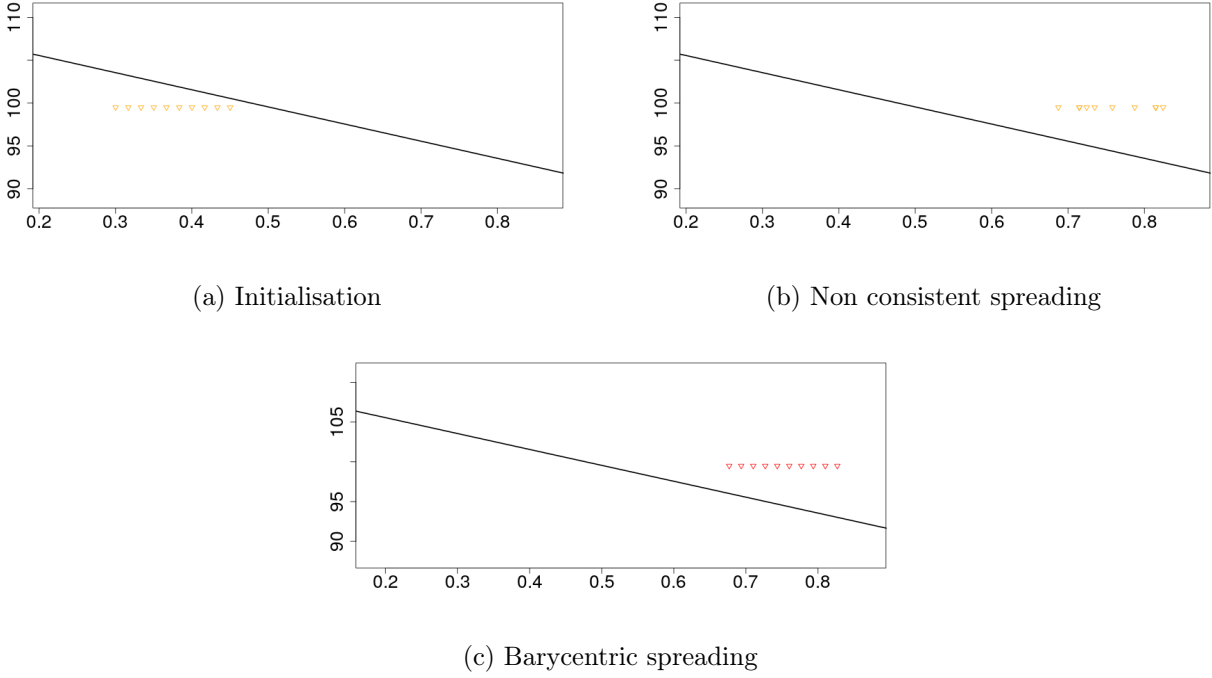


Figure 6.3: Comparison between two spreadings in uniform pressure gradient

6.5.2 On the transport equation

In the particle's description developed, the mass is entirely known by the position of the center of gravity of the particle. Thus, the transport is purely geometric. However, it is possible to mimic the transport equation to compare with a finite volume scheme (with an Eulerian mesh). The transport equation of the fluid in GEEC is:

$$m_c^{n+1} - m_c^n = \sum_d V_{dc}^n [\alpha \rho]_d^n - \sum_d V_{cd}^n [\alpha \rho]_c^n \quad (6.56)$$

$$= \Delta t^n \sum_d \frac{S_{dc}}{V_d} \cdot u_d^n \sigma_{dc} m_d^n - \Delta t^n \sum_d \frac{S_{cd}}{V_c} \cdot u_c^n \sigma_{cd} m_c^n. \quad (6.57)$$

With a mass distribution, the pseudo transport of particles yields

$$m_{pc}^{n+1} - m_{pc}^n = m_p [f_{m_{pc}}^{n+1} - f_{m_{pc}}^n] \quad (6.58)$$

$$= m_p \sum_i \frac{(\Delta x_p^n)^i}{i!} f_{m_{pc}}^{(i)}(x_p^n). \quad (6.59)$$

at the order (1), this restated as

$$m_{pc}^{n+1} - m_{pc}^n = m_p \Delta x_p^n \frac{\partial f_{m_{pc}}}{\partial x}(x_p^n) \quad (6.60)$$

$$= \Delta t^n u_p^n m_p \frac{\partial f_{m_{pc}}}{\partial x}(x_p^n) \quad (6.61)$$

With constant velocity, the two scheme correspond if the function $f_{m_{pc}}$ satisfies

$$\frac{\partial f_{m_{pc}}}{\partial x}(x_p^n) = \sum_d \frac{s_{dc}}{V_d} \sigma_{dc} f_{pd} - f_{pc} \sum_d \frac{s_{cd}}{V_c} \sigma_{cd}$$

This is a system of coupled equations

$$\partial_x F_p = \begin{pmatrix} -\sum_d \frac{s_{0d}}{V_0} \sigma_{0d} & \frac{s_{10}}{V_1} \sigma_{10} & \dots & \frac{s_{n0}}{V_n} \sigma_{n0} \\ \frac{s_{01}}{V_0} \sigma_{01} & -\sum_d \frac{s_{1d}}{V_1} \sigma_{1d} & \dots & \frac{s_{n1}}{V_n} \sigma_{n1} \\ \vdots & & \ddots & \vdots \end{pmatrix} F_p \quad (6.62)$$

This could be solvable for a constant sign of the velocity, otherwise the coefficient σ varies with u_p which lead to the introduction of a temporal derivative in the equation. Therefore, the choice of the transport in GEEC is a complex function of distribution which is probably non analytical.

6.5.3 Dissipation forms

Because these schemes are unstable in shocks, necessary dissipation must be added to carry on the computations. The dissipative forms added are introduced in a similar way that [Marboeuf \(2018\)](#)[chap 4] did. They consist on an artificial viscosity term and an anti-drift force. It must be underlined that these added forms should respect the following requirements:

- 1 Effective dissipation, i.e. destruction of kinetic energy into heat.
- 2 Impact the final result as little as possible which requires it to be activated only to dissipate in order to represent physical mechanisms (artificial viscosity) or when cells are nonphysically deformed.

The anti-drift force verifies only partially the requirement [2], [Marboeuf \(2018\)](#) proposed another way to counter non physical deformation modes with inertial filter. However, for simplicity, anti-drift force was implemented in the code.

6.6 Numerical results

6.6.1 Incompressible particles in compressible fluids

This section aims to test the schemes presented previously. No convergence analysis nor comparison with test cases in literature is done. The goal here is just to validate if our approach leads to physically relevant results and to evaluate its robustness. The CFL condition is captured with the fastest fluid's wave speed.

Shock tube test case

This test case is used because the analytical solution without particles is known. Also, it is a standard test case which allows to evaluate particles behavior in shocks and expansion waves. In all case the fluid is a perfect gas with $\Gamma = 2/5$.

First, 1D test cases are presented to focus on particles behavior (in 2D, other numerical issues appears). The fluid initialization is presented in (6.2).

x	pressure	velocity	density
$x \leq 0.5$	130	0.0	2
$x \geq 0.5$	100	0.0	1

Table 6.2: Initialization of the shock tube

Both simulations contains 1000 particles spread over 2 cells. The full domain is discretized with 100 cells. The aim is to verify that particles evolution are consistent with the physics in shock and expansion wave, i.e. that they are correctly accelerated. Therefore, the particles' density is imposed as the mean of fluid density before and after shock/expansion. Thus, particles density is set to 1.04 in shock and 1.88 in expansion¹. The first simulation is made with small particles which involves a volume fraction of 0.001. The second simulation is made with bigger ones which lets only half of the volume to the carrier phase. The end time is 0.03 s.

In the light of the figure (6.4), several points are raised. First, the scheme robustness is strongly reduced when particles' volume fraction increases. Instabilities appear in fluid's pressure which are tempered by artificial viscosity. The particle curtain gets highly dispersed in velocity. Secondly, the particles velocity is distributed around the fluid velocity (and thus without drag term). This means that pressure gradient is captured with some (but not perfect) accuracy.

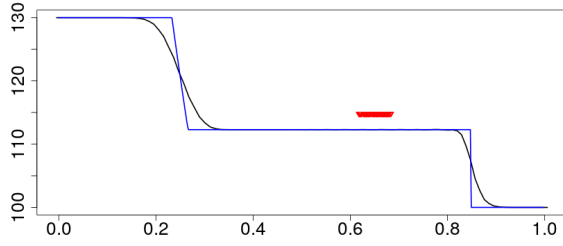
Other numerical experiments that are not shown here reveal that stability increases when particles are heavier.

Particles in expansion wave show good agreement with theoretical results. The velocity is dispersed around the fluid velocity value. Less stability issues are encountered as expected (the expansion profile is smoother than the shock). To conclude, the overall speeding up of particles is consistent which shows a correct capture of pressure gradients. However, stability issues are encountered with high volume fraction.

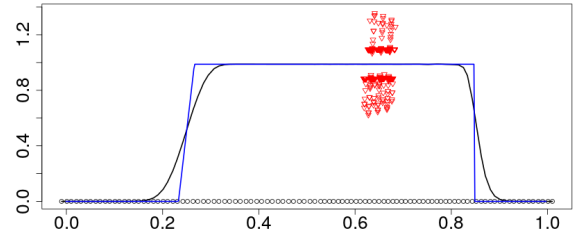
6.6.2 Dispersed curtains

The numerical test case presented in this section is designed to reproduce experiments made by Theofanous *et al.* (2018). The experiments consisted on dispersing a curtain of particles spread within a gas by a shock. The curtain is made of spherical particles whose density

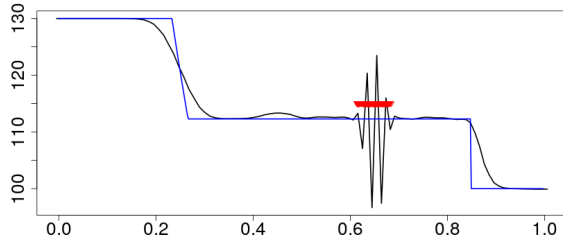
¹This is an approximation: $\int_T \frac{\nabla p(t)}{\rho(t)} dt \approx \frac{2}{\rho_i + \rho_f} \int_T \nabla p(t) dt$



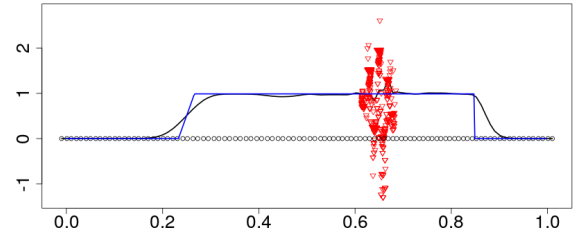
(a) Pressure with low volume fraction of particles



(b) Velocity with low volume fraction of particles

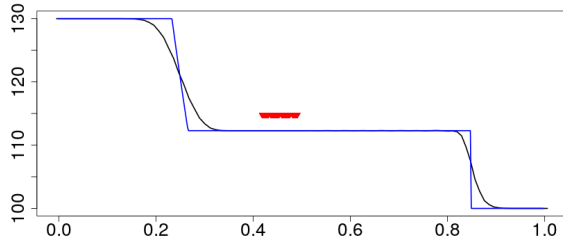


(c) Pressure with high volume fraction of particles

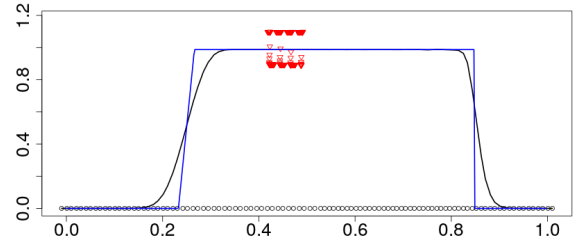


(d) Velocity with high volume fraction of particles

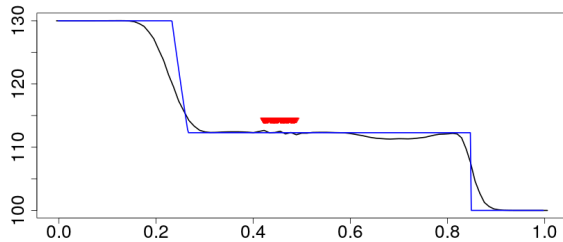
Figure 6.4: Particles under shock



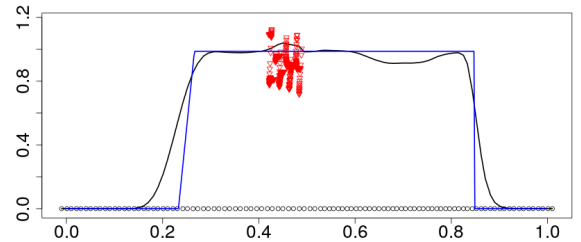
(a) Pressure with low volume fraction of particles



(b) Velocity with low volume fraction of particles

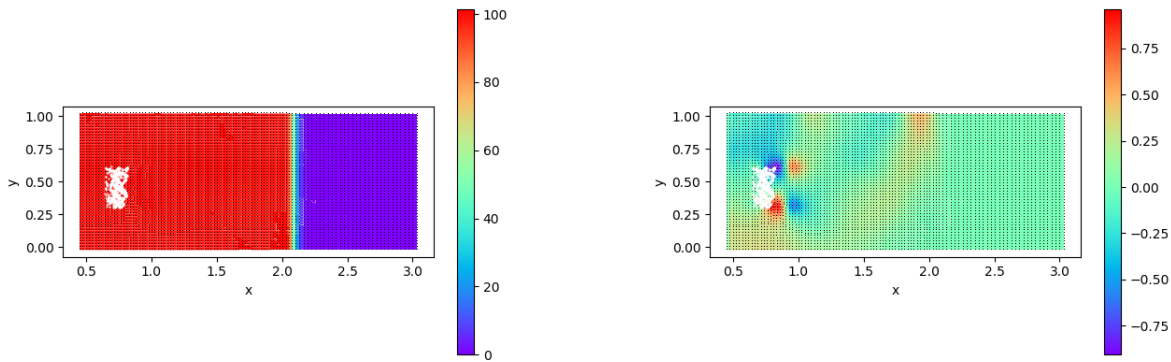


(c) Pressure with high volume fraction of particles



(d) Velocity with high volume fraction of particles

Figure 6.5: Particles in expansion wave



(a) Velocity in X direction, end time

(b) Velocity in Y direction, end time

Figure 6.6: Velocities at final time, particles are the white dots.

is 2.5 g.cm^{-3} . The loaded fraction is about 0.01. Therefore, the gas is slightly modified by the particles loading. However, the forward coupling essentially determines the particles behavior. In our model, the only coupling between both phases is the pressure gradient. But according to [Theofanous *et al.* \(2018\)](#), drag is responsible for the curtain dispersion. A simple drag force has been therefore implemented in the scheme

$$f_{pc} = 0.5 \sum_c v_{pc}^n f_{m_{pc}}^n \rho_c^n (u_c^{n+\frac{1}{2}} - u_p^{n+\frac{1}{2}}) \quad (6.63)$$

with $u_c^{n+\frac{1}{2}}$ the velocity interpolated in the center of the cell with nodes' velocity. No backward drag has been implemented because particles effects on fluid is negligible. The test case consists on a rectangular domain of $1 \times 3 \text{ m}^2$. The right boundary condition is a wall condition and the left one is a piston like boundary condition. The upper resp bottom nodes follow the closest bottom resp upper node. The piston velocity is set to 100 m.s^{-1} and the initial pressure and density for the gas are 1 atm and 1 kg.m^{-3} . 1000 hybrid particles are randomly initialized between $[0.5; 0.6] \times [0.3; 0.6]$. The simulation ends at time 5 ms. The CFL condition is determined by the fastest wave speed of the gas and is set to 0.2. The domain is discretized by 50×100 cells.

From the figures (6.6), the carrier phase is hardly influenced by the dispersed phase. However, the dispersed phase is influenced by the carrier phase as shown in figure (6.7b). The curtain is well dispersed by the shock after 5 ms (the shock hits the curtain at 1 ms). The curtain's width is multiplied by about 1.5 which is comparable to the results obtained by [Theofanous *et al.* \(2018\)](#) for the same Mach number.

6.6.3 Compressible particle in shock and expansion

The simulation presented here aimed to test the behavior of compressible particles inside shocks and rarefaction wave. The goal is to verify that particles described in a discrete

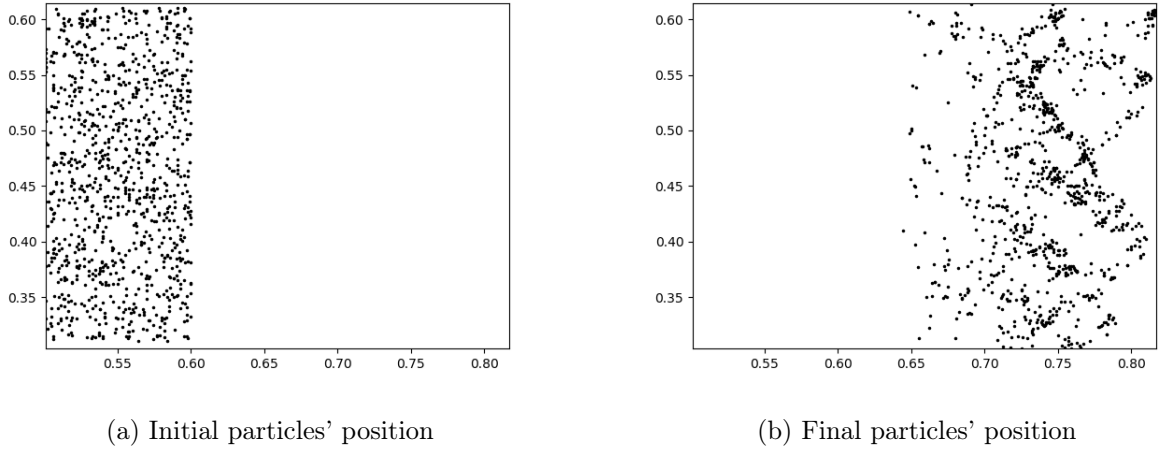


Figure 6.7: Dispersed curtain by a shock

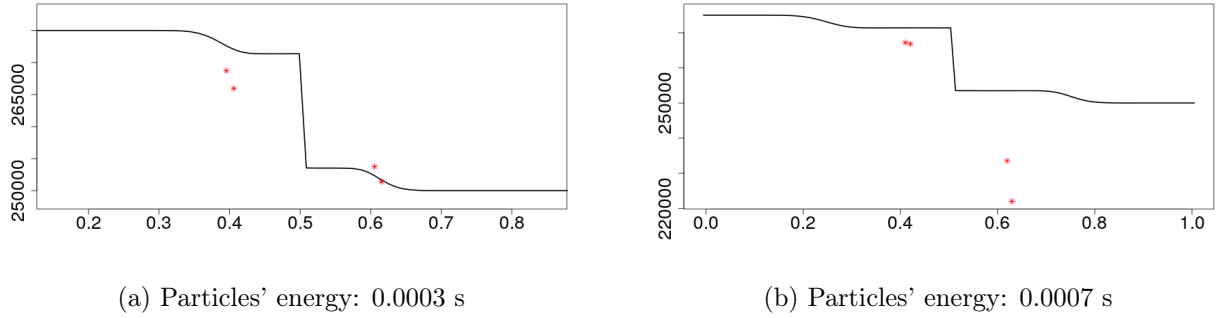


Figure 6.8: Fluid energy is drawn in black line, particle's energies are the red dots. Because it is a 1 D simulation, the particle is distributed in two cells. CFL = 0.5

way reproduce the fluid behavior if they possess the same thermodynamics (EOS, initial density...). We simulate one particle inside a shock tube. The particle and the fluid follow the perfect gas equation. Their initial density is 1. The pressure is set to 1.1×10^5 Pa on the left and 10^5 Pa on the right. The particles' volume are set to 10^{-4} of the cells volume. Computations are made with 100 cells.

The figure (6.8) reveals that the particle does not behave correctly. The internal energies strongly deviate from the fluid one's. This poses two problems: first the density of the particles is wrong, secondly, because internal energy intervenes in the momentum quantity, its gradient involves acceleration and thus the particle's velocity deviates from the fluid. After examination, it is shown that the problems comes from wrong transport approximation. Indeed, the term (2) in the equation (6.47b) stands from transport approximation $m_p^{n+1}c - m_{pc}^n$. However, this transport is badly predicted when particles' drift with respect to the nodes is high. To verify this, we proceed to a simulation where exact transport is prescribed into the internal energy equation.

It is shown in figure (6.9) that this correction allows to find the correct internal energy

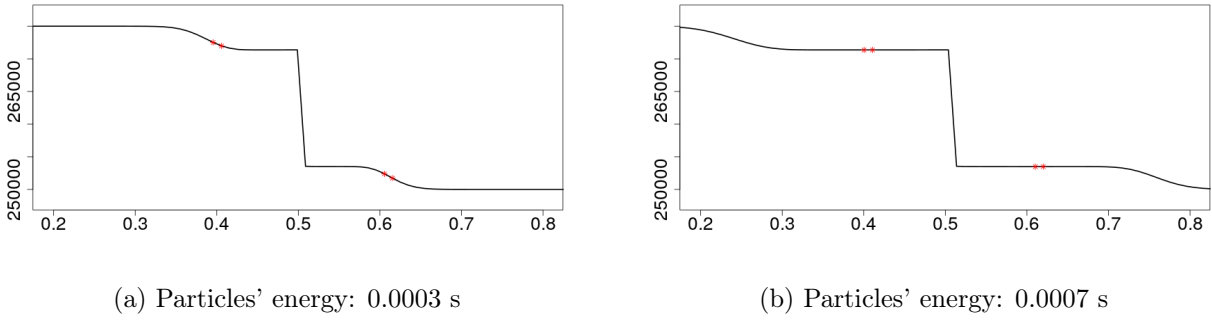


Figure 6.9: Fluid energy is drawn in black line, particles' energy are the red dots. The transport inside internal energy equation of particles has been introduced exactly. CFL = 0.5

evolution. However, this cannot preserve total energy conservation. Now, two options should be explored: i) reduce drastically the CFL in order to recover correct transport approximation, ii) use exact form of the transport.

The last option involves to add a correction in the scheme to preserve the total energy. But it remains to prove that this correction is dissipative.

Also, another problem that must be solved is the prescription of internal energy and specific volume when the particle's support (the cells on which it is distributed) is modified. Indeed, the internal energy in the new distribution is not determined by any equation. Therefore, physical reasoning must be used to distribute the internal energy of the particle into the new cells while conserving it. The specific volume may be then deduced from the EOS of the particle.

6.A Appendix

6.A.1 Continuous

Conservations in the full particles systems

$$\begin{aligned}
 m_p \dot{u}_p &= \int_{\partial\Omega} f_{m_p} [e_p + pv_p] DS - \int_{\Omega} f_{m_p} \underbrace{\partial_x [e_p + pv_p]}_{v_p \partial_x(p)} Dx \\
 \sum_p m_p \dot{u}_p &= \int_{\partial\Omega} \sum_p f_{m_p} [e_p + pv_p] DS - \int_{\Omega} \underbrace{\sum_p f_{m_p} v_p}_{=1} \partial_x(p) Dx \\
 \sum_p m_p \dot{u}_p &= \int_{\partial\Omega} \underbrace{\left(\sum_p f_{m_p} [e_p + pv_p] - p \right)}_{\sum_p f_{m_p} e_p} DS \\
 \sum_p m_p \dot{u}_p &= \sum_p \int_{\Omega} \partial_x (f_{m_p} e_p) Dx
 \end{aligned} \tag{6.64}$$

Full compressible fluid- particle systems

Momentum conservation

$$\begin{aligned}
 m_p \dot{u}_p &= \int_{\partial\Omega} f_{m_p} [e_p + p v_p] DS - \int_{\Omega} f_{m_p} \underbrace{\partial_x [e_p + p v_p]}_{v_p \partial_x(p)} dx \\
 \sum_p m_p \dot{u}_p &= \int_{\partial\Omega} \sum_p f_{m_p} [e_p + p v_p] DS - \int_{\Omega} \underbrace{\sum_p f_{m_p} v_p}_{=1-\alpha} \partial_x(p) dx
 \end{aligned} \tag{6.65}$$

Internal energies equations For each particle and for the fluid, the pressure equation yields

$$\begin{aligned}
 \partial_t(p) &= -\gamma_p p \frac{\partial_t(v_p)}{v_p} \\
 d_t(p) &= \gamma p \frac{d_t(\rho)}{\rho}
 \end{aligned} \tag{6.66}$$

This is restated as

$$\begin{aligned}
 \partial_t(p) \sum_p \eta_p &= -p \underbrace{\sum_p f_{m_p} \partial_t(v_p)}_{\sum_p \partial_t(f_{m_p} v_p) - \sum_p v_p u_p \partial_{x_p} f_{m_p}} \\
 \eta d_t(p) &= -p D_t(\alpha)
 \end{aligned} \tag{6.67}$$

Thanks to the volume filling constraint condition

$$\begin{aligned}
 \partial_t(p) \sum_p \eta_p &= p \partial_t(\alpha) + \sum_p v_p u_p \partial_{x_p} f_{m_p} \\
 \eta d_t(p) &= -p \partial_t(\alpha) - p (\alpha u_i)_{,i}
 \end{aligned} \tag{6.68}$$

with $\eta_p = \frac{f_{m_p} v_p}{\gamma_p}$ and $\eta = \frac{\alpha}{\gamma}$ By summing the equations, we obtain a similar relation as in the subsection (6.3.1),

$$\nu \partial_t(p) = -\eta u_i p_{,i} + \sum_p u_p v_p p \partial_{x_p} f_{m_p} - p (\alpha u_i)_{,i} \tag{6.69}$$

with $\nu = \sum_p \frac{f_{m_p} v_p}{\gamma_p} + \frac{\alpha}{\gamma}$ With this explicit equation on the common pressure, internal energies' dynamic is straightforward to derive.

6.A.2 Discrete

Full compressible fluid- particle systems

Momentum conservation

$$\begin{aligned} \sum_q m_q (u_q^{n+1/2} - u_q^{n-1/2}) + \sum_p m_p (u_p^{n+1/2} - u_p^{n-1/2}) &= \Delta t^n \sum_c \left(\sum_q \frac{\partial V_c^n}{\partial x_q} \right) p_c^n \\ &- \Delta t^n \sum_c \left(\sum_p \left(\frac{\partial f_{m_{pc}}^n}{\partial x_p} + \sum_q \frac{\partial f_{m_{pc}}^n}{\partial x_q} \right) (e_{pc} + v_{pc}^n p_c^n) \right) \end{aligned} \quad (6.70)$$

Internal energies equations For any particle p , the pressure evolution is

$$p_c^{n+1} - p_c^n = -\gamma_{pc}^n \frac{p_c^n}{v_{pc}^n} (v_{pc}^{n+1} - v_{pc}^n) + \Gamma^\phi \frac{W_{pc}^n}{v_{pc}^n} \quad (6.71)$$

and for the fluid

$$p_c^{n+1} - p_c^n = -\gamma_c^n \frac{p_c^n}{v_c^n} (v_c^{n+1} - v_c^n) + \Gamma_c \frac{W_c^n}{v_c^n} \quad (6.72)$$

with

$$v_c^n = \frac{V_c^n - \sum_p f_{m_{pc}}^n v_{pc}^n}{m_c} \quad (6.73)$$

By summing the equations (6.71) and (6.72) after isolating the specific volume difference, we obtain

$$\begin{aligned} \nu (p_c^{n+1} - p_c^n) &= -p_c^n \left[\sum_p (f_{m_{pc}}^n v_{pc}^{n+1} - f_{m_{pc}}^n v_{pc}^n) + (V_c^{n+1} - V_c^n) \right. \\ &\quad \left. - \sum_p (f_{m_{pc}}^{n+1} v_{pc}^{n+1} - f_{m_{pc}}^n v_{pc}^n) \right] + \sum \frac{mv}{\gamma} \Gamma \frac{W}{v} \\ &= -p_c^n \left[-\sum_p v_{pc}^{n+1} (f_{m_{pc}}^{n+1} - f_{m_{pc}}^n) + (V_c^{n+1} - V_c^n) \right] + \sum \frac{mv}{\gamma} \Gamma \frac{W}{v} \\ &= p_c^n \Delta t^{n+1/2} \left[\sum_p v_{pc}^{n+1} \underbrace{\left(\frac{\partial f_{m_{pc}}^n}{\partial x_p} u_p^{n+1/2} + \sum_q \frac{\partial f_{m_{pc}}^n}{\partial x_q} u_q^{n+1/2} \right)}_{\nabla f_{m_{pc}}^n \cdot u} \right. \\ &\quad \left. - p_c^n \Delta t^{n+1/2} \sum_q \frac{\partial V_c^n}{\partial x_q} u_q^{n+1/2} + \sum \frac{mv}{\gamma} \Gamma \frac{W}{v} \right] \\ &= -\Delta t^{n+1/2} p_c^n d_t V_{fc}^n + \sum \frac{mv}{\gamma} \Gamma \frac{W}{v} \end{aligned} \quad (6.74)$$

with $\nu = \sum_p \frac{f_{m_{pc}}^n v_{pc}^n}{\gamma_{pc}^n} + \frac{m_c v_c^n}{\gamma_c^n}$. Here, the total volume divergence is equal to

$$d_t V_c^n = \sum_q \frac{\partial V_c^n}{\partial x_q} u_q^{n+1/2} - \sum_p v_{pc}^{n+1} \left[\left(\frac{\partial f_{m_{pc}}^n}{\partial x_p} u_p^{n+1/2} + \sum_q \frac{\partial f_{m_{pc}}^n}{\partial x_q} u_q^{n+1/2} \right) \right] \quad (6.75)$$

This volume variation is similar to the variation of the volume occupied by the fluid.

$$\begin{aligned}
V_{f_c}^{n+1} - V_{f_c}^n &= \underbrace{V_c^{n+1} - V_c^n}_{\text{variation of the cell volume}} - \underbrace{\sum_p v_{pc}^{n+1} f_{m_{pc}}^{n+1} - \sum_p v_{pc}^n f_{m_{pc}}^n}_{\text{variation of the volume of particles inside the cell}} \\
&= \Delta t^n d_t V_{f_c}^n - \sum_p (v_{pc}^{n+1} - v_{pc}^n) f_{m_{pc}}^n + O((\Delta t^n)^2)
\end{aligned} \tag{6.76}$$

However, there is one form missing which is the variation of specific volume. It means that the term $d_t V_c^n$ contains the variation due to the volume of the cells and the variation of volume of the particle due to their variation of mass but not the variation of volume due to their variation of density at constant mass.

The discrete Gibbs relation yields

$$e_{pc}^{n+1} - e_{pc}^n = -p_c^n (v_c^{n+1} - v_c^n) + W_{pc}^n \tag{6.77}$$

The energy of the component ϕ may be found as

$$m_{\phi c}^{n+1} e_{\phi c}^{n+1} - m_{\phi c}^n e_{\phi c}^n = -p_c^n m_{\phi c}^n (v_{\phi c}^{n+1} - v_{\phi c}^n) + (m_{\phi c}^{n+1} - m_{\phi c}^n) e_{\phi c}^{n+1} \tag{6.78}$$

Internal energy dynamics of a particle p and of the fluid are then

$$\begin{aligned}
f_{m_{pc}}^{n+1} e_{pc}^{n+1} - f_{m_{pc}}^n e_{pc}^n &= -\Delta t^{n+1/2} \beta_{pc}^n D_t V_{f_c}^n + \Delta t^{n+1/2} e_{pc}^{n+1} \nabla f_{m_{pc}}^n \cdot u \\
&\quad + \sum_{\varphi} \mu_{\varphi p}^n (f_{m_{pc}}^n \Gamma_p^n W_p^n - m_{\varphi}^n \Gamma_{\varphi}^n W_{\varphi}^n) + W_{pc}^n
\end{aligned} \tag{6.79}$$

$$\begin{aligned}
m_c e_c^{n+1} - m_c e_c^n &= -\Delta t^{n+1/2} \beta_c^n D_t V_{f_c}^n \\
&\quad + \sum_{\varphi} \mu_{\varphi c}^n (m_c^n \Gamma_c^n W_c^n - m_{\varphi}^n \Gamma_{\varphi}^n W_{\varphi}^n) + W_c^n
\end{aligned} \tag{6.80}$$

The total internal energy evolution without dissipation is obtain by summation

$$\begin{aligned}
\sum_c m_c (e_c^{n+1} - e_c^n) + \sum_p (f_{m_{pc}}^{n+1} e_{pc}^{n+1} - f_{m_{pc}}^n e_{pc}^n) &= \\
&\quad -\Delta t^{n+1/2} \sum_c (p_c^n \sum_q \frac{\partial V_c^n}{\partial x_q} u_q^{n+1/2}) \\
&\quad + \Delta t^{n+1/2} \sum_c \sum_p \nabla f_{m_{pc}}^n \cdot u (v_{pc}^{n+1} p_c^n + e_{pc}^{n+1})
\end{aligned} \tag{6.81}$$

with $\beta_{pc}^n = \frac{f_{m_{pc}}^n v_{pc}^n}{\gamma_{pc}^n \nu}$, $\beta_c^n = \frac{m_c v_c^n}{\gamma_c^n \nu}$, $\mu_{\varphi c}^n = \beta_{\varphi c}^n \frac{m_c v_c^n}{\gamma_c^n}$.

Thus, there is a conservation default if the expressions above are used for energy equations. A modification at the order 2 is sufficient to obtain a correct compensation. The velocities $u_p^{n+1/2}$ and $u_q^{n+1/2}$ are modified to $\frac{1}{2}(u_p^{n+1/2} + u_p^{n-1/2})$ and $\frac{1}{2}(u_q^{n+1/2} + u_q^{n-1/2})$. Furthermore, we obtain the same enthalpy as in the kinetic energy equations by replacing internal energy and specific volume in $n+1$ by their values in n . Eventually, the time step $\Delta t^{n+1/2}$ is modified to Δt^n to preserve total energy.

Conclusion

The challenges of multiphase flow simulation addressed in this thesis are related to three main ideas: the capture of internal couplings, and the concepts of stiffness and entropy. These appear intertwined in various forms along the four chapters of the thesis:

- In chapter 3, a scheme to capture pressure work in *compressible contrasted flows* was built in compliance with the second law *even under fast (stiff) evolutions*. This challenge involved analyses about entropy and stiffness in multiphase flows.
- In chapter 4, the capture of isentropic couplings embedded in the averaged correlation terms coming from multifluid statistical descriptions are separated, analyzed, and consistently modeled. Questions about couplings and entropy are addressed there as well as in chapter 5 where collisions inside dispersed flows are modeled.
- In chapter 6, pressure work consistency is explored again, this time within the Lagrange–Euler framework. The main difficulty is then to properly capture the geometric character of this coupling, involving the concept of entropy.

The problems answered in these four chapters relate to modeling or numerical aspects. Less trivially, they also relate to their behavior in isentropic or dissipative situations: both are compatible with the second principle but the former is much more fragile than the second and requires special attention. As quoted from [Asher & McLachlan \(2005, § I\)](#) isentropy is “living at the edge of stability.” This separation between reversible and irreversible physics is fundamental and is much more general than the specific context of multiphase flows. For instance, it is illustrated in the development of time-stepping algorithms for non-linear

thermodynamic systems that preserve symmetries, energy and the laws of thermodynamics (Romero, 2009, § II). These desirable properties coming from the separate treatment of reversible and irreversible aspects are also illustrated in simulations where Reynolds numbers could be artificially reduced by spurious dissipation (Reiss, 2015, § 1.1). Results and perspectives are reviewed below according to these general lines.

The modeling of isentropic couplings in multiphase flows. In addition to the fundamental coupling by pressure, other couplings exist in multiphase flows hidden in interfacial effects whose description is lost in many formalisms, notably within the Euler–Euler description. A method is proposed in chapter 4 to capture their isentropic part in this framework through a variational approach. A procedure is then developed to obtain the explicit evolution equations of all these new energies, sometimes with corrections resulting from a pressure equality assumption.

This approach is tested in chapter 5 on the modeling of collisions in dispersed flows. The collisions are artificially divided in two types to adapt to the specific Euler–Euler formalism: collisions occurring inside a single phase or between different phases, the former being partly amenable to a variational approach. As a proof of concept, a new model is then developed, implemented, and tested on several numerical simulations showing the versatility and the robustness of the approach. The closure of the potentials does not aim at accurately describing real dispersed flows but rather at providing a founding ground on which building proper adapted models.

The approaches presented here are just proofs of concept and as such they have by no means the capacity to represent real industrial multiphase flows. More work must be added to define rigorously the potentials with careful analysis of the interactions between specific phases in specific systems. For this, closures of energy reservoirs presented in chapter 4 should be improved by DNS or experiments. Also, the closure of agitation potentials in chapter 5 is only provided here as a tool to prove the validity of the approach developed in chapter 4 to design models that can be integrated in a code to simulate multiphase flows. They could be improved for instance by including results from hard-spheres systems (Carnahan & Starling, 1969, etc.).

Dissipative phenomena and spurious dissipation in models. In this thesis, dissipative phenomena in the modeling of multiphase flows may be divided in two types: (i) the dissipation due to physical effects appearing as source terms in momentum equations, in particular here the drag force; (ii) spurious dissipation which is the consequence of the statistical averaging framework. Here, the averaging process of the Euler–Euler formalism leads to non physical dissipation in the capture of the collisions between two phases (see chapter 5). For now, the distribution of this dissipation has been prescribed at their extreme levels (all in the carrier phase as an example).

Improvements should be done in order to avoid spurious dissipation due to the Euler–

Euler formalism in the capture of collisions (for instance with the approach developed in section 5.6). Also, in order to represent real multiphase flows, the distribution of the dissipation must be crafted according to specific studies of the internal mechanisms based on experiments or DNS.

The other main modeling perspective is the consistency between the isentropic and the dissipative physics inside models. Indeed, as pointed out by M. Villedieu in his review of the thesis, the root of the explicit formulation of the energy equations comes from the Euler–Lagrange relations which lock to each other all the phase pressures. This relation, as seen in chapter 4, is used in the algebraic combination involving also the volume filling constraint and the pressures’ evolution to obtain the explicit isentropic evolution equations of energy. From there, the dissipation is simply added as source terms. However, pressure equilibration here appears as a consequence of strictly non-dissipative behavior and may not hold in the presence of dissipation (though it may still be a relevant approximation). A solution to recover the consistency between isentropic and entropic physics inside models could be the use of the virtual work principle.

Numerical capture of reversible physics. A quasi-symplectic discretization of the backbone model has been provided by *Vazquez-Gonzalez et al. (2020)* using a discrete variational approach leading to the GEEC scheme. The supplementary terms added to the backbone model in chapter 5 have been discretized by mimicking this scheme. The GEEC scheme is for now of order one in space, and studies may be conducted to improve it to order two while keeping its variational structure. Notable contributions towards this goal have been made by *Paulin (2021)* and further developments are being investigated.

In this spirit, exploratory works are proposed to capture pressure coupling in the Lagrange–Euler formalism in chapter 6 while keeping its geometric character. This is done by means of an hybrid description of particles introduced inside a discrete variational approach. Within this frame, discrete and almost-geometric evolution equations are obtained. The numerical tests show that the compressible version of the method suffers from serious defects revealed by the nonphysical behavior of particles in shocks and expansions. The method may be corrected but at the price of a loss of energy conservation. This is a challenging project which deserves further investigations and could potentially provide some indepth understanding applicable to other modeling and numerical approaches.

Enforcing the second law in scheme residuals. A particular focus is made on discretization of the coupling via pressure as it appears in all compressible models and connects most of the energy reservoirs. This coupling is known to be potentially extremely stiff when contrasted phases coexist within the flow, but furthermore, as examined in chapter 3, it is “stiffly stiff.” this new concept designates the sudden stiffness variations which may appear during the evolution of a contrasted mixture. A method is proposed to counter the challenging yet inevitable compressibility effects, adaptable to all models and schemes involving

the computation of pressure work. It is here tested first on the most extreme multiphase tests from the literature and then on even more extreme new tests exploring the horizon of multiphase stiffness and showing the potential of the method.

The general approach proposed in chapter 3 involves an implicit pressure in the pressure work discretization. This warrants to comply with the second law of thermodynamics even under stiff evolution. Now, the correspondingly modified GEEC scheme turns out to be identical to the native GEEC scheme (with explicit pressure) to which a linear artificial viscosity would be added. As reminded in chapter 2, the closure and amplitude of artificial viscosity should be defined from the EOS of the phases, notably by the fundamental derivative of the mixture; but, the artificial viscosity added through the implicit pressure is ruled by the pressure evolution and does not involve the fundamental derivative. It remains then to understand what is the link between artificial viscosity and the implicit pressure.

As mentioned previously, implicit pressure warrants compliance with the second law. This strong and convenient safety comes at a significant price that may appear too high: the scheme dissipates at each time step, possibly staying far away (at the order of the scheme) from the isentropic evolution (see for instance the isentropic expansions of Fig. 3.6). It thus appears highly relevant to investigate alternatives between fully explicit schemes (which anti-dissipates at each time step) and fully implicit schemes in order to reduce numerical dissipation while preserving the thermodynamic consistency.

Bibliography

- Aguilar-Corona, A., Zenit, R. & Masbernat, O., *Collisions in a liquid fluidized bed*, International Journal of Multiphase flow, vol. 37: 695 (2011)
- Allaire, G., Clerc, S. & Kokh, S., *A five-equation model for the simulation of interfaces between compressible fluids*, J Comput Phys, vol. 181: 577 (2002)
- Anderson, T. & Jackson, R., *Fluid mechanical description of fluidized beds. Equation of motion*, Industrial & Engineering Chemistry Fundamentals, vol. 6, 4
- Andrews, M. & O'Rourke, P., *The multiphase particle-in-cell (MP-PIC) method for dense particulate flows*, International Journal of Multiphase Flow, vol. 22
- Arnold, G., Drew, D. & Lahey, R., *An assessment of multiphase flow models using the second law of thermodynamics*, International Journal of Multiphase Flow, vol. 16
- Asher, U. & McLachlan, R., *On symplectic and multisymplectic schemes for the KdV equation*, Journal of scientific computing, vol. 25, 1: 83 (2005)
- Baer, M. R. & Nunziato, J. W., *A two-phases mixture theory for the deflagration to detonation transition (ddt) in reactive granular materials*, Int. J. Multiphase Flow, vol. 6
- Balachandar, S., *Turbulent dispersed multiphase flow*, Annual Review of Fluid Mechanics, vol. 42
- Bardenhagen, S., Brackbill, J. & Sulsky, D., *The material-point method for granular materials*, Computer methods in applied mechanics and engineering, vol. 187, 3–4: 529 (2000)
- Barlow, A., Hill, R. & Shashkov, M., *Constrained optimization framework for interface-aware sub-scale dynamics closure model for multimaterial cells in Lagrangian and arbitrary Lagrangian—Eulerian hydrodynamics*, J Comput Phys, vol. 276: 92 (2014)

- Bateman, H., *Notes on a differential equation which occurs in the two-dimensional motion of a compressible fluid and the associated variational problems*, Proceedings of the Royal Society A, vol. 125
- Baumgarten, A., Couchman, B. & Kamrin, K., *A coupled finite volume and material point method for two-phase simulation of liquid–sediment and gas–sediment flows*, Computers Methods in Applied Mechanics and Engineering, vol. 384: 113940 (2021)
- Bdzil, J. B., Menikoff, R., Son, S. F., Kapila, A. K. & Stewart, D. S., *Two-phase modeling of deflagration-to-detonation transition in granular materials: A critical examination of modeling issues*, Phys Fluids, vol. 11: 378 (1999)
- Bedford, A. & Drumheller, S., *A variational theory of immiscible mixtures*, Archive for Rational Mechanics and Analysis, vol. 68
- Benson, D. J., *Computational methods in Lagrangian and Eulerian hydrocodes*, Comput Methods Appl Mech Eng, vol. 99, 2–3: 235 (1992)
- Berdichevsky, V. L., *Variational principles*, Variational Principles of Continuum Mechanics, p. 3–44, Springer (2009)
- Bethe, H. A., *The theory of shock waves for an arbitrary equation of state*, Rap. tech. OSRD-545; NDRC-B-237, National Defense Research Committee of the Office of Scientific Research and Development, [also in Johnson & Chéret (1998, pp. 421–492)] (1942)
- Beylich, A. & Gülhan, A., *On the structure of nonlinear waves in liquids with gas bubbles*, Physics of Fluids, vol. 2: 1412 (1990)
- Bouré, J., *Dynamique des écoulements diphasiques: propagation de petites perturbations*, Rap. tech. CEA-R-4466, Commissariat à l'Énergie Atomique (1973)
- Boussinesq, J., *Essai sur la théorie des eaux courantes*, Mémoires présentés par divers savants à, Mém. Acad. Sci. Inst. Fr., vol. 23: 1 (1877)
- Brennen, C. E., *Fundamentals of multiphase flows*, Cambridge (2005)
- Bretherton, F., *A note on Hamilton's principle for perfect fluids*, Journal of Fluid Mechanics, vol. 44
- Burnett, S. C., Honnell, K. G., Ramsey, S. D. & Singleton, R. L., *Verification studies for the Noh problem using nonideal equations of state and finite strength shocks*, J Verif Valid Uncert, vol. 3: 021002 (2018)
- Burns, A., Frank, T., Hamill, I., Shi, J.-H. *et al.*, *The Favre averaged drag model for turbulent dispersion in Eulerian multi-phase flows*, 5th international conference of multiphase flow, ICMF, vol. 4, p. 1–17, ICMF (2004)

- Burton, D., *Exact conservation of energy and momentum in staggered-grid hydrodynamics with arbitrary connectivity*, Advances in the free-Lagrange method including contribution on adaptative gridding and the smooth particle hydrodynamics method, p. 7–19, Springer (1991)
- Cadzow, J. A., *Discrete calculus of variations*, International Journal of Control, vol. 11, 3: 393 (1970)
- Callen, H. B., *Thermodynamics: an introduction to the physical theories of equilibrium thermostatics and irreversible thermodynamics*, Wiley (1960)
- Callen, H. B., *Thermodynamics and an introduction to thermostatistics*, 2^e éd., Wiley, [1st ed. 1960] (1985)
- Capecelatro, J. & Desjardins, O., *An Euler–Lagrange strategy for simulating particle-laden flows*, Journal of Computational Physics, vol. 238: 1 (2013)
- Carnahan, N. F. & Starling, K. E., *Equation of state for nonattracting rigid spheres*, The Journal of chemical physics, vol. 51, 2: 635 (1969)
- Certaine, J., *The solution of ordinary differential equations with large time constant*, Math. methods for digital computing
- Chang, C. H. & Liou, M. S., *A robust and accurate approach to computing compressible multiphase flow: stratified flow model and AUSM⁺-up scheme*, J Comput Phys, vol. 225, 1: 840 (2007)
- Chang, C. H. & Ramshaw, J. D., *Dynamical evolution of volume fractions in multipressure multiphase flow models*, Phys. Rev. E, vol. 77: 066305 (2008)
- Channell, P. J., *Symplectic integration algorithms*, Los Alamos National Laboratory Internal Report AT-6: ATN-83-9
- Chardin, G., *À propos de : Sur un problème (élémentaire ?) de thermodynamique – 1 Objections*, B Union Phys, vol. 685: 1055 (1986)
- Chassaing, P., *La notion de moyenne en turbulence. quelques réflexions selon une perspective historique*, Comptes Rendus Mécanique, vol. 347, 3: 228 (2019)
- Chern, I.-L., Glimm, J., McBryan, O., Plohr, B. & Yaniv, S., *Front tracking for gas dynamics*, Journal of Computational Physics, vol. 62, 1: 83 (1986)
- Chiocchetti, S. & Müller, C., *A solver for stiff finite-rate relaxation in Baer–Nunziato two-phase flow models*, Droplet Interactions and Spray Processes, (édité par G. Lamanna, S. Toninia, G. E. Cossalia & B. Weigand), Fluid Mechanics and Its Applications, vol. 121, p. 31–44, Springer (2020)

- Chung, M., *Characteristic development of hyperbolic two-dimensional two-fluid model for gas-liquid flows with surface tension*, Applied Mathematical Modelling, vol. 31: 578–588 (2007)
- Clausse, A., *Lagrangian density equations of single-fluid and two-fluid flows*, International Journal of Heat and Technology
- Clausse, A. & López de Bertodano, M., *Natural modes of the two-fluid model of two-phase flow*, Physics of Fluids, vol. 33, 3: 033324 (2021)
- Clebsch, A., *Über die Integration der hydrodynamischen Gleichungen*, Journal für die Reine und Angewandte Mathematik, vol. 56
- Cournède, P., *Un schéma bilagrangé plus projection pour la simulation bifluide des instabilités de mélange*, Thèse de doctorat, École centrale de Paris (2001)
- Curtiss, C. & Hirschfelder, J., *Integration of stiff equations*, Proc. Nat. Acad. Sci., vol. 38
- Curzon, A. E. & Leff, H. S., *Resolution of an entropy maximization controversy*, Am J Phys, vol. 47, 4: 385 (1979)
- de Bertodano, L., *Turbulent Bubbly Two-Phase Flow in a Triangular Duct.*, Thèse de doctorat, Rensselaer Polytechnic Institute (1992)
- de Vogelaere, R., *Methods of integration which preserve the contact transformation property of the Hamiltonian equations*, Report No. 4, Dept. Math., Univ. of Notre Dame, Notre Dame, Ind.
- Delhaye, J.-M., *Équations fondamentales des écoulements diphasiques, première partie : Équations générales de conservation*, Rap. tech. CEA-R-3429, Commissariat à l'Énergie Atomique (1968)
- Denner, F., Xiao, C.-N. & van Wachem, B. G. M., *Pressure-based algorithm for compressible interfacial flows with acoustically-conservative interface discretisation*, J Comput Phys, vol. 367: 192 (2018)
- Despres, B. & Lagoutiere, F., *Numerical resolution of a two-component compressible fluid model with interface*, Progress in Computational Fluid Dynamics, An International Journal (PCFD), vol. 7
- Ding, J. & Gidaspow, D., *A bubbling fluidization model using kinetic theory of granular flow*, Aiche Journal, vol. 36: 523 (1990)
- Dinh, T., Nourgaliev, R. & Theofanous, T., *Direct numerical simulation of disperse multi-phase high-speed flows*, Conference: 42nd AIAA Aerospace Sciences Meeting and Exhibit

- Drew, D., *The analysis of virtual mass effects in two-phase flow*, International Journal of Multiphase Flow, vol. 5
- Drew, D., *Mathematical modelling of multiphase flow*, Annual Review of Fluid Mechanics, vol. 91
- Drew, D. A., *Averaged field equations for two-phase media*, Stud Appl Math, vol. 50, 2: 133 (1971)
- Eckart, C., *The electrodynamics of material media*, Phys. Rev., vol. 54: 920 (1938)
- Eckart, C., *Variation principle of hydrodynamics*, The physics of fluids, vol. 3
- Edwards, A. R. & O'Brien, T. P., *Studies of phenomena connected with the depressurization of water reactors*, J. British Nuc. Energy Soc, vol. 9, 2: 125 (1970)
- Eichwald, B., *Integrateur exponentiels modifiés pour la simulation des vagues non linéaires*, Université Nice Sophia Antipolis
- Elghobashi, S., *Particle-laden turbulent flows: direct simulation and closure models*, Applied Scientific Research, vol. 48: 301 (1991)
- Evans, M. & Harlow, F., *The particle in cells method for hydrodynamic calculation*, Rap. tech., Los Alamos Laboratory (1957)
- Fahrenthold, E. & Koo, J., *Discrete Hamilton's equations for viscous compressible fluid dynamics*, Computer methods in applied mechanics and engineering, vol. 178, 1–2: 1 (1999)
- Favre, A., *Équations statistiques des gaz turbulents*, C.R. Academie des Sciences, vol. 246: 2576 (1958)
- Ferrer, P. J. M., Flåtten, T. & Munkejord, S. T., *On the effect of temperature and velocity relaxation in two-phase flow models*, ESAIM: Math Model Num, vol. 46: 411 (2012)
- Flåtten, T. & Lund, A., *Relaxation two-phase flow models and the subcharacteristic condition*, Math Mod Meth Appl S, vol. 21, 12: 2379 (2011)
- François, M. M., Shashkov, M. J. & Dendy, E. D., *A comparative study of multimaterial Lagrangian and Eulerian methods with pressure relaxation*, Comput Fluids, vol. 83: 126 (2013)
- Galera, S., *Modélisation thermique de la turbulence de proche paroi en régime hypersonique*, Thèse de doctorat, Université Montpellier II (2005)
- Gallouet, Thierry, Helluy, Philippe, Hérard, Jean-Marc & Nussbaum, Julien, *Hyperbolic relaxation models for granular flows*, ESAIM: M2AN, vol. 44, 2: 371 (2010)

- Gavrilyuk, S., *Multiphase flow modeling via Hamilton's principle*, Variational models and methods in solid and fluid mechanics, p. 163–210, Springer (2011)
- Gavrilyuk, S. & Saurel, R., *Mathematical and numerical modeling of two-phase compressible flows with micro-inertia*, Journal of Computational Physics, vol. 175
- Geurst, J., *General theory unifying and extending the Landau–Khalatnikov, Ginzburg–Pitaevskii, and Hills–Roberts theories of superfluid ^4He* , Physical Review B: covering condensed matter and materials physics, vol. 22
- Geurst, J., *Virtual mass in two-phase bubbly flow*, Physica A: Statistical Mechanics and its Applications, vol. 129
- Gevrin, F., Masbernat, O. & Simonin, O., *Granular pressure and particle velocity fluctuations prediction in liquid fluidized beds*, Chemical Engineering Science, vol. 63
- Gidaspow, D., *Multiphase flow and fluidization: continuum and kinetic theory descriptions*, Academic Press (1994)
- Gidaspow, D., Lyckowski, R., Solbrig, C., Hughes, E. & Mortenson, G., *Characteristics of unsteady one-dimensional two-phase flow*, Trans. Amer. Nucl. Soc, vol. 17
- Gingold, R. & Monaghan, J., *Smoothed particle hydrodynamics: theory and application to non-spherical stars*, Monthly notices of the royal astronomical society, vol. 181, 3: 375 (1977)
- Glimm, J., Grove, J., Li, X., Oh, W. & Sharp, D., *A critical analysis of Rayleigh–Taylor growth rates*, Journal of Computational Physics, vol. 169, 2: 652 (2001)
- Glimm, J., Grove, J. W., Li, X. L., Shyue, K., Zeng, Y. & Zhang, Q., *Three-dimensional front tracking*, SIAM Journal on Scientific Computing, vol. 19, 3: 703 (1998)
- Greenberg, J., Silverman, I. & Tambour, Y., *On the origins of spray sectional conservation equations*, Combustion and Flame, vol. 93, 1: 90 (1993)
- Gruber, C., *Thermodynamics of systems with internal adiabatic constraints: time evolution of the adiabatic piston*, Eur J Phys, vol. 20: 259 (1999)
- Gueyffier, D., Li, J., Nadim, A., Scardovelli, R. & Zaleski, S., *Volume-of-fluid interface tracking with smoothed surface stress methods for three-dimensional flows*, Journal of Computational Physics, vol. 152, 2: 423 (1999)
- Hadamard, J., *Lectures on Cauchy's Problem in Linear Partial Differential Equations*, Yale University Press (1902)
- Hairer, E., Hochbruck, M., Iserles, A. & Lubich, C., *Geometric numerical integration*, Oberwolfach Reports, vol. 3, 1: 805 (2006)

- Hantke, M., Müller, S. & Grabowsky, L., *News on Baer–Nunziato-type model at pressure equilibrium*, Continuum Mech. Thermodyn., vol. 33: 767–788 (2021)
- Harten, A., *High resolution schemes for hyperbolic conservation laws*, Journal of Computational Physics, vol. 49: 357 (1983)
- Herard, J., *Numerical modeling of turbulent two phase flows using the two fluid approach*, 16th AIAA Computational Fluid Dynamics Conference
- Herivel, J., *The derivation of the equations of motion of an ideal flow by hamilton principle*, Proc. Cambridge Philos. Soc, vol. 51
- Hersh, R., *Mixed problems in several variables*, Journal of Mathematics and Mechanics, vol. 12, 3: 317 (1963)
- Heulhard de Montigny, E., Llor, A. & Poujade, O., *Backbone compressible multi-fluid equations in the presence of velocity fluctuations and surface tension*, To be submitted to Int J Multiph Flow (2021)
- Hinze, J., *Momentum and mechanical-energy balance equations for a flowing homogeneous suspension with slip between the two phases.*, Appl. sci. Res., vol. 11
- Hirt, C. & Nichols, B., *Volume of fluid (VOF) method for the dynamics of free boundaries*, Journal of Computational Physics, vol. 39, 1: 201 (1981)
- Holmas, H., Sira, T., Nordsveen, M., Langtangen, H. & Schulkes, R., *Analysis of a 1D incompressible two-fluid model including artificial diffusion*, IMA Journal of Applied Mathematics, vol. 73, 4: 651 (2008)
- Holmes, R., Grove, J. W. & Sharp, D. H., *Numerical investigation of Richtmyer–Meshkov instability using front tracking*, Journal of Fluid Mechanics, vol. 301: 51–64 (1995)
- Ishii, M., *Thermo-fluid dynamic theory of two-phase flow*, Collection de la Direction des Etudes et Recherches d’Electricite de France, vol. 22
- Ishii, M. & Ibiki, T., *Thermo-fluid dynamic theory of two-phase flow*, 2^e éd., Springer, [1st ed. 1975, Eyrolles] (2011)
- Jenkins, J. T. & Savage, S. B., *A theory for the rapid flow of identical, smooth, nearly elastic, spherical particles*, Journal of Fluid Mechanics, vol. 130: 187–202 (1983)
- Johnson, J. N. & Chéret, R. (Réds.), *Classic Papers in Shock Compression Science*, Springer (1998)
- Jordan, B. W. & E.Polak, *Theory of a class of discrete optimal control systems*, Journal of Electronics and Control, vol. 17, 6: 697 (1964)

- Kamenetsky, V., Goldshtein, A., Shapiro, M. & Degani, D., *Evolution of a shock wave in a granular gas*, Physics of fluids, vol. 12: 3036 (2000)
- Kamm, J. R., Shashkov, M. J., Fung, J., Harrison, A. K. & Canfield, T. R., *A comparative study of various pressure relaxation closure models for one-dimensional two-material Lagrangian hydrodynamics*, Int J Numer Meth Fluids, vol. 65, 11–12: 1311 (2011)
- Kang, F., *On difference schemes and symplectic geometry*, Beijing Symposium on Differential Geometry and Differential Equations, p. 42–58
- Kapila, A., Menikoff, R., Bdzil, J. & Son, S., *Two-phase modeling of ddt transition in granular materials: Reduced equations*, Physics of fluids, vol. 13: 3002 (2001)
- Kataoka, I., *Local instant formulation of two-phase flow*, Int J Multiph Flow, vol. 12, 5: 745 (1986)
- Keyfitz, B. L., *Mathematical properties of nonhyperbolic models for incompressible two-phase flow*, Orleans (CD ROM). Tulane University (2001)
- Khalil, N., *Mesoscopic description of the adiabatic piston: kinetic equations and H-theorem*, J Stat Phys, vol. 176: 1138 (2019)
- Kitamura, K., Liou, M.-S. & Chang, C.-H., *Extension and comparative study of AUSM-family schemes for compressible multiphase flow simulations*, Commun Comput Phys, vol. 16, 3: 632 (2014)
- Koo, J. & Fahrenthold, E., *Discrete Hamilton’s equations for arbitrary Lagrangian–Eulerian dynamics of viscous compressible flow*, Computer methods in applied mechanics and engineering, vol. 189, 3: 875 (2000)
- Kraus, M., Kormann, K., Morrison, P. & Sonnendrücker, E., *GEMPIC: geometric electromagnetic particle-in-cell methods*, Journal of Plasma Physics, vol. 83, 4
- Kreeft, J. J. & Koren, B., *A new formulation of Kapila’s five-equation model for compressible two-fluid flow, and its numerical treatment*, J Comput Phys, vol. 229, 18: 6220 (2010)
- Kreiss, H.-O., *Initial boundary value problems for hyperbolic systems*, Communications on Pure and Applied Mathematics, vol. 23, 3: 277 (1970)
- Kuropatenko, V., *On difference methods for the equations of hydrodynamics*, Difference Methods for Solutions of Problems of Mathematical Physics, vol. 1: 287 (1967)
- La Spina, G. & de’ Michieli Vitturi, M., *High-resolution finite volume central schemes for a compressible two-phase model*, SIAM J Sci Comput, vol. 34, 6: B861 (2012)
- Lagoutière, F., *Modélisation mathématiques et résolution numérique de problèmes de fluides compressibles à plusieurs constituants*, Thèse de doctorat, Paris 6 (2000)

- Lallemand, M.-H., Chinnayya, A. & Metayer, O. L., *Pressure relaxation procedures for multiphase compressible flows*, International journal for numerical methods in fluids, vol. 49: 1 (2005)
- Laurent, F. & Massot, M., *Multi-fluid modelling of laminar polydisperse spray flames: origin, assumptions and comparison of sectional and sampling methods*, Combustion Theory and Modelling, vol. 5, 4: 537 (2001)
- Le Métayer, O., Massoni, J. & Saurel, R., *Dynamic relaxation processes in compressible multiphase flows. application to evaporation phenomena*, ESAIM: Proc, vol. 40: 103 (2013)
- Leveque, R., *Numerical methods for conservation laws*, Lecture in Mathematics
- Lhuillier, D., Chang, C.-H. & Theofanous, T. G., *On the quest for a hyperbolic effective-field model of disperse flows*, Journal of Fluid Mechanics, vol. 731
- Lhuillier, D. & Raviart, P., *Continuum-mechanics of fluid-particle mixtures Part I: The two-fluid model*, accessible upon request to the authors (2020)
- Lhuillier, D., Theofanous, T. & Meng, L., *Handbook of nuclear engineering*, Multiphase Flows: Compressible Multi-Hydrodynamics, p. 1813–1912
- Li, Q. B., *An improved gas-kinetic scheme for multimaterial flows*, Commun Comput Phys, vol. 27, 1: 145 (2020)
- Lin, C., *Hydrodynamics of liquid Helium II*, Phys. Rev. Lett, vol. 51
- Liou, M.-S. & Chang, C.-H., *Computing multiphase flows using AUSM⁺-up scheme*, 2006, (édité par D. A. Caughey & M. M. Hafez), Frontiers of Computational Fluid Dynamics, p. 367–394, World Scientific (2005)
- Liou, M.-S., Chang, C.-H., Nguyen, L. & Theofanous, T. G., *How to solve compressible multifluid equations: a simple, robust, and accurate method*, AIAA J, vol. 49, 9: 2345 (2008)
- Liu, H., Valocchi, A. J. & Kang, Q., *Three-dimensional lattice boltzmann model for immiscible two-phase flow simulations*, Physical Review E, vol. 85
- Llor, A., *Statistical hydrodynamic models for developed mixing instabilities flows: analytical 0D evaluation criteria, and comparison of single-and-two-phase flow approaches*, Lect Notes Phys, vol. 681, Springer (2005)
- Llor, A., Claisse, A. & Fochesato, C., *Energy preservation and entropy in Lagrangian space- and time-staggered hydrodynamic schemes*, Journal of Computational Physics, vol. 309: 324 (2016)

- Logan, J., *First integrals in the discrete variational calculus*, *aequationes mathematicae*, vol. 9, 2: 210 (1973)
- Loubère, R., Braeunig, J. P. & Ghidaglia, J. M., *A totally Eulerian finite volume solver for multi-material fluid flows: Enhanced Natural Interface Positioning (ENIP)*, *Eur J Mech B/Fluids*, vol. 31: 1 (2012)
- Lucy, L., *A numerical approach to the testing of the fission hypothesis*, *The astronomical journal*, vol. 82: 1013 (1977)
- Luo, D. M., Qiu, J. X., Zhu, J. & Chen, Y. B., *A quasi-conservative discontinuous Galerkin method for multi-component flows using the non-oscillatory kinetic flux*, *J Sci Comput*, vol. 87: 96 (2021)
- Lyczkowski, R. W., *The History of Multiphase Science and Computational Fluid Dynamics: A Personal Memoir*, Springer (2017)
- Marboeuf, A., *Schemas ALE multi-matériaux totalement conservatifs pour l'hydrodynamique*, Thèse de doctorat, Université Paris Saclay (2018)
- Margolin, L. G., *The reality of artificial viscosity*, *Shock Waves*, vol. 29, 1: 27 (2019)
- Marsden, J. E., Patrick, G. W. & Shkoller, S., *Multisymplectic geometry, variational integrators, and nonlinear PDEs*, *Communications in Mathematical Physics*, vol. 199, 2: 351 (1998)
- Marsden, J. E. & West, M., *Discrete mechanics and variational integrators*, *Acta numerica*, vol. 10: 357 (2001)
- Marx, C., *Intégrateurs géométriques: Application à la Mécanique des Fluides*, Theses, Université de La Rochelle (2008)
- Mattsson, A. E. & Rider, W. J., *Artificial viscosity: back to the basics*, *International Journal for Numerical Methods in Fluids*, vol. 77, 7: 400 (2015)
- Mecredy, R. & Hamilton, L., *The effects of nonequilibrium heat, mass, and momentum transfer on two-phase sound speed*, *International Journal Heat Mass Transfer*, vol. 15, 1: 61 (1972)
- Menikoff, R. & Plohr, B. J., *The Riemann problem for fluid flow of real materials*, *Rev Mod Phys*, vol. 61, 1: 75 (1989)
- Mesina, G., *A history of RELAP computer code*, *Nuclear Science and Engineering*, vol. 182, 1: v (2016)

- Miller, D. S. & Zimmerman, G. B., *An algorithm for time evolving volume fractions in mixed zones in Lagrangian hydrodynamics calculations*, Russ J Phys Chem B, vol. 3, 1: 117 (2009)
- Miller, G. H. & Puckett, E. G., *A high-order Godunov method for multiple condensed phases*, Journal of Computational physics, vol. 128, 0200: 134–164 (1996)
- Minchev, B. & W.Wrigh, *A review of exponential integrators for first order semi-linear problems*, Tech. report 2/05, Department of Mathematics, NTNU
- Monaghan, J., *An introduction to SPH*, Computer Physics Communications, vol. 48: 89–96 (1988)
- Montini, M., *Closure Relations of the one-dimensional two-fluid model for the simulation of slug flows*, Thèse de doctorat, Imperial College (2011)
- Morel, C., *Mathematical modeling of disperse two-phase flows*, Fluid Mechanics and Its Applications, vol. 114, Springer (2005)
- Morrison, P., *Hamiltonian fluid mechanics*, Encyclopedia of Mathematical Physics, vol. 2
- Morrison, P. J., *Hamiltonian description of the ideal fluid*, Reviews of modern physics, vol. 70, 2: 467 (1998)
- Munkejord, S., S.Evje & T.Flatens, *A MUSTA scheme for a nonconservative two-fluid model*, Sciam J. of science computing, vol. 31
- Murray, J., *On the mathematics of fluidization Part 1. Fundamental equation and wave propagation*, Journal of Fluid Mechanics, vol. 21, 3
- Murrone, A. & Guillard, H., *A five equation reduced model for compressible two phase flow problems*, J Comput Phys, vol. 202: 664 (2005)
- Murrone, A. & Villedieu, P., *Numerical modeling of dispersed two-phase flows*, Aerospace-Lab, vol. 2, 4: 1 (2011)
- Nigmatulin, R. I., *Equations of hydromechanics and compression shock in two-velocity and two-temperature continuum with phase transformations*, Fluid Dyn, vol. 2, 5: 20 (1967), [Translated from 1967. Izv AN SSSR Mekhanika Zhidkosti Gaza 2, 33–47]
- Noh, W. F., *Errors for calculations of strong shocks using an artificial viscosity and an artificial heat flux*, J Comput Phys, vol. 72, 1: 78 (1987)
- Noh, W. F. & Woodward, P., *Slic (simple line interface calculation)*, Proceedings of the Fifth International Conference on Numerical Methods in Fluid Dynamics June 28 – July 2, 1976 Twente University, Enschede, (édité par A. I. van de Vooren & P. J. Zandbergen), p. 330–340, Springer Berlin Heidelberg, Berlin, Heidelberg (1976)

- O'Rourke, P. J., Brackbill, J. & Larrouturou, B., *On particle-grid interpolation and calculating chemistry in particle-in-cell methods*, Journal of Computational Physics, vol. 109, 1: 37 (1993)
- Osher, S. & Sethian, J. A., *Fronts propagating with curvature-dependent speed: Algorithms based on Hamilton–Jacobi formulations*, Journal of computational physics, vol. 79, 1: 12 (1988)
- Padding, J. T., Deen, N. G., Peters, E. F. & Kuipers, J. H., *Euler–Lagrange modeling of the hydrodynamics of dense multiphase flows*, Advances in Chemical Engineering, vol. 46, p. 137–191, Elsevier (2015)
- Pandare, A. K., Luo, H. & Bakosi, J., *An enhanced AUSM⁺-up scheme for high-speed compressible two-phase flows on hybrid grids*, Shock Waves, vol. 29, 1: 629 (2019)
- Paulin, C., *Improved numerical schemes for monotonic conservative scalar advection: tackling mesh imprinting and numerical wetting.*, Thèse de doctorat, Université Paris-Saclay (2021)
- Paulin, C., Heulhard de Montigny, E. & Llor, A., *Towards isotropic transport with co-meshes*, Coupled Syst Mech, vol. 9, 1: 63 (2020)
- Paulin, C., Llor, A., Vazquez-Gonzalez, T., Perlat, J. & de Montigny, É. H., *Doubly-monotonic constraint on interpolators: bridging second-order to singularity preservation to cancel numerical wetting in transport schemes.*, submitted to SIAM J. Sci. Comput. (Methods and Algorithms for Scientific Computing)
- Pavlov, D., Mullen, P., Tong, Y., Kanso, E., Marsden, J. E. & Desbrun, M., *Structure-preserving discretization of incompressible fluids*, Physica D: Nonlinear Phenomena, vol. 240, 6: 443 (2011)
- Plesset, M. S., *The dynamics of cavitation bubbles*, J. Appl. Mech., vol. 16, 3: 277 (1949)
- Poroshyna, Y. & Utkin, P., *Pressure relaxation procedure with compaction for the problems of shock wave – particles beds interaction*, Proceedings of the 32nd International Symposium on Shock Waves (ISSW32 2019)
- Price, D., *Smoothed particle hydrodynamics and magnetohydrodynamics*, Journal of Computational Physics, vol. 231: 759–794 (2012)
- Ramshaw, J., *Characteristics, stability and short-wavelength phenomena in two phases flow equation systems*, Nuclear Science and Engineering, vol. 66
- Ransom, V. & Hicks, D., *Hyperbolic two-pressure models for two phases flow*, Journal of Computational Physics, vol. 53: 124 (1984)

- Reiss, J., *A family of energy stable, skew-symmetric finite difference schemes on collocated grids*, Journal of Scientific Computing, vol. 65, 2: 821 (2015)
- Reynolds, O., *IV. on the dynamical theory of incompressible viscous fluids and the determination of the criterion*, Philosophical Transactions of the Royal Society of London. (A.), vol. 186: 123 (1895)
- Richardson, L. F. & Lynch, P., *Weather prediction by numerical process*, Cambridge Mathematical Library, 2^e éd., Cambridge University Press (1922)
- Richtmyer, R., *Proposed numerical method for calculation of shocks*, Rapp. tech. LANL, vol. LA-671
- Romenski, E. & Toro, E., *Compressible two-phase flows: two-pressure models and numerical methods*, Comput. Fluid Dyn. J, vol. 13: 403 (2004)
- Romero, I., *Thermodynamically consistent time-stepping algorithms for non-linear thermo-mechanical systems*, International journal for numerical methods in engineering, vol. 79, 6: 706 (2009)
- Rousseau, J., *Le module de base du code CATHARE. Développements physiques et performances*, La Houille Blanche, vol. 3–4: 209 (1984)
- Ruth, R., *A Canonical Integration Technique*, IEEE Trans. Nucl. Sci., vol. 30: 2669 (1983)
- Salas, M., *The curious events leading to the theory of shock waves*, Shock waves, vol. 16, 6: 477 (2007)
- Sanz-Serna, J. M., *Symplectic integrators for Hamiltonian problems: an overview*, Acta numerica, vol. 1: 243 (1992)
- Saurel, R. & Abgrall, R., *A multiphase Godunov method for compressible multifluid and multiphase flows*, Journal of Computational Physics, vol. 150
- Saurel, R. & Abgrall, R., *A simple method for compressible multifluid flows*, SIAM J Sci Comput, vol. 21, 3: 1115 (1999b)
- Saurel, R., Franquet, E., Daniel, E. & Le Métayer, O., *A relaxation-projection method for compressible flows. Part I: The numerical equation of state for the Euler equations*, J Comput Phys, vol. 223: 822 (2007)
- Saurel, R., Gavriluk, S. & Renaud, F., *A multiphase model with internal degrees of freedom: application to shock-bubble interaction*, Journal of Fluid Mechanics, vol. 495
- Saurel, R. & Le Métayer, O., *A multiphase model for compressible flows with interfaces, shocks, detonation waves and cavitation*, J Fluid Mech, vol. 431: 239 (2001)

- Saurel, R., Petitpas, F. & A.Berryc, R., *Simple and efficient relaxation methods for interfaces separating compressible fluids, cavitating flows and shocks in multiphase mixtures*, Journal of Computational Physics, vol. 228, 5: 1678 (2009)
- Saurel, R., Petitpas, F. & Abgrall, R., *Modelling phase transition in metastable liquids: application to cavitating and flashing flows*, J Fluid Mech, vol. 607: 313 (2008)
- Schutz, B. F. & Sorkin, R., *Variational aspects of relativistic field theories, with application to perfect fluids*, Annals of Physics, vol. 107
- Sciarra, G., Hutter, K. & Maugin, G., *A variational approach to a micro-structured theory of solid-fluid mixtures*, Archive of applied mechanics, vol. 73
- Seliger, R. L. & Whitham, G. B., *Variational principles in continuum mechanics*, Proceedings of the Royal Society of London. Series A. Mathematical and Physical Sciences, vol. 305, 1480: 1 (1968)
- Shen, Z., Yan, W. & Lv, G., *Behavior of viscous solutions in Lagrangian formulation*, Journal of Computational Physics, vol. 229, 12: 4522–4543 (2010)
- Shi, P. & Rzehak, R., *Bubbly flow in stirred tanks: Euler–Euler/RANS modeling*, Chemical Engineering Science, vol. 190: 419 (2018)
- Snider, D., *An incompressible three-dimensional multiphase particle-in-cell model for dense particle flows*, Journal of computational physics, vol. 170, 2: 523 (2001)
- Snider, D., ORourke, P. & Andrews, M., *An incompressible two-dimensional multiphase particle-in-cell model for dense particle flows*, Rap. tech., Los Alamos National Lab., NM (United States) (1997)
- Snider, D. M., *Three fundamental granular flow experiments and CPFD predictions*, Powder Technology, vol. 176, 1: 36 (2007)
- Solbrig, C. & Hughes, E. D., *Two phase flow equations which account for unequal phase velocities and unequal phase temperatures*, Rap. tech. INL/EXT-16-38913, Idaho National Laboratory (1971)
- Soo, S., *Pipe flow of suspension*, Applied Scientific Research, vol. 21
- Squire, J., Qin, H. & Tang, W., *Geometric integration of the Vlasov–Maxwell system with a variational particle-in-cell scheme*, Physic of Plasmas, vol. 19, 8: 084501 (2012)
- Stuhmiller, J., *The influence of interfacial pressure forces on the character of two-phase flow model equations*, International Journal of Multiphase Flow, vol. 3
- Subramaniam, S., *Lagrangian–Eulerian methods for multiphase flows*, Progress in Energy and Combustion Science, vol. 39, 2–3: 215 (2013)

- Sun, M., *A thermodynamic and dynamic subgrid closure model for two-material cells*, Int J Numer Meth Fluids, vol. 73: 130 (2013)
- Sussman, M., Smereka, P. & Osher, S., *A level set approach for computing solutions to incompressible two-phase flow*, Journal of Computational physics, vol. 114, 1: 146 (1994)
- Tambour, Y., *Sectional model for evaporation and combustion of sprays of liquid fuels*, Isr. J. Technol., vol. 18, 1–2
- Terashima, H. & Tryggvason, G., *A front-tracking/ghost-fluid method for fluid interfaces in compressible flows*, Journal of Computational Physics, vol. 228, 11: 4012 (2009)
- Theofanous, T. & Chang, C.-H., *On the computation of multiphase interactions in transonic and supersonic flows*, Conference: 46th AIAA Aerospace Sciences Meeting and Exhibit, TP-8: Computational Multi-Phase Flow
- Theofanous, T., Mitkin, V. & Chang, C.-H., *Shock dispersal of dilute particle clouds*, Journal of fluid mechanics, vol. 841: 732 (2018)
- Toumi, I., *An upwind numerical method for two-fluid two-phase flow models*, Nuclear Science and Engineering, vol. 123: 147 (1996)
- Toumi, I. & Kumbaro, A., *An approximate linearized riemann solver for a two-fluid model*, J Comput Phys, vol. 124: 286 (1996)
- Truesdell, C., *Rational Thermodynamics*, 2^e éd., Springer, [1st ed. 1969, McGraw-Hill] (1984)
- Tryggvason, G., *A front-tracking/finite-volume Navier–Stokes solver for direct numerical simulations of multiphase flows*, Rap. tech. (2012)
- Tsuji, Y., Kawaguchi, T. & Tanaka, T., *Discrete particle simulation of two-dimensional fluidized bed*, Powder Technology, vol. 77: 79 (1993)
- van Deemter, J. & van der Laan, E., *Momentum and energy balances for dispersed two-phase flow*, Appl. sci. Res., vol. 10, 102
- van der Pijl, S., Segal, A., Vuik, C. & Wesseling, P., *A mass-conserving level-set method for modelling of multi-phase flows*, International Journal for Numerical Methods in Fluids, vol. 47: 339 (2005)
- Vazquez-Gonzalez, T., *Schemas numeriques mimétiques et conservatifs pour la simulation d'écoulements multiphasiques compressibles*, Thèse de doctorat, Université Paris-Saclay (2016)
- Vazquez-Gonzalez, T., A.Llor & C.Fochesato, *Ransom test results from various two-fluid schemes: Is enforcing hyperbolicity a thermodynamically consistent option?*, International Journal of Multiphase flow, vol. 81

- Vazquez-Gonzalez, T., A.Llor & C.Fochesato, *A mimetic numerical scheme for multi-fluid flows with thermodynamic and geometric compatibility on an arbitrarily moving grid*, International Journal of Multiphase Flow, vol. 132
- von Kármán, T., *Progress in the statistical theory of turbulence*, Proceedings of the National Academy of Sciences, vol. 34, 11: 530 (1948)
- VonNeumann, J. & Richtmyer, R. D., *A method for the numerical calculation of hydrodynamic shocks*, Journal of applied physics, vol. 21, 3: 232 (1950)
- Vreman, A., *Stabilisation of the Eulerian model for incompressible multiphase flow by artificial diffusion*, Journal of COmputational Physics, vol. 230: 1639 (2011)
- Wachem, B. V., Schouten, J., den Bleek, C. V., Krishna, R. & Sinclair, J., *Comparative analysis of CFD models of dense gas–solid systems*, Aiche Journal, vol. 47, 5: 1035 (2001)
- Wendroff, B., *Two-fluid models; a critical survey*, Los Alamos Scientific Laboratory, LA-UR, p. 79–291
- Wijngaarden, L., *Shock waves in bubbly liquids*, Multiphase Flows I, Shock Wave Science and Technology Reference Library, vol. 1, p. 3–33, Springer (2007)
- Wilkins, M. L., *Calculation of elastic-plastic flow*, Rap. tech., California Univ Livermore Radiation Lab (1963)
- Williams, A., *Spray combustion and atomization*, The physics of fluids, vol. 1, 6: 541 (1958)
- Wörner, M., *A compact introduction to the numerical modeling of multiphase flows*, Rap. tech. FZKA 6932, Forschungszentrum Karlsruhe (2003)
- Yanilkin, Y. V., Goncharov, E. A., Kolobyanin, V. Y., Sadchikov, V. V., Kamm, J. R., Shashkov, M. J. & Rider, W. J., *Multi-material pressure relaxation methods for Lagrangian hydrodynamics*, Comput Fluids, vol. 83: 137 (2013)
- Youngs, D. L., *Modelling turbulent mixing by Rayleigh–Taylor instability*, Physica D: Non-linear Phenomena, vol. 37, 1–3: 270 (1989)
- Zel'Dovich, Y. B. & Raizer, Y. P., *Physics of shock waves and high-temperature hydrodynamic phenomena*, Courier Corporation (2002)
- Zhang, D. & VanderHeyden, W., *High-resolution three-dimensional numerical simulation of a circulating fluidized bed*, Powder Technology, vol. 116, 2: 133 (2001), modelling and Computational analysis of a collection of particulate and fluid-solid flow problems
- Zhang, D. & VanderHeyden, W., *The effects of mesoscale structures on the macroscopic momentum equations for two-phase flows*, International Journal of Multiphase Flow, vol. 28

Zhong, G. & Marsden, J., *Lie–Poisson Hamilton–Jacobi theory and Lie–Poisson integrators*,
Physical Letters A, vol. 133, 3: 134 (1988)